MRI analysis of brain connectivity in a mouse model of Alzheimer's disease

Laetitia Degiorgis

UNIVERSITE DE STRASBOURG

ÉCOLE DOCTORALE MSII

Laboratoire ICube UMR 7357

THÈSE présentée par :

Laetitia Degiorgis

soutenue le : **11 septembre 2019**

pour obtenir le grade de : **Docteur de l'université de Strasbourg**

Discipline/ Spécialité : **Neurosciences**

Analyse des réseaux cérébraux par IRM chez un modèle souris de la maladie d'Alzheimer

THÈSE dirigée par :

M. BLANC Frédéric	Professeur, Université de Strasbourg
M. ARMSPACH Jean-Paul	Ingénieur de recherche, Université de Strasbourg

ENCADRANTE :

Mme HARSAN Laura	MCU-PH, Université de Strasbourg

RAPPORTEURS :

Mme. KIEFFER Brigitte	Professeur, Université McGill, Montréal
M. DHENAIN Marc	Directeur de Recherche, Université Paris-Saclay

Table of contents

Table of contents 3

Table of figures 6

List of abbreviations 8

Summary 9

A) Introduction 10

I. The Alzheimer's disease 10

1. General context 10
   a. History 10
   b. Epidemiology 11
2. Anatomo-pathology in AD 12
   a. Amyloidopathy 12
   b. Tauopathy 13
   c. Longitudinal evolution of amyoïdopathy and tauopathy in AD patients 15
   d. Other mechanisms of AD 16
3. Clinic of Alzheimer's disease 17
   a. Etiology of the pathology 17
   b. Diagnostic and symptoms 18
   c. Therapeutic strategies 20
4. Transgenic animal models of Alzheimer's disease 20

II. Brain wide connectome analysis with MRI 21

1. Principle of the MRI 21
2. Resting-state functional MRI 23
   a. The BOLD signal 23
   b. From BOLD signal to the concept of functional connectivity 26
   c. Approaches for mapping functional brain networks 27
      - Seed-based analysis 27
      - Independent component analysis 28
      - Dictionary learning 28
      - Modelling functional connectivity with graph theory 28
      - Characterizing the dynamic functional connectivity 29

d. Organization of intrinsic functional architecture in human brain 29
e. Rodent brain functional networks 31
3. Structural MRI: from anatomy to structural connectivity mapping 34
a. Brain morphometry measures 34
b. Diffusion tensor imaging and fiber tracking 35
- DTI derived maps for quantitative analysis of microstructural features 36
- Fiber tractography 37
4. Graph theory for modelling functional and structural connectivity 37
5. The connectome in neurodegenerative diseases 41
III. Brain MRI in Alzheimer's disease: anatomy and brain connectome features 43
1. Human imaging studies 43
2. Precilinical MRI in animal models of AD: state of the art 45
3. The place of the thesis project in the current scientific context 48
B) Study 1 49
1. Remodeling of cerebral networks architecture anticipate behavioral deficits in a tauopathy mouse model of Alzheimer's disease 50
2. Additional results to the study 1 78
3. Conclusion 79
C) Study 2 80
1. Longitudinal Evaluation of the brain connectome of a mouse model of Alzheimer's disease 81
2. Additional results to the study 2 121
D) Discussion 127
1. Memory and learning behavior profiles 127
2. Patterns of functional and structural connectivity in Thy-Tau22 mouse model 128
a. Network signatures of early stage of the pathology 128
a.1 Hippocampal connectivity 128
a.2 Early prefrontal cortex connectivity impairments in Thy-Tau22 mice 131

b. Longitudinal profile of functional and structural brain networks alterations in Thy-Tau22 tauopathy model 132

b.1 Functional networks signatures 132

b.2 Progressive microstructural alterations along major cholinergic pathways 133

3. Conclusion and Outlook 136

a. Major findings of the study 136

b. Perspectives 138

E) References 139

F) Annexes 160

1. Preprocessing pipeline of the MRI images 160
2. Résumé de la thèse en français 163
3. Other paper's involvment 172
4. List of presentations 204

List of figures and tables

Introduction

Figure 1: *Geographic repartition of people living with a dementia worldwide* 11
Figure 2: *The amyloidotic mechanism in AD* 13
Figure 3: *The mechanism of tauopathy in AD* 14
Figure 4: *Longitudinal progression of amyloidopathy and tauopathy* 15
Figure 5: *The Neuroinflammation mechanism in AD* 17
Figure 6: *Evolution of AD biomarkers* 19
Figure 7: *The BOLD signal mechanism* 24
Figure 8: *The Hemodynamic Response Function* 25
Figure 9: *Resting-state functional analysis using the seed-based approach* 28
Figure 10: *Relevant functional networks in the Human brain* 31
Figure 11: *Seed-based networks in mice* 32
Figure 12**:** *Hierarchical clustering methods in mice* 33
Figure 13: *Human vs mice networks* 34
Figure 14: *Parametric maps extracted from the tensor of a mouse brain* 36
Figure 15: *The brain connectome organization* 39
Figure 16: *The Rich-club organization of the brain* 40
Figure 17: *Connectome's modification in neurodegenerative diseases* 41
Figure 18: *Summary of differences in local connectivity in AD versus control group* 45

Study 1

Figure 1: *Behavioral evaluation of Thy-Tau22 mice at 5 months* 56
Figure 2: *Mean correlation analysis of ROIs involved in AD* 57
Figure 3: *dHIP hyperconnectivity in Thy-Tau22 mice* 59
Figure 4: *vHIP functional modifications in Thy-Tau22 mice* 60
Figure 5: *Microstructural modifications at early stage of tauopathy* 62
Figure 6: *Representative immunofluorescence coronal slices* 64

Supplementary table 1: *MRI acquisition parameters for the three used sequences* 74
Supplementary Figure 1: *Ranking of the most connected brain areas in WT and Thy-Tau22 mice* 75
Supplementary Figure 2: *Dynamic Functional Connectivity* 76
Supplementary Figure 3: *Pathological Tau staining in the septo-hippocampal pathway* 77

Additional result to the study 1

Annex figure 1: *Early functional prefrontal cortex connectivity modifications in Thy-Tau22 mice* 78

Study 2

Figure 1: *Methodological pipeline of the study* 83
Figure 2: *Memory and learning assessment in Thy-Tau22 mice over time* 87
Figure 3: *Morphological changes between Thy-Tau22 and WT mice* 88

Figure 4: *Fractional anisotropy and Fiber density maps* 89
Figure 5: *Longitudinal graph theory functional analysis* 92-93
Figure 6: *Septal functional connectivity modifications in Thy-Tau22 mice over time* 95
Figure 7: *Functional connectivity changes over time in the hippocampus* 97
Figure 8: *Default-mode network functional modifications over time* 99
Figure 9: *Representative sagittal slices and corresponding magnified images of immunological staining* 100

Supplementary table 1: *MRI acquisition parameters* 116
Supplementary table 2: *Abbreviations of regions of interests used in the partial correlation analysis* 116
Supplementary table 3: *Most changed edges* 117
Supplementary figure 1: *Seed-based analysis of the lateral septum at 5, 9 and 13 months* 118
Supplementary figure 2: *Seed-based analysis of the dorsal hippocampus at 5, 9 and 13 months* 119
Supplementary figure 3: *Seed-based analysis of the ventral hippocampus at 5, 9 and 13 months* 120

Additional results to the study 2

Annex figure 1: *Radial diffusivity increases over time in Thy-Tau22 mice* 121
Annex figure 2: *Axial diffusivity modifications in Thy-Tau22 mice* 122
Annex figure 3: *A preliminary evaluation of early hippocampal functional connectivity changes in early AD patients and prodromal Thy-Tau22 mice* 125

List of abbreviations

Aβ: Amyloid-β
AD: Alzheimer's disease
ADif: Axial Diffusivity
ATP: Adenosinie Triphosphate
BGN: Basal Ganglia Network
BOLD: Blood-oxygen level dependent
CBF: Cerebral blood flow
CBV: Cerebral blood volum
CSF: Cerebro spinal fluid
DCM: Dynamic causal modality
DFC: Dynamic functional connectivity
DMN: Default-mode network
DTI Diffusion tensor imaging
ECN: Executive control network
EGG: Electroencephalogram
EPI: Echo-planar imaging
FA: Fractional anisotropy
FC: Functional connectivity
FD: Fiber density
fMRI: Functional MRI
Hb: Hemoglobin
HARDI: High angular resolution diffusion imaging
IADLs: Instrumental activities of daily living
ICA: Independent component analysis
MCI: Mild cognitive impairment
MD: Mean diffusivity
MEG: Magnetoencephalography
MR: Magnetic resonance
MRI: Magnetic resonance imaging
MTL: Medial temporal lobe
NFT: Neurofibrillary tangles
NMR: Nuclear magnetic resonance
PET: Positron emission tomography
PS: Presenilin
QPP: Quasi-periodic patterns
RD: Radial diffusivity
RF: Radiofrequence
ROI: Region of interest
SAD: Sporadic alzheimer's disease
SCI: Subjective cognitive impairments
SMN: Sensory-motor network
SNR: Signal-to-noise ratio
TC: Timecourse
TE: Time of echo
TR: Time of repetition

Summary

Our brain is a network, built from efficient structural and functional connections between cerebral regions, sharing information continuously. Exploring brain-wide neural communications is providing unique perspective about the cerebral networks topology and their interactions as an integrative system, called the connectome. In the brain, selected "hubs", are sustaining and integrating efficiently the communication between intrinsic functional and/or structural networks, and represents key cerebral areas spreading information across the whole brain.

A hierarchical organization emerges, and the complex architecture of functional and structural connections can be affected by numerous factors such as metabolic changes, genetic alterations, behavioral affectations, or environment. In neurodegenerative diseases, exploring the connectome features becomes a crucial step towards the discovery of the mechanisms of the pathology and towards an early and specific diagnosis. It offers a unique way for understanding how the functional and structural connectivity are affected, which are the vulnerable nodes and pathways and what's driving the brain network remodeling or damaging, potential future treatments for pathologies such as Alzheimer's disease.

Alzheimer's disease (AD) is the most widespread cause of dementia in the world and constitutes one of the biggest challenges for society. This neurodegenerative disorder is inducing structural, functional and cognitive dysfunctions over time. Despite the accumulation of strong knowledge about the pathology over the years, the establishment of specific and non-invasive biomarkers of AD, to help both early diagnosis and detection of the disease's development, is still of paramount importance. Among dominant mechanisms of the disease is the abnormal change of conformation and accumulation of the protein Tau, leading to a tauopathy, a pathological process known to strongly underlie memory impairment in patients.

In Human and animal models of cerebral pathology, Magnetic Resonance Imaging (MRI) is a unique approach allowing the investigation of the connectome in a longitudinal, non-invasive and in-vivo manner. In the exploration of neurodegenerative diseases, resting state MRI has opened a new window into the brain and its connectome, proposing abnormal functional connectivity as a candidate biomarker of brain pathologies, such as AD. Combining the analysis of resting-state functional MRI images, revealing networks of synchronous functional connectivity between regions, and diffusion tensor imaging (DTI) analysis, allowing the mapping of fiber bundles to explore the structural connectivity, a complete and robust overview of the connectome can be acquired.

In this context, we explored this pathway, and combined these two approaches *in vivo* in a longitudinal study to follow-up and characterize the Thy-Tau22 transgenic mouse model of tauopathy that develops overtime classical AD hallmarks. We identified possible network signatures of pathological states evolving from early to intermediate and late stages. We associate behavioral assessment and histological staining of neurotoxic protein to the MRI approach, in order to relate pathological mechanism at both network and cellular level, to connectome's affectations in AD.

A) Introduction

I. The Alzheimer's disease

1. General context

a. History

In 1907, Alois Alzheimer described the first case of the eponymous disease in a state asylum in Frankfurt. His patient, Auguste Deter, was a 51 years old woman presenting progressive cognitive impairment.

"*Her memory is seriously impaired. If objects are shown to her, she names them correctly, but almost immediately afterwards she has forgotten everything. When reading a test, she skips from line to line or reads by spelling the words individually, or by making them meaningless through her pronunciation. In writing she repeats separate syllables many times, omits others and quickly breaks down completely. In speaking, she uses gap-fills and a few paraphrased expressions ("milk-pourer" instead of cup); sometimes it is obvious she cannot go on. Plainly, she does not understand certain questions. She does not remember the use of some objects*." *(Alzheimer, 1907* [1]*; for an English translation, see Stelzmann et al., 1995)*

After she passed away, he performed a brain autopsy and revealed the two main neuropathological lesions known in Alzheimer's disease (AD): amyloid plaques and neurofibrillary tangles (NFT).

It's only in the 80's that the proteins associated with these lesions were highlighted. The American pathologist George Glenner discovered the major constituent of amyloid plaques, the amyloid Beta (Aβ) protein, and the Belgian Jean-Pierre Brion revealed that an abnormal phosphorylation of the protein Tau was responsible of NFT's formation. Over the years, scientists also linked genetic anomalies with AD's development. Indeed, in the 90's several mutations located on genes involved in the amyloid process, the APP gene and Presenilin (PS) 1 and 2 genes, were discovered responsible for a genetic form of AD. As important as they are, the APP, PS1 and PS2 mutations are only responsible for 1 to 2% of AD patients. However, involvement of genetic determinants such as the APOE4 allele which was highlighted as a major risk factor of AD the same decade, is attributed to 60% cases of sporadic development of the disease. Thanks to the development of "Genome Wide Association Studies" (GWAS) methodology, investigating simultaneously thousands of late onset patients and even more polymorphisms, several loci were identified as susceptible to be involved in AD, such a rare variant of the TREM2 gene, BIN1, or CLU genes -to only cite few examples. Large-scale meta-analysis of GWAS using a two-stage study design led to the discovery of additional risks factors of the disease, identifying in 2013 11 new susceptible loci involved in AD, in addition to the already known genes [2]. More recently, Jansen et al., 2019 [3] performed a three stages meta-analysis on a large cohort of AD patients, including offspring with one or two parents with AD, leading to the identification of 9 new risk loci implicating 215 potential causative genes, in addition to the already 20 known genetic determinants' risk factors. These studies highlight the strong and complex implication of multiple genetic variants factors in the development of sporadic forms of AD.

Despite many years of knowledge accumulation and crucial discoveries about the mechanisms of AD, no clear etiology nor curative treatment has been proposed yet, and neurodegenerative diseases like AD are still a serious challenge for society. One of the drawbacks in their management and treatment is the absence of clear biomarkers of early phases of the disease, leading to a late diagnosis, and expansion of cases worldwide.

b. Epidemiology

Alzheimer's disease is the most widespread cause of dementia in the world. According to the World Alzheimer Report 2015 [4], more than 35 million people would be affected worldwide, adding 7.7 million more every year. Predictions from the OMS (Organisation Mondiale de la Santé) suggest that this number will double every 20 years (Fig. 1). Among patients, women represent 60% of the diseased, a higher percentage than men that could be related to several factors including brain structure differences, hormonal changes, or the differences between gender in their vulnerability to genetical risk factors such as the APOE4 allele [5–7]. Despite the discovery of several genetic implications in AD, mutations-related forms of the pathology only represent 1 to 2% of AD patients, while most forms of the disease are coming from multifactorial determinism, starting with age [8]

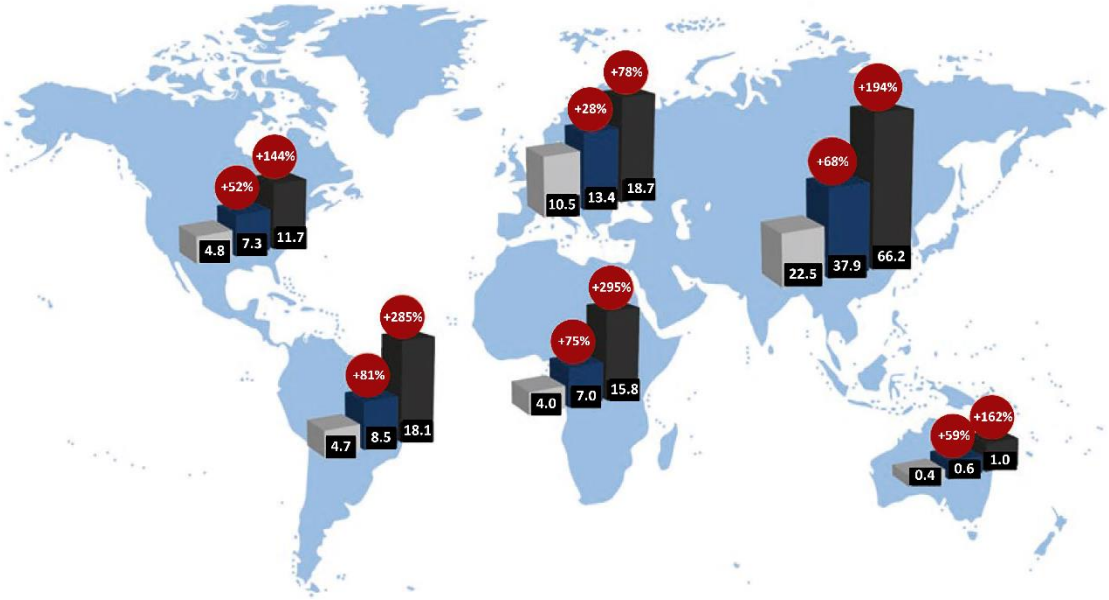

Figure 1: *Geographic repartition of people living with a dementia worldwide. In grey, number of patient (in million) in 2015, projection in 2030 in blue and in 2050 in black. From Wolters and Ikram, 2018* [9]

In France 900 000 people are affected by AD, which represents the 4th cause of mortality in the country. Every year, 225 000 individuals are diagnosed with AD, which has been estimated to represent only half of patients. Among French 75 years old and ager people, 14.2% are affected by AD or an associated dementia [10]. This increasing number of AD patients over the years could be explained by the combination of 1) an expansion of AD, 2) a higher life expectancy in human, and/or 3) a better specificity of diagnosis.

2. Anatomo-pathology in AD

In AD, many molecular lesions have been highlighted. Among them, two mechanisms involving the accumulation of misfolded proteins are emerging as the major abnormalities of the disease.

a. Amyloidopathy

In AD's research field, the "amyloid cascade" is one of the strongest hypotheses about the disease progress [11], supported by the fact that familial forms of AD are only involving amyloid-related gene mutations. In the amyloidogenic pathway (Fig. 2), a neurotoxic peptide named Aβ-42 is originated from a wrong cleavage of the APP protein by a β-secretase (BACE-1) [12]. An imbalance between the production and clearance of this neurotoxic peptide is responsible for its accumulation and aggregations throughout the brain. When spontaneously aggregating, Aβ-42 peptides adopt an oligomer conformation, which can then coalesce together to adopt a protofibrils form [13]. All those structures of Aβ-42 are soluble and the most toxic forms of amyloids in the brain [14,15]. Insoluble amyloids conformations can also be observed in AD patients' brain, such as amyloid β-sheet fibrils and the well-known amyloid plaques. Several Aβ production's pathways have been demonstrated in the literature [16]. The main characterized mechanism involves an internalization of APP at the cell membrane, were the protein can either be processed to produce extracellular Aβ, either be subject to endocytosis leading to its expression at the surface of an endosome, or a lysosome, where γ-secretase are responsible for its wrong cleavage into intracellular Aβ [17]. Other studies suggest the existence of alternative pathways for Aβ production, showing a direct pathway from APP secretion to the lysosome, without involving a cell membrane internalization [18], or a direct production from autophagic vacuoles [19,20]

Both soluble and insoluble Aβ are impacting several cell processes inducing oxydatif stress, synaptic dysfunction, neuroinflammation, excitotoxicty, and -according to the amyoid cascade hypothesis-, NFT [12,21–23]

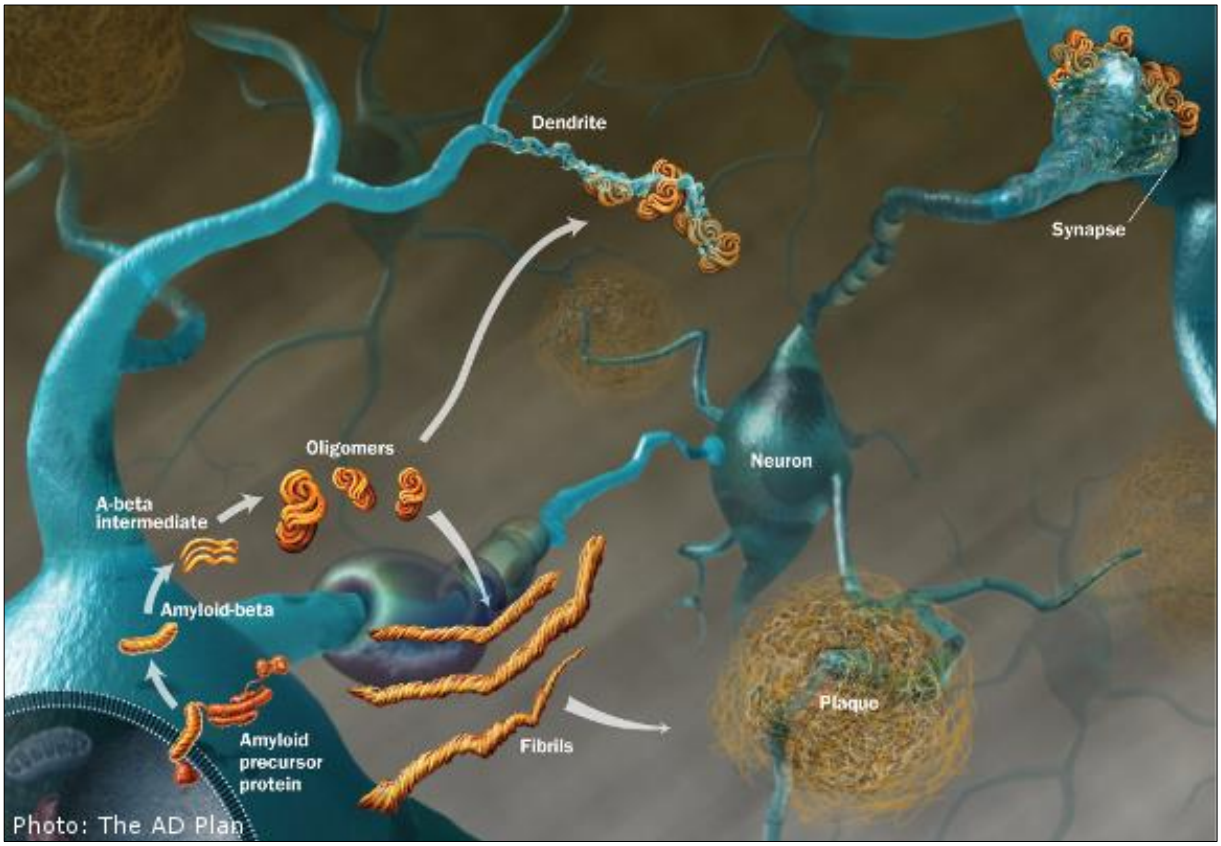

Figure 2*: The amyloidotic mechanism in AD: from the wrong cleavage of the amyloid precursor protein (APP), a soluble and neurotoxic monomer, called* Aβ-42*, is generated. The aggregation of several monomer is first inducing* Aβ*-intermediate dimer's formation that then assembled into* Aβ *oligomers. These soluble forms of the protein are the most toxic for neurons, and are thus involved in many of the neurotoxic processes in AD. Oligomers can also aggregated into a non-soluble fibrillar form that accumulate to generate amyloid plaques.*

b. Tauopathy

Among crucial mechanisms known to be responsible for cognitive deficits in AD is a progressive tauopathy, following a selective and predictable course defined by Braak stages [24](Fig. 3). An imbalance of specific kinases and phosphatases of the Tau protein in the brain is inducing its pathological phosphorylation and/or hyperphosphorylation, leading to its malfunction in AD [25–27]. The main known task of this Microtubule Associated Protein's (MAP) in healthy brain is to stabilize and assemble axonal microtubules [28], but recent advances have shown that Tau could also be produced in neurons' cell bodies, found in synapses, or transmitted to cellular structures other than synapses through a "transcellular" prion-like pathway, giving this protein multiple roles to play in healthy and pathologic cellular processes [27].

In AD, the abnormal phosphorylation of this protein is leading to a misfolded state of Tau which presents a modified molecular structure, induces the dissociation of microtubules and therefore, alterations of axonal transport leading to neurodegeneration. In later stages of AD, the misfolded Tau protein can form prefibrillar oligomers, a soluble and toxic form of Tau aggregation [29]. Tau protein are then agglomerating into insoluble paired helicoidal filaments

[30,31], which are involved in synapses dysfunction, mitochondrial loss and neuronal death [31,32]. Such filaments are then agglomerating to form NFT that are the most toxic form or Tau for neurons.

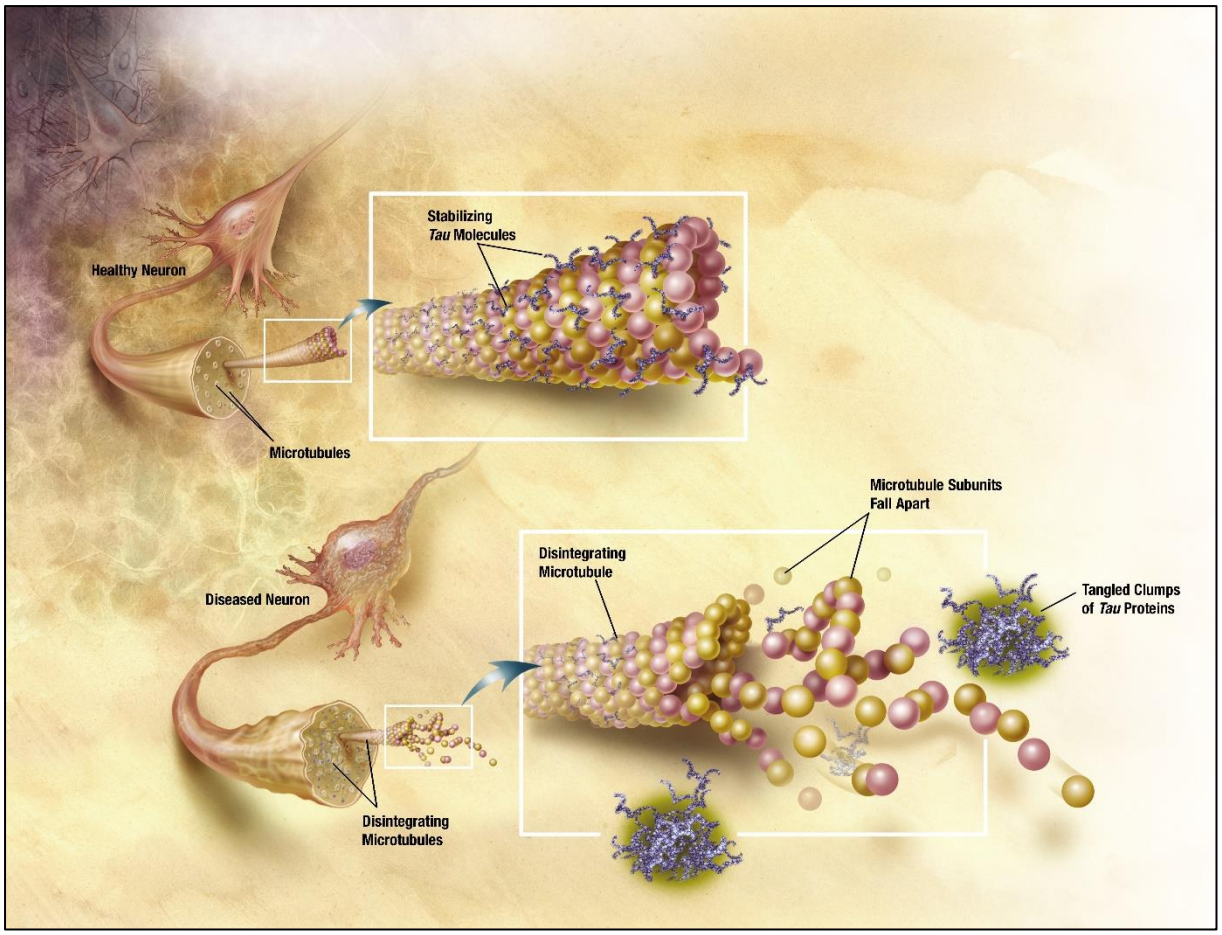

Figure 3*: The mechanism of tauopathy in AD (from the National Institute on Aging): Tau protein is a microtubule associated protein-kinase (MAP-kinase) that bind to microtubule via a microtubule-binding domain (MBD) of four repeated sequences (R1 to R4), and stabilize microtubules assembly in healthy neurons. In AD, the Tau protein is hyperphosphorylated and insoluble, and cannot support microtubule integrity anymore. Therefore, microtubules in axons are destabilized and their subunits fall apart, disturbing the axonal transport. Free hyperphosphorylated Tau proteins are then aggregating into paired helical filaments, which might be a protective mechanism sequestering toxic Tau species* [12]*. From the aggregation of those filament, cytotoxic filamentous inclusions called NFT are generated in pyramidal neurons, and impair cognition.*

c. Longitudinal evolution of amyloidopathy and tauopathy in AD patients

In AD patients, both described mechanisms are affecting the brain regions following relatively known pathway established in Braak and Braak, 1997 using a silver impregnation method on 2661 brains, as illustrated in figure 4 [33,34]. For years, the most dominant hypothesis about the progression of amyloidopathy and tauopathy in AD suggested that amyloid deposits were preceding Tau alterations such as NFT [34–36]. Toxic amyloid deposits would originate in the frontal and temporal lobes, affecting the hippocampus and the limbic system, and then spread all over the brain, from cortical to subcortical areas. Tau pathology on the other hand, would begin in the entorhinal cortex induced by toxic mechanisms from Aβ deposits, and progress to the hippocampus and limbic areas such as the amygdala, temporal and frontal cortices. Finally, both amyloidopathy and tauopathy would widespread in the neocortex, sparing the cerebellum [34]. However, this "amyloid cascade" hypothesis has been largely reconsidered in more recent years and remains debated. In fact, a "continuum" hypothesis [37] attests that the existence of a particular case of patients presenting tau pathology in the entorhinal cortex and the hippocampus with minimal, or without Aβ deposits, would reflect the possibility of a tauopathic origin of AD. Over the years, the "amyloid cascade" hypothesis have been repeatedly challenged, based on failed anti-amyloid clinical trials in Human [38,39], on literature reviewing about AD findings [40–42]or on mouse model studies showing for example a potential stronger impact of the Asp-664 site of cleavage in the APP gene than Aβ deposits [43]. Therefore, the "amyloid cascade" hypothesis as dominant as it is, still remain to be either proved, or revoked.

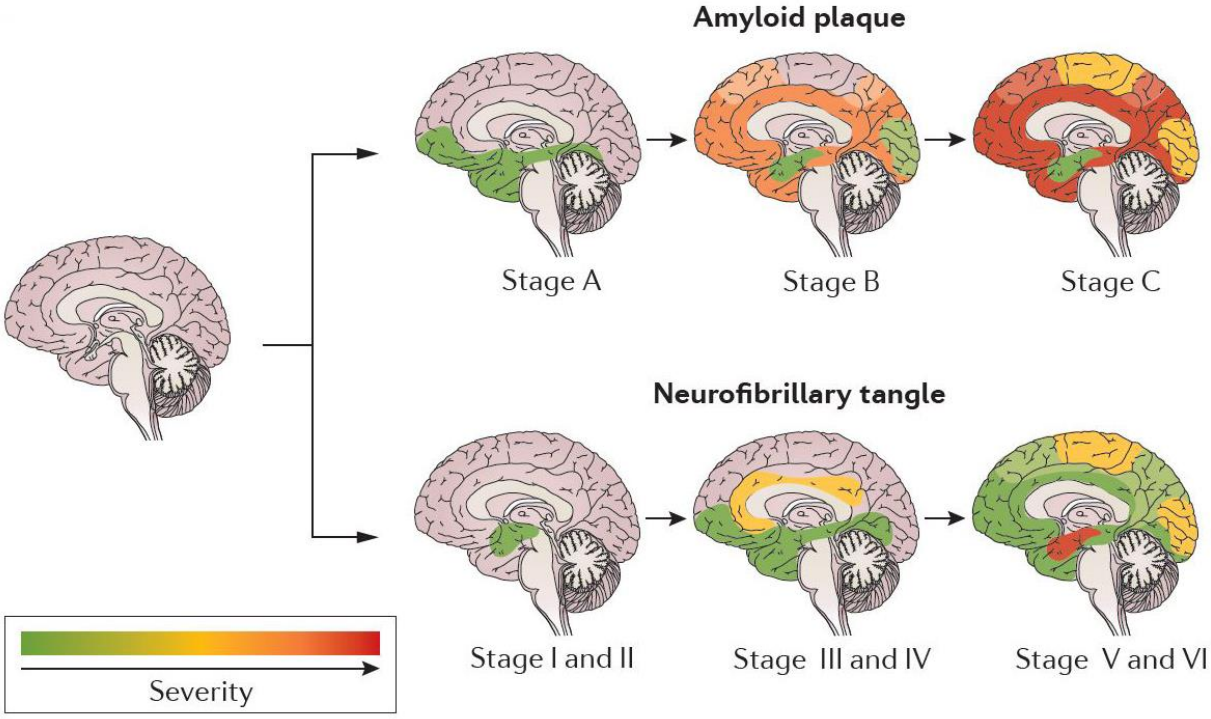

***Figure 4**: Longitudinal progression of amyloidopathy and tauopathy evaluated using a silver impregnation method on 2661 brains (figure from Masters et al., 2015* [34]*)*

d. Other mechanisms of AD

Besides amyoïdopathy and tauopathy, other noxious processes evolving from genetic to cellular level, are occurring in the brain of AD patients. In fact, vascular dysfunctions and oxidative stress in association with mitochondrial failure are all largely contributing mechanisms to AD progression [22,44]. Particularly, numerous evidences point out a strong involvement of the brain inflammation in AD (Fig. 5) [45,46], mostly supported by the discovery of the mutation in the Triggering Receptor Expressed on Myeloid Cells 2 (TREM2) gene involved in neuroinflammatory processes, as a great risk factor of the disease [47].

In healthy brain, inflammation response mainly involves the activation of microglial cells -the macrophage of the brain- inducing acute neuroinflammation reactions playing a protective role of neurons [45]. However, in AD the neuroinflammation response become chronical, leading to brain damages instead. At early stage of AD, deposits of toxic Aβ induce the activation of microglia, therefore releasing pro-inflammatory factors and toxic species such as cytokines, nitric oxide and reactive oxygen species (ROS). Despite the protective feature of this response that first help the clearance of the protein, sustained activation of microglia quickly leads to an exacerbation of AD. As a result of this chronic inflammatory response, the level of pro-inflammatory factors, neurotoxins, and cytokines release from microglia increases, contributing to neurodegeneration, increased Aβ-42 production, and exacerbation of the neuroinflammation. At the same time, efficiency of microglia decreases and Aβ-42 deposits accumulate in the brain. Among released cytokines by the microglia is the Interleukine 6 (IL-6), involved in the stimulation of the CDK kinase known to hyperphospholate Tau [46]. In response to neuroinflammation signal, reactive astrocytes are also recruited. Similarly to microglia, astrocytes would present a biphasic effect, depending on the severity of AD, and would have neuroprotective role at first, followed by a neurotoxic implication when accumulating. Thus, neuroinflammation is one of the main contributing mechanisms to accelerate core AD pathologies such as the amyoïdopathy and tauopathy.[48].

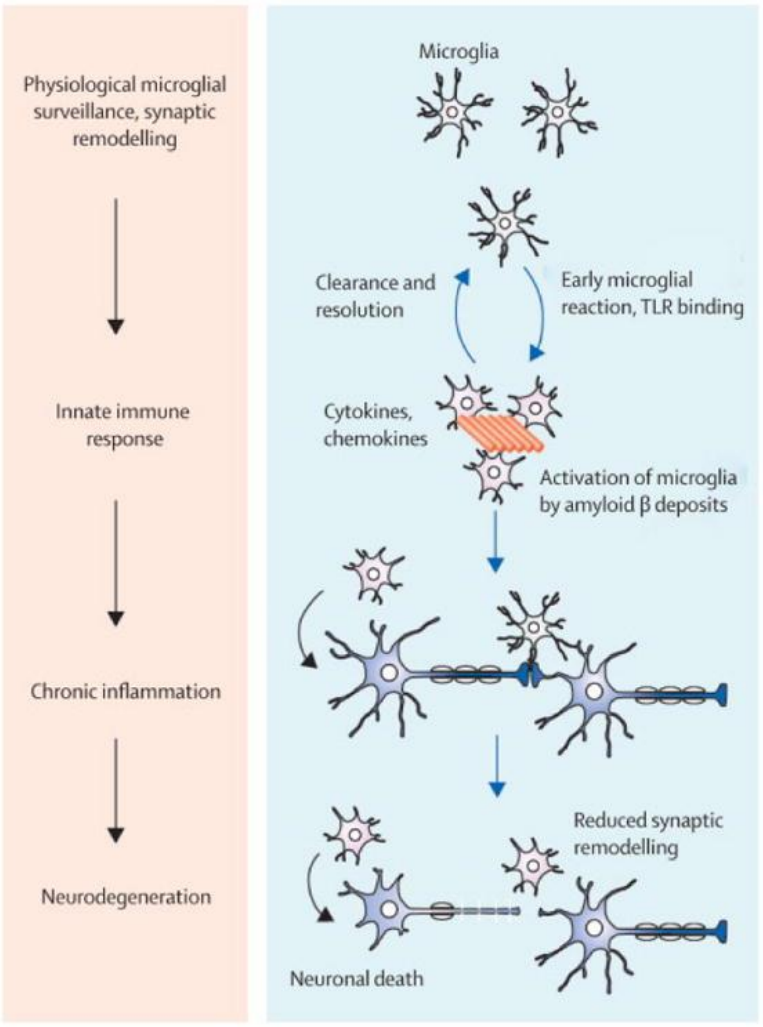

Figure 5*: The Neuroinflammation mechanism in AD (from Heneka et al., 2015* [45]*). In AD, the neuroinflammation mechanism mostly involves microglial activation by Aβ deposits, notably through toll-like receptors (TLR). The reaction starts with an acute response of inflammatory cells, with cytokines and chemokines' production from microglia, and therefore the clearance of Aβ. However, the chronic activation of microglial cells is leading to a toxic production of pro-inflammatory factors that contribute to functional and structural changes in neurons, exacerbating neurodegeneration.*

3. Clinic of Alzheimer's disease

a. Etiology of the pathology

According to their etiology, two different forms of AD are described:

1) The Sporadic form of AD represents most of AD patients. Despite that, no specific cause has been described to be responsible for its development. A combination of several factors including the environment, the lifestyle, the genetic, and aging, are responsible for this AD form. The most studied susceptibility gene related to the sporadic AD (SAD) development is the isoform 4 of the APOE gene, encoding for a lipoprotein binding amyloid proteins [49]. Other molecular factors would have an influence on the susceptibility to SAD, such as a variant of TREM2 gene -coding for a transmembrane receptor expressed in cells involved in neuroinflammation processes

[47]. Besides genetic susceptibility, environment would play a major role in the development of the disease: head injury, cardiovascular diseases, repeated anesthesia, and inactivity are as many risk factors of SAD. On the opposite, some factors are thought to prevent/delay the beginning of AD, such as a rich social life, stimulating cognitive activities or physical exercise [8].

2) The Familial form of AD referred to patient developing the disease in relation to genetic alterations inherited from a parent. These rare form of AD (1 to 2%) [8] are associated with genetic mutations in one of the three genes previously evoked: APP, PS1 or PS2. With these mutations, if a parent is diagnosed with AD, siblings and children each have 50% chance to develop the pathology as well. Patients display similar symptoms as SAD, but the disease usually starting at younger age (45 years old).

b. Diagnostic and symptoms

In AD, the diagnosis is essentially based on medical history and clinical features identified in the "*Diagnostic and Statistical Manual of mental disorders, fifth edition"*[50] (DSM V).

According to DSM V, disorders are ranked either as: (i) major neurocognitive disorders (NCD) if they display impairments in at least 2 cognitive domains along with altered *Instrumental Activities of Daily Living* (IADLs); or (ii) mild NCD if they present one or more cognitive domains impaired and intact IADLs. Concerning dementia such as AD, patients are categorized as Subjective Cognitive Impairment (SCI) or pre-clinical state if they don't present any clinical signs yet, Mild Cognitive Impairment (MCI) or pre-dementia when IADLs are intact, and finally dementia.

In this manual, dementia is defined by: memory deficits, at least one other affected cognitive domain such as executive functions or speech alterations, impaired IADLs, and the absence of confusion or psychiatric disorder. To be diagnosed with AD the evolution of the symptoms must be progressive and continuous.

In both AD forms, patients exhibit the same phenotype, presenting symptoms that can appear several years after the beginning of the disease [51]. The pathology begins to manifest with progressive episodic memory impairment, related to memories of personal experience associated with a spatio-temporal context. This type of memory is therefore combining perceptive, sensorial, emotional, and cognitive information specific to an event, and is the basis of autobiographical memories [52]. Later, other types of memory are affected, with first semantic memory that store language information (semantic, lexical) and facts about the world [53]; followed by procedural memory, which gives the capacity to automatized behavior based on learned skills [54]. However, behavioral changes in AD also include depression, anxiety, attention dysfunction, and disturbance of executive functions that develop over time [55]. Clinical symptoms can therefore overlap with features of other types of dementia [56–58] as well as with normal aging [59], reducing the specificity of diagnosis using clinical DSM criteria to 51% only, versus 85% of sensitivity. To exclude other possible etiologies, evaluation of the distribution and presence of amyloid plaques, NFT and neurodegeneration is essential.

To detect changes in those biomarkers and improve AD diagnosis, both biochemical and imaging analysis are providing great information. The analysis of cerebro-spinal fluid (CSF) through lumbar puncture is a tool to evaluate Aβ-42, total Tau and hyperphosphorylated Tau concentration [60]. A decrease of Aβ-42 concentration measured in the CSF is correlating with both clinical diagnosis of AD and histopathology of amyloid plaques at autopsy. On the opposite, an increase of Tau and hyperphosphorylated Tau concentration in the CSF is illustrating an accumulation of the protein in neurons, and correlates with the presence of NFT at autopsy [60]. To reveal Aβ deposits and neuronal injury in the brain, positrons emission tomography (PET)-imaging has been used in association with specific probes such as the Pittsburgh compound B (PiB) that specifically binds to fibrillar Aβ, or fluorodeoxyglucose uptake associated with net brain metabolism [61]. However, changes in these biomarkers' concentrations are reaching their maximum at early stages of AD, limiting their use to predict cognitive decline (Fig. 6).

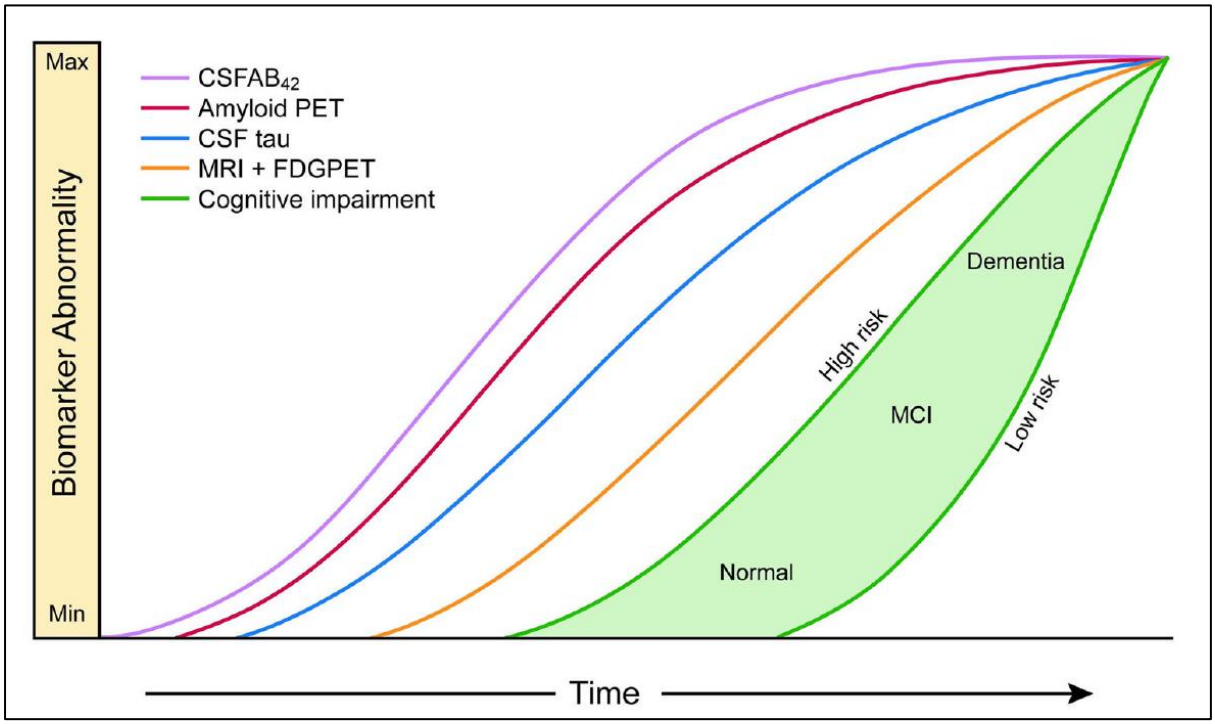

***Figure 6**: Evolution of AD biomarkers (from Jack et al., update version in 2013)*

To reveal pathological evolution in patients, Magnetic Resonance Imaging (MRI) has been mainly used to follow structural alterations such as atrophy of the brain caused by dendritic pruning and loss of synapses and neurons. Despite that brain atrophy is not specific to AD, the severity of the atrophy correlates with rates of cognitive decline, and its topographic distribution is following Braak stages of NFT in AD patient. In addition to morphological measurement, MRI is providing the unique possibility to explore non-invasively the brain communication at network levels, and to provide an overview of the whole brain hierarchical architecture.

c. Therapeutic strategies

Several strategies have been explored in an attempt to find effective treatment of AD. Despite the fact that no curative treatment has been discovered yet, medications are used to help controlling symptoms of the pathology. Currently, different drugs are used, targeting either neurotransmitters systems of the brain, either pathological proteins of the disease. One of the first damaged system in AD is the cholinergic system, whose alteration well correlates with early cognitive affection [62]. In this context, acetylcholinesterase inhibitors have been used to increase levels of acetyl-choline at synapses, and thus improving memory functions and attention deficits in AD. Three different drugs are prescribed to patients at early to moderate stages of AD: Donezepil, Rivastigmine and Galantamine. For later stages, an antagonist for NMDA glutamate receptors, the Memantine, has also been approved by the FDA (Food and Drug Administration). Its role is to reduce the excitotoxicity induced by a higher glutamate concentration, and restore homeostasis in the glutamatergic system that is perturbed at later stages of AD [62,63].

Besides these treatments, pharmaceutical industry has been trying to produce drugs directed against neurotoxic proteins of AD, especially to reduce Aβ-42 protein deposition in the brain [64]. The main used strategy is immunotherapy, by injecting anti-Aβ-42 antibodies (passive immunization) or vaccinating patients (active immunization). Another used technic is the inhibition of enzymes responsible for the production of the neurotoxic peptide. However, none of these clinical trials succeeded to pass the phase three, and other therapeutic strategies are being investigated. Alongside other amyloid-based therapies, one of the most promising approaches is triggering the development of the Tau pathology, which correlates with the evolution of cognitive deficits in AD and is one of the main mechanisms of the disease.

4. Transgenic animal models of Alzheimer's disease

From causative genes of the familial form of AD, genetically modified animals have been created, providing a significant insight into the underlying mechanism of the disease and giving the opportunity to perform preclinical evaluation of potential therapeutic interventions. Currently, no genetic model recapitulates all of the aspects of the disease spectrum. However, each model allows for in-depth analysis of one or two components of the disease, which is not readily possible or ethical with human patients or samples [65].

To create animal models of amyloidopathy, modifications of the APP gene have been largely used. The overexpression of human-APP mediates by various promoters, with or without mutations on the gene, is leading to a similar development of amyloidopathy to that found in the human brain. A constant Aβ production leads to amyloid plaques formation in mild of late adulthood in mice, displaying an age-dependent evolution of the pathology. These models allow the analysis of Aβ production and deposition, the investigation of Aβ associated neuroinflammation processes, the exploration of behavioral modifications related to Aβ, drug development and identification of CSF biomarkers [66]. Combined with other mutations such as PS1, an increases of the pathology Aβ is generated, resulting in an acceleration of Aβ deposition, behavioral impairment, and neuronal loss. A second-generation of mouse models

of amyloidopathy, based on APP knock-in strategy in which the murine Aβ sequence is humanized and FAD mutations introduced, generates an overproduction of pathogenic Aβ without overexpressing APP. Thus, this second generation of models aims at overcome drawbacks of APP overexpression paradigm such as unphysiological interactions between non-Aβ APP fragments with cellular proteins, or atypical region specificity of Aβ pathology related to promoters [66]. However, despite a strong hypothesis about the amyloid cascade that would induce pathological tau mechanisms, neither APP-overexpressing transgenic mice, neither knock-in mice exhibit NFTs. To replicate the NFT pathology, crossbreeding of Tau transgenic mice and APP transgenic mice have been created. A triple transgenic mice model (3xTg-AD) has been generated by Oddo et al., in 2003 [67] overexpressing human-APP and Tau transgene on a PS1 knock-in background, and presenting Aβ plaques and NFTs formation, gliosis, synaptic damages and memory deficits. However, these multiple genes overexpression is leading to an increased risk of artificial phenomena.

To model the tauopathy, and therefore NFTs development, mice model expressing human Tau mutations have been generated. The most commonly used models are P301L and P301S mutations models, developing NFTs, neurodegenerations and atrophy [68]. However, these models are also displaying motor deficits, that are not hallmarks of AD. These two mutations are indeed found in a specific form of the fronto-temporal dementia, called Frontotemporal dementia with parkinsonism linked to chromosome 17 (FTDP-17). This pathology shows, together with personality disturbances and a cognitive decline, some motor affectations [69–71] [72]. Other mutations involving the Tau protein have been generated, such as G272V [73], V337M [74], or R406W [75], however showing motor deficits and hind limb paralysis causing by Tau expression in the spinal cord. Expressing human Tau isoform, a non-mutant model of the hyperphosphorylated form of the protein was also generate, exhibiting an aggregation of pathological Tau and paired-helical filaments formation in a spatiotemporal distribution [76,77]. One transgenic model has been created combining G272V and P301S Human Tau mutations under the Thy1.2 promoter, called Thy-Tau22 mice [78]. Compared with other transgenic Tau models, this mice model does not present motor deficits, while showing other main AD-related affectations such as memory impairment [79], disinhibition behavior, age dependent pathological Tau deposition starting in the hippocampus, NFTs formation, neuronal death [80], and gliosis. Therefore, the Thy-Tau22 mice model represents a valuable model to explore and understand the Tau pathology, displaying the main features observed in AD.

II. Brain Wide connectome analysis with MRI

1. Principle of the MRI

The MRI technic stands on the principle of the Nuclear Magnetic Resonance (NMR). NMR is based on *the quantum property of spin*, possessed by all electron, proton and neutron. In atomic nucleus, all cited particles possess a spin of ½. To record a signal in NMR, the most widely used nuclei is the hydrogen (H_1), composed of a single proton and thus possessing a spin of ½. In literature, the word "spin" is commonly used as a general term to talk about *the quantum property of spin*, or an ensemble of spin in one voxel, or the magnetic moment of particles. In this manuscript we'll further use the same designation "spin" as a general term, to

ease our speech. To characterize the spin's interaction with a magnetic field, two mathematical perspectives known as the classical or the quantum perspective, can be applied. In MRI, both models can be used to predict the behavior of a spin, and we'll focus for our description on the classic view.

In the classical model, the proton is described as a rotating charge of an angular moment called a spin, in which circulating electric currents lead to a magnetic moment. When applying a magnetic field B0 to the system, the spin is forced into a precessing motion around the magnetic axis at a frequency depending to the gyromagnetic ratio (proper to the proton), and the magnetic field B0, known as the Larmor frequency. When a radiofrequency (RF) radiation B1, orthogonal to B0, is applied to the system, the magnetic moment of the proton will rotate toward the transverse plane depending on the strength and duration of the RF radiation, and following a flip angle α.

In one voxel, the net magnetization vector reflects an accumulation of individual's spin magnetic moment. When a magnetic field B0 is applied to the system, spins will mostly align to the state of lower energy, that is the direction of the magnetic field B0. A small part of the spin's population will align to the opposite orientation of B0, a state of higher energy, in order to reach a thermal equilibrium. This same principle applied to the macroscopic scale of several voxels, such as in organic tissue.

After the RF pulse, the transverse component of the magnetization (Mt) starts to precesses with the Larmor frequency in the transverse plan. In MRI, this change of magnetic flux is recorded using a reception coil that is inducing the corresponding voltage, which is the signal basis for MRI acquisition. Along time, the magnitude of the magnetization is decreasing with a time constant T2*, following a shape referred as Free induction decay (FID). To reverse the relaxation phase of individual spin, a 180° pulse can be applied after the excitation pulse: spins are then refocusing, which give rise to an "echo", following a T2 decay that is longer than T2*, and get rid of field inhomogeneity. At the same time, the magnetization is also relaxing in the longitudinal axis, following a characteristic time constant T1.

To create an average image the FID experiment is repeated multiple times, and several excitation pulses are run separated by a repetition time (TR). The TR determines to what extent the longitudinal magnetization can regrow and what's available for the next run. The time between the beginning of a run -a of the excitation pulse- and half TR in called echo time (TE). These two parameters are the main settings of an acquisition sequence in MRI.

In the brain, grey matter, white matter and CSF differ in content of water, macromolecules or fat. According to the chemical properties of a tissue, spins are presenting specific relaxation properties, and thus T1 and T2 relaxation constants. Depending on the TE/TR combination applied, tissue contrasts can be created in the image, highlighting a chosen feature of the tissue. To image organs, magnetic gradients can be used to create gradient echo sequences originally based on a single RF pulse of a limited angle (inferior to 90°), creating an echo using a bipolar frequency gradient instead of a 180° pulse as in spin-echo sequences, allowing a decrease of the acquisition time. To then record the signal, three gradients are applied thanks to gradient coil to select the slice, encode the frequency of spins, and encode the phase (or transverse plan) of spins, corresponding respectively to the z, x and y axis of the

tissue. The received signal from the manipulations of gradient is a matrix called K-space and is a Fourrier Transform of the underlying spatial distribution of transverse magnetization. Using an inverse Fourrier Transformation is giving a classical MRI image thanks to a spatial coding of the frequential image.

To conclude, in MRI acquisition the choice of RF pulses, TE and TR is orienting the weighted contrast of the future image, gradients are coding for the frequential plan of the image to then obtain an image, and according the combinations of all those features that are used, different properties of biologicals tissues can be revealed.

Indeed, specific adjustment of those physical parameters in a sequence of acquisition produce different type of images that can be further analyzed to reveal a property of interest. For example, the fMRI sequence is based on T2* weighted contrast and encode images used to detect functional connectivity; anatomical sequence which create T2 weighted images are providing a contrast segregation of the signal in CSF, white matter and grey matter allowing morphological analysis; diffusion weighted images reveal the diffusion property of water molecule, used as an indirect index for structural connectivity analysis. These three particular sequences are of great interest to explore the anatomical, microstructural and functional brain features, in addition with analyzing methods, will be further details.

2. Resting-state functional MRI

a. The BOLD signal

Blood oxygenation level dependent (BOLD) imaging is the standard methodology used in functional MRI (fMRI) studies. This signal was described in 1990 by Ogawa et al., [57] which performed a magnetic resonance microimaging in-vivo experiment on rat's brain under different anesthesia. They detected variations in the BOLD signal depending on physiological state of rats, correlated with changes in the blood oxygen level. This BOLD contrast MRI of brain relies on the magnetic properties of the hemoglobin (Hb), a protein whose main function is to transport oxygen (O2) in the blood. Hb can be found in two different states of conformation: oxyhemoglobin (oxy-Hb) when O2 molecules are attached to Hb, and deoxyhemoglobin (dHb) when there're not. These two conformations have different magnetic properties, in relation with their oxidation levels of the Fe complex. This results in a diamagnetic oxyhemoglobin that negligibly affects the magnetic resonance (MR) signal, while deoxyhemoglobin is paramagnetic and acts as an endogenous paramagnetic contrast agent and strongly attenuates it [81] in fMRI.

In case of a neuronal activation, the cell's demands for oxygen (O_2) and glucose, the main energy source to synthetize Adenosine Triphosphate Protein (ATP), are increasing. The increase of the metabolism mediate by ATP generation, is first leading to substrate depletion and induction of variety of signals enhancing astrocytes' function. Mitochondria are particularly involved in energy generation, and its use during ATP hydrolysis mediates a considerable heat generation. Metabolic signals from both neurons and astrocytes can modulate blood flow and substrate availability (i.e., glucose and O_2), leading to a vascular response that mediates an increase of the cerebral blood flow (CBF) to increase the substrate delivery, but

also help cool the brain and remove waste by-product [82]. This vascular response is also involving an increase of the cerebral blood volume (CBV).

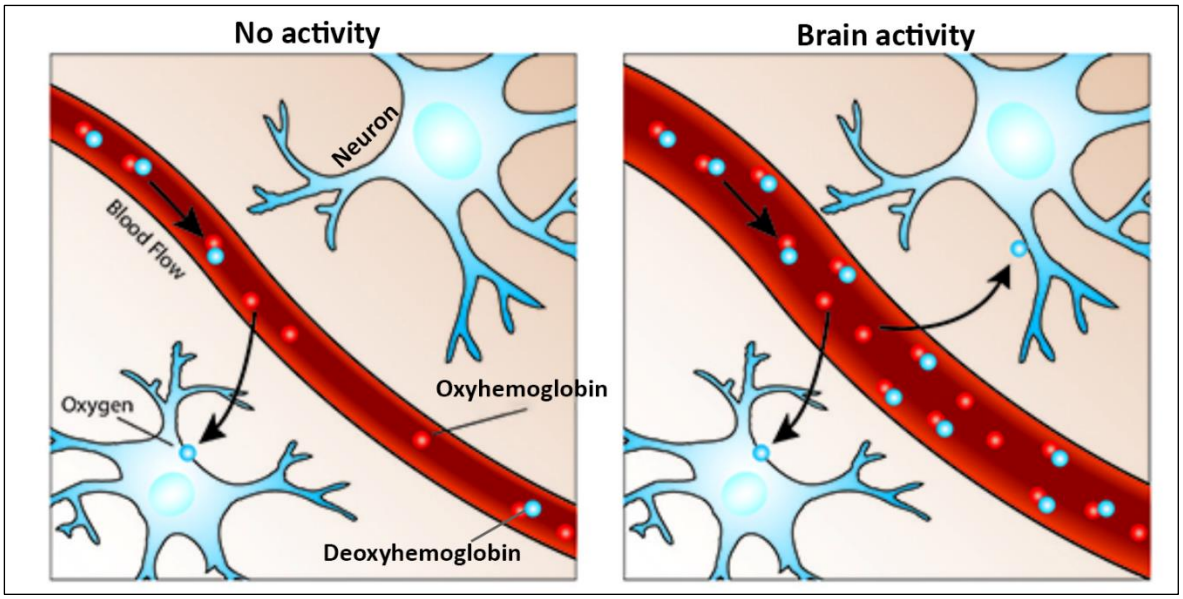

Figure 7: *The BOLD signal mechanism – adapted from fMRIB. Following a brain activity, the cerebral blood flow is increasing, leading to an increase of oxyhemoglobin and a decrease of deoxyhemoglobin.*

Therefore, in the short-term response to a brain activity, the deoxygenated blood will first decrease following the increase O_2 metabolism, to then increase synchronously to a higher CBF and CBV. Indeed, neural activity augments the CBF in excess of the O_2 consumption (CMRO2). Therefore, the rate of O_2 delivery to activate the cortex exceeds its rate of consumption, resulting in locally increased capillary-venous O_2 saturation, and, therefore, an increased ratio of oxygenated to deoxygenated hemoglobin. This mechanism is known as a neuro-vascular coupling, and forms the basis of the BOLD signal (Fig. 7). Thus, the activity-induced increase in oxy-Hb/dHb ratio augments the MR signal, constituting the BOLD response. This signal is therefore assumed to indirectly measure the neuronal activity via the neurovascular coupling (Fig. 8).

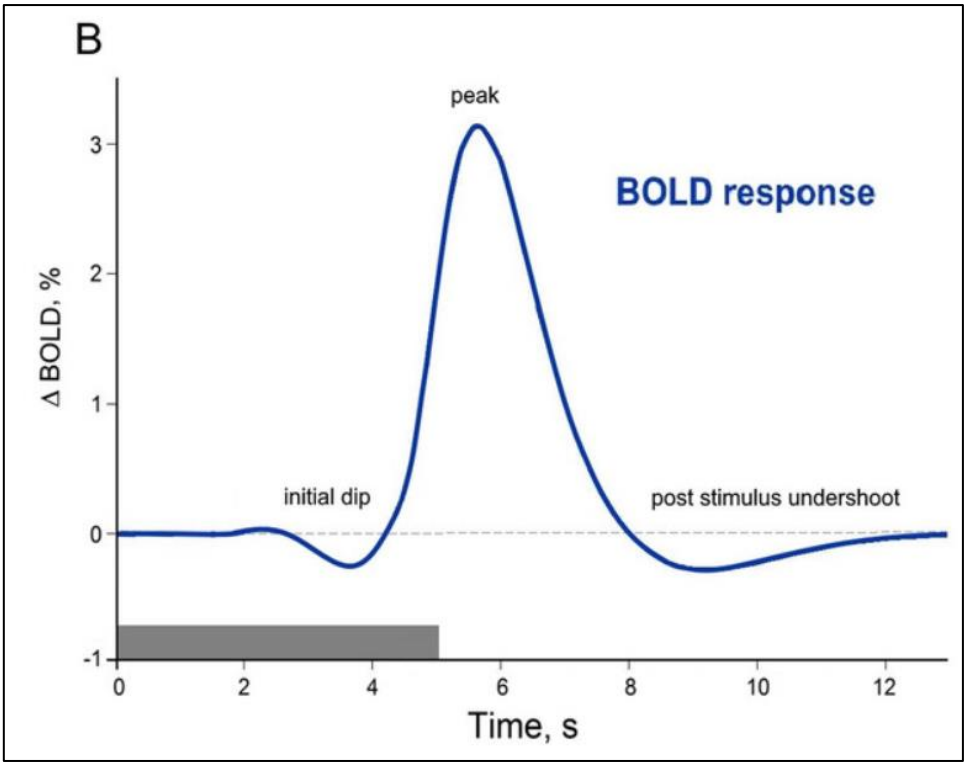

Figure 8: *The Hemodynamic Response Function (HRF) from Cinciute 2019* [83]. *Following a brief stimulus, the typical hemodynamic response demonstrates a small negative initial dip, that is more commonly observed at very high field (from 7.0T). This decrease of the BOLD signal would come from either a) the early extraction of blood O_2, or b) the increase of the CBV. Following the initial dip, the positive dominant peak reflects the phase of the increased of CBF out of proportion to immediate metabolic needs. A post-stimulus undershoot is then observed. Despite its debated mechanism, the most popular theory is that it would be the result from a slow recovery of the arterial blood volume.*

In fMRI, gradient echo T2* weighted sequences are used to detect this effect. Usually, a single excitation pulse is used to obtain a T2* contrast image. An echo train of the signal is obtained by applying a bipolar gradient of frequency: a prior dephasing gradient is first accelerating the dephasing of the FID, followed by a reversed process using the same strength but in opposite polarity to rephase the spins and generate an echo. This gradient is allowing a simultaneous acquisition of the signal and its frequency encoding. Variations of the BOLD signal are measured by acquiring several volumes of the brain during the same imaging session, allowing the extraction of the time-course (TC) of the BOLD signal in all voxels of the brains, along the acquisition. BOLD fMRI studies require rapid acquisition of multiple brain slices through the whole brain at high temporal resolution. Echo-planar imaging (EPI) is by far the most widely used imaging technique to achieve these goals. Since the nuclear magnetization and BOLD contrast increase with magnetic field strength, high magnetic field is advantageous. In addition, multichannel head coils (e.g., 32 channels) and parallel imaging are valuable to increase acquisition speed and signal-to-noise ratio. These techniques can acquire whole-brain volumes every 2–3 seconds with a typical voxel size of $3mm^3$ in the human brain. Comparing to other functional measurement such as electro-encephalography (EEG) or magneto-encephalography (MEG), which detect more direct information, fMRI is providing the best three-dimensional spatial resolution covering the entire brain.

To image the rodent brain's activity, optimized protocols of the imaging set-up have been created, mostly to overcome the low signal-to-noise ratio (SNR) in small tissue imaging. Most rodent imaging has been performed in rats, related to the difficulty to acquire reproducible brain activation upon stimulation in mice. However, since the introduction of cryo-coils [84] that significantly enhanced the sensitivity in small animal fMRI, more studies have been conducted on mice. These coils are based on the principle that for small volumes of tissue, both sample noise and thermal noise are of comparable magnitude. Therefore, considerable noise reduction can be achieved by reducing the temperature of the receiver system using cold helium gas. In order to improve the SNR and enabling a higher spatial resolution that is needed in rodents' acquisition, higher field MRI are used for rodent imaging than in human MRI. Small animal MRI systems usually operate from 4.7 to 11.4 Tesla, whereas human acquisition in clinic are performed using 1.5 to 3T MRI system. Using a higher magnetic field is clearly increasing the SNR for rodent's imaging, however it also leads to more prominent artifacts [85]. One of the main limitations imaging the head at higher field, is the increase of susceptibility artifacts. Indeed, related to the different physico-chemical properties of the multiple compartments in the head, artifacts can be generated due to susceptibility and different relaxation properties at a higher field strength, leading to distortions of the image [86].

In addition, fMRI studies in rodents require the use of anesthesia, in order to reduce the stress of the animal, and prevent motion artifacts during the acquisition. However, these anesthetic agents are affecting the neuronal response and the hemodynamic response of the brain [87]. Therefore, a highly optimized anesthesia protocol has to be applied in the same manner to each animal included in a study. The most commonly used agents are the medetomidine -resulting in sedation rather than deep anesthesia-, isoflurane, or a combination of the two, which have proved to sustain a robust and reproducible BOLD response in mice [87,88]. In both rats and mice, protocols have been established in order to reduce the stress of the animal during the acquisition, allowing awake procedure [89,90]. However, depending on how well the animal have been acclimatized to the MRI, its brain functional states may be different, and more likely related to stress, which increases variability in the fMRI analysis of brain networks.

b. From BOLD signal to the concept of functional connectivity

In fMRI, recording of the BOLD signal is based on the brain neuro-vascular response following a task. However, Biswal et al., in 1995 [91] showed a significant temporal correlation of the BOLD signal between brain areas in subjects at rest. These correlations came from spontaneous fluctuations of the fMRI signal at rest, in a range of frequency between 0.01 and 0.1 Hz, or 0.2Hz. Five years later in 2001, Raichle et al., [92] proved for the first-time using PET-scan imaging, that most of the brain's energy consumption occurred at rest, describing the baseline state of brain areas called Default Mode Network (DMN). From those findings emerged the concept of resting-state functional MRI (rsfMRI), which investigates the brain functional organization at rest. RsfMRI infers functional connectivity as the statistical dependency between low frequency fluctuations of the BOLD fMRI signal acquired at rest from distinct brain regions. The synchrony between these low frequency BOLD signal

fluctuations is associated with functional brain communication [93], which was for a long time assumed to have stationary nature.

Therefore, when talking about static functional connectivity, one refers to the correlations between TCs of BOLD signal from distinct brain areas, without including the potential temporal changes along the acquisition. This connection is considered stronger the higher the statistical correlation is, for both positive and negative correlations.

However, in recent years the dynamic behavior of functional connectivity was revealed, showing that on top of correlational patterns of spontaneous fMRI signal fluctuations, connectivity between different brain regions exhibits meaningful variations within a typical resting-state fMRI experiment. As a consequence, a considerable amount of studies has been directed to assessing dynamic functional connectivity (DFC) patterns, and several different approaches were explored to identify relevant functional connectivity fluctuations

We will further describe the main approaches used for mapping the static and dynamic functional connectivity in human and animal models.

c. Approaches for mapping functional brain networks

Seed-based analysis

To study the static functional connectivity, one straight forward method [94] called the "seed-based analysis" is largely used (Fig. 9). This technic relies on the extraction of the mean TC of the BOLD rsfMRI signal from a brain region of interest (ROI), or a seed, chosen on the basis of *a priori* knowledge. The correlation of TC with all other voxels' TCs of the image is then statistically assessed using a voxel-wise analysis. This analysis leads to the creation of a functional connectivity map of a specific brain region, known as its functional network. Another possibility is to evaluate the correlation of the mean TC of the BOLD rsfMRI signal between several brain areas, gathered as a group of voxels based on an atlas parcellation. From there, connectivity matrices can be created, evaluating the functional correlations between several selected brain regions. The main drawback of this method is the restriction based on the selection of ROIs, limiting the whole-brain connectivity analysis.

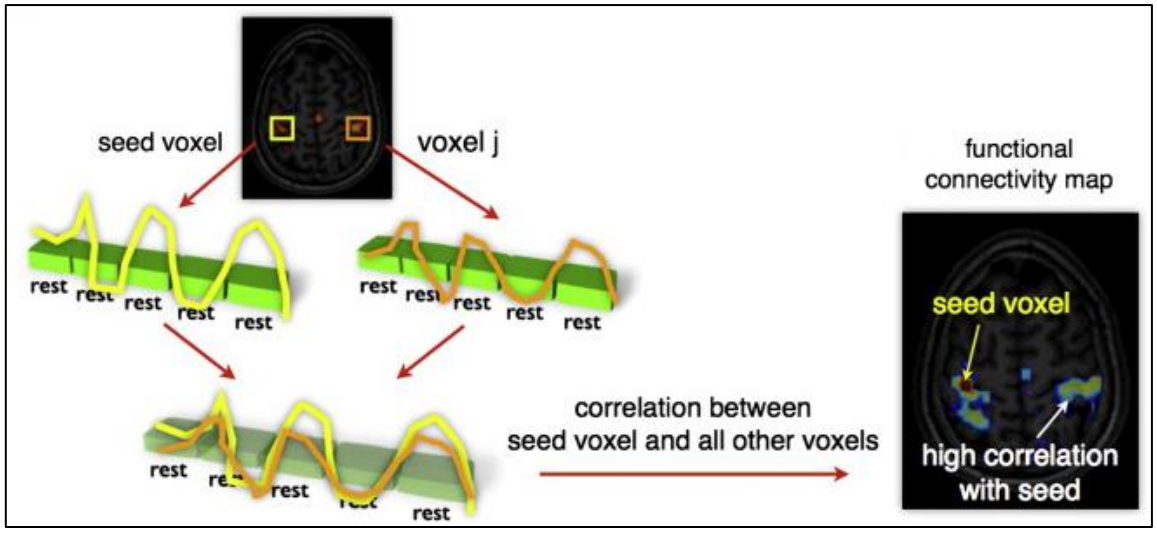

Figure 9: *Resting-state functional analysis using the seed-based approach (from Van den Heuvel and Hulshoff Pol, 2010* [95]*)*

Independent component analysis

To overcome the *a priori* selection of brain areas for the analysis, one widely used model-free method is the independent component analysis (ICA) [95–98]. This approach uses a blind-source separation algorithm, which assumes that the brain is organized into spatially or temporally separated, independent, sources of signal, called components. Using appropriate tools extracting TCs of each component, correlations analysis between pairs of components can be performed. Therefore, ICA is allowing to examin whole-brain level networks of functional analysis. This technic however needs an estimation beforehand of the number of components, leading to a potential artefactual separation or gathering of functional networks depending on the chosen number.

Dictionary learning

Similarly to ICA the dictionary learning method is aiming at decompose the signal of the brain to reconstruct functional networks [99,100]. However, instead of the assumption of an independence of the components -or atoms in this case- the dictionary learning technic is based on a sparsity hypothesis, which would be more in line with the sparseness of neuronal activity property. The algorithm aims to learn an over-completed dictionary, or sources, corresponding to the decomposed fMRI signal in a dense matrix, to then sparsely separate the sources. As exposed previously with ICA, dictionary learning needs a prior estimation of the number of atoms, which could mediate segmentation differences for two similar atoms.

Modelling functional connectivity with graph theory

The graph theory analysis can be applied to model functional connectivity analysis to reconstruct large-scale brain networks and characterize local functional regions. With this technic, brain areas extracted either from an atlas parcellation, either from a model-free analysis such as ICA or dictionary learning, are defined as nodes. Features such as strength of the functional connectivity, define by the sum of weighted correlation coefficients for one node, or the degree representing the number or functional connections of a node. More detailed description of the graph theory modelling will be explained later in this manuscript.

Characterizing the dynamic functional connectivity

Using dynamic functional connectivity analysis is providing information about the spatiotemporal organization of spontaneous brain activity during the rsfMRI acquistion. Temporal fluctuations in functional connectivity are thought to reflect dynamic changes in brain organization and non-stationary switching of discrete brain states.

In order to explore the evolution of correlations between TCs along the acquisition time, algorithms where calculating DFC between ROIs were created. There is currently no consensus about the methodology to use to extract this information; however, one strategy has been most commonly used based on a sliding-windows approach. As reported in Preti et al., 2017, [101] this approach evaluates the connectivity between brain regions from the correlation between pairs of BOLD TCs over a temporal interval, called a temporal window. This computation is then repeated by shifting the window by a specific step every time, to cover the whole acquisition time, and create a connectivity TC corresponding to the DFC between two ROIs. To characterize the DFC of a group of selected ROIs, this procedure is performed for all pairs of ROIs, and connectivity matrix per time windows are generated. From the matrix, all possible brain states of DFC can be extracted, representing patterns of connectivity that repetitively occur during the resting-state acquisition. Applied to brain disorders, dynamic functional connectivity alterations have been proposed to reflect inner dynamic nature of functional connectivity dysfunctions. Studies in Human already used dynamic functional connectivity to discriminate schizophrenia from healthy subjects based on the dynamic occurrence and connectivity strength of DFC states [102,103]. Grandjean et al., in 2017 [104] explored the dynamic functional connectivity in anesthetized mice using a sliding windows correlation approach, and identified several states of dynamic connectivity, which fluctuated depending on the depth of the anesthesia and the stress.

Therefore, static and dynamic analysis of functional connectivity are providing complementary information about interactions of brain areas, allowing the mapping of the whole-brain functional organization.

d. Organization of intrinsic functional architecture in human brain

Since the seminal discovery that brain regions can be synchronized in activity despite the absence of any task or stimulus [105], a rich and complex mapping of resting state networks (RSNs) has emerged, inferred from coherent fluctuations in sets of distributed brain regions [106–108]. Using several methods and variety of MRI acquisition protocols, a large overlap of the results allowed the description of robust functional resting-state networks in the brain (Fig. 10) [91,106–109].

The Default Mode Network (DMN) is the most explored network in resting-state studies. Originally from Raichle's description, the DMN referred as the functional communication of the ventral and dorsal prefrontal cortex, the posterior cingulate cortex, the precuneus, and the lateral/posterior cortex [110]. Other brain areas are sometimes attached to this network such as the thalamus, the entorhinal cortex and the hippocampal formation [111]. This network is particularly active at rest, showing lower level of activity during a task. The main hypothesis about its function is that it would underly the wandering mind, involving specific domains of

cognition including social cognition, semantic and episodic memory, and future planning [112]. Several studies have linked affectations of the DMN with brain diseases, such as depression [113], schizophrenia [114] or AD [115].

The salience network is strongly related to affective arousal and memory consolidation. It is defined by the resting-state functional connectivity between the insula and the dorsal anterior cingulate area. It's function aim at guide behavior through the segregation of the most relevant stimuli among internal and extrapersonal information [116]. The communication between the insula and the dorsal cingulate area can be divided in two submodules. The ventral salience network including the ventral insula, predicts subjective ratings or arousal and would sustain the affective functions of the salience network. Defined by the dorsal insula, the module of the dorsal salience network predicts executive function, and mediate attentional function of the network [117]. In AD, a neuropsychiatric symptoms have been associated to dysfunction of the salience network [118], and the disruption of communication between the dorsal part of this module and other networks would drive neuronal changes associate with cognitive impairment in early AD [119].

The executive control network (ECN), typically shows an increased activity during tasks, but can still be detected during rest. This module is critical for actively maintaining and manipulating information in working memory, for the judgement and decision-making for goal-directed behavior, and drives in part emotions [120–122]. It involved cortical areas including superior and middle prefrontal cortices, anterior cingulate and paracingulate gyri, and ventrolateral prefrontal cortex; in addition to the thalamus [106]. Perturbation of communication in this network have been associated with brain disorders, including AD [123,124]

The sensory-motor network (SMN) includes synchronous functional activation of the precentral and postcentral gyri [106]. It's the first functional network described by Biswal et al., in 1995 [91]. They showed that this network is particularly activated during a motor task such as finger tapping, and would therefore be involved in performance and coordination during this type of tasks. As for previously described modules, the SMN connectivity was found altered in brain pathology, particularly involving motor neurons as in amyotrophic lateral sclerosis [125]. In AD, several studies highlighted an increase of the sensory functional connectivity at early stages of the disease [126,127].

The basal ganglia network (BGN) was originally described by Albin et al., in 1989 [128], suggesting that the dorsal striatum – or caudate-putamen nucleus - would be a main node of this circuit. In addition to this area, the subthalamic nucleus, the substantia nigra and the pallidum are all involved in the BGN [129]. This network particularly detected at rest [130] would correspond to the motor control circuit, and have been associated with Parkinson's disease especially [131,132]. In AD, a group detected specific pattern of alterations for intergration and segregation in several network using graph theory applied analysis, including the BGN [133].

We listed here some of the main functional networks found in the Human brain at rest. However, it is important to note that numerous other networks have been described in Human,

such as the dorsal attention network, the visual network or the auditory network (Fig. 10) particularly activated during task.

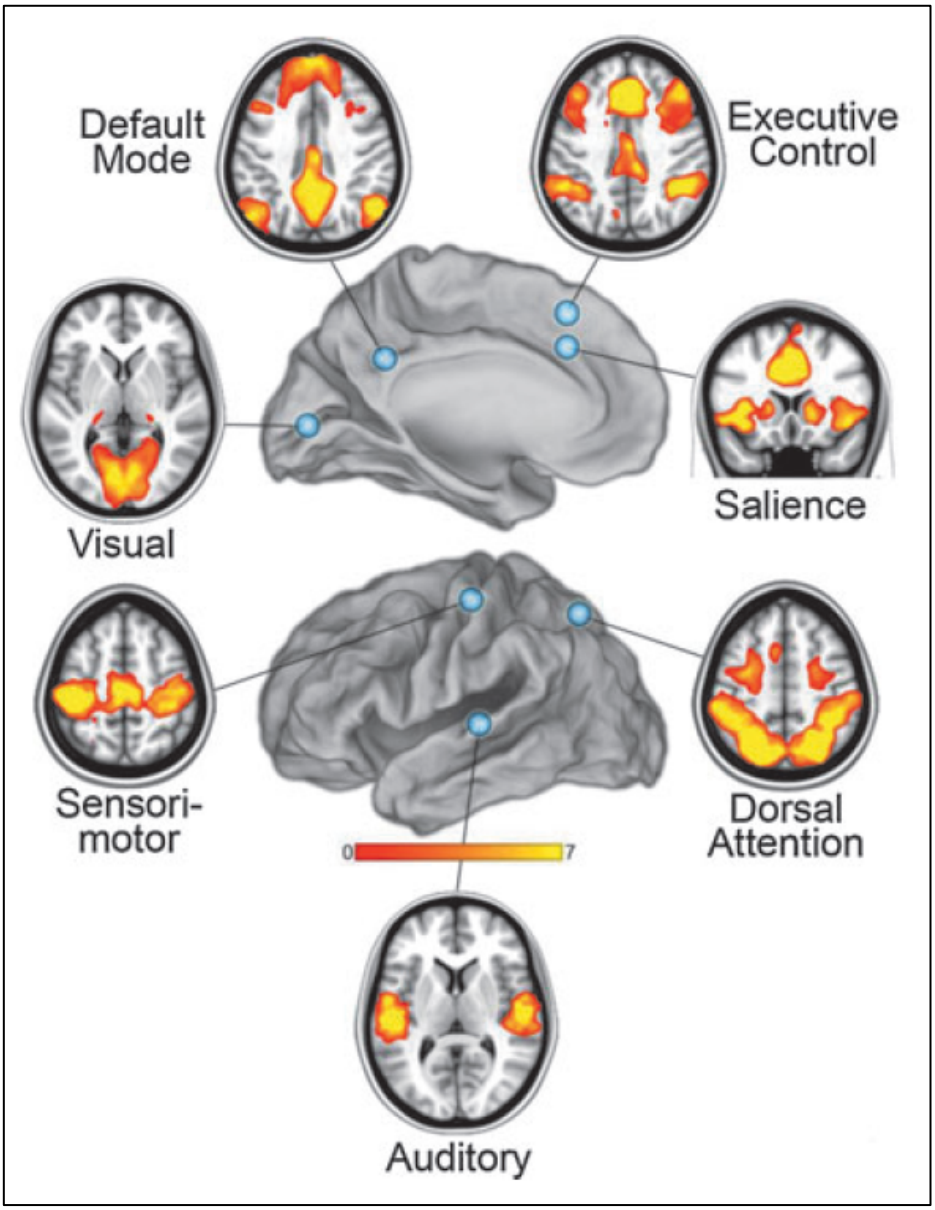

Figure 10: *Relevant functional networks in the Human brain, from Raichle et al., 2011*[110]

e. Rodent brain functional networks

Human MR based connectomics studies demonstrate now that such network topology metrics are able to localize brain pathology, track patterns of disease spread and even generate hypotheses about underlying pathophysiological mechanisms and clinically useful predictions concerning key prognostic indicators [134]. Translation of these approaches into the animal imaging field provides further invaluable opportunity to test and validate these pathophysiological mechanisms by pairing the network analysis with behavioral, genetic, molecular and histological studies. It can reveal the complex interplay between structure and function in the mammalian brain and can identify specific therapeutic targets. Such multi-approach strategies in the mouse, the most used model organism in fundamental neuroscience, may provide a unique window to bridge the gap between pre-clinical and clinical

investigations, by direct comparison of whole brain networks reconfigurations in response to pathological conditions and/or therapeutic manipulations.

To this end, several groups worked towards extracting reproductible functional network in mice [135–137]. Comparatively analyzing rats and mice functional connectivity using ICA and different numbers of components (15 or 40), relevant functional networks were highlighted [136]: separate sensorimotor, visual and auditory networks were described, comparable to Human. Focusing on the DMN in mice, Stafford et al., in 2014 [138] showing a correspondence in both functional and structural connectivity analysis. They described overlapping regions to the Human DMN, such as the cingulate cortex, the orbitofrontal cortex and parietal cortices, both structurally and functionally connected. Different from primate studies, but consistent with rat, the primary visual and somatosensory cortices were also found is the mouse DMN the group described [138].

Potential homologues salience network and DMN were found comparing BOLD and CBV analysis using ICA and seed-based approaches in mice (Fig. 11) [137]. Moreover, a resembling ECN was found anti-correlated to the mice DMN, and a somatosensory network (Fig. 11) was highlighted, driving the possibility of such network existence in mice as well. Strong inter-hemispheric correlations of functional signals were also found in somatosensory, visual, and motor cortices, in addition to subcortical thalamic, hippocampal and striatal areas [139].

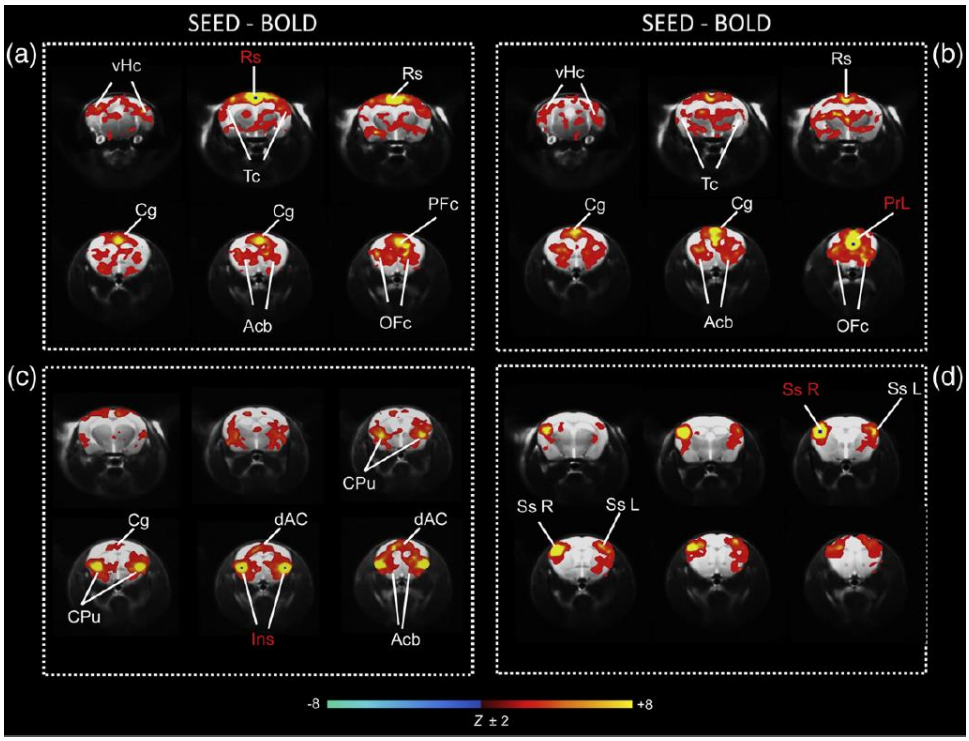

Figure 11: *Seed-based networks from Sforazzini et al., 2014* [137]. *a) DMN-like network using the retrosplenial cortex (Rs) as a seed and b) using the prelimbic area (PrL). c) Seed-based functional connectivity of the bilateral insula (Ins) seed, showing a resembling salience network. d) Somatosensory network highlighted using seed-based analysis of the right somatosensory (Ss R) area.*

More recently in 2015, Zerbi et al., [135] described a methodology to extract relevant networks in mice, including a DMN-like circuits. They used a hierarchical clustering method to further enhanc the relevance of 23 functional networks, and how they are related (Fig. 12).

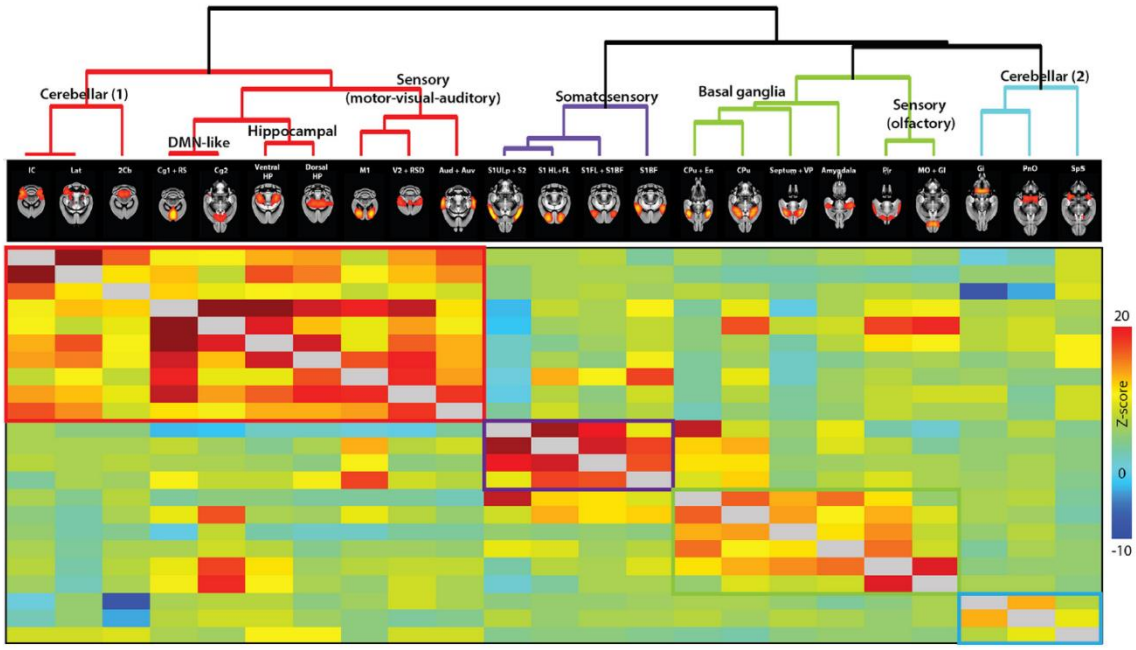

Figure 12: *Hierarchical clustering methods illustrating the closest relations between 23 bilateral component from Zerbi et al., 2015* [135]

The consistency of those functional network across studies and species is not without difficulties. For example, regions included in the DMN are not completely similar depending on the methodological approach used. While Stafford et al., [138] detected a DMN gathering the cingulate, orbital, parietal, in addition with visual and somatosensory components; Sforazzini et al.,[137] included also the nucleus accumbens in the DMN they found. However, Gozzi and Schwarz reviewed in 2016 [140] the progresses in the study of functional connectivity in rodents, and showed the enormous potential to the application of functional connectivity mapping in transgenic models of neuropathological disease, as a tool to explore underpinnings of the mesoscale communications alterations in Human (Fig. 13).

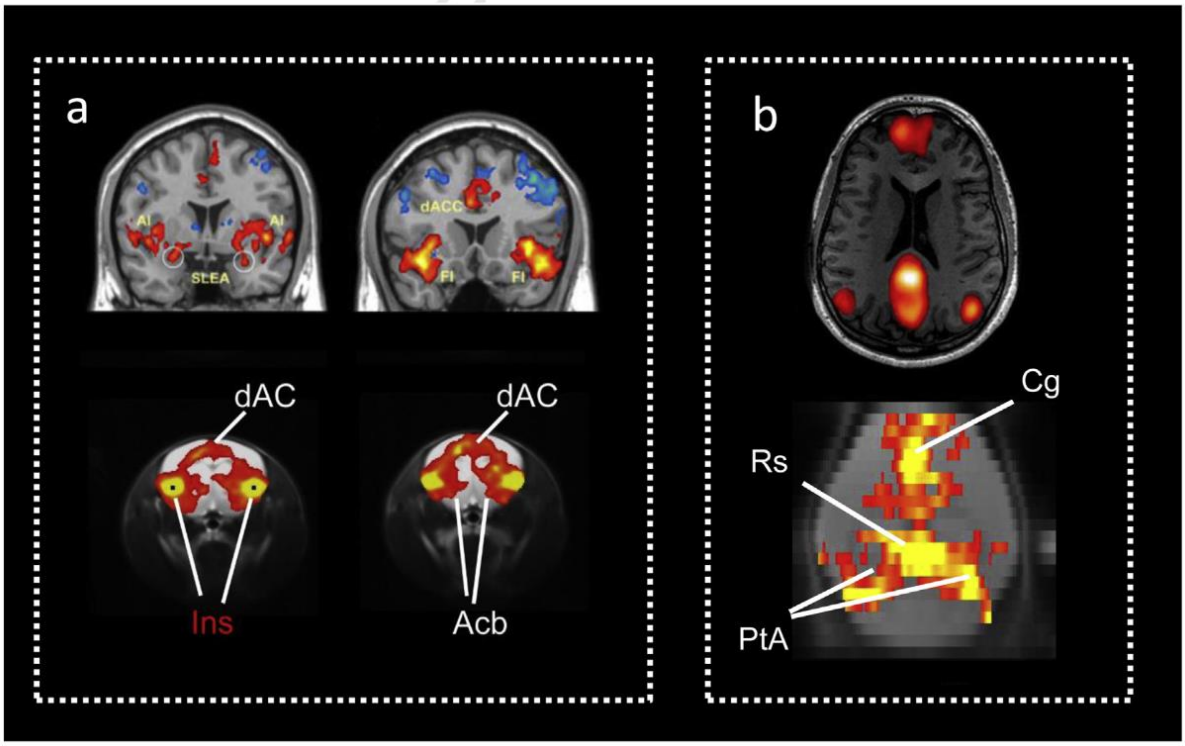

Figure 13: *Comparison of two key functional networks between Human and rodents (Gozzi and Schwarz., 2016* [140]*). a) The salience network. B) The DMN.*

3. Structural MRI: from anatomy to structural connectivity mapping

a. Brain morphometry measures

To assess morphological changes in the brain with MRI, voxel-based morphometry (VBM) have been highlighted as the gold standard methods [141,142]. Such approaches are essential in studies of neurodegenerative diseases where progressive neuronal loss and atrophy are part of the definition of the pathology [143]. The analysis of volume changes is based on voxel-wise deformation fields maps calculated from the spatial transformations applied on every voxel of one image (T2 weighted image for example), to best fit a template image known as the spatial normalization process. In other words, the deformation field is describing how local structures were adjusted to match two brains to each other [144], which illustrates enlargement or compression of brain areas. Jacobian determinants derived from these deformation fields are then used to perform deformation-based morphometry and therefore reveal morphological changes from one brain to another. In addition, Jacobians determinants can be used to correct artefactual volume changes resulting from the normalization, by modulating the difference between the true volume and apparent volume [144]. Using high magnetic field, which provides an excellent spatial resolution, is allowing a high quality of differentiation of brain tissues and therefore, finer grained morphological analysis of surface contour with VBM [145]. To explore neurodegenerative disease such as AD in animal models, VBM have been largely used, in ex-vivo [146,147] and in-vivo MRI studies [148–150], to detect anatomical changes of the brain.

To explore structural modifications in neurodegenerative brains, in addition to anatomical measurement of surface contour changes, evaluation of the microstructural

architecture of fiber connectivity and integrity can be detected using specific MRI sequences and analysis processes.

b. Diffusion tensor imaging and fiber tracking

The driving force of diffusion-based MRI is to monitor microscopic, random walk of water molecules as a probe of tissue microstructure and therefore inferring - in the brain - structural connectivity pathways and fine architecture of the neural tissue via tractography algorithms [151,152]. Diffusion is a three-dimensional process, and water molecular mobility in cerebral tissues is not the same in all directions. Limitations are imposed by water molecules environment. As described by Denis Le Bihan in 2003 [151], water molecules are moving distances of 10µm on average in the brain for 50ms diffusion times. During their displacement, these molecules can bounce off, cross or interact with many tissue components, such as cell membranes, fibers or macromolecules. Statistically evaluating the motion of water molecules is providing unique clues to the structural features and the geometric organization of neural tissues, and allows the detection of specific changes of these features in the diseased brain. The investigation of differences of motion according to the cellular organization is therefore providing an indirect measure of the microscopic architecture [153]. The use of MRI to create contrast based on the Brownian water motion characteristics within biological tissue has been first described by Denis Le Bihan in 1995 [154].

To obtain an MRI signal sensitive to diffusion, a pair of magnetic field gradient pulses are use defined by their duration time and separation tie. The first pulse aimed at detecting the spatial location of hydrogen nuclei carried by water, and magnetically labels them. Depending on the chosen separation time -or diffusion time- a second pulse is applied slightly later to detect changes in the nuclei's location along the gradient direction, leading to a change in the magnetic field, reflecting the displacement of the water molecules. When looking at a large-scale population of diffusion water molecules, various magnetic field changes will reflect the statistical displacement distribution of this population. The MRI signal resulting from the diffusion of the population of water molecules is lower than the signal from a perfectly homogeneous magnetic field, and its amplitude is directly linked to the displacement distribution and speed of water molecules. The b-factor is defined by the amplitude, timing, and spacing of the applied magnetic field gradients. Therefore, depending on its values, different degrees of diffusion weighted images can be obtained, from the attenuation of the signal. In ventricles, the diffusion of water is fast and induce a fast decrease of the signal when the b-factor is increased. On the opposite, the signal in tissues with low diffusion such as grey and white matter, decays more slowly using the same b-value [151,155].

To provide a strong diffusion weighting contrast there is a need to use hardware that can provide stable gradients of the utmost intensity. This requirement can be best satisfied with small-bore MRI scanners that are dedicated to small animals (delivering gradient intensities of up to 1,000 mT/m). In terms of sequences, the diffusion tensor EPI technique is the method of choice for in vivo diffusion imaging, but as for EPI technique fMRI the sequence is susceptible to certain artefacts. Magnetic interfaces between bone or air-filled cavities (sinuses) and water-containing tissues might result in local image distortion or signal dropout. To overcome this

localized shimming procedures are applied to increase the field homogeneity in areas of interest.

To have an optimal characterization of the complex brain fibers architecture the acquisition schemes should include a minimum of 6 non-collinear gradient diffusion directions, allowing the application of tensor formalism in analyzing the data [156,157]. Its use became apparent in the description of the white matter anisotropy. This anisotropy originates roughly from the specific organization of this tissue as bundles of more or less myelinated axonal fibers running in parallel. Diffusion in the direction of the fibers (whatever the species or the fiber type) is about three to six times faster than in the perpendicular direction. To quantify this anisotropy, the model of an ellipsoid calculated as a tensor can be used, which is a 3 x 3 symmetric matrix that features three-dimensional water displacements [158]. As said previously, the calculation of the 3D diffusion tensor requires at least 6 diffusion gradient directions, but can be multiplied to improve the quality of the tensor construction.

DTI derived parametric maps for quantitative analysis of microstructural features

Parametric maps can be extracted from the tensor, depending on the three principals axes of the model: the extraction of the main diffusion axis in a voxel is giving information about the longitudinal diffusivity called Axial Diffusivity (λ_1, Adif); information about the perpendicular axis to the longitudinal diffusion is giving Radial Diffusivity ((λ_{2+} λ_3)/2, RD) maps; and Mean diffusivity ($\lambda_1 + \lambda_2 + \lambda_3$)/3 , MD) is extracted from the measure of rotationally invariant diffusion in a voxel. Finally, one of the most used parameters is fractional anisotropy (FA), which correspond to a normalized measure of the direction of the diffusion [159] (Fig. 14). This last parameter is calculated from all three eigenvalues ($\lambda_1 + \lambda_2 + \lambda_3$) representing the lengths of the three principal axes if the tensor:

$$FA = \sqrt{\frac{3}{2}\frac{(\lambda_1 - \langle\lambda\rangle)^2 + (\lambda_2 - \langle\lambda\rangle)^2 + (\lambda_3 - \langle\lambda\rangle)^2}{\lambda_1^2 + \lambda_2^2 + \lambda_3^2}}$$

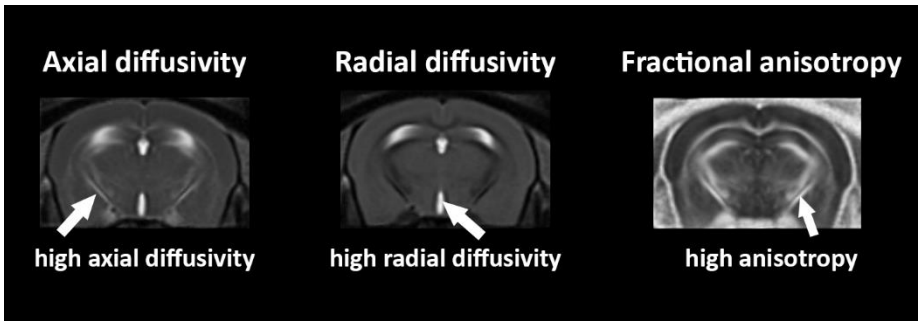

Figure 14: *Parametric maps extracted from the tensor of a mouse brain*

Fiber Tractography

Based on the anisotropy of water diffusion, and using tractography algorithms, the intervoxel connectivity can be calculated [160]. Propagation techniques to follow the estimates of main diffusion direction can be applied on diffusion tensor data to generate "streamlines", hypothesized to correspond to the fiber trajectories. Such methods allowed the reconstruction of some of the major white matter bundles of the living human brain for the first time, and triggered tremendous hopes and expectations [161]. Yet, the model is "imperfect" [162,163] as it can only characterize one fiber compartment per voxel – a problem in regions of "crossing / kissing /fanning" fibers. Indeed, propagation methods can only operate when anisotropy is high and therefore, in practice, the tractography is based on the use of anisotropy thresholds (typically 0.2) and terminate a pathway when anisotropy drops below this level. Moreover, such methods are generally using starting point, a "seed" from which the tracts are inferred independently in successive steps, either deterministically or probabilistically [160,164]. The procedure can induce the accumulation of small errors in path estimation over the large number of steps and lead to major errors in the final result.

Consequently, several alternatives have been proposed to overcome this limitation. Most of them are based on high angular resolution diffusion imaging (HARDI) [165], which uses acquisitions based on several tens to a few hundreds of different diffusion gradient directions, allowing for a more complete description of the water diffusion displacements at voxel level. Such approaches can resolve multiple fiber orientations within a voxel and provide insights into orientation structure a high angular resolution. To this type of data, global tractography approaches can further be applied. This method is reconstructing all fibers simultaneously by estimating the configuration that fit best to the data [166], without the need of a seed region or anisotropy thresholds. Using this type of algorithm is much more time consuming than seed-based algorithms, but gets the advantage of being more stable in terms of noise and imaging artefacts. From the reconstruction of fiber pathways in the whole brain, fiber density (FD) maps can be calculated. This quantitative measure extract from the tractogram is based on the calculation of the number of distinct tracts that pass through a voxel [167]. Thus, FD evaluation constitute a fine-grained measure to detect potential alterations in white matter density, relative to fiber loss and neurodegeneration in brain diseases including AD [168–171].

In brain pathology, DTI imaging can be used to detect myelination processes alterations and axonal damages [172]. Indeed, an increase of RD have been linked to demyelination in several studies [173–175], and an decrease of ADif is usually associated with axonal damages [174,176]. However, increased of this last parameter have already been associated to a pathological state, in both Human and mice studies [177,178]. A decrease in FA or FD is usually related to pathological processes leading to loss of tissue [179,180] such as in Wallerian degeneration [181–183], or inflammatory processes [184].

4. Graph theory for modeling functional and structural connectivity

Exploring and understanding the brain's communication, in healthy and pathological brain, is one of the biggest challenges for scientists. One on its major particularity when compared to other organs, resides in its multiple functionality enabling for instance cognition,

memory, perception or action; all of them emerging from an apparently invariant anatomy. In the field of connectomics, mathematic models have been developed describing - as closely as possible - the topology of functional and structural connectivity, attempting to resolve this highly complex puzzle of brain's multiple and diverse functionalities (Fig. 15). Such models can be applied at mesoscale on brain MRI data – that can be acquired in longitudinal and non-invasive studies – and therefore providing insight into the dynamics of the brain-wide connectome features in health and disease. [93,134,185].

Studying **structural - or anatomical connectivity** in MRI aim at describing physical, axonal based connections between spatially separate brain areas. It refers to the existence and structural integrity of tracts connecting brain areas, generally involving white matter projections linking cortical and subcortical regions. Using specific MR acquisition sequences described previously, fiber bundles and their orientations -but not their directions- can be detected to recreate the complex map of the structural architecture organization of brain networks. While this hierarchical structural organization is thought to be relatively stable during short periods of time (seconds to minutes), over hours, plastic dependent changes would happen, modifying the anatomical architecture of the brain [186]

This anatomical circuitry is in strong relationship with **functional communication** between brain areas. This functional coupling of cerebral regions in MRI is evaluated measuring statistical dependence of the TC of the BOLD signal between neural element. Therefore, two brain regions are considered functionally connected when the TCs of the signal of their activity, at rest or during a task, are correlated. From there, several regions exhibiting a synchronous signal in a given time period are considered part of one functional network. The functional communication between brain areas is highly time-dependent, displaying dynamic modulations in a range of tens or hundreds of milliseconds. In most cases, structural connectivity is directly supporting functional communication. However, functional network can also be completely independent to axonal projections between regions [93,186].

While structural and functional connectivity analysis in MRI cannot provide information about the excitatory or inhibitory feature of a path, the **effective connectivity** can be calculated to reveal the influence from a brain region to another. This concept is modelling neuronal-like circuitries that would produce signals of the same temporal relationships observed in MRI between small groups of neurons [187]. Indeed, the dynamic causality model (DCM), grounded from a structural connectivity model of interactions, can estimate the best parameters that explain BOLD signals according to the biophysics of neuronal interactions [188].

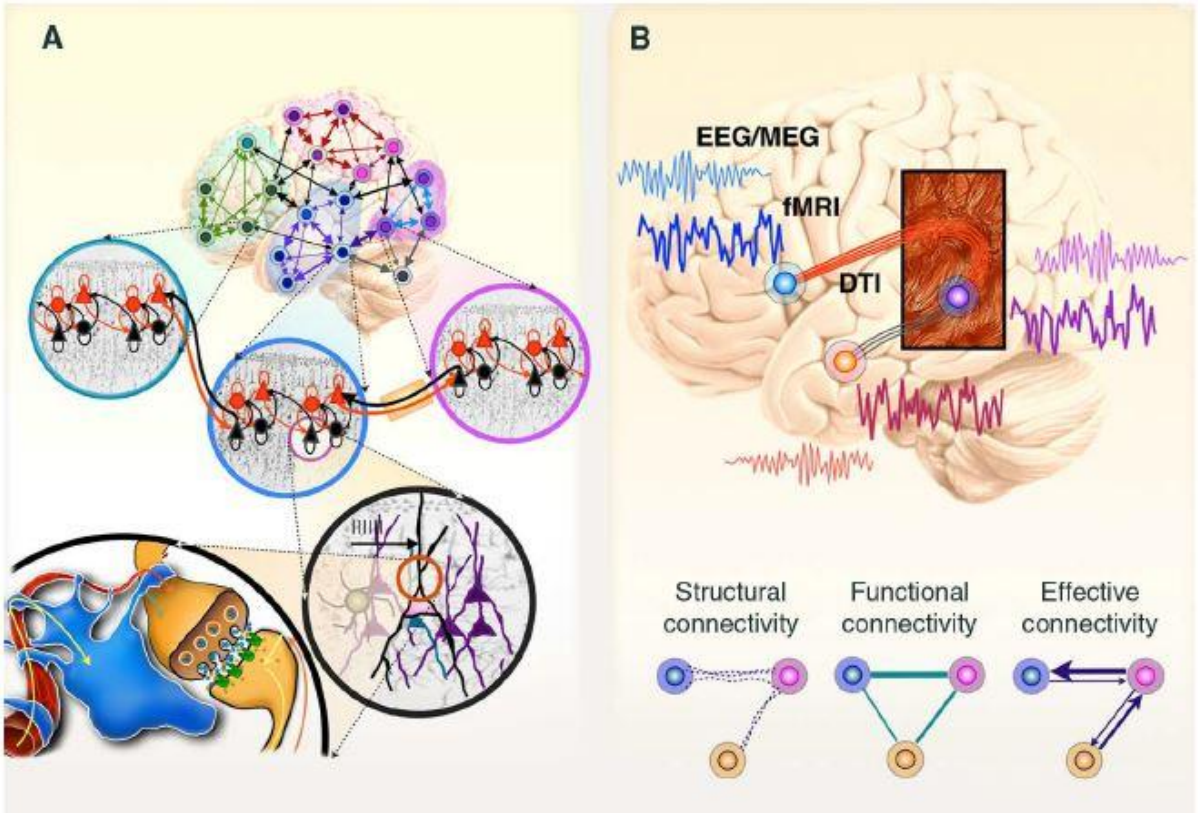

Figure 15*: The brain connectome organization (from Park & Friston* [93]*). A. In the brain, neurons are projecting axons from one region to another, communicating through synapses, and creating structural links between brain areas. In addition, a functional dialogue between brain cells is strengthening anatomical relations. When selected regions are cooperating through structural and functional relations to achieve a specific function, they form what's called a brain network. B. Several technics are used to record functional activity (EEG, MEG, functional MRI (fMRI)) and detected structural architecture (Diffusion Tensor Imaging (DTI) in MRI) of the brain. Analyzing signals from these technics, structural, functional and effective connectivity can be calculated in order to understand underlying organization to the numerous functions of the brain.*

To understand the complexity of the brain communication at network level, huge effort was dedicated during the last years to find reliable modelling of structural and functional network topology, supporting biological interactions [93,186], and aiming at identify the "**nodes"** – the interacting unit/brain areas of a network - and define the parameters acting as "connectors" or **"edges**" between nodes. In this context, **graph theory** approaches demonstrated common but also divergent features of structural and functional connectivity [189]. A general consensus however exists on the hierarchical cerebral network organization, at both structural and functional levels [93,190], involving a **small-worldness** organization with **modularity features**.

The **small-worldness** organization of the brain is represented by short paths lengths between pair nodes of a specific network and high local clustering, promoting high efficiency for information integration. A path corresponds to any unique sequence of edges that connects two nodes with each other. The length of this path is evaluated from the sum of edges lengths or

the number of steps from the origin to the end of the path. Therefore, a short path length promote functional integration by minimizing the steps of the path and the signal degradation [186].

Clusters of connected nodes form **modules**, or community structures that support functional segregation of the brain, and relate with specific cognitive or sensory processes; while inter-modular communication is insured via highly interconnected nodes of different modules. These long-range connections between modules such as cortico-cortical relationships, would support higher cognition processes by connecting modules between them through highly interconnected brain areas called **hubs**, and would be responsible for the global integration of the brain. In the human brain, hubs connecting modules are located in the precuneus, superior frontal and superior parietal cortex, the hippocampus, putamen, and the thalamus [191].

In the concept of graph theory, the **degree** is giving the number of edges -that can be structural, functional or effective- of a node, forming function-related modules. This measure attempt to quantify the importance of a node, and is associated with its influence on a given network. A high degree is usually a defining feature of a hub.

The model extracted from this theory that is approaching the representation of brain interactions most closely is called the **rich-club** model (Fig. 16). This type of network configuration is mediated by a dense connectivity supporting the local integration of functional processes within a module, but sparse between module connectivity.

Thus, the brain connectome appears to follow a hierarchical and modular arrangement, presenting lots of subnetworks, with a rich-club organization. Investigating structural and functional network communication in MRI study using graph theory approaches is providing a unique point of view of the highly complex brain topology, its evolution along time and its modulation following environmental changes. In a given context, the configuration and collaborations between modules -both functional and structural- will generate a global integration in the brain specifically associated to this context. In a neuropathological context this principle also applies, suggesting a strong interest in investigating the modifications of this highly organized brain communication in the diseased brain, such as in neurodegenerative diseases.

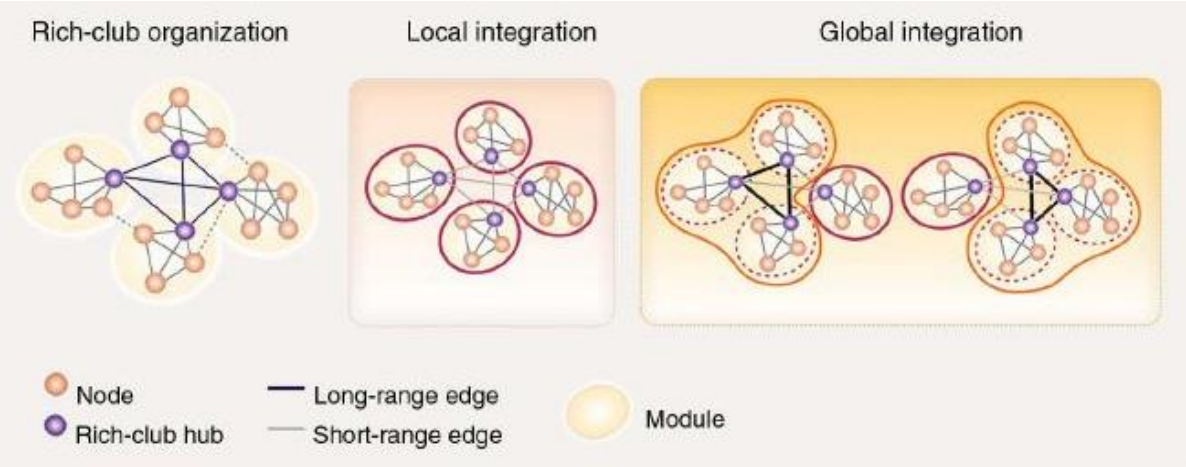

***Figure 16**: The Rich-club organization of the brain (from Park & Friston 2013* [93]*)*

5. The connectome in neurodegenerative diseases

Relation between connectome's changes and neurodegenerative diseases have already been shown in Human [134,185] and animal models. Characterized by its non-invasive property, the MRI technic associated with network analysis is providing an exclusive tool to study the beginning, the course and predict future event in neurodegenerative diseases. Changes of the brain connectome occurring in such pathology are related to both structural affectations and functional communication. Main functional alterations are sustained by structural modifications, however metabolic modifications can also impact the functional communication mediating structural scaffolding affectations.

Two types of brain architecture modifications can be observed in pathological brain: maladaptative or adaptative responses, as described by Fornito, Zalesky and Breakspear in 2015 [134]. Those include **diaschisis**, **transneuronal degeneration** and **dedifferentiation** concerning maladaptative behavior; **compensation**, **neural reserve** and **degeneracy** **adaptative** responses (Fig. 17).

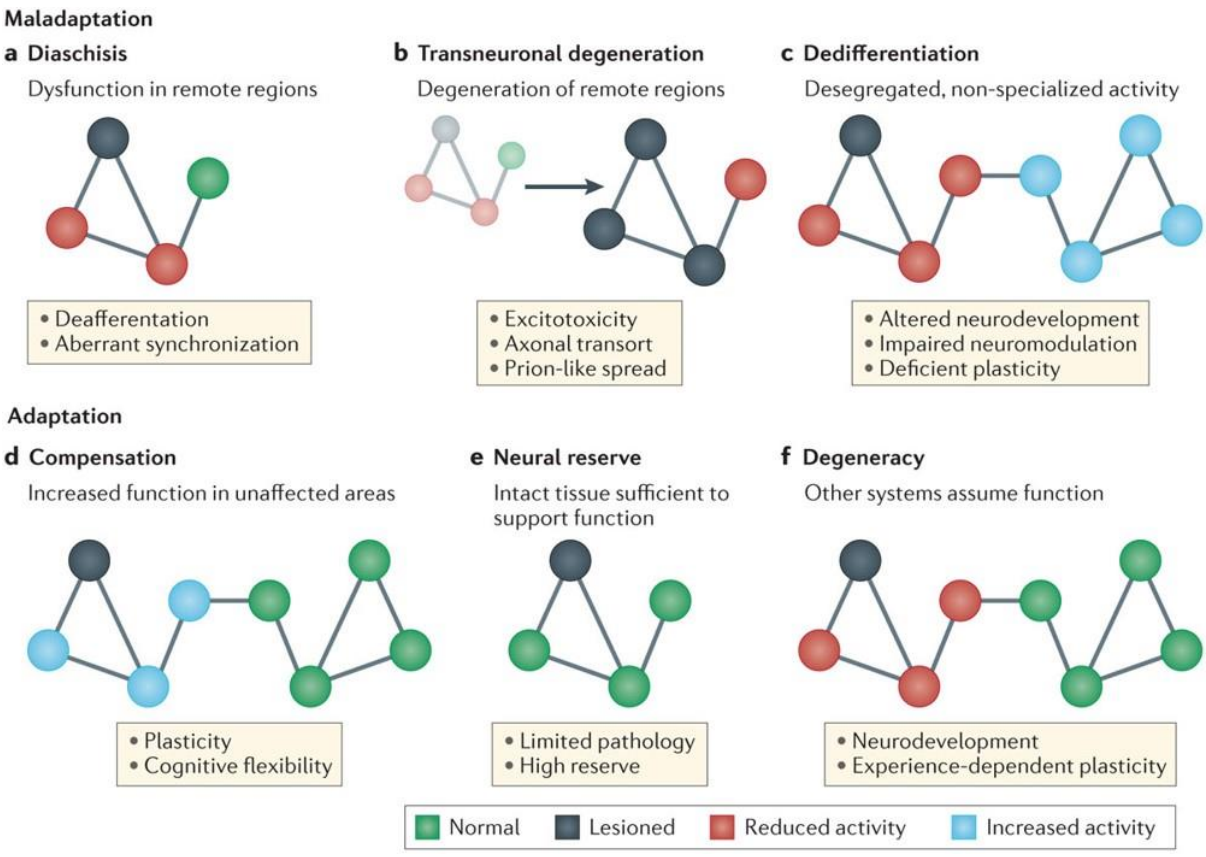

Figure 17*: Connectome's modification in neurodegenerative diseases (from Fornito, Zalesky and Breakspear 2015).*

The diaschisis (Fig. 17.a), a phenomenon described by Von Monakow [192], is affecting a remote region of a leased area by disrupting its function, and leading to behavioral impairment. The alteration can originate from the suppression of afferences from a leased brain region toward other areas, known as deafferentation processes. This processe can also be mediated by

an aberrant synchronization of the functional communication of an affected area with other brain structures. This response is particularly observed following stroke [193], and while it was first described as a transient mechanism, more persistent forms are also detected.

Transneuronal degeneration (Fig. 17.b) is detected in longitudinal analysis only, and leads to alterations along time of remote regions from the first site of affectation, through excitotoxicity, axonal transport disruption, or prion-like spreading. The degeneration can be related to a diminution of the number of dendrites, synapses, or fibers, the alteration of the myelin organization, neuronal shrinkage, or neuronal death [194]. Studying AD, it was shown using PET imaging that Aβ-42 accumulation in one brain area can lead to its reduced functional communication with other distal related regions, mediating metabolism dysfunction [195]. In addition, white matter affectation in transneuronal degeneration is particularly affecting the axonal transport, which leads to a spreading of the atrophy following the structural architecture of the brain. Thus, transneuronal degeneration mediates both anatomical and functional network longitudinal dysfunction in the brain in neurodegenerative diseases such as AD.

Dedifferentiation (Fig. 17.c) is mediated by neural activity dysfunction in a network, leading to the recruitment of other brain regions to perform its task. Disruption of neuromodulatory systems for instance, or a regional alteration of the inhibitory/excitatory balance can engender this mechanism, that have been shown to lead to cognitive deficits in aging [196,197].

Compensation mechanisms: (Fig. 17.d) are allowing the maintenance of the behavioral output following brain injury. An increase of the functional connectivity between the affected regions and a remote brain area can be observed, leading to hypersynchrony of the functional network. This phenomenon has been described in early stages of neurodegenerative diseases such as AD, where hippocampal hyperconnectivity was identified in presymptomatic familial AD patient [198]. Moreover, a compensatory reallocation of cognitive resources has been found in AD patients performing a memory task compared to healthy subjects [199].

Neural reserve (Fig. 17.e) refers to the ability of a neuronal network to keep ensuring its function despite brain damages from an injury or disease. In AD, the accumulation of pathological proteins begins years before the detection of clinical symptoms [200], supporting the hypothesis of a neuronal reserve that would allow patients to carry out given tasks. This adaptative mechanism is closely related to compensation and degeneracy.

Degeneracy, in opposition to pluripotentiality, is related to the capacity of several brain structures to sustain the same function [201]. The degeneracy of a system allows the maintenance of its function despite neuronal damages, and is in relation with neural reserve and compensation mechanism. Indeed, the better degeneracy of a system is, the better compensation and cognitive reserve are.

Thus, connectome's evaluation of neurodegenerative diseases such as AD using MRI is providing great information about the network reorganization, supported by known mechanisms in relation with biological substrate deposition. Static and dynamic analysis of functional connectivity are providing complementary information about functional interactions of brain areas. However, as previously explained, functional connectivity alterations in neurodegenerative diseases are mostly sustained by structural alterations, such as brain

morphological changes and white matter dysfunctions, that can be as well explored synergistically with MRI.

III. Brain MRI in Alzheimer Disease: anatomy and brain connectome features

1. Human imaging studies

Most AD studies investigating with MRI the brain connectome features highlighted strong modifications at the level of functional brain circuitry. In this context, DMN that is constituted of brain regions whose activity increases at rest, is one of the most studied networks in AD. Indeed, as the disease progresses, the functional connectivity of the DMN decreases [202] Moreover, Greicius et al., in 2004 [115] specifically associated functional connectivity disruption of the DMN using ICA in AD patient compared to healthy subjects. They also highlighted a strong implication of the hippocampus in AD patient's connectivity, showing a deficient hippocampal functional communication especially with the posterior cingulate cortex (PCC) in the DMN. Other groups reported a strong relation between AD and the disrupted functional connectivity of the medial temporal lobe (MTL), where the hippocampus lies [203], suggesting a key role of this region's connectivity alteration in the pathology. In addition to the hippocampus, the amygdala functional network was also identified as functionally disrupted in AD, showing a decreased of its connectivity [204,205].

Using fMRI coupled with perfusion analysis, it was also shown a positive correlation between hypoperfusion and functional connectivity [206] contributing to cognitive impairment in AD. Moreover, the disrupted perfusion in AD patients appeared to occur in hippocampal-related regions such as left inferior temporal gyrus and left parahippocampal gyrus. In addition, the cerebral blood flow seems to be positively correlated with cognition scores of the patients [207], reinforcing a relationship between vascularization processes in the brain of AD patients and cognitive deficits.

To detect patterns of white matter alterations in AD, DTI has been largely used. Those modifications would rather be associated with NFT than amyloid plaques: indeed, in regions at higher NFT pathologic stages such as the ventral cingulum tract, the fornix, and the entorhinal white matter including the perforant path connecting the hippocampus, AD patients exhibit a lower FA and a higher MD [208]. Thus, the limbic pathway, involved in connection between the medial parietal lobes, the subcortical grey matter and the medial parietal lobes, appears strongly impacted in AD. Additionally, degenerative changes in white matter have been shown to correlate with CSF measures of biomarkers of AD [209], more precisely in DMN regions.

Measuring brain atrophy is one of the main applications of MRI in AD. The evolution of atrophy in this disease is following Braak stages, and therefore NFT progression. Thus, similarly to NFT, neuronal loss starts in the transentorhinal region in patients that does not display clear clinical symptoms yet. Later, the atrophy spreads to the entorhinal cortex and the hippocampus. Patient starts exhibiting cognitive impairment at stages V and VI, when neocortical association areas begin to shrink [210]. According to the Alzheimer's Disease

Neuroimaging Initiative (ADNI) study, grey matter atrophy in medial and lateral temporal lobes would be correlated with memory impairment, and with executive functions alterations in parietal and temporal lobes [211].

Recently, investigation of the atrophy evolution from prodromal to AD stage in human subjects has highlighted susceptible brain areas that would predict AD development. Indeed, Coupé et al., 2019 [212] compared normal and pathological models of lifespan changes of the human brain, estimating pathological trajectory of brain structure over the entire lifespan. They revealed that the hippocampus would be the first region in the pathological group to diverge from normal aging model before 40 years old, closely followed by the amygdala and lateral ventricles around 40 years old. Moreover, amygdala and hippocampus both displayed an abnormal longitudinal evolution in the AD group compared to normal subjects, supporting a specific role in those regions involved in very early stages and pathological development of AD. These findings are in accordance with a previous investigation of the same group showing a reduced medial temporal lobe in preclinical phases of AD [213]. In line with these studies, other groups investigated possible brain modifications that could predict the conversion from mild cognitive impairment to AD. Using spectroscopy and atrophy measures, Mitolo et al., 2019 suggested predictive morphological changes of the parahippocampal gyrus and fusiform gyrus from healthy subjects to MCI and AD, in addition with metabolites alterations in the posterior cingulate cortex, a core area of the DMN.

Looking at later stages, a study modeled the evolution of morphological changes associated with either normal aging or AD, and similarly showed AD's specific changes located in the temporal lobe and the hippocampal area [214]. Interestingly and contrary to Coupé et al., 2019, they associated ventricles modifications with normal aging evolution, illustrating that the detection of predictive markers for AD remains challenging in Human studies, where including patient at very early stages, before cognitive alterations, is a real problematic issue.

Using fMRI to investigate disrupted functional wiring in initial stages of the disease, several groups studied the functional connectivity of MCI patients. They revealed a paradoxical increase in the functional response of MCI's memory-related structures during a task compared to healthy subjects [198,215–218], while structural analysis demonstrated either no modifications [217], either atrophy of this same region [218]. Magnetoencephalography analysis of the SS cortex revealed a larger amplitude response in MCI than in AD patients [219]. Other studies using the DTI technique, allowing analysis of white matter changes supplied evidences of early microstructural affectations of brain fibers in familial AD mutation carriers, and especially in tract connecting limbic structures [220].

Finally, a graph theory description of AD patient's connectome from Tijms et al., 2013 [221], gathered results of 13 studies showing important loss in highly connected areas in AD (Fig. 18). In particular, several studies highlighted a decreased number of hubs in AD compared to control groups, in addition with an increase of unnormalized path length. However, diverging results were found when comparing different imaging modalities such as EEG, DTI or fMRI, illustrating the difficulty to interpret graph measurements, and more importantly the need of multimodal research to better understand the relationship between structure and function in AD brain.

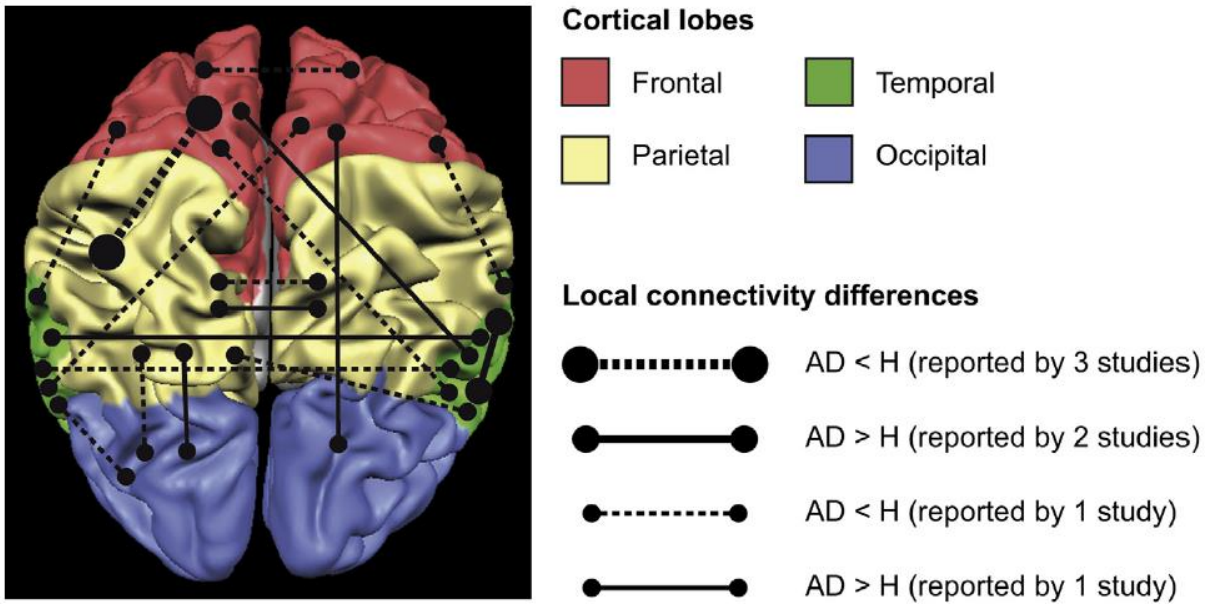

Figure 18: *Summary of differences in local connectivity in AD versus control group (H) extracted from 4 studies in graph theory [Stam et al., 2007 (EEG), He et al., 2008 (fMRI), Yao et al., 2010 (fMRI), and Stamet al. (2009) (MEG)] – from Tijms et al., 2013* [221].

2. Preclinical MRI in animal models of AD: state of the art

To better understand the complexity of the connectome's modifications in AD, the use of genetically modified animal models provides advantages of robustness, reproducibility and specificity, allowing the characterization of selected mechanisms of interest of the pathology. Moreover, such animal models bring the possibility to investigate very early onset of the disease, before the beginning of cognitive or memory impairment, and thus, give a great edge to uncover early biomarkers of cerebral pathology like AD. MRI characterization of the brain connectivity in rodents have already revealed the high potential of this technique as a tool to explore brain circuitry in neurodegenerative models, as well as its strong translational power [140,222,223].

In AD, most mouse models are generated based on the two main neuropathological mechanisms of the disease, the amyloidopathy and the tauopathy. In order to evaluate initial stages of AD, several studies were conducted on different amyloid mouse models using resting state fMRI. One study [224] detected functional alterations of the connectivity of TG2576 mice and PDAPP mice, both amyloidosis model overexpressing mutations specifically affecting amyloid processes. They showed early hypersynchrony in the hippocampus in both models, in addition with frontal network hypersynchrony only in PDAPP mice, before detections of amyloid plaques. Hyposynchrony of memory-related regions were detected at later stages of the disease. Interestingly, they managed to reverse the early functional modifications using an anti-Aβ -antibody, suggesting that soluble Aβ would be responsible for the early alterations of functional connectivity. However, several studies reported potential neurodevelopmental alterations of the hippocampus and the corpus collosum starting 3 months in the PDAPP model [225–229]. Therefore, the hyperconnectivity detected in the hippocampus in this model might be the result of a combined effect from the early AB deposits and the structural prodromal

alterations inherent to PDAPP mice.Similarly, the same group recently found an increased prefrontal-hippocampal network synchronicity in young knock-in APP^{NL-G-F} mice that presented only subtle behavioral alterations such as a reduced anxiety, which could be associated with disinhibition resulting from AD pathology [230]. Grandjean et al., 2014 [231] also revealed abnormal functional connectivity between several networks such as the somatosensory cortex and the motor cortex, along with alterations in the microstructure of the white matter in transgenic mice model of amyloidopathy, before the beginning of cerebral amyloidosis. Moreover, a recent study [232] linked a local hypersynchrony of the hippocampal neuronal activity with the Tau pathology in young mice model of AD, displaying both amyloid and tau alterations.

Thus, as in MCI patients, alterations of the functional connectivity in young transgenic mice expressing tauopathy and/or amyloidosis, seem to manifest as a hyperconnectivity of networks, particularly memory related networks. Interestingly, the cerebrovascular response appears to be particularly affected by the APP genotype, but not the Tau genotype, at a pre-symptomatic stage of the pathology [233]. Accordingly, a study using MRI and histological methods showed cerebrovascular affectations in APP/PS1 mice that would start at the same time as extracellular amyloid deposits in 4 months old mice displaying cerebral amyloid angiopathy [234].

At later stages of the disease, an amyloid-mice model exhibits a decrease of interhemispheric functional connectivity compared to wild-type mice in the hippocampus and somato-sensory cortex [235]. Moreover, Quasi-Periodic Patterns (QPPs) analysis, representing dynamic recurring periods of infraslow neural activity (inferior to 1 Hz) along the acquisition time, reflected a lowered DMN functional connectivity in a mouse model of amyloidosis, and a compromised dynamic anti-correlation between the DMN and the task positive network [236]. These changes in static and dynamic functional connectivity at later stages of the diseases in those amyloid models are close to results found in AD patients [115].

In adequation with those findings, Zerbi et al., 2014 [237] demonstrated that both adult and old (12 and 18 months of age) APOE4 mice expressed functional connectivity deficits, and microstructural modifications in external capsule, corpus callosum and dorsal hippocampus, associated with neurodegenerative processes such as myelin degradation of axonal bundles, and inflammation processes. Other groups revealed microstructural alterations in mouse models of AD. For example, longitudinal studies of mice developing amyloidopathy, especially associated: late amyloid deposit with axonal injury and myelin damages of the corpus callosum [174], Aβ induced inflammation with an age-related decreased mean diffusivity in the hippocampus, or very early cholinergic affectations associated with septal changes [238]. In addition, significant alterations of grey and white matter were highlighted in a triple transgenic mice model expressing both amyloid and Tau pathology using a DTI approach [239,240]. These studies revealed age-related microstructural modifications particularly in the fimbria/fornix fibers -the major output tract of the hippocampus- and the external capsule, starting at 9 months [239]. At later stages, grey matter alterations were found in the hippocampus showing a decreased FA and ADif [240]. To explore the brain connectome of 5XFAD transgenic mice developing an accelerated amyloidosis, a preliminary study applied

the graph theory on ex vivo DTI and in vivo resting-state fMRI [241]. In transgenic mice, a higher path length was found, suggesting a disconnection within the network in favor to long and less efficient routes of information. They also observed a lower small-worldness index reflecting lower normalized clustering and/or higher path length. However, as in Human studies, there is no standard in graph theory regarding threshold to apply, nor scheme for connectome analysis, increasing the difficulties to extract results.

Using other imaging modalities such as [18F]-Fluoro-2-deoxy-D-Glucose-Positron Emission Tomography ([18F]-FDG-PET), longitudinal evaluation of the cerebral glucose uptake has been explored in the APP/PS1 model. The results showed an age-related increase of [18F]-FDG uptake in the cortex, hippocampus and striatum of transgenic mice, and are consistent with the increased cerebral metabolism found in prodromal stages of AD [242], and functional hyperactivity described earlier in mice and human. Investigating morphological changes over time in the brain of two mice models expressing both amyloid and Tau lesions, a group showed age-related entorhinal and striatal atrophy using MRI and gliosis markers with spectroscopy approach [243].

From this section, it is easily noticeable that most MRI studies have been done on mouse model of amyloidosis. This can be explained by the fact that familial AD forms are only coming from mutations in genes involved in the toxic amyloid pathway. Moreover, the main hypotheses about AD etiology is the amyloid cascade. Therefore, only a few recent studies used combined mutations to express both tauopathy and amyoidopathy in mice [232,239,240] and investigate the brain connectome of AD mice models. Up until now, only two studies focused on the tauopathy, exploring longitudinal alterations in functional and structural connectivity in mice [244,245]. Using DTI, Sahara et al., compared transgenic mice rTg4510 expressing the human P301L Tau to wild-type. They showed that from 2.5 to 8 months old, transgenic mice developed an age-related Tau pathology -mostly affecting older mice- in white matter tracts such as the corpus callosum, splenium and the fimbria. A decrease of FA and an increase of radial diffusivity in those regions may reflect axonal alterations in this mouse model of tauopathy. In a recent study, functional and structural modifications were investigated on two mouse models expressing tau pathology in addition with either a pro-aggregant mutation, either an anti-aggregant mutation [245]. Interestingly, they found a decreased functional connectivity in both models, highlighting a neurotoxic effect of the overall soluble Tau independently to its aggregation. They evaluated the density of fibers in both models and revealed changes mostly between the motor cortex and white matter tracts, and a noticeable change of structural connectivity in the fimbria-fornix complex with most cortical nodes.

3. Place of the thesis project in the current scientific context

An important imbalance in the research field of mouse model in AD can be observed, in favor of amyloidosis processes investigations. In addition, among the few studies exploring the tauopathy in mice using MRI, only one combined functional and structural connectivity analysis [245] for the best of our knowledge. However, this study is limited in its longitudinal investigation, to the extent that only two structural and functional MRI datasets were acquired over the limited time course of 2 months.

OBJECTIVES and WORK STRATEGY:

In this context, the main objective of this PhD work was to explore the longitudinal evolution and modifications of the connectome of a mouse model of tauopathy.

For this purpose, I applied non-invasive, in vivo brain MRI technology in a longitudinal experimental design for mapping the dynamics of brain cerebral networks in the Thy-Tau22 mice, over a time course of 8 months. Three MRI methods were used in this work: HARDI to examine microstructural substrates underlying functional brain responses, resting-state fMRI to reconstruct the overall architecture of brain functional communication pathways and anatomical imaging to track morphological alterations using VBM methods.

We associated connectomics analysis of MRI data, with behavioral experiments in the same mice and ex-vivo histological staining of pathological proteins. This aimed at constructing a robust longitudinal picture of three main stages of the pathology: prodromal, intermediate and tardive tauopathy in Thy-Tau22 model.

The final goal was to decipher network signatures of the pathology, discover vulnerable pathways and network's hubs that are critical for early onset of the pathology and coordinate the development - as potential imaging biomarkers of AD. These signatures could further be used in translational investigations as a lead toward early diagnosis and new targets for future treatments.

Indeed, probing the brain networks in animal models is a key strategy to shed light on the mechanisms of the pathology and advance the translational research. MRI is today part of this synergistic strategy, as its non-invasive and versatile nature allow for both clinical and preclinical analysis.

Therefore, the presentation of the results and discussion of this thesis are given in the following investigations:

(i) A first study was performed to evaluate the remodeling cerebral architecture of the brain network at very early stages of the disease, before memory impairments.

(ii) An exploration the morphological, structural and functional changes over time in relation with AD spectrum was completed to highlighted specific modifications of pattern of connectivity along the pathology.

(iii) A general discussion is given in order to build hypothesis regarding the evolution of the pathology from previous described findings.

B) Study 1 – Submitted to Alzheimer and Dementia

Remodeling of cerebral networks architecture anticipate behavioral deficits in a tauopathy mouse model of Alzheimer's disease

Authors: Laetitia Degiorgis[a*], Meltem Karatas[a,b,c], Marion Sourty[a,d], Emilie Faivre[e] Julien Lamy[a], Vincent Noblet[a], Thomas Bienert[b], Marco Reisert[b], Dominik von Elverfeldt[b], Luc Buée[e], David Blum[e], Anne-Laurence Boutillier[f], Jean-Paul Armspach[a], Frédéric Blanc[a,g], Laura-Adela Harsan[a,h*]

Affiliations:

[a]University of Strasbourg and CNRS, ICube Laboratory UMR 7357 and FMTS, Team IMIS, Strasbourg, France

[b]Department of Radiology, Medical Physics, University Medical Center Freiburg, Freiburg, Germany

[c]CNRS, University of Strasbourg, INCI, UMR 7168, Strasbourg, France

[d] The University of Sydney, Faculty of Engineering, School of Aerospace, Mechanical and Mechatronic Engineering, Sydney, Australia

[e]Univ. Lille, Inserm, CHU Lille, UMR-S 1172 - JPArc, LabEx DISTALZ, F-59000 Lille, France.

[f] Laboratoire de Neuroscience Cognitives et Adaptatives (LNCA), CNRS UMR 7364, Strasbourg, France

[g]University Hospital of Strasbourg, CM2R (Memory Resource and Research Centre), Day Hospital, Geriatrics Department, Strasbourg, France

[h]Department of Biophysics and Nuclear Medicine, University Hospital of Strasbourg, Strasbourg, France

***Corresponding author:** Laetitia Degiorgis: ldegiorgis@unistra.fr and Laura-Adela Harsan: harsan@unistra.fr

Meltem Karatas: meltemkaratas@gmail.com

Marion Sourty: marion.sourty@sydney.edu.au

Emilie Faivre: emilie.faivre@inserm.fr

Julien Lamy: lamy@unistra.fr

Vincent Noblet: vincent.noblet@unistra.fr

Thomas Bienert: thomas.bienert@uniklinik-freiburg.de

Marco Reisert: marco.reisert@uniklinik-freiburg.de

David Blum: david.blum@inserm.fr

Anne-Laurence Boutillier: laurette@unistra.fr

Jean-Paul Armspach: jparmspach@unistra.fr

Frédéric Blanc: f.blanc@unistra.fr

Abstract

INTRODUCTION: In Alzheimer's disease (AD), the tauopathy is known as a major mechanism responsible for cognitive deficits development. Early biomarkers of such affectations for diagnosis/stratification are a "Holy Grail" of AD research and intensively sought, and brain connectome studies increasingly show their potential establishing pathology fingerprints at network level.
METHODS: We conducted an in-vivo MRI study on Thy-Tau22 transgenic mice expressing tauopathy, performing functional and structural brain imaging on young mice to identify early connectome signatures of the pathology, relating with behavioral and histological investigations.
RESULTS: Thy-Tau22 mice displayed a functional hyperconnectivity of several networks, including memory-related circuits, supported by dynamic functional connectivity alterations and microstructural modifications, identified before the emergence of cognitive impairments.
DISCUSSION: We found early and specific changes in the connectome of transgenic mice that might be related to combined: early Tau deposition, astrogliosis and/or functional compensation. These specific patterns of connectivity could be used as potential early biomarkers of AD.

Keywords: Alzheimer's disease; Tauopathy; resting-state MRI; functional connectivity; structural connectivity; Thy-Tau22; hypersynchrony; prodromal

Highlights

- Thy-Tau22 mice display hippocampal functional hyperconnectivity before memory impairment
- Memory-related pathway present microstructural alterations consistent with functional changes, without brain atrophy
- The architecture of the hippocampus-amygdala connectivity seems to be strongly involved in early onset of AD
- Dynamic functional connectivity between key regions involved in AD is disrupted at very early stage of the disease
- Early pathological Tau deposition in association with astrogliosis could lead to modifications of the connectome in prodromal stages of AD

Research in context

1. **Systematic review**: The authors reviewed the literature about early Alzheimer's disease (AD) in rodent models of the disease using PubMed. Several groups used amyloidopathy models of AD to identify early alterations of the connectome, but only one recent report investigated the impact of tauopathy on brain communications in a triple transgenic mouse. All those studies are appropriately cited.
2. **Interpretation**: We found a specific pattern of the prodromal brain connectivity of transgenic mice developing tauopathy, showing structural connectivity alterations and functional networks hypersynchrony which may be mediated by early pathological tau deposition. This finding is supported by other preclinical and human studies, reinforcing its potential as a biomarker of AD that can be used for early diagnosis.
3. **Future directions**: Longitudinal study of this mouse model should provide crucial information about the evolution of the brain circuitry alterations at later stages of the pathology, specifically mediated by tauopathy-related affectations.

1. Introduction

Alzheimer's disease (AD) is the most widespread cause of dementia in the world. The belated diagnosis of this pathology, essentially based on clinical features [1] appearing several years after the beginning of the disease [2], maintains the important challenge to reveal an early, robust and specific biomarker of AD.

So far Magnetic Resonance Imaging (MRI) is the only methodology able to give a non-invasive insight into the large-scale functional and structural cerebral networks architecture, providing the unique possibility to study neurodegenerative diseases at connectome level [3]. Resting state functional MRI (rsfMRI) and diffusion tensor imaging (DTI) are both staple techniques to explore, respectively, brain functional connectivity (FC) modifications in relation with fibers integrity. In AD patients, FC modifications of specific networks – including the so called "default mode network (DMN)" - have been highlighted [4,5], and recent studies showed a link between patterns of dynamic FC changes during the rsfMRI scan, and neuropathological affectations [6]. Studies using DTI to analyze white matter [7] supplied evidence of early microstructural changes in AD mutation carriers [8].

In rodents, MRI studies highlighted the great potential of this technique as a tool to explore functional and structural brain connectivity in neurodegenerative models [9,10]. To evaluate initial stages of AD, several studies were conducted on different amyloid mouse models using rsfMRI. They revealed abnormal FC in several networks along with alterations in the microstructure of the white matter before cerebral amyloidosis [11], or associated with toxic soluble Amyloid-β [12]. A recent study [13] however, linked a local abnormal neuronal activity with the Tau pathology in young mice model of AD, displaying both amyloid and tau alterations.

Nevertheless, the relation between alterations of the brain connectome and specific biological substrates of AD remain ill-defined. Particularly, despite the strong implication on the tauopathy in cognitive decline, its impact on circuitry patterns in AD is still poorly studied. In this context, we performed a non-invasive and in vivo brain MRI study of the Thy-Tau22 mouse model progressively expressing brain tauopathy paralleling neuroimmune and cognitive

alterations [14-16]. We evaluated possible network signatures at an early pathological stage and identified specific patterns of resting-state FC associated with microstructural alterations. Such circuitry features might underpin early pathological mechanisms in AD - appearing before behavioral impairment – and constitute new potential biomarkers of prodromal AD.

2. Material and methods

2.1. Animals

All experimental protocols were approved by the Regional Committee of Ethic in Animals Experiment of Strasbourg (CREMEAS, APAFIS n°2016033011298450). Sixteen transgenic Thy-Tau22 and thirteen littermates wild-type (WT) male mice aged 5 months were used for both behavioral experiments and MRI studies. Mice were randomly housed in pairs allowing social behavior. Thy-Tau22 mice overexpressed the human mutated tau protein (G272V and P301S) under the Thy1.2 promoter, inducing formation of phosphorylated Tau and later on neurofibrillary tangles (NFT), throughout the brain [14].

2.2. Behavioral tests

"Object tasks" behavioral tests in rodents classically evaluate subtle memory impairments based on animals' spontaneous behavior to explore novelty in their environment. We used 3 types of tests to evaluate the episodic-like memory in mice (Fig 1, A, B, C): object recognition (OR), object-in-place (OIP) and object location (OL). These tests were adapted according to previous optimizations [17]. Spatial reference learning and memory abilities were evaluated using the Morris Water Maze (MWM), as described in Chatterjee et al., 2018 [18] (Fig 1, D). See supplementary material 1.

2.3 MRI experiments: images acquisition and processing

Brain MRI was carried-out in the two animal groups using a 7T small bore animal scanner (BioSpec 70/30, Bruker, Germany), a mouse head adapted room temperature surface coil combined with a volume transmission coil, and Paravision 6.0.1 (PV6, Bruker, Ettlingen, Germany). Anatomical images were acquired using a multislice (34 slices of 0.4 mm) Turbo Rapid Acquisition with Relaxation Enhancement (RARE) T2-weighted sequence. RsfMRI data were acquired in 16 min using single shot gradient-echo, echo-planar imaging (GE-EPI). 27 axial slices of 0.4 mm thickness were recorded to cover the entire brain (Echo Time/Repetition Time=15/2000ms, spatial resolution=0.14x0.22x0.4). A diffusion tensor imaging – echo planar imaging (DTI-EPI) sequence was used to perform High Angular Resolution Diffusion Imaging (HARDI). 27 slices of 0.5 mm were recorded with 30 diffusion directions and 5 b-values (500, 1000, 1500, 1750, and 2000 s/mm^2), covering the equivalent partition of the brain as in the rsfMRI scan (See supplementary table 1). For rsfMRI the animals were briefly anesthetized with isoflurane for initial animal handling. The anesthesia was further switched to medetomidine sedation (MD, Domitor, Pfizer, Karlsruhe, Germany, bolus of 0.6 mg MD per kg body weight in 100 µl 0.9% NaCl-solution and infusion of 0.3 mg/kg body weight in 200 µl/hour). Mouse physiological conditions (body temperature and respiration) were monitored continually during the imaging. After the experiment, the animals were allowed to spontaneously recover. See supplementary material 2.1. for detailed procedure.

Preprocessing of fMRI data was performed using Statistical Parametric Mapping (SPM8, http://www.fil.ion.ucl.ac.uk/spm/) with SPMmouse (www.spmmouse.org) for MATLAB (The MathWorks, Natick, Massachusetts) as previously described [19] and given in the supplementary material 2.2.

Partial Correlation (PC) analysis was performed to evaluate direct temporal correlations between spatially separated regions of interest (ROIs) [20]. ROIs (42) covering the major mouse brain areas were extracted from the Allen Mouse Brain Atlas (AMBA) (http://mouse.brain-map.org/static/atlas), using an in-house built MATLAB tool. We created: i) a 42x42 ROIs matrix covering the major brain areas, to create a ranking of the number of significant connections per ROI in each group (one sample t-test, $p<0.001$, FDR corrected), and ii) a mean PC matrix for each group to specifically evaluate FC of 22 key ROIs involved in AD (Fig 2, supplementary Figure 1 and supplementary material 2.3.).

Seed-based voxel wise analysis was performed to evaluate the correlation (Spearman's rho) between the rsfMRI signal's time-course (TC) of a ROI, and the TCs from all other voxels of the brain. We generated Fisher-transformed spatial correlation maps and investigated group averaged FC maps of representative areas showing changed connectivity patterns in PC matrices (i.e. CA1, primary somatosensory cortex (SSp), and dorsal hippocampus (dHIP)). Group-wise statistical analysis was performed to evaluate FC modifications of several brain areas, including the dHIP and ventral hippocampus (vHIP) networks. These two ROIs were created based on parcellation of the whole hippocampus area extracted from AMBA. We used a two-sample t-test ($p<0.05$) and applied a cluster-based threshold at $t<2.1$, corrected for multiple comparisons (FDR) by using the null distribution of the max cluster size from FSL software to compare networks in both groups.

Dynamic functional connectivity (DFC) analysis was performed on preprocessed mean TCs extracted from 8 ROIs selected on the bases of their known involvement in AD and our histological results: dHIP and vHIP, entorhinal cortex (ENT), SSp, orbitofrontal area (ORB), lateral septal complex (LS), bed nuclei of the stria terminalis (BST), and amygdalar nuclei (AMG). We used a sliding-window method described in [6] to compare and characterize connectivity state changes between ROI's TCs. Group differences were evaluated using two-sample t-tests ($p<0.05$). See supplementary material 2.4 and supplementary figure 2 for further details.

For *structural analysis*, HARDI data were denoised using the MRtrix software [21], and parametric maps derived from HARDI were generated for each mouse (fractional anisotropy (FA), radial diffusivity (RD) and axial diffusivity (ADif)). A Global fiber tracking approach was used as described previously [22,23], to perform global mouse brain tractography. Fiber density (FD) maps were constructed for each mouse from the number of streamlines passing in each voxel. We then performed a voxel-based quantification (VBQ) for each type of HARDI derived maps, followed by a two-sample t-test to infer microstructural alterations ($p<0.01$, FDR cluster corrected).

2.4 Immunofluorescence

To investigate astrogliosis and hyperphosphorylated Tau distribution on histological brain slices, we used antibodies directed against GFAP (glial fibrillary acidic proteins) and phosphorylated Tau at Ser202/Thr205 sites (AT8 antibody), respectively (procedure in supplementary material 3).

3. Results

3.1 Five-month-old Thy-Tau22 mice exhibit preserved memory abilities

To assess the cognitive state of 5-months -old Thy-Tau22 mice, we first performed object memory tests, allowing highlighting mild memory alterations in mice. The results showed that in all tasks, Thy-Tau22 mice did not show any deficit relative to WT mice, as they spent significantly more time exploring the rearranged object during the retention than would be expected from chance ($p<0.0001$ for each test) (Fig 1, A, B, C). Mice were then submitted to the MWM (Fig 1, D). During the learning phase, both Thy-Tau22 and WT mice displayed significant acquisition of the platform location (day 1 vs day 5: $p<0.01$ for Thy-tau22 and $p<0.0001$ for WT) (Fig 1, E). Analysis of long-term retention (10-days probe test) later showed that both groups were able to remember the location of the hidden platform, as they spent significantly more than 25% of the time in the target quadrant (Fig 1, F; $p<0.01$). There was no genotype effect ($p=0.42$). Therefore, these data show that different type of memory -relying on different brain structure interactions- are preserved in Thy-Tau22 mice at this age.

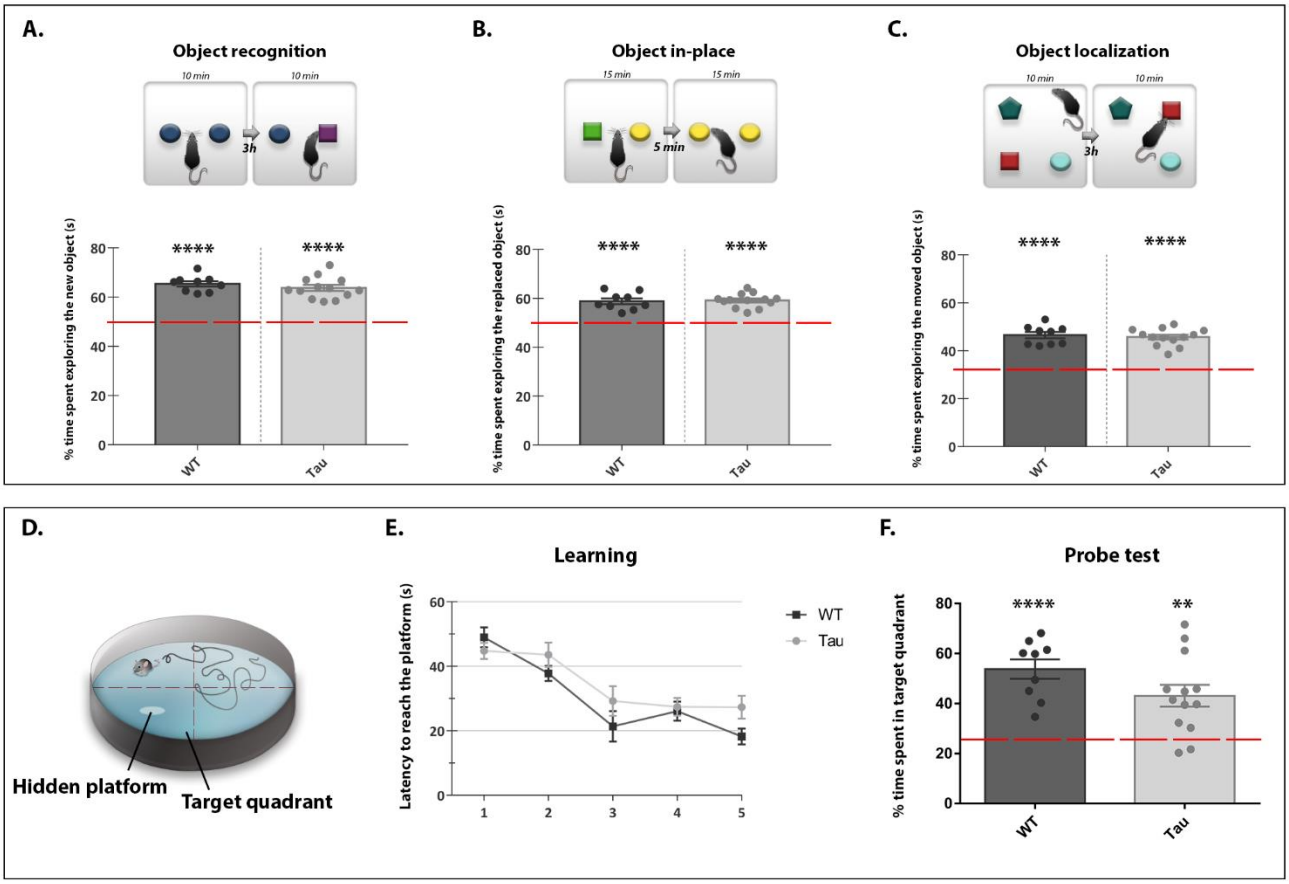

Figure 1: *Behavioral evaluation of Thy-Tau22 mice at 5 months. (A) Novel object recognition test, (B) object in-place, and (C) object localization, showing the percentage (%) of time spent exploring the changed object in each test, for both groups (Thy-Tau22 mice and WT) compared with the level of chance (one sample t-test, **** p<.0001; +/- mean standard error). In the MWM test (D) learning abilities (E) are evaluated in each group timing the mean latency to reach the plateform over days. Statistical group comparison is performed for each day of training, showing no differences. (F) Probe test performance are evaluated in each group comparing the % of time spent in the target quadrant with the level of chance (25%), (one sample t-test, ** p<.01; *** p<.001; **** p<.0001; mean +/- standard error).*

3.2 rsfMRI modifications in Thy-Tau22 before memory deficits

Analysis of the mean PC connectivity matrix of 22 key ROIs (see Supplementary Fig 1, A), -brain areas representative for AD – showed increased FC of hippocampal subregions (CA1, CA2, CA3) in Thy-Tau22 mice towards cortical areas such as SSp (right and left), retrosplenial cortices as well as most amygdalar nuclei (anterior, central, lateral (LA), basolateral (BLA), basomedian (BME) and medial amygdala) (Fig 2, A). The mean correlation maps of the CA1 network (Fig 2, B) suggested a hyperconnectivity of this area especially directed toward SSp cortex, amygdala and other hippocampal subregions (CA2, CA3 and the dentate gyrus). Similarly, the mean correlation maps of AMG (data not shown) and SSp

networks (Fig 2, B), indicate increased connectivity patterns of these areas toward HIP. Analysis of the whole brain PC matrix (42 x 42 ROIs) suggest a global increase of the FC in the Thy-tau22 mice, as the mean number of significant functional connections per ROIs in Thy-tau22 was higher (14.5) than in WT (11.47), as well as the number of regions displaying a significant number of connections (Suppl Fig 1, B, $p<0.001$). Moreover, the ranking of the most connected regions is changed in the transgenic group, particularly highlighting an increase of the connectivity of CA1, SSp, cortical amygdala (COA), perirhinal cortex (PERI), ORB, anterior cingulate area (ACA) and Caudate-Putamen (CPu), all above the mean number of connections per ROI (Suppl Fig 1, A, B).

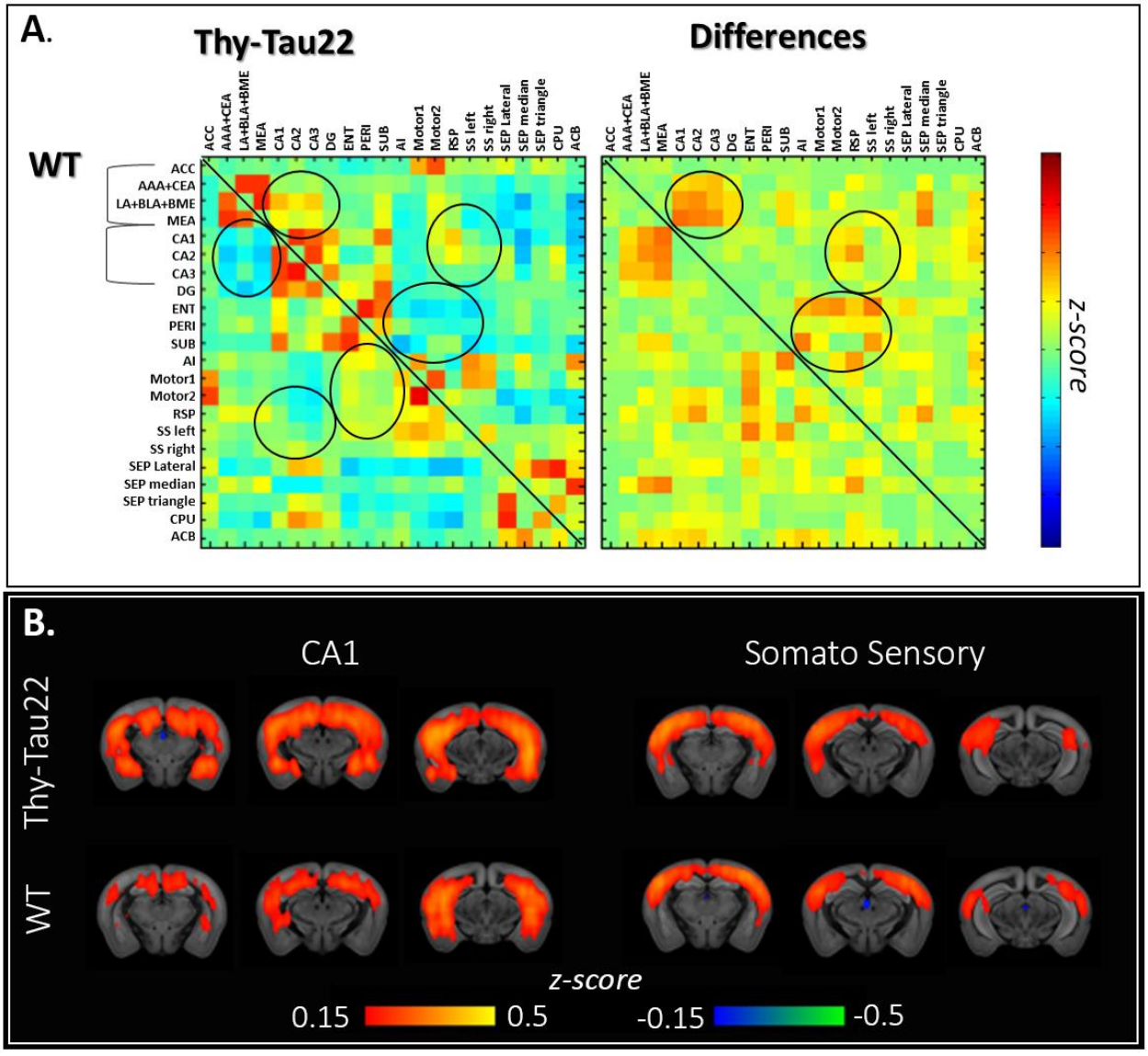

Figure 2: *Mean correlation analysis of ROIs involved in AD. (A) Mean correlations matrices of BOLD FC in Thy-Tau22 mice (upper half) versus WT (lower half) on the left, showing functional correlations between pairs of ROIs. On the right, the matrix is showing the mean differences in FC strength in Thy-Tau22 mice versus WT. (B) Coronal slices of the seed-based analysis of CA1 and SSp networks showing the mean correlation between the mean BOLD signal in a ROI and all other voxels of the brain, in Thy-Tau22 mice and WT. The color scale*

represents the strength of the functional correlation normalized with a fisher z-transformation. Abbreviations are listed in Supplementary Figure 1.

To further investigate the pattern of these hippocampal functional modifications, we analyzed dorsal and ventral hippocampal networks separately. RsfMRI mapping of dHIP showed a strongly increased mean FC of this network in Thy-Tau22 compared to WT mice (Fig 3, A) towards isocortical regions, within HIP and towards amygdala (AMG; LA, BLA, BME). In-between groups statistical comparison showed specific hyperconnectivity of the dHIP in Thy-Tau22 with cortical areas (Fig 3, B), such as a significant bilateral increase of the dHIP-SSp connectivity, and higher correlations with primary motor cortex. dHIP was also more strongly connected to associative areas like temporal associative (TEa) and posterior parietal associative (PTLp) areas in Thy-tau22 than in WT as well as PERI and ectorhinal (ECT) cortices. FC of dHIP with caudate-putamen (CPU) was also found to be stronger in transgenic than WT mice.

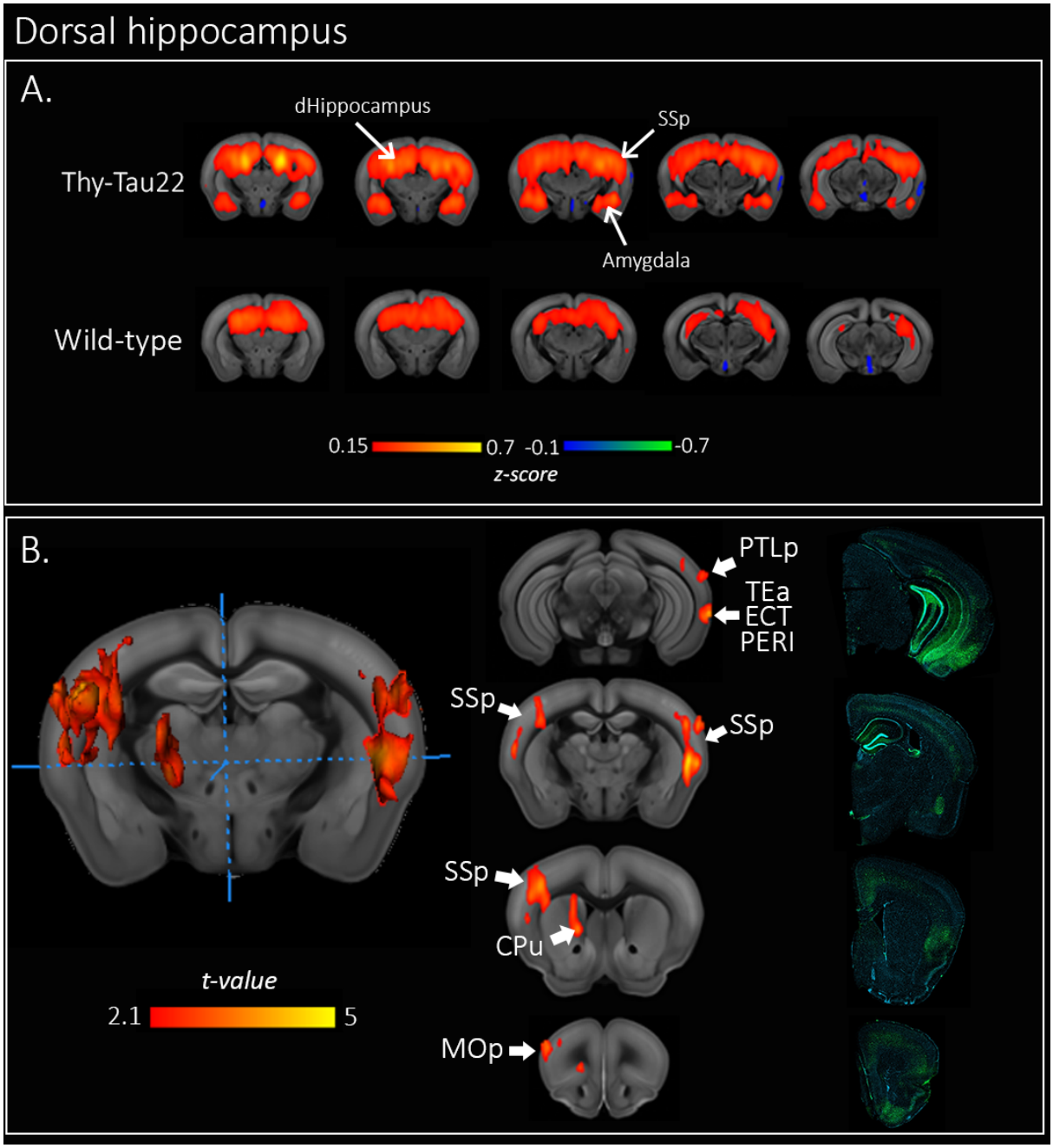

Figure 3: *dHIP hyperconnectivity in Thy-Tau22 mice. (A) Coronal slices of the seed-based analysis of the dHIP network showing the mean correlation between the mean BOLD signal in the dHIP and all other voxels of the brain, in Thy-Tau22 mice and WT. The color scale represents the strength of the functional correlation normalized with a fisher z-transformation. (B) Statistical analysis map of the group comparison of the dHIP FC, in red showing a significantly higher FC in Thy-Tau22 mice compared to WT. 3D representations of statistically significant differences (two sample t-test, $p<0.01$, FDR cluster corrected) is showed on the left. Coronal slices of the FC statistical map and corresponding slices of immunofluorescence staining in a Thy-Tau22 mice: AT8 staining (green) and DAPI (blue); in the middle and on the right respectively. Abbreviations are listed in Supplementary Figure 1.*

Statistical analysis of vHIP network (Fig 4) showed functional modifications in the olfactory system of transgenic mice with decreased FC strength toward the olfactory bulb (OB), and increased toward piriform (PIR) and ORB cortices. Similarly to the dHIP, a significant increase of the vHIP-striatum connectivity was found. Interestingly, and opposed to dHIP FC patterns, vHIP decreases its FC with AMG in Thy-tau22 mice, suggesting that hippocampal sub-regions communications (dHIP, vHIP) are differently affected with this limbic brain area.

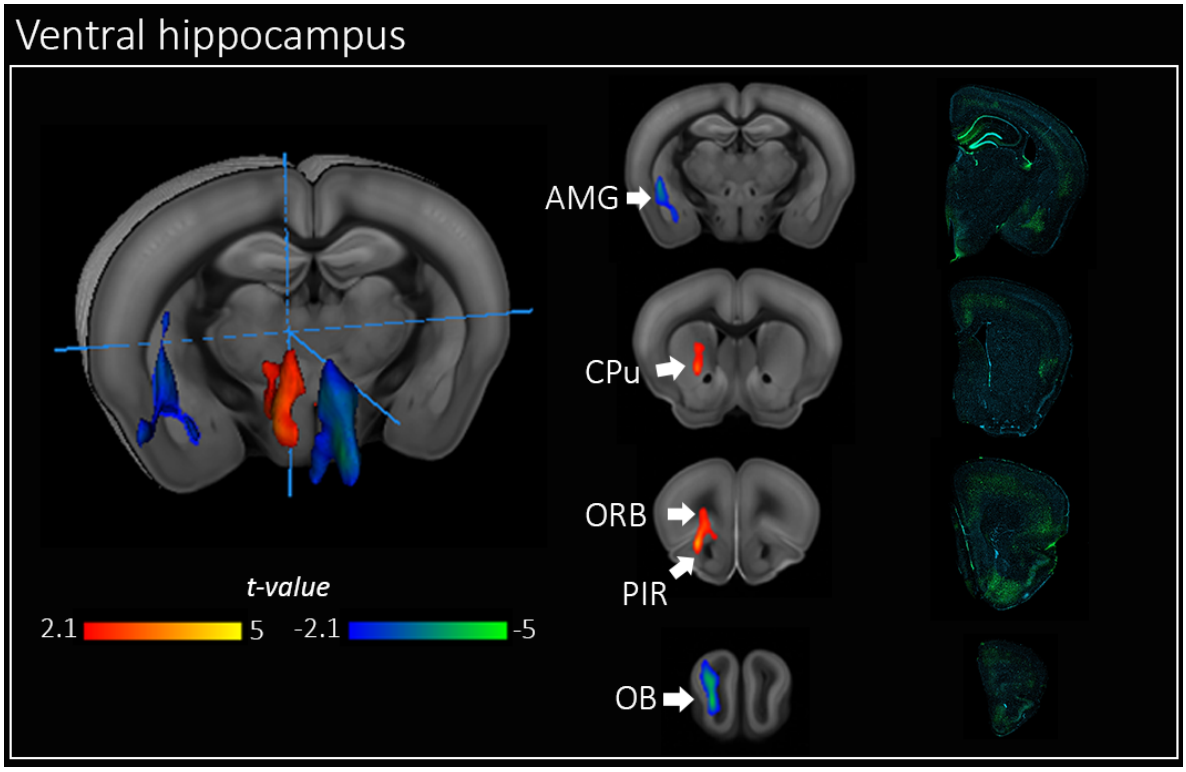

Figure 4: *vHIP functional modifications in Thy-Tau22 mice. Statistical analysis results of the group comparison of the vHIP FC, in red representing a significantly higher FC and a significantly lower FC in blue, in Thy-Tau22 mice than in WT. 3D representations of statistically significant differences (two sample t-test, p<.01, FDR cluster corrected) is showed on the left. Coronal slices of the FC statistical map and corresponding slices of immunofluorescence staining in a Thy-Tau22 mouse: AT8 staining (green) and DAPI (blue); in the middle and on the right respectively. Abbreviations are listed in Supplementary Figure 1.*

We then evaluated DFC features within 8 chosen ROIs. Our results showed that the DFC within those selected ROIs was significantly different between groups (two-sample t-test, $p<0.001$). Specific changes of the dynamic features occurred in vHIP DFC and AMG DFC ($p<0.001$ and $p<0.0013$ respectively, Suppl Fig 2). We performed further analysis on these 2 ROIs focusing on only 4 cognitive states, described in Suppl Fig2. The time spent in each of these 4 states is significantly different between groups for both ROIs and for 3 of these 4 states. WT reached more uncorrelated states than the Tau animals who tended to stay in states where more ROIs are correlated (Suppl Fig 2).

3.3 Microstructural alterations in 5 months Thy-tau22 mice

The group-wise analysis of FA maps showed a significant decrease ($p<0.01$, FDR cluster corrected) of the FA in Thy-Tau22 (Fig 5, A) located bilaterally in the fornix and fimbria, in the internal capsule, and in the CPu. In coherence with these findings, the group-wise FD maps statistical comparison showed a decreased density of fibers in transgenic mice in the fornix and fimbria, the HIP, LS, CPu, the internal capsule and in thalamus (both medial and ventral part) ($p<0.01$, FDR cluster corrected; Fig 5, B). However, no statistically significant changes were detected in RD or ADif. The estimation of volumetric brain changes in Thy-tau22 mice using voxel-based morphometry (see supplementary material 2.5) analysis showed no differences between groups (data not shown).

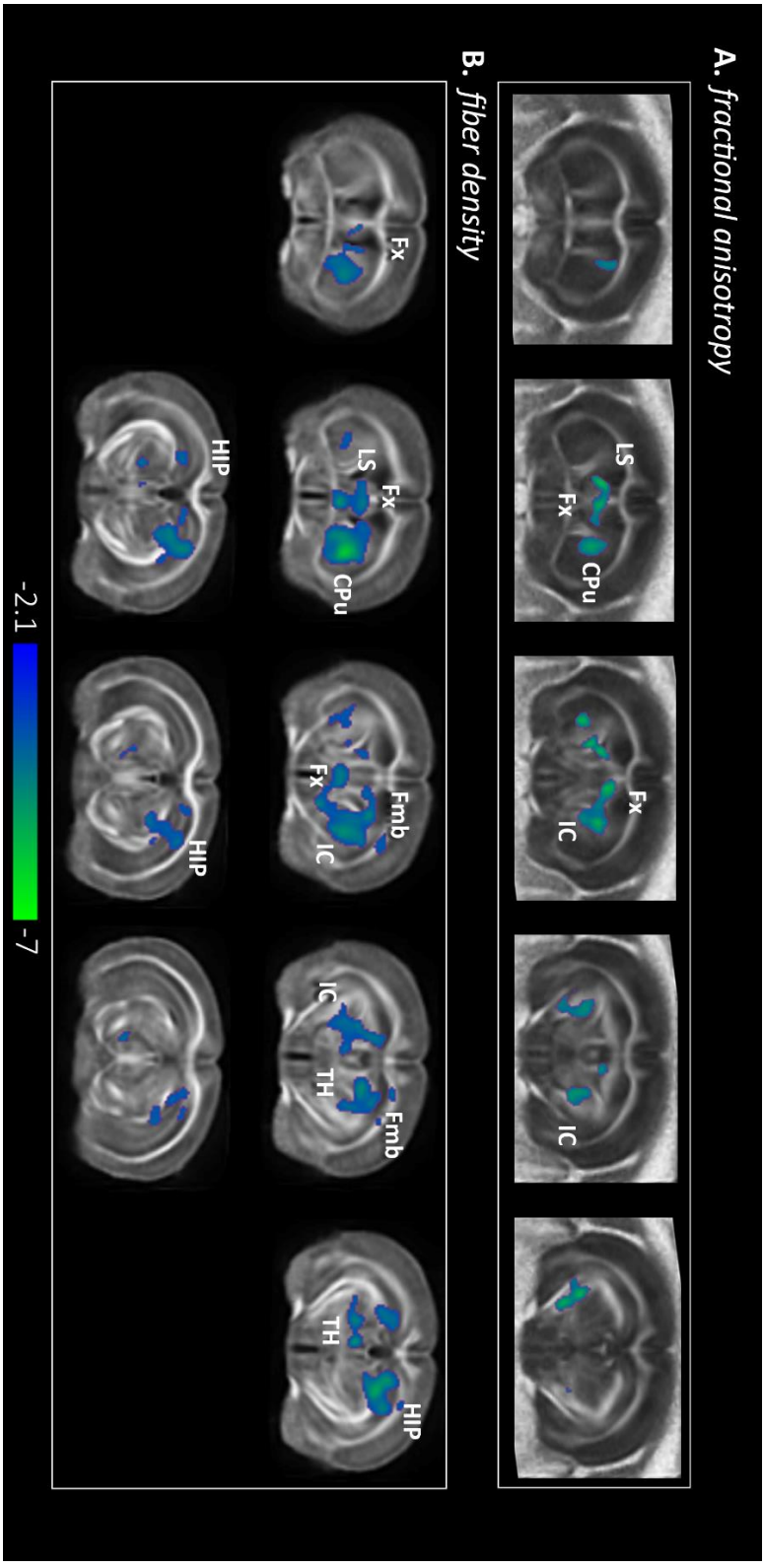

Figure 5: *Microstructural modifications at early stage of tauopathy. Statistical group comparison of the fractional anisotropy (A) and of the fiber density (B) between Thy-Tau22 and WT (two sample t-test, p<.01, FDR cluster corrected). Color scale representing a significant decrease in FA and FD in Thy-Tau22 mice. (Fornix: fx; internal capsule: IC; fimbria: Fmb; thalamus: TH; caudate-putamen: CPu; hippocampus: HIP).*

3.4 AD brain tissue histology correlates of MR based connectivity modifications

To further explore the pathological microstructural substrate in Thy-Tau22 mice, we performed GFAP and AT8 immunostaining (Fig 6). GFAP staining revealed astrogliosis features in dHIP, vHIP, AMG but also in the fimbria and the internal capsule. AT8 staining showed a higher concentration of phosphorylated tau in cortical areas like ORB, SSp, TEa, ECT, PERI, and ENT cortices. Several other brain areas showed pathological tau depositions but the highest extent was located in the HIP and in the AMG of Thy-Tau22 mice (Fig 6).

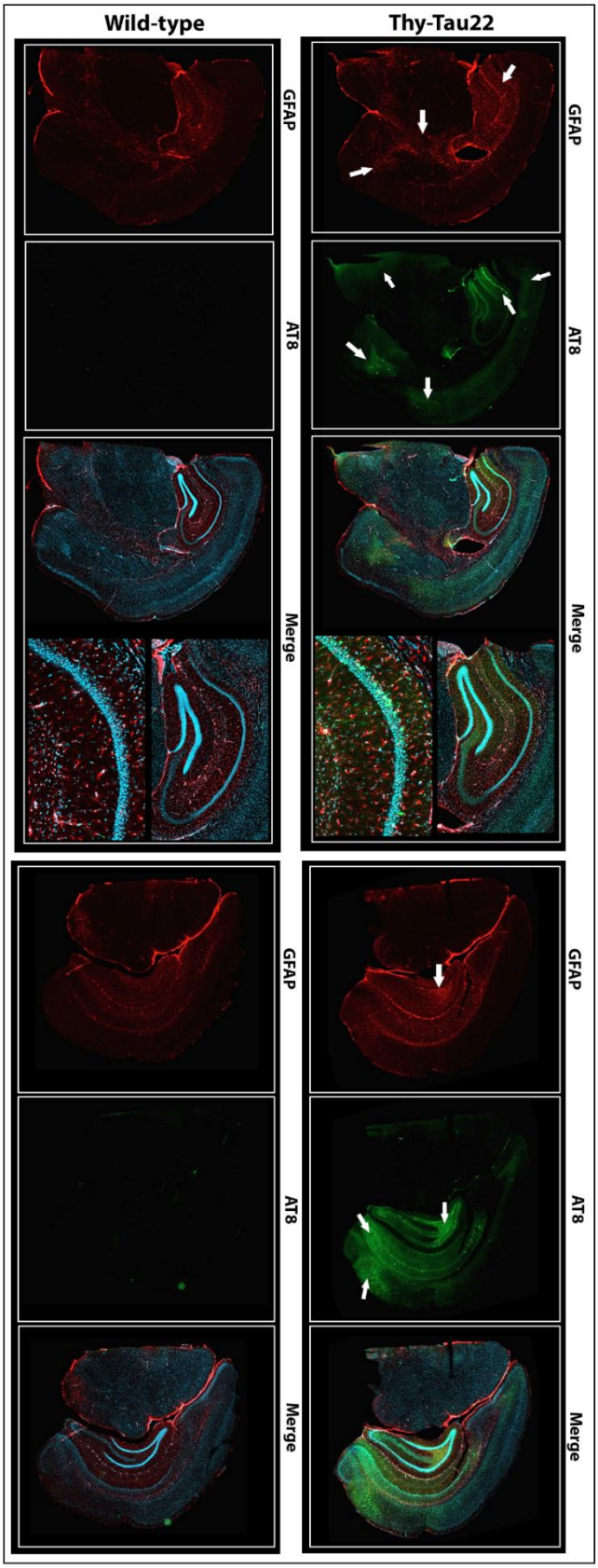

Figure 6: *Representative immunofluorescence coronal slices of AT8 (green), GFAP (red), and merged images with DAPI (blue) staining in Thy-Tau22 mice and WT. Arrows are showing the highest intensity of staining.*

4. Discussion

This study provides strong evidence regarding the early tauopathy impact on the brain connectivity, demonstrating that dysregulation of neuronal network activity precedes memory and learning deficits. We show specific modifications of the functional brain communication of key memory regions, such as the HIP, AMG and cortical areas, in a tauopathy mouse model of AD. We equally show for the first time that dynamic features of the FC between such regions are also perturbed. Moreover, these FC results were attuned with microstructural alterations along HIP related pathways (supplementary Fig 3).

We tested memory and learning abilities of 5 months-old Thy-tau22 mice using established approaches, recruiting key memory areas presenting tauopathy in AD [24]: HIP, ENT, PERI and cortical regions [25-27]. In all tests, Thy-Tau22 mice demonstrated good performance, supported by previous study showing spatial memory impairment starting around 8-9 months, and non-spatial memory impairment starting at around 6 months of age in Thy-Tau22 mice [15]. Despite this lack of AD specific phenotype at 5 months, these mice are developing pathological Tau hyperphosphorylation in HIP as early as 3 months of age, according to litterature [15,28]. Altogether those results show that 5 months-old Thy-Tau22 mouse model is reliable for studying early onset of the disease, with neither cognitive impairment, synaptic degeneration (occurring from 9 months of age [18,29]) nor neuronal loss (occurring after 12 months).

We quantified global remodeling of the functional connectome in these mice, revealing a hyperconnectivity signature of HIP-cortical and altered HIP-AMG functional communication in Thy-Tau22 brain, but also major modifications of the intra-HIP network, and HIP vs. temporal areas, prefrontal cortices.

Interestingly, those same functional paths have been shown to be affected in patients with mild cognitive impairments (MCI) [30]. Several groups showed functional hyperconnectivity of the HIP in MCI patients during memory tasks while structural analysis demonstrated atrophy of this same region [31,32]. Moreover, a recent study modeling structural changes in brain areas across lifespan in AD patients vs controls revealed an early vulnerability of the HIP and AMG, and a close abnormal evolution of these structures [33]. Other groups showed early modifications of the FC in the SSp and motor cortices functional circuitry [11] and hyperconnectivity of the HIP [12] before amyloid plaques depositions in mice models of amyloidosis. Using 3 months-old amyloid mice, a study detected hypersynchronous signals in the HIP and frontal networks of mice presenting early impairment in cognitive flexibility but not in classic memory test [34]. Recently a regional homogeneity study of the BOLD signal in young transgenic mice expressing both amyloid and tau pathologies established a correlation between the hypersynchronous signal in the HIP, parietal, and temporal cortices; and the presence of pathological tau [13]. Despite the trend to interpret hypersynchrony as a compensatory mechanism that might help the maintenance of a normal behavior by several authors, other evidence supports the idea that an increased hippocampal FC could reflect a dysfunctional condition, whose reduction could improve cognition in patients [31].

We further investigated the hippocampal connectivity studying dorsal and ventral HIP functional networks separately [35]. We found an increase FC of the dHIP network toward cortical brain areas -a pathway that has been proved to be indispensable especially in spatial memory processes [36] - in Thy-Tau22 mice. This hyperconnectivity may indeed reflect a compensatory adaptation regarding the strong pathological tau deposition in the dHIP, inducing an increase FC toward recruited remote brain areas, and allowing the preservation of the behavioral output in Thy-Tau22 mice [3]. However, this hyperactivity could eventually stimulate the spreading of the tauopathy in those recruited areas [37], sustaining a pathological loop. The astrogliosis found in the same regions also raises the hypotheses of astrocytes involvement in this abnormal signal, as supported previously in a study of a mouse model of amyloidopathy [38].

The vHIP is a crucial area involved in olfactory processes, exhibiting numerous afferences directed to the OB and the PIR cortex, before projecting to the ORB cortex [35]. Major modifications of functional interaction with those three regions has been found while investigating the vHIP FC, despite the fact that Thy-Tau22 mice are only presenting olfactory impairment from 12 months as shown on Martel et al., 2015 [39]. These alterations might illustrate a compensatory increase of the vHIP-PIR and vHIP-ORB cortices FC, counteracting the decrease of its functional communication with the OB. In accordance with Human studies [40], we detected a high density of pathological tau in these brain regions in Thy-Tau22 mice. These results are reinforcing a link between pathological Tau depositions and FC disruptions in AD. The decrease of the vHIP-OB FC could reflect a threshold level of the phosphorylated Tau density that would rather induce functional hypoconnectivity than hyperconnectivity. Supporting evidences of early olfactory dysfunction in presymptomatic AD patients [41], have already been shown and proposed as an early marker of AD.

Specific connections between the AMG and the vHIP are responsible for the emotional arousal effect on encoding and consolidation of memories [42]. AD patients are displaying atrophy of the AMG and disruptions in related function relying on the HIP-AMG complex [33, 43, 44]. Our investigation of the vHIP functional network showed a decrease of the vHIP-AMG FC in Thy-Tau22. Supporting these results, analysis of the DFC demonstrated specific modifications in vHIP and in AMG dynamic communication in transgenic mice, which preferentially stayed in highly correlated states suggesting a compensatory mechanism. Additionally, a high density of hyperphosphorylated Tau deposition in most of amygdalar nuclei was found. Thus, the decrease of the vHIP-AMG functional interaction could lead to a compensatory hypersynchrone response from dHIP toward AMG. Early pathological Tau deposition in those areas in Thy-Tau22 may contribute to create such an effect. Evidence of functional alterations of the AMG in MCI patients [45, 46] are in line with our findings suggesting a specific alteration of the HIP-AMG pathways of connectivity, leading to differential affectations of dorsal and ventral HIP at early stage of AD.

Our diffusion MRI investigation of white matter integrity showed alterations of the internal capsule connecting the basal ganglia, the HIP and cortical centers. Linking structural with FC, it has been shown that minimal structural damage can be sufficient to trigger an increase of FC toward compensatory mechanisms [3]. Therefore, microstructural alterations

along this cortico-subcortical pathway may result in failure of the efficient functional reorganization, participating to the functional hyperconnectivity in these regions in Thy-Tau22 mice. A decrease of the FA and a decline of the FD in the fornix, the lateral septum, the fimbria and the HIP, illustrated microstructural modifications of the septo-hippocampal pathway in transgenic mice, a cholinergic tract connecting the HIP with septal nuclei [47]. Affectations of the fornix-fimbria complex have also been shown in AD patients [47, 48], Thy-Tau22 mice [28] and on the VLW mouse strain expressing tauopathy [49], but never at a prodromal stage of the disease. Moreover, a great amount of pathological tau deposition was noticed in the septum of Thy-Tau22 that might enhance structural affectation of projecting tracts from this area to the HIP. With this, altered FD and FA found in CPu and TH of transgenic mice provide evidences of structural affectations to the whole limbic system architecture [50]. Therefore, the alteration of the dorso-ventral structural connectivity of the limbic system may be a crucial mechanism underlying early functional alterations in AD, suggested by the functional hypersynchrony of dHIP toward AMG and CPu, and a higher FC in prefrontal areas.

Our findings are giving supporting evidence of specific modifications of the connectome of a mouse model of tauopathy, at a time when mice do not present cognitive impairments yet. Functional and structural alterations of the HIP network notably toward AMG at such early stage of the disease constitute a strong lead toward the discovery of an early biomarker of AD.

Acknowledgments

The authors wish to thank Dr.Céline Meillier for very helpful discussions regarding functional image processing, Dr. Chantal Mathis for kindly providing supply and guidance for behavioral tests, and Dr. Chrystelle Po for her technical support at the MRI scanner. The project was developed using the IRIS imaging facility of ICube lab, Strasbourg. We thank the Alsace Region for the PhD Fellowship of Laetitia Degiorgis and Alsace Alzheimer Foundation for further support. LB's laboratory is supported by Programs d'Investissements d'Avenir LabEx (excellence laboratory) DISTALZ (Development of Innovative Strategies for a Transdisciplinary approach to ALZheimer's disease).

References

[1] Association AP. DSM-5 - Manuel diagnostique et statistique des troubles mentaux. Elsevier Masson; 2015.

[2] Serrano-Pozo A, Frosch MP, Masliah E, Hyman BT. Neuropathological alterations in Alzheimer disease. Cold Spring Harb Perspect Med 2011;1:a006189. doi:10.1101/cshperspect.a006189.

[3] Fornito A, Zalesky A, Breakspear M. The connectomics of brain disorders. Nat Rev Neurosci 2015;16:159–72. doi:10.1038/nrn3901.

[4] Greicius MD, Srivastava G, Reiss AL, Menon V. Default-mode network activity distinguishes Alzheimer's disease from healthy aging: evidence from functional MRI. Proc Natl Acad Sci U S A 2004;101:4637–4642.

[5] Sheline YI, Raichle ME. Resting State Functional Connectivity in Preclinical Alzheimer's Disease. Biol Psychiatry 2013;74:340–7. doi:10.1016/j.biopsych.2012.11.028.

[6] Sourty M, Thoraval L, Roquet D, Armspach J-P, Foucher J, Blanc F. Identifying Dynamic Functional Connectivity Changes in Dementia with Lewy Bodies Based on Product Hidden Markov Models. Front Comput Neurosci 2016;10. doi:10.3389/fncom.2016.00060.

[7] Bihan DL, Mangin J-F, Poupon C, Clark CA, Pappata S, Molko N, et al. Diffusion tensor imaging: Concepts and applications. J Magn Reson Imaging 2001;13:534–46. doi:10.1002/jmri.1076.

[8] Ringman JM, O'Neill J, Geschwind D, Medina L, Apostolova LG, Rodriguez Y, et al. Diffusion tensor imaging in preclinical and presymptomatic carriers of familial Alzheimer's disease mutations. Brain J Neurol 2007;130:1767–76. doi:10.1093/brain/awm102.

[9] Harsan L-A, Paul D, Schnell S, Kreher BW, Hennig J, Staiger JF, et al. In vivo diffusion tensor magnetic resonance imaging and fiber tracking of the mouse brain. NMR Biomed 2010;23:884–96. doi:10.1002/nbm.1496.

[10] Gozzi A, Schwarz AJ. Large-scale functional connectivity networks in the rodent brain. NeuroImage 2015. doi:10.1016/j.neuroimage.2015.12.017.

[11] Grandjean J, Schroeter A, He P, Tanadini M, Keist R, Krstic D, et al. Early Alterations in Functional Connectivity and White Matter Structure in a Transgenic Mouse Model of Cerebral Amyloidosis. J Neurosci 2014;34:13780–9. doi:10.1523/JNEUROSCI.4762-13.2014.

[12] Shah D, Praet J, Latif Hernandez A, Höfling C, Anckaerts C, Bard F, et al. Early pathologic amyloid induces hypersynchrony of BOLD resting-state networks in transgenic mice and provides an early therapeutic window before amyloid plaque deposition. Alzheimers Dement 2016;12:964–76. doi:10.1016/j.jalz.2016.03.010.

[13] Liu D, Lu H, Stein E, Zhou Z, Yang Y, Mattson MP. Brain regional synchronous activity predicts tauopathy in 3×TgAD mice. Neurobiol Aging 2018;70:160–9. doi:10.1016/j.neurobiolaging.2018.06.016.

[14] Schindowski K, Bretteville A, Leroy K, Bégard S, Brion J-P, Hamdane M, et al. Alzheimer's Disease-Like Tau Neuropathology Leads to Memory Deficits and Loss of Functional Synapses in a Novel Mutated Tau Transgenic Mouse without Any Motor Deficits. Am J Pathol 2006;169:599–616. doi:10.2353/ajpath.2006.060002.

[15] Van der Jeugd A, Vermaercke B, Derisbourg M, Lo AC, Hamdane M, Blum D, et al. Progressive age-related cognitive decline in tau mice. J Alzheimers JAD 2013;37:777–788.

[16] Laurent C, Dorothée G, Hunot S, Martin E, Monnet Y, Duchamp M, et al. Hippocampal T cell infiltration promotes neuroinflammation and cognitive decline in a mouse model of tauopathy. Brain 2017;140:184–200. doi:10.1093/brain/aww270.

[17] Hamm V, Héraud C, Bott J-B, Herbeaux K, Strittmatter C, Mathis C, et al. Differential contribution of APP metabolites to early cognitive deficits in a TgCRND8 mouse model of Alzheimer's disease. Sci Adv 2017;3. doi:10.1126/sciadv.1601068.

[18] Chatterjee S, Cassel R, Schneider-Anthony A, Merienne K, Cosquer B, Tzeplaeff L, et al. Reinstating plasticity and memory in a tauopathy mouse model with an acetyltransferase activator. EMBO Molecular Medicine 2018:e8587. doi:10.15252/emmm.201708587.

[19] Hübner NS, Mechling AE, Lee H-L, Reisert M, Bienert T, Hennig J, et al. The connectomics of brain demyelination: Functional and structural patterns in the cuprizone mouse model. NeuroImage 2017;146:1–18. doi:10.1016/j.neuroimage.2016.11.008.

[20] Smith SM, Miller KL, Salimi-Khorshidi G, Webster M, Beckmann CF, Nichols TE, et al. Network modelling methods for FMRI. NeuroImage 2011;54:875–91. doi:10.1016/j.neuroimage.2010.08.063.

[21] Veraart J, Novikov DS, Christiaens D, Ades-aron B, Sijbers J, Fieremans E. Denoising of diffusion MRI using random matrix theory. NeuroImage 2016;142:394–406. doi:10.1016/j.neuroimage.2016.08.016.

[22] Harsan L-A, David C, Reisert M, Schnell S, Hennig J, von Elverfeldt D, et al. Mapping remodeling of thalamocortical projections in the living reeler mouse brain by diffusion tractography. Proc Natl Acad Sci 2013;110:E1797–806. doi:10.1073/pnas.1218330110.

[23] Reisert M, Kiselev VG. Fiber Continuity: An Anisotropic Prior for ODF Estimation. IEEE Trans Med Imaging 2011;30:1274–83. doi:10.1109/TMI.2011.2112769.

[24] Braak H, Alafuzoff I, Arzberger T, Kretzschmar H, Del Tredici K. Staging of Alzheimer disease-associated neurofibrillary pathology using paraffin sections and immunocytochemistry. Acta Neuropathol (Berl) 2006;112:389–404. doi:10.1007/s00401-006-0127-z.

[25] Clarke JR, Cammarota M, Gruart A, Izquierdo I, Delgado-García JM. Plastic modifications induced by object recognition memory processing. Proc Natl Acad Sci U S A 2010;107:2652–7. doi:10.1073/pnas.0915059107.

[26] Lee I, Solivan F. The roles of the medial prefrontal cortex and hippocampus in a spatial paired association task. Learn Mem 2008;15:357–67. doi:10.1101/lm.902708.

[27] Van Cauter T, Camon J, Alvernhe A, Elduayen C, Sargolini F, Save E. Distinct Roles of Medial and Lateral Entorhinal Cortex in Spatial Cognition. Cereb Cortex 2013;23:451–9. doi:10.1093/cercor/bhs033.

[28] Belarbi K, Schindowski K, Burnouf S, Caillierez R, Grosjean M-E, Demeyer D, et al. Early Tau pathology involving the septo-hippocampal pathway in a Tau transgenic model: relevance to Alzheimer's disease. Curr Alzheimer Res 2009;6:152–7.

[29] Burlot M-A, Braudeau J, Michaelsen-Preusse K, Potier B, Ayciriex S, Varin J, et al. Cholesterol 24-hydroxylase defect is implicated in memory impairments associated with Alzheimer-like Tau pathology. Hum Mol Genet 2015;24:5965–76. doi:10.1093/hmg/ddv268.

[30] Stephen JM, Montaño R, Donahue CH, Adair JC, Knoefel J, Qualls C, et al. Somatosensory responses in normal aging, mild cognitive impairment, and Alzheimer's disease. J Neural Transm Vienna Austria 1996 2010;117:217–25. doi:10.1007/s00702-009-0343-5.

[31] Bakker A, Krauss GL, Albert MS, Speck CL, Jones LR, Stark CE, et al. Reduction of Hippocampal Hyperactivity Improves Cognition in Amnestic Mild Cognitive Impairment. Neuron 2012;74:467–74. doi:10.1016/j.neuron.2012.03.023.

[32] Dickerson BC, Salat DH, Greve DN, Chua EF, Rand-Giovannetti E, Rentz DM, et al. Increased hippocampal activation in mild cognitive impairment compared to normal aging and AD. Neurology 2005;65:404–11. doi:10.1212/01.wnl.0000171450.97464.49.

[33] Coupé P, Manjón JV, Lanuza E, Catheline G. Lifespan Changes of the Human Brain In Alzheimer's Disease. Sci Rep 2019;9. doi:10.1038/s41598-019-39809-8.

[34] Latif-Hernandez A, Shah D, Craessaerts K, Saido T, Saito T, De Strooper B, et al. Subtle behavioral changes and increased prefrontal-hippocampal network synchronicity in APPNL−G−F mice before prominent plaque deposition. Behav Brain Res 2019;364:431–41. doi:10.1016/j.bbr.2017.11.017.

[35] Fanselow MS, Dong H-W. Are the Dorsal and Ventral Hippocampus Functionally Distinct Structures? Neuron 2010;65:7–19. doi:10.1016/j.neuron.2009.11.031.

[36] Jones MW, Wilson MA. Theta Rhythms Coordinate Hippocampal–Prefrontal Interactions in a Spatial Memory Task. PLoS Biol 2005;3. doi:10.1371/journal.pbio.0030402.

[37] Wu JW, Hussaini SA, Bastille IM, Rodriguez GA, Mrejeru A, Rilett K, et al. Neuronal activity enhances tau propagation and tau pathology in vivo. Nat Neurosci 2016;19:1085–92. doi:10.1038/nn.4328.

[38] Kuchibhotla KV, Lattarulo CR, Hyman BT, Bacskai BJ. Synchronous Hyperactivity and Intercellular Calcium Waves in Astrocytes in Alzheimer Mice. Science 2009;323:1211–5. doi:10.1126/science.1169096.

[39] Martel G, Simon A, Nocera S, Kalainathan S, Pidoux L, Blum D, et al. Aging, but not tau pathology, impacts olfactory performances and somatostatin systems in THY-Tau22 mice. Neurobiol Aging 2015;36:1013–28. doi:10.1016/j.neurobiolaging.2014.10.033.

[40] Kovács T. Mechanisms of olfactory dysfunction in aging and neurodegenerative disorders. Ageing Res Rev 2004;3:215–32. doi:10.1016/j.arr.2003.10.003.

[41] Wilson RS, Arnold SE, Schneider JA, Boyle PA, Buchman AS, Bennett DA. Olfactory; Impairment in Presymptomatic Alzheimer's Disease. Ann N Y Acad Sci 2009;1170:730–5. doi:10.1111/j.1749-6632.2009.04013.x.

[42] Phelps EA. Human emotion and memory: interactions of the amygdala and hippocampal complex. Curr Opin Neurobiol 2004;14:198–202. doi:10.1016/j.conb.2004.03.015.

[43] Poulin SP, Dautoff R, Morris JC, Barrett LF, Dickerson BC, Alzheimer's Disease Neuroimaging Initiative. Amygdala atrophy is prominent in early Alzheimer's disease and relates to symptom severity. Psychiatry Res 2011;194:7–13. doi:10.1016/j.pscychresns.2011.06.014.

[44] Miller MI, Younes L, Ratnanather JT, Brown T, Trinh H, Lee DS, et al. Amygdalar atrophy in symptomatic Alzheimer's disease based on diffeomorphometry: the BIOCARD cohort. Neurobiol Aging 2015;36 Suppl 1:S3–10. doi:10.1016/j.neurobiolaging.2014.06.032.

[45] Yao H, Liu Y, Zhou B, Zhang Z, An N, Wang P, et al. Decreased functional connectivity of the amygdala in Alzheimer's disease revealed by resting-state fMRI. Eur J Radiol 2013;82:1531–8. doi:10.1016/j.ejrad.2013.03.019.

[46] Ortner M, Pasquini L, Barat M, Alexopoulos P, Grimmer T, Förster S, et al. Progressively Disrupted Intrinsic Functional Connectivity of Basolateral Amygdala in Very Early Alzheimer's Disease. Front Neurol 2016;7:132. doi:10.3389/fneur.2016.00132.

[47] Thomas AG, Koumellis P, Dineen RA. The Fornix in Health and Disease: An Imaging Review. RadioGraphics 2011;31:1107–21. doi:10.1148/rg.314105729.

[48] Copenhaver BR, Rabin LA, Saykin AJ, Roth RM, Wishart HA, Flashman LA, et al. The fornix and mammillary bodies in older adults with Alzheimer's disease, mild cognitive impairment, and cognitive complaints: A volumetric MRI study. Psychiatry Res Neuroimaging 2006;147:93–103. doi:10.1016/j.pscychresns.2006.01.015.

[49] Soler H, Dorca-Arévalo J, González M, Rubio SE, Ávila J, Soriano E, et al. The GABAergic septohippocampal connection is impaired in a mouse model of tauopathy. Neurobiol Aging 2017;49:40–51. doi:10.1016/j.neurobiolaging.2016.09.006.

[50] Rajmohan V, Mohandas E. The limbic system. Indian J Psychiatry 2007;49:132–9. doi:10.4103/0019-5545.33264.

Supplementary material

1. Behavior tests

1.1. Objects tasks

To assess the cognitive state of mice, we performed object memory tests, allowing to highlight mild memory alterations in mice in different brain structures, including the hippocampus, entorhinal, perirhinal cortex and frontal cortices [1].We used a square Plexiglas open-field (52cmx52cm) for the tests and spatial cues were disposed on the wall of the open-field. Each task was divided in 2 phases: a habituation phase, and a retention phase. In the first phase of habituation, the mouse was allowed to explore the objects in the open-field for 10 minutes in the object recognition (OR) and object location (OL) tests, and for 15 minutes in the object in-place (OIP) task. The mouse was then put back in its cage and after 3h in the case of OR and OL tasks, and 5min for the OIP task, one object was either changed, moved or replaced for the retention phase. We then measured the time spend by the mouse exploring each of the objects, and, based on the spontaneous behavior of rodents to preferentially explore novelty, expected the mouse to spend significantly more time exploring the either changed, moved or replaced object (one-sample t-test comparing with the level of chance, $p<0.05$). Therefore, if the mouse does not detect the novelty, it is considered that it does not correctly remember the previous configuration of objects, and thus has memory disruptions in this task. Each task was divided in 2 phases: a habituation phase, and a retention phase. In the first phase of habituation, the mouse was allowed to explore the objects in the open-field for 10 minutes in the object recognition (OR) and object location (OL) tests, and for 15 minutes in the object in-place (OIP) task. The mouse was then put back in its cage and after 3h in the case of OR and OL tasks, and 5min for the OIP task, one object was either changed, moved or replaced for the retention phase. We then measured the time spend by the mouse exploring each of the objects, and, based on the spontaneous behavior of rodents to preferentially explore novelty, expected the mouse to spend significantly more time exploring the either changed, moved or replaced object (one-sample t-test comparing with the level of chance, $p<0.05$). Therefore, if the mouse does not detect the novelty, it is considered that it does not correctly remember the previous configuration of objects, and thus has memory disruptions in this task.

1.2. The Morris Water Maze

Mice were submitted to a classical hippocampus dependent task, spatial reference memory tested in the MWM. After 2 days of habituation, mice have to learn the fixed position of a platform hidden beneath opacified water in a circular pool with the help of distal cues. They were trained for 5 days, 4 trials a day. The time spent and the path length before reaching the

platform was measured using a video tracking system (Anymaze). Ten days after the learning phase, a probe test was performed where the platform was removed. In this phase mice had 60s in the pool during which we evaluated the time spent in the target quadrant, corresponding to the quadrant where the platform was previously located. Analysis of long-term retention (10-day probe test) is mainly dependent on hippocampus and frontal cortex interactions [1]. We used a one-way ANOVA with repeated measures and corrected for multiple comparison by a Tukey test, to analyze and compare learning abilities of mice. For the probe test, the time spent in the target quadrant was compared with the chance level (15s for a test duration of 60s in four quadrants) using a one-sample t-test.

2. MRI experiments

2.1. Animal preparation

For rsfMRI acquisition, moderate MD sedation was initially induced by a subcutaneous (*sc*) bolus injection (0.6 mg MD per kg body weight in 100 µl 0.9% NaCl-solution). 15 min later, the animals received a continuous *sc* infusion of MD through an MRI compatible catheter (0.3 mg per kg body weight in 200 µl per hour) inserted at the mouse shoulder level. During the whole acquisition a 2 mm thick agar gel (2% in NaCl) was applied on the mouse head to reduce any susceptibility artifacts arising at the coil/tissue interface. MD infusion was stopped and replaced by anesthesia through isoflurane (∼1.5 % of volume) for further morphological and diffusion-based imaging protocol.

2.2. Preprocessing

The SPM function of co-registration was used to realign each functional scan to its corresponding T2-weighted image. A step of realignment of the 500 volumes to the first scan was applied as a motion correction (using a least square approach and a 6-parameters rigid body transformation in space). Normalization of the data was done on a template extracted from the Allen Brain Atlas (http://mouse.brain-map.org/static/atlas) involving a linear registration – 12-parameters affine transformation – accounting for major differences in head shape and position in between subjects as well as nonlinear registration – warping – accounting for smaller-scale anatomical differences. We performed a Gaussian smoothing with a kernel of 2 voxels FWHM to all fMRI image volumes and a zero-phase band-pass filter was applied to extract frequencies between 0.01-0.1 Hz, representatives of the Blood Oxygen Level Dependent (BOLD) signal. The signal from ventricles was regressed out using a least square approach in order to reduce non-neural detection from the cerebro-spinal fluid.

2.3. Partial correlation (PC) analysis

PC coefficients between each pair of ROIs, by controlling correlation mediated by other ROIs, were calculated using their associated preprocessed mean time-course (TC) of the signal. Each element of the matrix represents the strength of functional connectivity between two ROIs. PC matrices were generated for each mouse separately and normalized with a Fisher's z-transformation. To create a ranking of the number of significant connections per ROI in each

group, we assessed the significance of positive correlations with a one sample t-test thresholded at $p<0.001$ and corrected for multiple comparison (False Discovery Rate), as previously described [2].

2.4. Dynamic functional connectivity (DFC)

This method from Sourty et al., 2016 [3], based on multidimensional hidden Markov models and sliding-window correlation approach, captures both statistical and temporal aspects of DFC. An assumption is made that the brain is in one global brain connectivity pattern, called state, at each time point. The relationship between one ROI and all the other ROIs is modeled at subject-level with this method to obtain a temporal state sequence. This sequence of states and specific dynamic features can then be used for group comparison.

2.5. Voxel based morphometry (VBM) analysis was performed on T2-weighted images, registered and normalized to a common template using ANTS tool [4]. Jacobians determinants were calculated for each mouse from the deformation fields applied for spatial normalization, and smoothed with a spatial smoothing full width at half-maximum (FWHM) of 0.5mm. Voxel-based statistics were applied (two-sample t-test, $p<0.05$ FDR cluster corrected) on deformation maps.

3. Immunofluorescence

Animals used for immunohistochemical studies were deeply anesthetized with pentobarbital sodium (50 mg/kg, i.p.), then transcardially perfused with cold NaCl (0.9%). Brains were removed, post-fixed for 48h in 4% paraformaldehyde fixative in PBS (pH 7.4) and cryoprotected in 30% sucrose before being frozen at -40°C in isopentane (methyl-butane) and stored at -80°C. Coronal brains sections (35 µm) were obtained using a Leica cryostat. Free-floating sections were chosen according the stereological rules, with the first section taken at random and every twelve's sections afterwards, and were stored in a PBS-azide (0.2 %) at 4°C. Two successive staining were realized to investigate astrogliosis and hyperphosphorylated tau using antibodies directed against GFAP (glial fibrillary acidic proteins) and phosphorylated Tau at Ser202/Thr205 sites (AT8 antibody), respectively. First, brain cryosections were washed three times in 0.2% Triton X-100/PBS prior being incubated for 1h in normal goat serum (NGS, Vector Laboratories). The sections were then incubated overnight with primary rabbit anti-GFAP antibody (1/500; Dako Laboratories) diluted in NGS (5%) at 4°C. Alexa Fluor 568 goat anti-rabbit secondary antibody (1/500; Life technology) was used on sections for 1h at room temperature. After three additional wash steps with PBS, slices were incubated with 10% of Mouse On Mouse Kit serum (Vector Laboratories) for 1h and then with mouse anti-AT8 antibody (1/1000, Thermofisher) overnight at 4°C. Primary antibody was revealed using Alexa Fluor 488 goat anti-mouse secondary antibody (1/500, Life technology). Sections were counterstained with DAPI (1/5000, 62248, Thermoscientific) to reveal nuclei and treated in 0.3% Suden Black (Sigma-Aldrich) with 70% ethanol for 10 min to block autofluorescence. Slices were mounted with Dako Fluorescent mounting medium. Images were acquired using Zeiss Axioscan Z1 slide scanner.

Supplementary table and figures

Supplementary table 1: MRI acquisition parameters for the three used sequences.

	T2-RARE	GE-EPI	DTI-EPI
Acquisition time	9min47sec	16min40sec	1h1min3sec
Field of view	2,1 x 2 cm^2	2.1 x 2 cm^2	2.1 x 2 cm^2
Resolution	0.08 x 0.07 mm^2	0.14 × 0.22 mm^2	0.1 x 0.1 mm^2
Slice thickness	0.4 mm	0.4 mm	0.5 mm
Echo time/repetition time	40/4500 ms	15ms/2000 ms	28/3000 ms
Number of volumes	/	500 volumes	/
B-values	/	/	500, 1000, 1500, 1750, 2000 s/mm^2
Diffusion parameters	/	/	Diffusion gradient duration (δ): 5 ms Time between the two diffusion gradients (Δ) = 10.64 ms

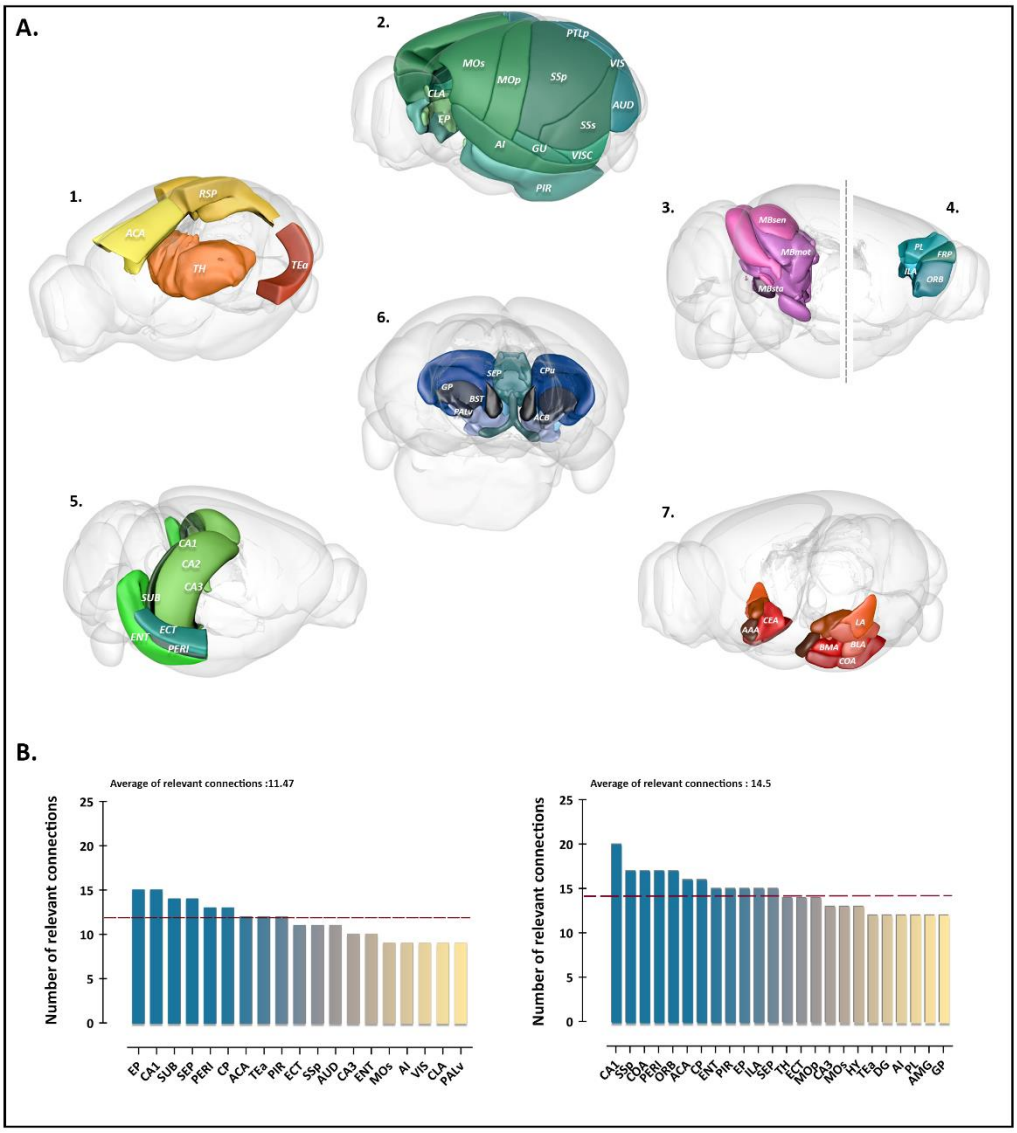

1. DMN-like network
ACA: Anterior cingulate area
RSP: Retrosplenial area
TEa: Temporal Association area
TH: Thalamus
2. Cortical areas
MOp: primary Motor area
MOs: secondary Motor area
SSp: primary Somatosensory area
SSs: supplemental Somatosensory area
PTLp: Posterior parietal association areas
VIS: Visual areas
AUD: Auditory areas
AI: Agranular Insula
GU: Gustatory areas
VISC: Visceral areas
PIR: Piriform area
CLA: Claustrum
EP: Endopiriform nucleus
3. Midbrain
MBsen: sensory related
MBmot: motor related
MBsta: behavior related
4. Frontal regions
FRP: Frontal pole
PL: Prelimbic area
ILA: Infralimbic area
ORB: Orbital area
5. Memory-related regions
CA1-CA2-CA3: Ammon's horn
SUB: Subiculum
ENT: ENtorhinal area
ECT: Ectorhinal area
PERI: Perirhinal area
6. Striato-pallidal system
CPu: Caudoputamen
ACB: Nucleus Accumbens
SEP: Septum
GP: Globus Pallidus
BST: Bed nuclei of the Stria Terminalis
PALv: ventral Pallidum
7. Amygdalar nuclei
CEA: Central Amygdalar nucleus
AAA: Anterior Amygdalar nucleus
LA: Lateral Amygdalar nucleus
BLA: Basolateral Amygdalar nucleus
BMA: Basomedial Amygdalar nucleus
COA: Cortical Amygdalar Area

Supplementary Figure 1: *Ranking of the most connected brain areas in WT and Thy-Tau22 mice. (A) 3D representations of the 42 ROIs included in the 42x42 matrix used to generate the ranking of the highest number of relevant functional connections, associated with their corresponding abbreviations (right column). (B) Ranking of the most functionally connected ROIs in WT (left) and Thy-Tau22 mice (right), calculated from a weighted undirected matrix (WUM) associated with the relevance of significant positive correlation ($p<0.01$; one sample t-test; FDR voxel corrected) given by a binary undirected matrix (BUM) as previously described (Mechling et al, 2014).*

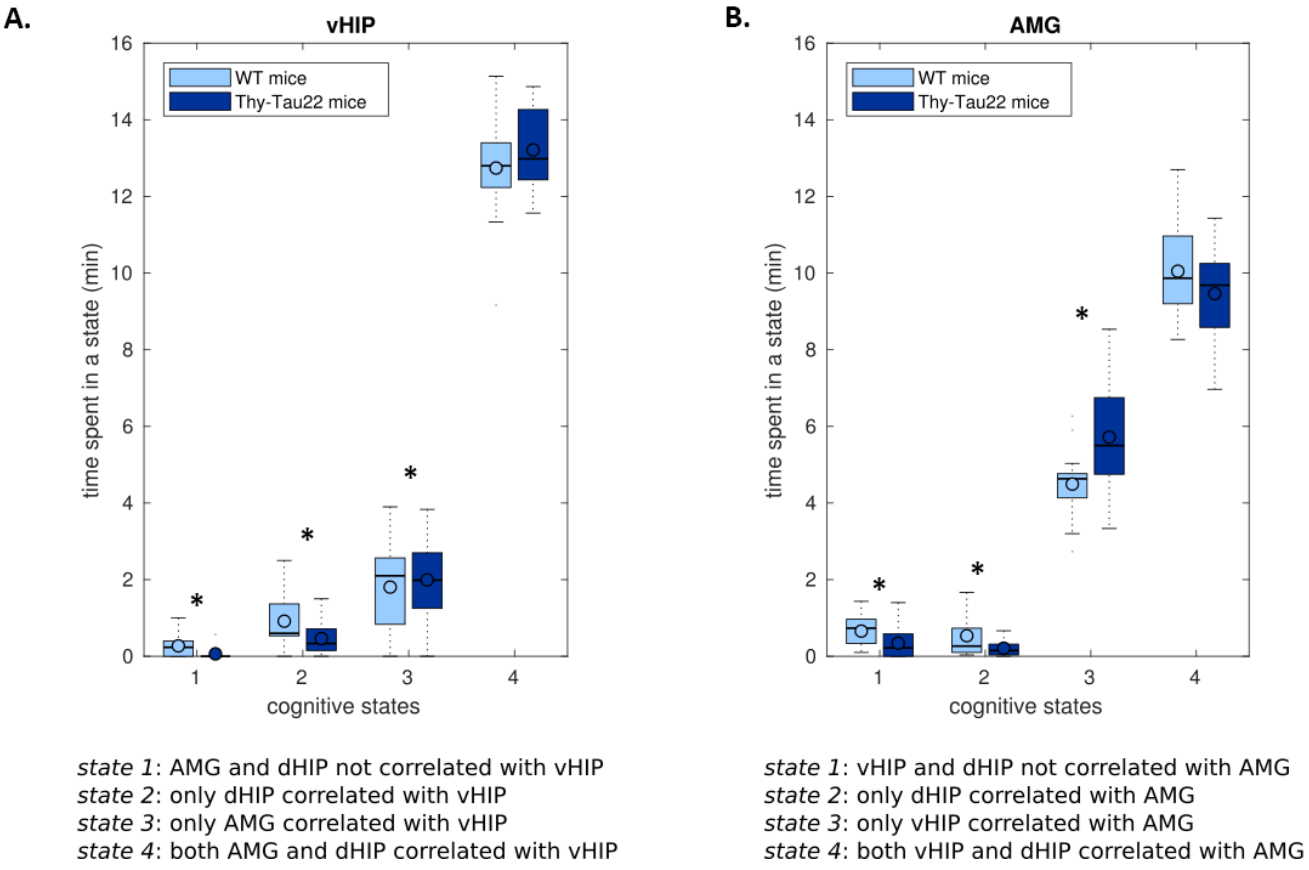

state 1: AMG and dHIP not correlated with vHIP
state 2: only dHIP correlated with vHIP
state 3: only AMG correlated with vHIP
state 4: both AMG and dHIP correlated with vHIP

state 1: vHIP and dHIP not correlated with AMG
state 2: only dHIP correlated with AMG
state 3: only vHIP correlated with AMG
state 4: both vHIP and dHIP correlated with AMG

Supplementary Figure 2: *Dynamic Functional Connectivity of vHIP and AMG toward dHIP, generating 4 possible states of connectivity: all ROIs correlated, all decorrelated, only the first one correlated, only the second one correlated. (A) Time spent in each state of connectivity of vHIP toward dHIP and AMG during the whole acquisition time of the fMRI sequence, for each group. Results show significant differences between groups in state 1,2 and 3, when at least one ROI is decorrelated to vHIP. WT mice spent significantly more time in states presenting decorelations to vHIP, compared to Thy-Tau22. Transgenic mice are thus spending most time in highly correlated states (B) Time spent in each state of connectivity of AMG toward vHIP and dHIP during the whole acquisition time of the fMRI sequence, for each group. Results show significant differences between groups in state 1,2 and 3, when at least one ROI is decorrelated to AMG. WT mice spent significantly more time in states presenting decorelations to vHIP, compared to Thy-Tau22. Transgenic mice are thus spending most time in highly correlated states.*

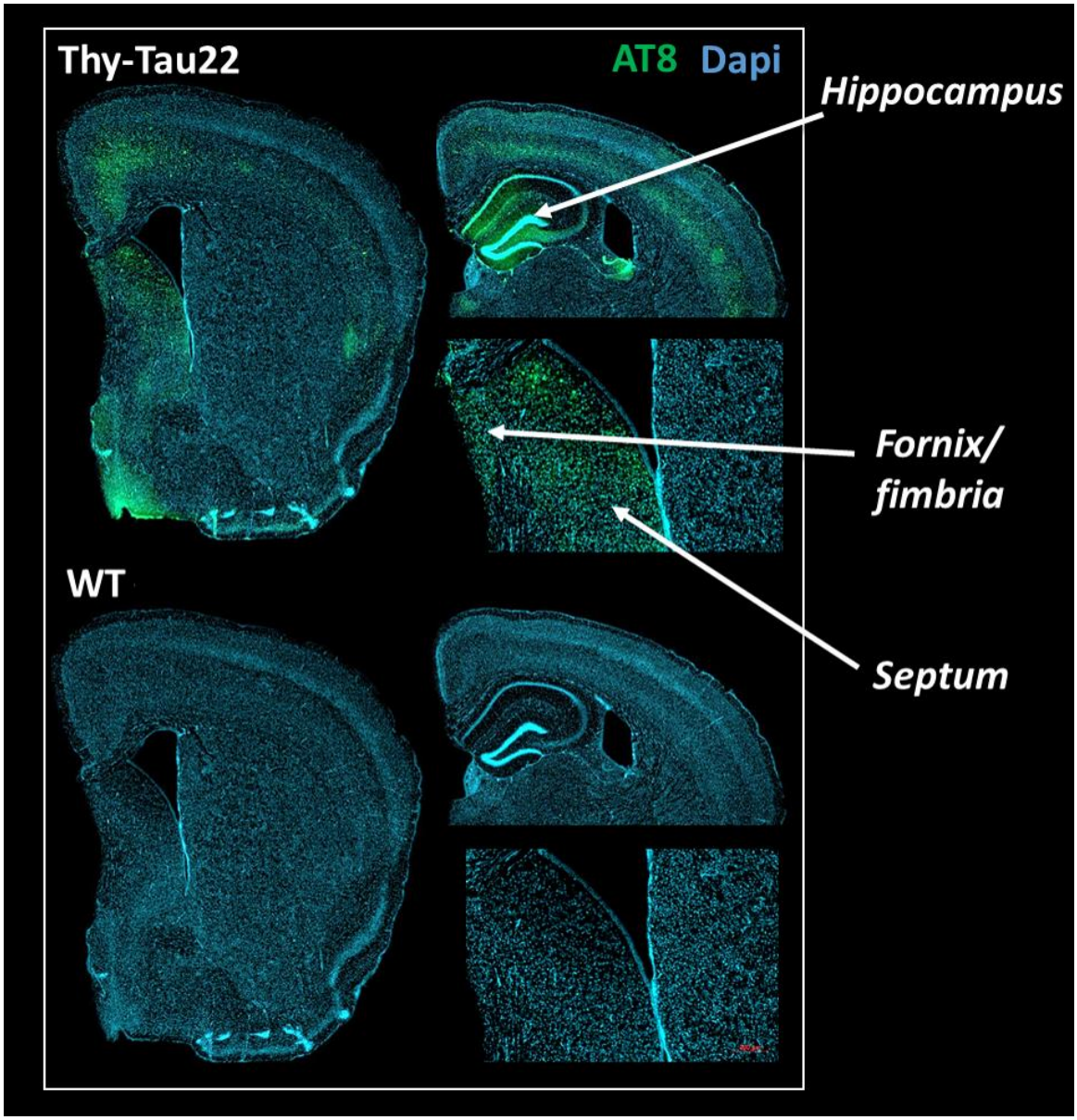

Supplementary Figure 3: *Pathological Tau staining in the septo-hippocampal pathway. Immunofluorescence of the AT8 marker of hyperphosphorylated Tau revealed a high deposit of the pathological protein in the hippocampus, the fornix, the fimbria and the septum.*

References

[1] Frankland PW, Bontempi B. The organization of recent and remote memories. Nature Reviews Neuroscience 2005;6:119. doi:10.1038/nrn1607.

[2] Mechling AE, Hübner NS, Lee H-L, Hennig J, von Elverfeldt D, Harsan L-A. Fine-grained mapping of mouse brain functional connectivity with resting-state fMRI. NeuroImage 2014;96:203–15. doi:10.1016/j.neuroimage.2014.03.078.

[3] Sourty M, Thoraval L, Roquet D, Armspach J-P, Foucher J, Blanc F. Identifying Dynamic Functional Connectivity Changes in Dementia with Lewy Bodies Based on Product Hidden Markov Models. Frontiers in Computational Neuroscience 2016;10. doi:10.3389/fncom.2016.00060.

[4] Avants BB, Tustison NJ, Song G, Cook PA, Klein A, Gee JC. A reproducible evaluation of ANTs similarity metric performance in brain image registration. Neuroimage 2011;54:2033–44. doi:10.1016/j.neuroimage.2010.09.025.

Additional results to the study 1:

While investigating hyperphosphorylated Tau staining in 5 months-old brains of Thy-Tau22 mice, we detected a substantial amount of pathological Tau in prefrontal areas. Moreover, AD has been associated with noncognitive behavioral changes, such as depression, apathy, agitation, psychosis or anxiety, especially manifesting at very early stages of the disease [246]. These phenotypes are particularly associated with frontal areas connectivity alterations, as reviewed in Victoroff et al., 2018 [247]. Therefore, we performed a seed-based analysis of the frontal pole functional connectivity, in addition with group comparison analysis between Thy-Tau22 and WT mice (annex Fig.1). Results showed a global increased of the functional connectivity of the frontal pole. We found a significantly higher functional relation between this region and the hippocampus, in addition with related memory areas such as the entorhinal cortex and the subiculum. Moreover, the functional communication of the frontal pole was found higher with several cortical areas, notably the primary somatosensory cortex, the posterior parietal associative area, the temporal associative area, and the piriform cortex. Similarly to the ventral and dorsal hippocampus functional connectivity in Thy-Tau22, we highlighted an increase of the connectivity of the frontal pole with the caudate putamen nucleus. Finally, we detected a higher functional relation with the midbrain, a projecting area of the prefrontal cortex [248]. A decrease of the frontal pole functional connectivity was found with only two areas: the triangle nucleus of septum, and the thalamus. These all three regions are part of the limbic system [249], playing a role in controlling emotions.

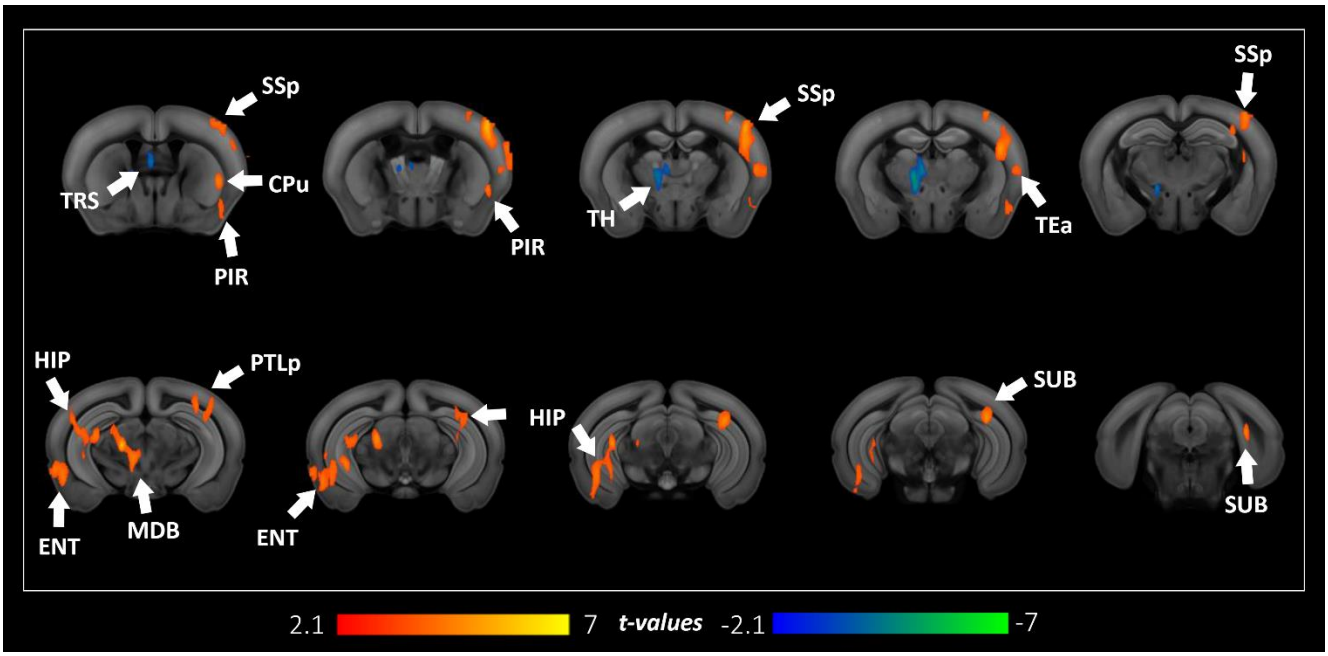

Annex figure 1: Early functional prefrontal modifications in Thy-Tau22 mice. *Coronal slices of the seed-based analysis of the frontal pole functional network showing statistical group comparison maps. An increased functional connectivity in Thy-Tau22 compared to WT mice is illustrated with positive values (red), and a decrease in negative values (blue). Only statistically significant differences calculated using a two-sample t-test, $p<0.05$, FDR cluster-corrected, are shown.*

Conclusion:

From this first study, we detected alterations of specific patterns of the connectome, combining both functional and structural analysis, in a mouse model of AD. In particular, we revealed an early hyperconnectivity of the hippocampus, with differential affectations of the dorsal and ventral subregions, especially with the amygdala. We looked at the prefrontal connectivity based on literature findings, and observed a higher global functional connectivity of this area. We also explored early microstructural affectation in transgenic mice and highlighted damaged in the septo-hippocampal pathway, a cholinergic pathway affected in AD. Those connectomics modifications and pathological deposition of hyperphosphorylated Tau and astrocytes at this age were found overlapping, suggesting a toxic mechanism that might trigger the remodeling of functional architecture and microstructural affectations. We hypothesized that the functional modifications showing an increased connectivity in several AD-related areas might result from a compensatory mechanism, driven by microstructural damaged induce by toxic protein activity.

To further explore the morphological, functional, and structural changes in the brain of Thy-Tau22 mice, we conducted a longitudinal analysis of the connectome's modification over a period of time of 8 months, including investigations of prodromal, intermediate and tardive states of the disease. We combined for the first time in a mouse model of tauopathy, MRI analysis with behavioral assessment of memory abilities in mice, and histological staining of tauopathy-related proteins in order to obtain a complete overview of the brain-related changes in this model.

C) Study 2 – In Preparation

Longitudinal evaluation of the brain connectome of a mouse model of Alzheimer's disease

1. Introduction

Alzheimer's disease (AD) is a neurodegenerative disease exhibiting progressive brain alterations such as synapses dysfunction and neuronal loss and functional modifications, leading to cognitive impairment especially involving mnesic abilities [1]. To understand the mechanisms mediating those progressive changes, longitudinal investigations are as inevitable as they are complex, regarding the difficulty of an early and robust diagnosis of AD.

Using Magnetic Resonance Imaging (MRI) as a non-invasive tool gives the opportunity to carry out a follow-up of the brain connectivity -or connectome-, providing the keys to understand how the brain architecture and network communication's modifications relate to the evolution of the symptomatology, cognitive abilities or response to therapeutic strategies [2]. This growing way of studying neurodegenerative disorders is probing both functional and structural connectivity in the brain, reflecting respectively the detection of coordinated activity between brain areas, and the exploration of the fiber bundles organization [3]. For modeling and characterizing the topological properties of the cerebral networks, graph theory approaches have been developed [4] and applied extensively in recent years in both, humans and animal models. Therefore, in association with morphological evaluation overtime, connectomics MRI open up the opportunity to get a unique overview of the brain longitudinal evolution in AD. Cognitive disorders have already been associated with connectome's affectations in AD patients [5], and functional communication dysfunctions have been highlighted especially in the default mode network (DMN) [6] and in limbic areas networks such as the hippocampus and amygdala [7,8]. AD patients also exhibit microstructural alterations in white matter tracts such as the cingulum bundle, the fornix, and the perforant path, all three connecting memory regions [9]. However, only a few recent MRI studies have been performed in Human in a longitudinal manner, mostly following the morphological evolution overtime [10–13], or inferring microstructural changes [14] using diffusion tensor imaging (DTI). Such features however most likely appear several years after the onset of the pathology [15].

Longitudinal brain MRI studies in rodent models of neurodegeneration offer the unique opportunity of exploring the brain structure and function even before the emergence of cognitive decline, and following up the modifications across lifespan along with the progression of the pathology. As one of the most informative approaches on the disease's mechanisms, mapping of the connectome can be done in preclinical models at different levels meso- and micro- scale. High resolution DTI and resting state functional MRI (fMRI) - probing brain wide communication - can be combined with intra-vital multi-photon microscopy [16] or ex-vivo histopathology to investigate specific microcircuits. Together with behavioral evaluation such approaches may identify susceptible pathways or vulnerable cerebral network hubs, triggered by the main mechanisms of AD. While several previous imaging studies in mice evaluated the connectome features in relationship with the amyloïd hypothesis [17–19] only a few recent reports focused on the tauopathy, a crucial mechanism known to strongly

correlate with cognitive deficits in AD [20]. Following a selective and predictable course defined by Braak stages [21], an imbalance of specific kinases and phosphatases of the Tau protein in the brain is inducing its pathological phosphorylation and/or hyperphosphorylation, conducting to its malfunction in AD [22–24]. This abnormal mechanism leads to a misfolded state of tau, which then agglomerates into toxic neurofibrillary tangles (NFT). Pathological forms of the Tau protein are involved in progressive axonal disturbance, synapses dysfunction, mitochondrial loss and neuronal death [25], and are thus likely to trigger cascades of functional and structural network affectations in AD. Circuitry malfunctions can however be accompanied by circuity remodeling and activation of compensatory pathways, especially in the early phases of the disease.

A comprehensive picture of the evolution of both structural and functional network reorganization across lifespan in specific tauopathy models was not mapped so far. A recent DTI study investigated white matter (WM) changes and linked microstructural alterations in the hippocampus of 3xTG mice expression both amyloïd and Tau pathology [26]. A longitudinal study on the same model also revealed important microstructural changes from early onset of the disease to late stages in the fimbria -the main output of the hippocampus- and the external capsule, both being route for cholinergic fibers from basal forebrain [27]. Using fMRI measures, tau pathology has been associated with an early functional hyperconnectivity in the hippocampus in the 3xTG mice [28]. Only one longitudinal study using DTI focused on a tauopathy mouse model, investigating fibers alterations overtime and described early cortical modifications, along with later WM affectations associated with tauopathy development [29].

In our study, we associated longitudinal MRI investigation of the brain structural and functional connectome of the Thy-Tau22 mouse model of tauopathy with the behavioral evolution of memory abilities and histopathological staining detecting the progression of neurotoxic mechanisms. This study is thus providing a comprehensive and robust insight of the Tau pathology evolution and its impact on the brain connectivity from early onset to late stage of the disease, combining morphological, microstructural and functional findings in relation with cognitive and biological evolution.

2. Material and methods

2.1. Animals

All experimental protocols were approved by the Regional Committee of Ethic in Animals Experiment of Strasbourg (CREMEAS, APAFIS n°2016033011298450). 16 transgenic Thy-Tau22 and 13 littermates wild-type (WT) male mice were used for both behavioral experiments and MRI studies at 5, 9 and 13 months (Fig.1). A second cohort matching in age was used for histological staining. Mice were randomly housed in pairs allowing social behavior. In this model, the human mutated tau protein (G272V and P301S) is overexpressed under the Thy1.2 brain promoter, leading to abnormal phosphorylation of the Tau protein, and later to neurofibrillary tangles' (NFT) formation.

2.2. Behavioral tests

Classical behavior tests evaluating memory in mice have been used on both WT and Thy-Tau22 group of mice at 5, 9 and 13 months, before the MRI experiment (Fig. 1, A). We used the object recognition test and the object in place test at all three investigated time-points, and the Morris Water Maze (MWM) in 5 and 13 months-old mice, following protocols previously described in Hamm et al., 2017 [30] and Chatterjee et al., 2018 [31] (See supplementary material 1).

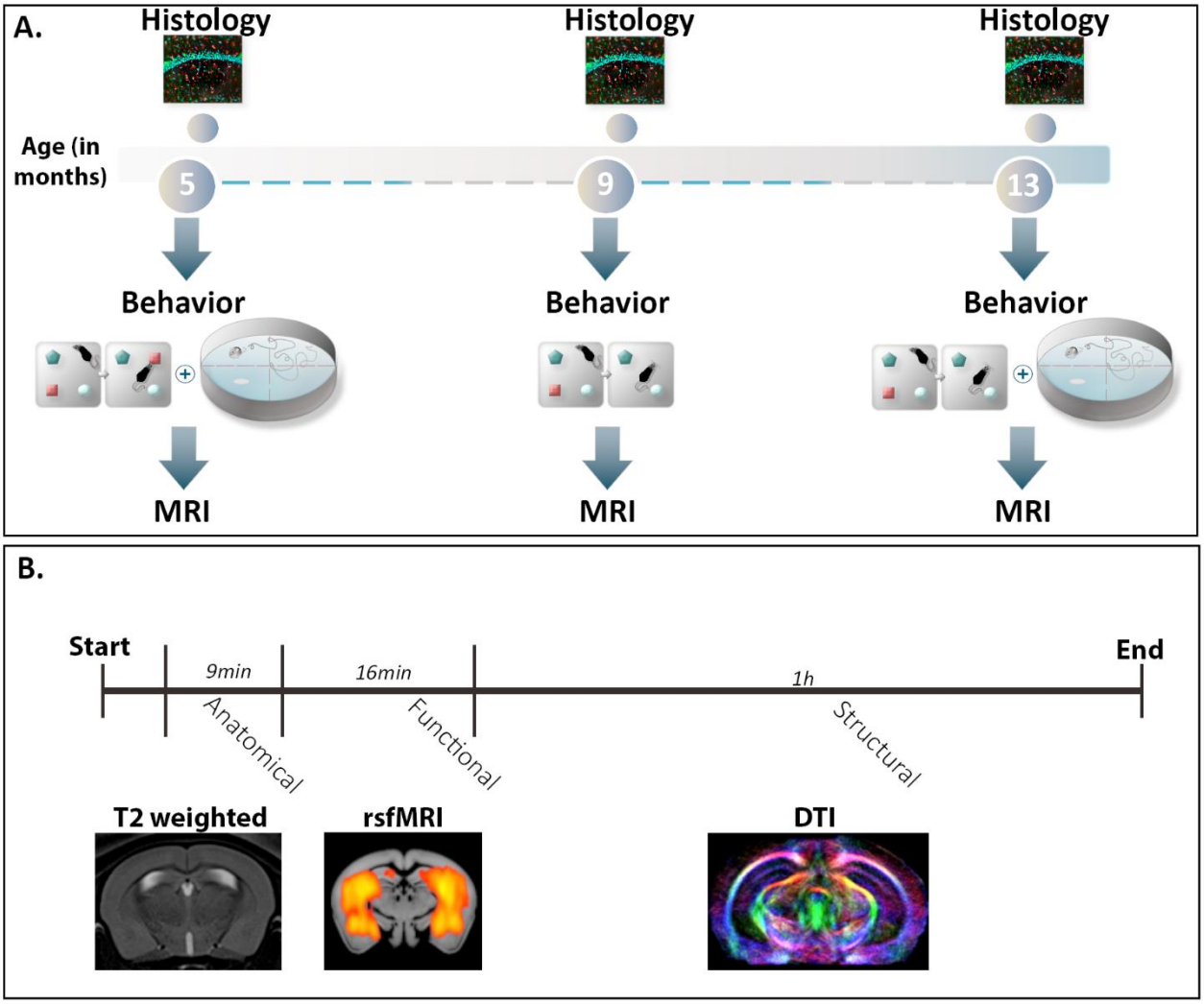

Figure 1: *Methodological pipeline of the study. A) Illustration of the study timeline. The MRI experiments and the behavioral tests were performed on the same groups of mice (n=13 WT and n=16 Thy-Tau22) at three time-points, reflecting early (5 months), intermediate (9 months) and tardive (13 months) stages of the disease in Thy-Tau22 mice. Brain tissue histological staining was carried-out on another cohort of mice matched in age. B) Illustration of the MRI acquisition. For each mouse, we performed T2-weighted imaging, resting-state fMRI (rsfMRI) and DTI acquisition. Those images were further analyzed to explore morphological, functional and structural changes in both Thy-Tau22 and WT mice.*

1.1. MRI experiments: images acquisition and processing

Brain MRI was carried-out in the two animal groups using a 7T small bore animal scanner (BioSpec 70/30, Bruker, Germany), a mouse head adapted room temperature surface coil combined with a volume transmission coil, and Paravision 6.0.1 (PV6, Bruker, Ettlingen, Germany), following a protocol illustrated in figure 1, B. The animals were briefly anesthetized with isoflurane for initial animal handling. The anesthesia was further switched to medetomidine sedation (MD, Domitor, Pfizer, Karlsruhe, Germany, bolus of 0.6 mg MD per kg body weight in 100 µl 0.9% NaCl-solution followed after 25 min by continuous sc infusion of medetomidine - 0.3 mg/kg body weight in 200 µl/hour). Mouse physiological conditions (body temperature and respiration) were monitored continually during the imaging. RsfMRI data were acquired in 16 min using single shot gradient-echo, echo-planar imaging (GE-EPI), imaging 500 volumes. 27 axial slices of 0.4 mm thickness were recorded in interlaced fashion, covering the entire brain (Echo Time/Repetition Time=15/2000ms, spatial resolution=0.14x0.22mm^2; slice thickness = 0.4mm; Field Of View (FOV) = 2.1 x 2 cm^2). A diffusion tensor imaging – echo planar imaging (DTI-EPI) sequence was used to perform High Angular Resolution Diffusion Imaging (HARDI). 27 slices of 0.5 mm were recorded (spatial resolution = 0.1x0.1mm^2; FOV = 2.1 x 2 cm^2) with 30 gradient diffusion directions of 5 ms duration (δ) and separated of 10.64 ms (Δ), 5 b-values (500, 1000, 1500, 1750, and 2000 s/mm^2). The imaging covered the equivalent partition of the brain as in the rsfMRI scan (See supplementary table 1). Anatomical images were acquired using a multislice (34 slices of 0.4 mm; spatial resolution = 0.08 x 0.07 mm^2; FOV = 2.1 x 2 cm^2) Rapid Acquisition with Relaxation Enhancement (RARE) T2-weighted sequence (TE/TR = 40/4500ms). After the experiment, the animals were subcutaneously injected with 100µl of saline solution and allowed to spontaneously recover from anesthesia. See supplementary material 2.1 for detailed procedure.

Data processing and analysis:

We first performed *microstructural HARDI data analysis and fiber tractography*. After HARDI data denoising, using the MRtrix software [32], parametric maps of fractional anisotropy (FA) were generated for each mouse and spatially normalized to an average template using the ANTS tools [33]. A Global fiber tracking approach was further used as previously described [34], to perform global mouse brain tractography. Fiber density (FD) maps were constructed for each mouse brain from the number of streamlines passing in each voxel, and registered to an average template (ANTS, [33]). We then performed an inter-group voxel-based quantification (VBQ) of FA, FD maps and statistical analysis using a two-sample t-tests to infer microstructural modifications related to the tau pathology (Thy-Tau22 group *vs.* WT group at different timepoints; $p<0.01$, cluster-based correction thresholded at $p<0.01$, corrected for multiple comparisons (FDR) by using the null distribution of the max from FSL software).

Voxel based morphometry (VBM) analysis was performed on T2-weighted images, registered and normalized to a common template using ANTS tool [33]. Jacobians determinants were calculated for each mouse from the deformation fields applied for spatial normalization, and smoothed with a spatial smoothing full width at half-maximum (FWHM) of 0.5mm. Voxel-

based inter-groups statistics (Thy-Tau22 group *vs.* WT group at different timepoints; two-sample t-test, $p<0.001$ FDR cluster corrected) were applied on deformation maps.

Preprocessing of fMRI data was performed using Statistical Parametric Mapping (SPM8, http://www.fil.ion.ucl.ac.uk/spm/) with SPMmouse (www.spmmouse.org) for MATLAB (The MathWorks, Natick, Massachusetts) as previously described [35] and given in the supplementary material 2.2).

Partial Correlation (PC) analysis was performed to evaluate direct temporal correlations between spatially separated regions of interest (ROIs) [36]. 20 ROIs (see supplementary table 2) gathering specific brain regions selected for their known involvement in the AD mechanisms and based on the results of our structural MRI analysis, were extracted from the Allen Brain Atlas (AMBA) (http://mouse.brain-map.org/static/atlas) using an in-house built MATLAB tool. We created mean 20x20 ROIs PC matrix for each mouse, at each age (See supplementary material 2.3.), normalized with a Fisher's z-transformation. PC coefficients between each pair of ROIs (defined as the "nodes" or "interacting units" of the PC matrix), by controlling correlation mediated by other ROIs, were calculated using their associated preprocessed mean time-course (TC) of the signal. Each element of the matrix represents the strength of functional connectivity (FC) between two ROIs ("edges").

The PC matrices were further statistically compared, testing: either Thy-Tau22 group *vs.* WT group differences at various timepoints; either the evolution of the Thy-Tau22 FC from 5 months to 9 and 13 months. For each inter-group statistical analysis ($p<0.05$, uncorr.) a group comparison matrix (GCM) was generated and graphically represented, as in each panel of Fig 4. On these GCM we used two measures derived from the graph theory to identify the most vulnerable nodes: (i) we first highlighted the regions exhibiting the major changes of connectivity between the two groups using the Stouffer's method [37], computing a single p-value for each region based on the combination of the p-values derived from the statistical tests made on the correlations with all other regions; (ii) we next ranked the nodes showing the highest number of statistically significant changed connections, "the degree". Comparisons between time-points (5 to 9 months-old and 9 to 13 months-old differences) were performed using paired t-test ($p<0.05$, uncorr.) revealing the most changed nodes and modifications in "degrees" over time. Tau vs WT differences were calculated using two sample t-tests ($p<0.05$, uncorr.), and most changed "edges" between groups (Tau compared to controls-WT), based on significant change in the strength of FC between two ROIs, were reported ($p<0.05$, uncorr., see supplementray table 3).

Seed-based voxel wise analysis was conducted using as seeds several regions of interests (ROIs): the lateral septum complex (including the lateral septum, medial septum and triangular nucleus of the septum), the dorsal and ventral hippocampus, and the retrosplenial cortex, to evaluate the correlation (Spearman; rho) between the rsfMRI signal's time-course (TC) of each ROI, and the TCs from all other voxels of the brain. Statistical analysis was performed to evaluate FC modifications of those selected ROIs between Thy-Tau 22 and WT over time. All areas were specifically selected for fine grained analysis of their connectivity changes, based on combined findings from the graph functional analysis, and DTI maps group comparisons. We used a full factorial ANOVA of the two factors: group and age; associated with two and

three levels (Thy-Tau22 and WT for the group factor; 5, 9 and 13 months for the age factor) to compare longitudinal evolution of functional modifications between groups in all selected areas. We investigated these functional networks in mice from 5 to 9 months old, from 9 to 13 months old and along all three time points ($p<0.05$, FDR cluster corrected). In addition, we generated Fisher-transformed spatial correlation maps of the retrosplenial cortex, and investigated group averaged FC maps at 5, 9 and 13 months. We used two-sample t-tests to compare FC differences between groups in the lateral septum, dorsal and ventral hippocampus, at each time-point ($p<0.05$, FDR cluster corrected).

Immunohistology

To investigate the evolution of the spatial distribution of phosphorylated Tau on histological brain slices, we used antibodies directed against phosphorylated Tau at the pSer422 site of phosphorylation. Brains sections (35 µm) were obtained from cohorts of Thy-Tau22 mice aged of 3, 7 and 12 months. The staining of free-floating sagittal sections was performed. Slices were first incubated in 0.3% hydrogen peroxide (H_2O_2) for 30 min and permeabilized with 0.2% Triton X-100/sodium phosphate buffer (PBS). Sections were then blocked with 5% of Normal Goat Serum (NGS; Vector Laboratories) for 1h, and incubated overnight with a primary rabbit anti-pSer422 antibody (Invitrogen). After washing in PBS, slices were incubated for 1h with an anti-rabbit biotinylated secondary antibody (Vector Laboratories). Incubation for 2h with the ABC kit (Vector Laboratories) was performed after washing the tissue sections, followed by the revelation of the staining using DAB (Sigma). Images were acquired using Leica ICC50 HD microscope.

3. Results

3.1. Prodromal, intermediate and tardive behavioral stages in Thy-Tau22 mice

Using object-tasks, we evaluated episodic-like memory of Thy-Tau22 mice and WT mice at 5, 9 and 13 months. At 5 months, transgenic mice were able to detect changes in both objects test (one-sample t-test compared to the level of chance of 50%, $p<0.001$; Fig.2 A), and remembered the platform location in the probe of MWM ($p<0.01$; Fig.2, B), similar to WT mice. The results showed that starting with 9 months, transgenic mice failed in both objects tests, spending an equal time exploring both changed and familiar objects. On the contrary, WT mice spent significantly more time exploring either the new or replaced object, showing their ability to remember the original combination of objects (Fig.2, A). The memory impairments are worsening overtime as the Thy-Tau22 mice poorly performed in all tests at 13 months-old (Fig.2, A, B).

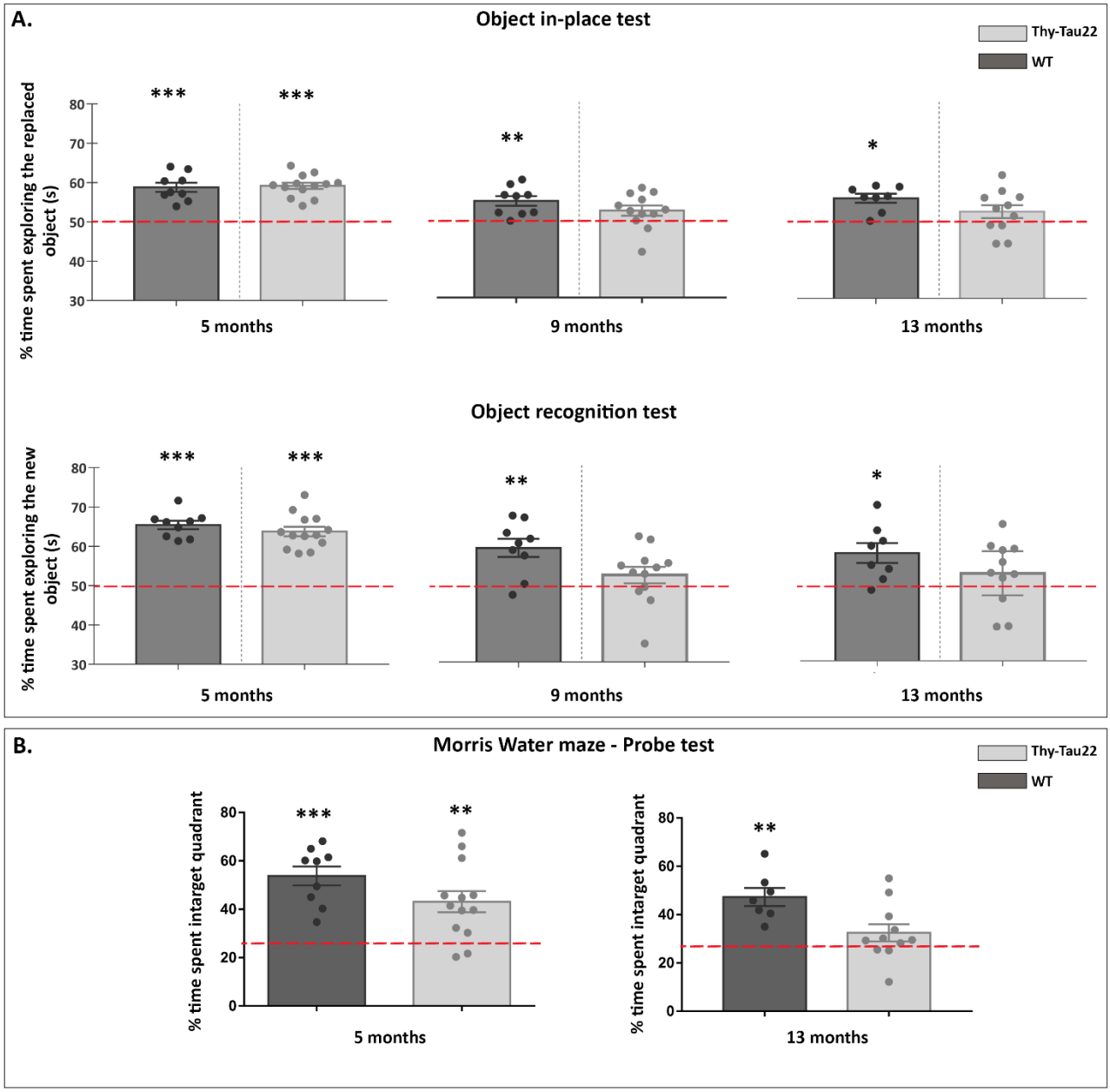

Figure 2: *Memory and learning assessment in Thy-Tau22 mice over time**.** A) Object in-place and novel object recognition showing the percentage (%) of time spent exploring the changed object in each test, for both groups (Thy-Tau22 mice and WT) at each time point, compared with the level of chance (one sample t-test, *p<0.05, **p<0.01, *** p<.0001; +/- mean standard error). In the Morris Water Maze (WM) test (B) performances are evaluated in each group comparing the % of time spent in the target quadrant with the level of chance (25%), (one sample t-test, ** p<.01; *** p<.001; **** p<.0001; mean +/- standard error).*

3.2 Morphological and microstructural modifications across lifespan in Thy-Tau22 mice

In 5 months Thy-Tau22 mice, no brain morphological differences could be found when compared to WT mice (data not shown). At 9 months, significant smaller brain volumes of the hippocampus, the amygdala and the entorhinal cortex of transgenic mice were measured when compared to WT mice ($p<0.001$; Fig. 3, A). These affectations were found in same brain areas, yet larger, in 13 months-old Thy-Tau22 ($p<0.001$; Fig 3, B). In addition, larger than WT cerebral volume was detected in several cortical areas, such as the primary somatosensory cortex, the auditive, visual and the posterior parietal associative cortical areas of transgenic mice starting with 9 months, and extending at 13 months ($p<0.001$; Fig 3. A, B).

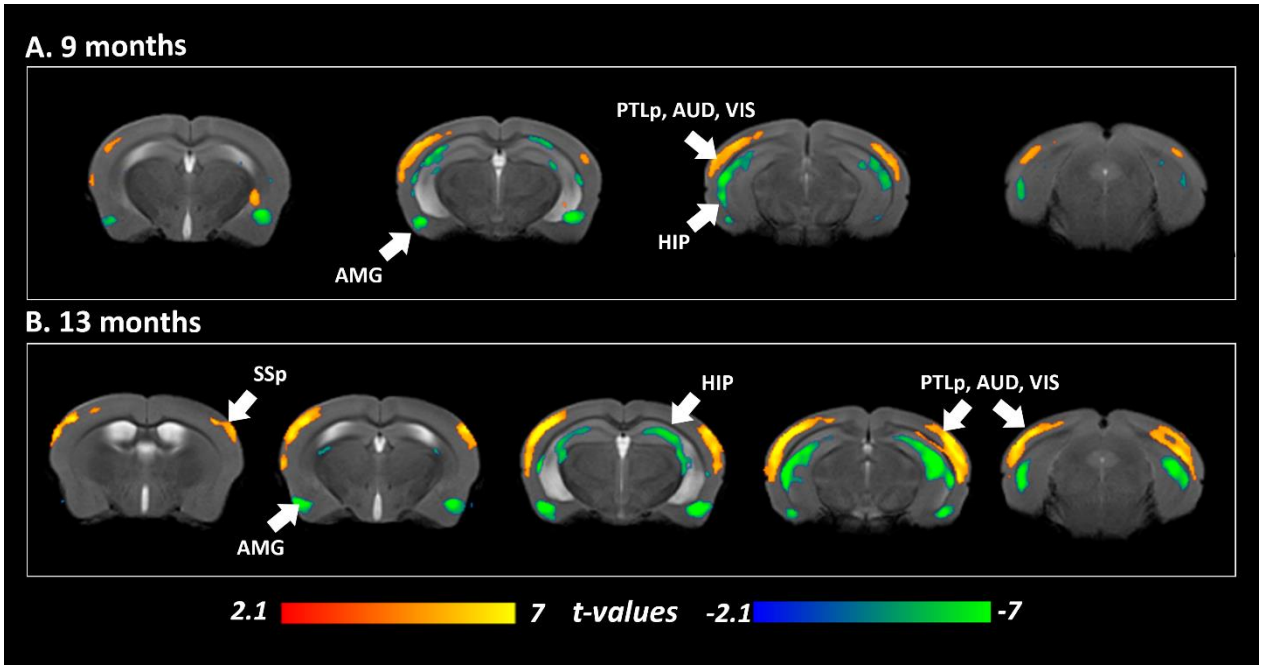

Figure 3: *Morphological changes between Thy-Tau22 and WT mice. Coronal slices of the voxel-based quantification, showing statistical differences between Thy-Tau22 group and WT group at 9 months (A) and 13 months (B) using two-sample t-test, p<0.001 FDR cluster corrected. Contrasts:* ***Thy-Tau22*** *< WT (blue scale);* ***Thy-Tau22*** *> WT (red scale).*

Microstructural modifications were assessed measuring voxel-vise FA differences in Thy-Tau22 and WT groups, at each age of the analysis. Significantly lower FA values along the lateral septum, the caudate-putamen nucleus and the fornix's were found in 5 months-old Thy-Tau22 ($p<0.05$; Fig. 4, A). In addition to 5 months' alterations, broader areas of decreased FA in related grey and white matter structures were observed at 9 months ($p<0.05$; Fig. 4, B) encompassing hippocampal areas, the fimbria, and the stria terminalis. The internal capsule and the cerebral peduncle presented both an early and at each time point decrease in FA in Thy-Tau22 compared to WT (Fig 4. A, B, C; FDR cluster corrected, $p<0.05$).

A similar decrease over time of the density of fibers was observed in transgenic mice compared to WT (Fig 4. D, E, F). Starting at 5 months, the FD were reduced in the septum, the

fornix, the fimbria, the caudate putamen and the hippocampus, revealing affectations of the whole septo-hippocampal pathway (Fig.4, D). Altered density of fibers was also observed in the internal capsule, the stria terminalis and the thalamus. The same white and grey matter areas were found affected at 9 months (Fig.4 E), in addition with the basal nucleus of the stria terminalis (BST) and the medial lemniscus. At 13 months, significant FD loss was also detected in the caudate putamen, together with increased affectation in the thalamus of the Thy-Tau22 (Fig.4 F).

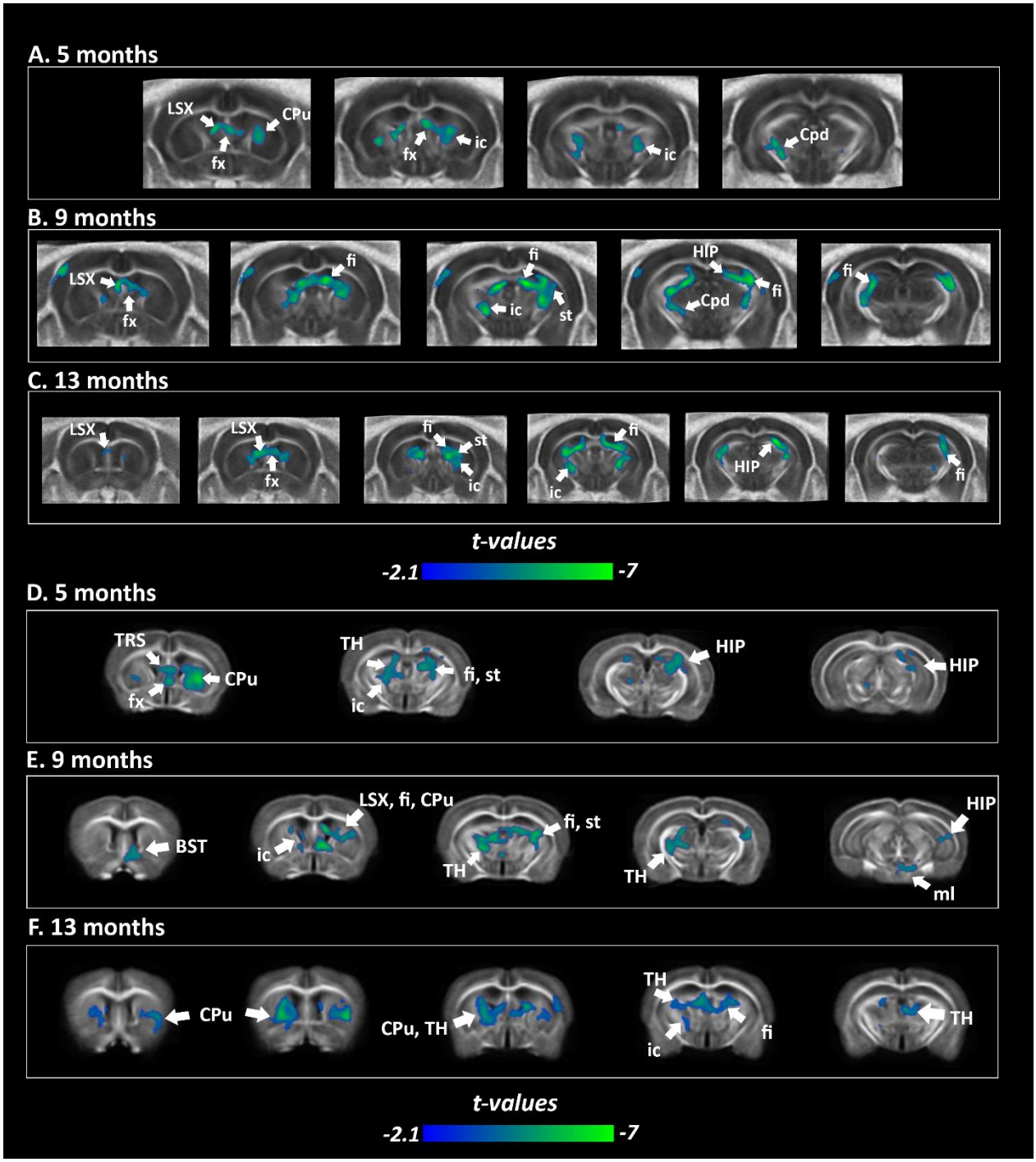

Figure 4: *Fractional anisotropy (FA) (A, B, C) and Fiber density maps (FD) (D, E, F) reveal microstructural modifications at early, intermediate and late stages of tauopathy. Statistical*

group comparison of the fractional anisotropy at 5 (A), 9 (B) and 13 months-old (C) and of the fiber density at the same timepoints (5 months, D; 9 months, E; 13 months; F) between Thy-Tau22 and WT (two sample t-test, p<0.01, FDR cluster corrected). Color scale represents significant decrease in FA and FD in Thy-Tau22 mice compared to WT group. (Fornix: fx; internal capsule: ic; fimbria: Fi; Cpd: cerebral peduncles; stria terminalis: st; hippocampus: HIP; lateral septum: LSX; medial septum: MSC; bed nuclei of the stria terminalis: BST; thalamus: TH; caudate-putamen: CPu; hippocampus: HIP).

3.3 Functional network disruption in Thy-Tau22 mice: longitudinal profile

We further evaluated FC changes within a circuit including 20 brain areas selected based on our VBM and DTI findings, and including other regions known for their involvement in memory and learning processes and AD mechanisms. This functional network is corresponding to the 20x20 PC matrices used for testing: (i) group differences (Thy-Tau22 group *vs.* WT) at various timepoints; (ii) the evolution of the Thy-Tau22 FC from 5 months to 9 and 13 months.

To highlight group differences between Thy-Tau22 and WT mice along time, we used the results of the group-matrices direct statistical comparison (two sample t-test, $p<0.05$) to identify vulnerable nodes and connections. We established a ranking of the "most changed nodes" (based on Stouffer coefficient that includes the weight of the change towards each other node, $p<0.05$ uncorr.) and graphically presented it as the node size in Fig. 5. As a second measure of the nodal changes we color coded the number of significantly different connections/node, the "degree" (see as well Fig. 5). The group comparison results are graphically shown for 5, 9, and 13 months in Fig 5 A, B and C, respectively. At 5 months, we found early significant FC changes in septal areas (lateral septum, medial septum and triangular nucleus of the septum (TRS), ranked 1, 2 and 4 according to Stouffer coefficient. Consistently, the same areas are showing significant changed connections within the analyzed network accounting for high degrees (Fig. 5, A). In addition, somatosensory cortex FC alterations were highlighted (ranked 3rd), sustained by high degree of this region. Amygdala nuclei (lateral, basolateral, and basomedial), the nucleus acumbens, and hippocampal formation regions (entorhinal cortex, dorsal and ventral hippocampus) displayed as well significantly changed connections in the Thy-Tau22 compared to WT at this age. Among the changed connections we note the amygdala – ventral hippocampus pathway as well as dorsal hippocampus – somatosensory areas, connections that were found as well remodeled at this age in our previous seed-based analysis (Degiorgis et al., submitted)

Differences between groups at 5 months seemed to persevere along time, illustrated by significant differences in septal nuclei at 9 months (Fig.5 B; TRS and medial septum ranked 2 and 3), according to both Stouffer coefficient and degree. Dorsal hippocampus appeared to be the area with strongest FC modifications in Thy-Tau22 compared to WT at 9 months, in synergy with other memory related areas (subiculum and perirhinal cortex) that show significant connectivity changes at this age. We also found a disrupted FC of the amygdala and FC affectation of the anterior cingulate cortex (ACA) in degree. Moreover we showed that one of the most significantly changed connections at this age is between anterior cingulate area and retrosplenial cortex (RSP), suggesting modifications within the default mode network at this timepoint (See Supplementary Table 1).

Further, at 13 months of age, septal area - including the medial septum (ranked 1) and triangular nucleus of the septum - showed strongest FC changes in the Thy-Tau22 mice compared to age matched WT animals also exhibiting high degree (Fig. 5C). The somatosensory cortex and the insula were found particularly different between Thy-Tau and WT mice, showing the 2nd and 3rd most functional changes at this age.

We next performed a longitudinal analysis of FC matrices (PC 20x20 ROIs matrices) of Thy-Tau22 mice, to assess the network remodeling in parallel with the progression of the pathology during the time intervals: from 5 to 9 months (paired t test between 5 and 9 months PC matrices of Thy-Tau22 group and from 9 to 13 months (paired t test between 5 and 9 months PC matrices of Thy-Tau22 group) (Fig. 5, D and E).

From prodromal to intermediate stage (from 5 to 9 months) most affected nodes regarding their FC included known "aversive" centers involved in mood/affective aspects of the pathology: anterior and central amygdala as well as basolateral and basomedial amygdala nuclei (ranked 1 and 3). These areas significantly changed their connectivity - among others - towards memory core centers, dorsal and ventral hippocampus respectively. The retrospenial cortex was found particularly affected during this time period, being the 2nd most changed node and showing the highest degree. Dorsal hippocampus showed as well significant modifications, particularly towards the lateral septum and amygdala. From early to intermediate phase, lateral septal area was ranked 4 among the most changed areas.

A higher number of brain nodes were found to significantly alter their connectivity patterns from 9 to 13 months in Thy-Tau22 mice, than from 5 to 9 months (Fig. 5 E vs D) accounting most probably for a stronger decline of cognitive processes from intermediate to tardive stages of the pathology. Lateral, basolateral and basomedial amygdala presented the most significant changes from 9 to 13 months (rank 1) and high degree. Memory-related regions of Thy-Tau22 mice displayed overtime modifications in functional communication: the ventral hippocampus was the 2nd most changed node and presented the highest degree in Thy-Tau22 mice, in addition with dorsal hippocampus and subiculum modifications in both graph features (ranked 5 and 9 respectively). The septum and related areas -lateral septum, caudate putamen, medial septum, TRS- also showed functional modifications from 9 to 13 months, ranked 3, 4, 6, and 7 in the importance of the changes during this time window.

Overall, our graph measures indicated several brain areas as distinct targets during the disease progression and guided further our seed-based mapping of the connectivity patterns. Among these regions, septal complex emerged as a particular vulnerable node: the segregated nuclei of this region showed strong FC alterations both in the inter-group comparison (Thy-Tau22 vs. WT and longitudinal investigation). Further, both dorsal and ventral hippocampal connectivity showed changes overtime in the AD model particularly towards the aversive nodes of the limbic basal ganglia, the amygdala nuclei. Moreover, RSP, the core default mode network player displayed significant alterations overtime (See Supplementary table 1).

A. **Thy-Tau22 vs WT - 5 months**

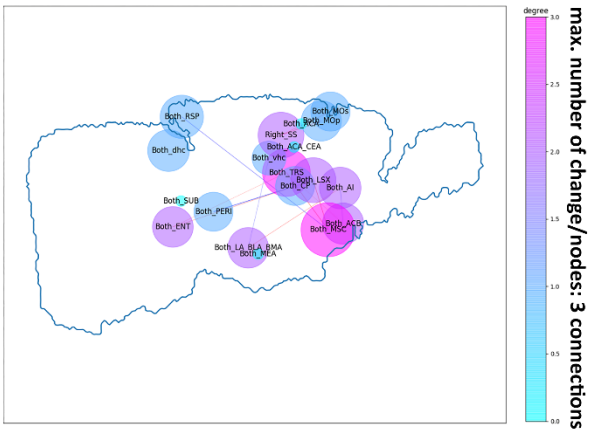

Most changed nodes (Stouffer coef.)
1. Lateral Septum
2. Triangular nucleus of Septum
3. Somatosensory cortex
4. Medial Septum

B. **Thy-Tau22 vs WT - 9 months**

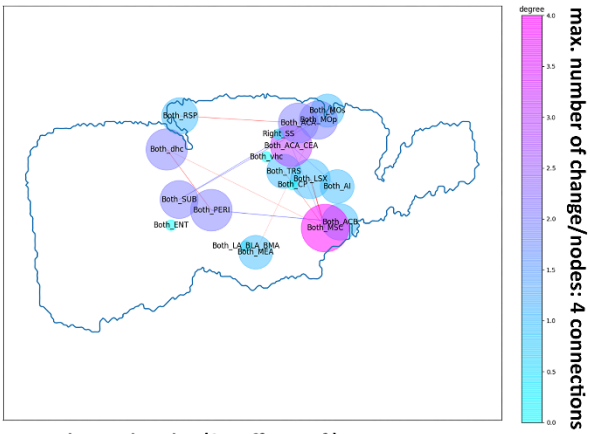

correlation

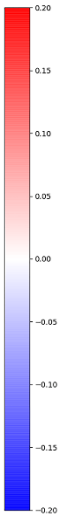

Most changed nodes (Stouffer coef.)
1. Dorsal Hippocampus
2. Medial Septum
3. Triangular nucleus of Septum

C. **Thy-Tau22 vs WT - 13 months**

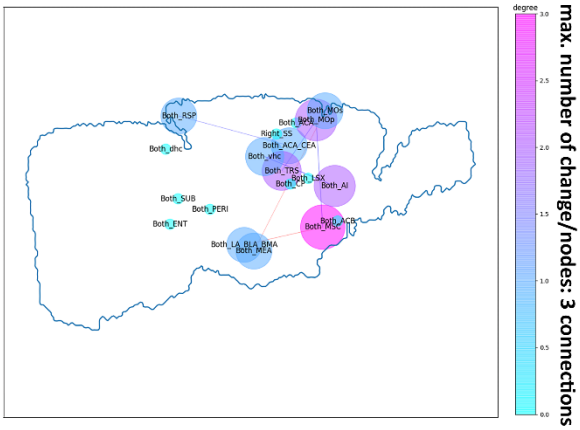

Most changed nodes (Stouffer coef.)
1. Medial Septum
2. Somatosensory
3. Insula

Nodes size according to Stouffer coef.

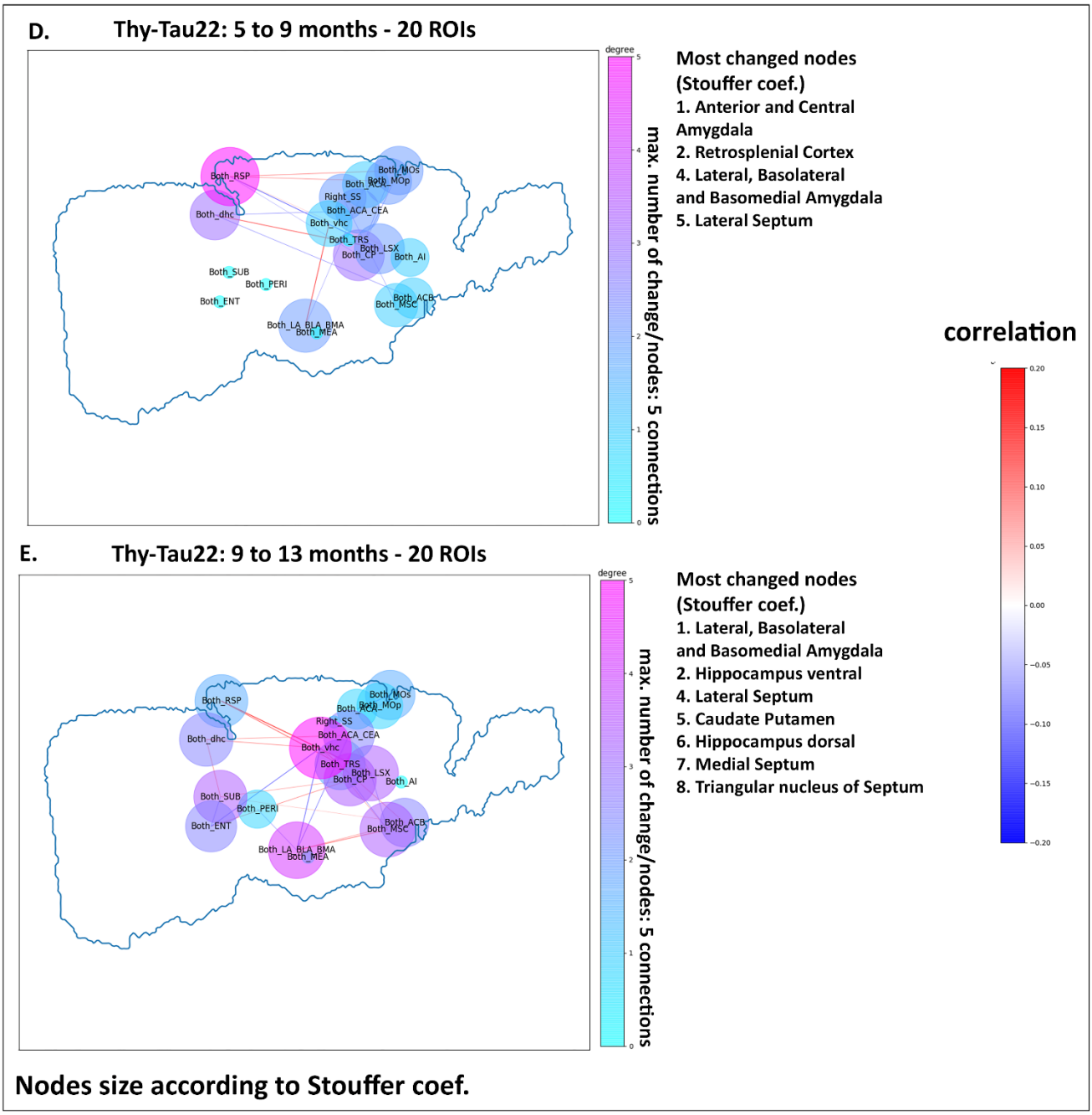

Figure 5: *Longitudinal graph theory functional analysis showing significant differences (two-sample t-test, p<0.05, uncorr.) between Thy-Tau22 and WT at 5, 9 and 13 months-old (A, B, C). Significant changes over time in Thy-Tau22 are showed in (D) from 5 to 9months old, and in (E) from 9 to 13 months-old. In the whole figure, significant differences are shown for (i) the "edges" strength based on correlation coefficient; (ii) the "degree" according to the number of changed connections per nodes; and (iii) Stouffer coefficient assessing for the most changed nodes. Node size are displaying according to the Stouffer coefficient. (Bilateral Anterior and central amygdala: Both_AAA_CEA; Bilateral Lateral, basolateral and basomedial amygdala: Both_LA_BLA_BMA; Bilateral Medial amygdala: Both_MEA;*

Bilateral Anterior cingulate cortex; Both_ACA; Bilateral Retrosplenial cortex: Both_RSP, Bilateral Dorsal Hippocampus: Both_dhc; Bilateral Ventral Hippocampus: Both_vhc; Bilateral Entorhinal cortex: Both_ENT; Bilateral Subiculum: Both_SUB; Bilateral Perirhinal cortex: Both_PERI; Bilateral Nucleus accumbens: Both_ACB; Bilateral Lateral septum: Both_LSX; Bilateral Medial septum: Both_MSC; Bilateral Triangular nucleus of the septum: Both_TRS; Left Primary somatosensory: Left_SS; Right Primary somatosensory: Right_SS; Bilateral Primary motor cortex: Both_MOp; Bilateral Secondary motor cortex: Both_MOs).

Septo-hippocampal functional alterations from 5 to 13 months

Combining graph analysis and structural connectivity evaluation results, the lateral septum complex appeared to be both early and longitudinally affected in Thy-Tau22 mice. We explored the temporal evolution of the functional network of this specific region between groups (Fig. 6). Statistical analysis showed that from 5 to 13 months, Thy-Tau22 mice presented significant changes of the lateral septum FC compared to WT mice (Fig. 6 A $p<0.05$, FDR cluster corrected). These modifications involved mostly functional relations with basal ganglia nuclei, such as the diagonal band nucleus, the medial septum, the bed nuclei of the stria terminalis and the lateral septum's intrinsic connectivity. Significant changes in functional communication between the lateral septum and the infralimbic areas, the entorhinal, and the piriform cortices were also observed in Thy-Tau22 mice.

Similar analysis war further performed to probe the changes of the septal FC in transgenic mice within 2 time-windows: from 5 to 9 months of age and then from 9 to 13 months. From 5 to 9 months, Thy-Tau22 presented significant changes in septal this functional network patterns (Fig. 6, B). As previously, the connectivity with the medial septum, the diagonal band nucleus and the lateral septum itself was significantly changing over time. In addition to the entorhinal cortex, other regions involved in memory processes such as the subiculum and the hippocampus, presented modified connectivity patterns with the lateral septum. Alterations of the septo-cortical amygdala connectivity was also revealed, and a changed functional communication between the primary motor cortex and the lateral septum was highlighted during the same time-lapse in Thy-Tau22 mice.

Progressive modifications of the septal FC were found to affect both groups at older ages (Fig. 6, C), from 9 to 13 months. While transgenic mice showed fronto-septal functional changes (infralimbic and anterior cingulate areas) and septo-hippocampal modifications, WT mice presented significant variations of the lateral septum functional network involving interactions with the caudate-putamen and within the lateral septum.

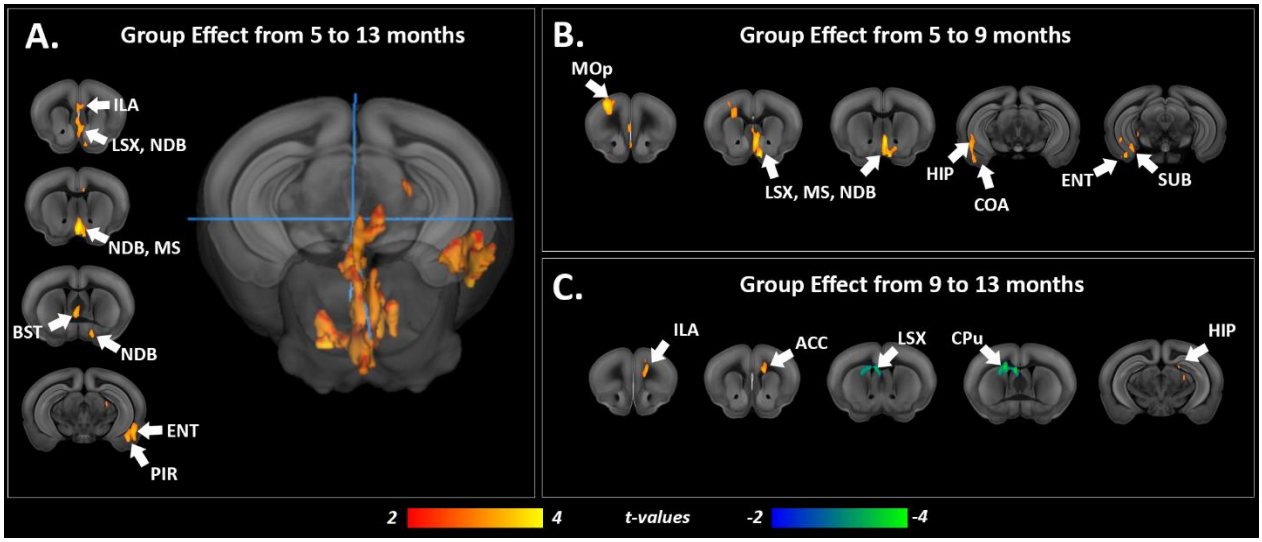

Figure 6: *Septal functional connectivity modifications in Thy-Tau22 mice over time. Coronal brain slices showing statistically significant group-differences in the evolution of the septum functional connectivity patterns from: 5 to 13 months (A); from 5 to 9 months (B) and from 9 to 13 months (C). In the whole figure, higher changes over time of functional connectivity in Thy-Tau22 compared to WT mice are illustrated with positive values (red), and higher over time changes in WT in negative values (blue). Only statistically significant differences calculated using a full factorial approach, $p<0.05$, FDR cluster-corrected, are shown.*

Next, based on graph analysis that indicated in Thy-Tau22 mice perturbed FC of the dorsal and ventral hippocampus we probed the functional communication changes in those hippocampal subregions over time (Fig.7). Statistical results revealed a longitudinal affectation in Thy-Tau22 mice within both time windows: from 5 to 9 months-old (3D brain and left column, Fig. 7, A) and from 9 to 13 months-old (right column Fig.7, A) between the dorsal hippocampus FC and the primary somatosensory cortex, the thalamus and the caudate-putamen. The hippocampus intrinsic functional communication was also found modified along the entire time-period of the pathology development. Specifically from 5 to 9 months, altered FC between the dorsal hippocampus and motor areas was detected. Over this same timespan, dorsal hippocampus FC in WT mice also displayed changes, particularly with the lateral septum. At later stages, modifications of the dorsal hippocampus-Insula functional communication, as well as with the hypothalamus were observed in Thy-Tau22 mice (right column Fig.7, A).

Functional changes of the ventral hippocampus connectivity occurred in Thy-Tau22 mice towards motor areas, the caudate-putamen nucleus and within hippocampus itself, similarly to the dorsal hippocampus connectivity, but only across the 5 to 9 months timespan (3D brain and left column, Fig 7, B). Later, (right column Fig.7, B) an altered functional relation between the ventral hippocampus and the lateral septum was highlighted in addition with the anterior cingulate area. We also found several changes over time in the FC of the ventral hippocampus in WT mice. Indeed, amygdala nuclei as well as the caudate-putamen showed modifications of FC towards the ventral hippocampus from 5 to 13 months-old in WT (Fig. 7, blue patterns). In addition, the ventral hippocampus presented stronger evolution of

functional communication with several cortical areas from 9 to 13 months in WT, such as motor areas, the primary somatosensory cortex, and the insula. The taenia tecta and the piriform cortex, both olfactory areas, also presented modified FC with the ventral hippocampus in later stage in WT mice compared to Thy-Tau22 mice.

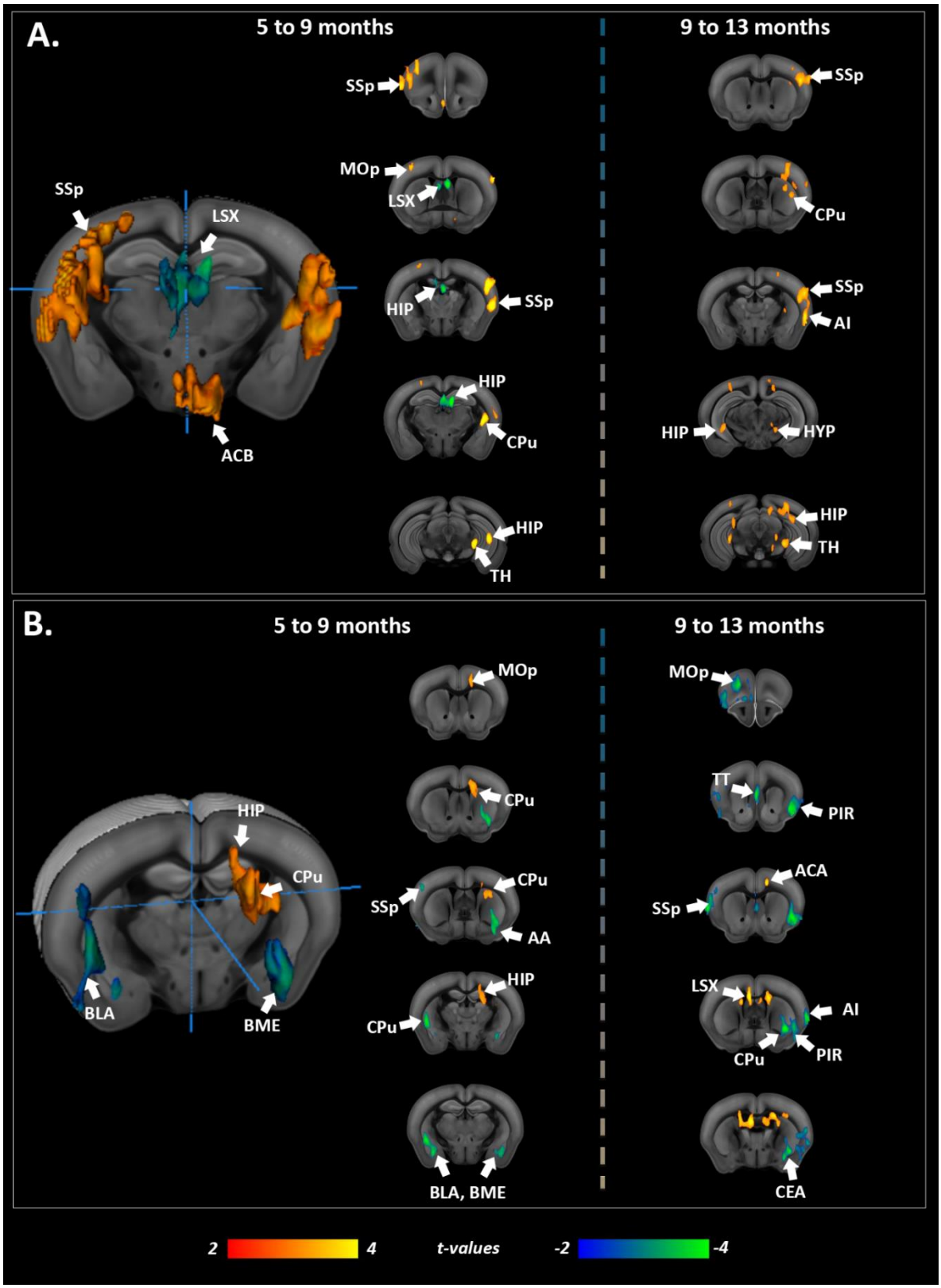

Figure 7: *Functional connectivity changes over time in the hippocampus. A) Dorsal hippocampus and B) ventral hippocampus functional connectivity changes over time in Thy-Tau22 mice compared to WT mice from 5 to 9 months (3D illustration and left column), and from 9 to 13 months (right column). In the whole figure, higher changes over time in functional connectivity in Thy-Tau22 compared to WT mice are illustrated with positive values (red), and*

higher changes in WT over time in negative values (blue). Only statistically significant differences calculated using a full factorial approach, p<0.05, FDR cluster-corrected, are shown.

Default-mode networks modifications in Thy-Tau22

Analysis from graph theory indicated particular affectations of the retrosplenial functional connectivity, suggesting alterations of the default-mode network (DMN) in Thy-Tau22 mice over time (Fig. 5D and Supplementary Table 3, A, B - most changed "edges"). Therefore, we explored the longitudinal modifications of this network using seed-analysis of RSP, a core node of the rodent DMN. We found a continuous hypersyncrony of DMN rsfMRI signal in Thy-Tau22 compared to WT mice (Fig. 8, A). Mean functional correlation maps of this network illustrated a synchronous FC particularly towards medial and basolateral amygdala at 5, 9 and 13 months in Thy-Tau22 mice. At each time-point, an increased functional communication was also found between the retrosplenial cortex and the somatosensory and posterior parietal associative cortices, when compared to WT FC correlation maps. At later stages of the pathology in transgenic mice, the auditory and temporal associative cortices presented a hypersynchrony of the BOLD signal with the retrosplenial cortex.

In coherence with previous results, between groups cross-analysis of the longitudinal evolution of DMN patterns from 5 to 9 months and 9 to 13 months (Fig. 8, B) highlighted modified DMN in Thy-Tau22 mice with limbic areas -including septal nuclei and the caudate putamen- and the anterior cingulate cortex ($p<0.05$, FDR cluster corrected). FC changes of the DMN in Thy-Tau22 were also observed toward the orbitofrontal cortex and the taenia tecta of the olfactory system, and the motor cortex. From intermediate to late stage, Thy-Tau22 mice showed significantly remodeled DMN connectivity ($p<0.05$, FDR cluster corrected) with the lateral septum and the motor cortex, in addition to functional modification towards the hippocampus (Fig.8 C). WT mice presented, during this same time period, significant modification in the DMN functional connectivity. Changes with the basal ganglia were detected, involving, the medial septum, the nucleus accumbens and the ventral pallidum (Fig. 8, C). Modified FC in WT was also found between the DMN and the amygdala, and towards cortical areas such as the insula and the somatosensory cortex (Fig. 8, C) at this more advanced age.

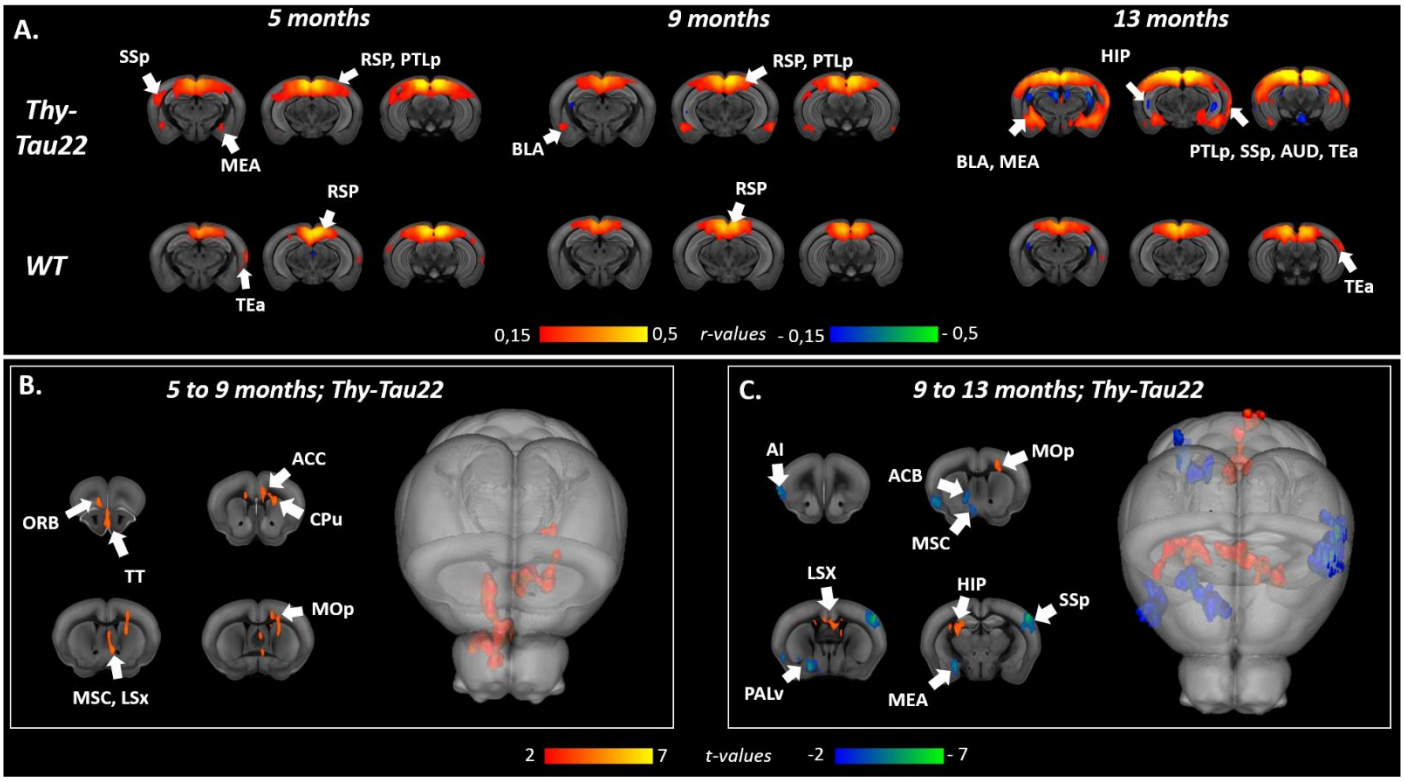

Figure 8: *Default-mode network functional modifications over time. (A) Coronal slices of the seed-based analysis of the retrosplenial network, showing the mean correlation between the mean BOLD signal in this ROI and all other voxels of the brain, in Thy-Tau22 mice (upper row) and WT (lower row). The color scale represents the strength of the functional correlation normalized with a fisher z-transformation. (B) Coronal brain slices and 3D brain representation showing statistically significant group-differences in the evolution of the retrosplenial functional connectivity patterns from: 5 to 9 months (B) and from 9 to 13 months (C). Higher changes over time of functional connectivity in Thy-Tau22 compared to WT mice are illustrated with positive values (red), and higher over time changes in WT in negative values (blue). Only statistically significant differences calculated using a full factorial approach, $p<0.05$, FDR cluster-corrected, are shown. (Accumbens: ACB, agranular insula: AI, anterior cingulate cortex: ACC, auditive cortex: AUD, basolateral amygdala: BLA, caudate putamen: CPu, hippocampus: HIP, lateral septum: LSX, medial amygdala: MEA, medial septum: MSC, orbitofrontal cortex: ORB, posterior parietal associative cortex: PTLp, primary motor cortex: MOp, retrosplenial cortex: RSP, somatosentosory cortex: SSp, taenia tecta: TT, temporal associative: TEa, ventral pallidum: PALv).*

3.4. Pathological Tau expansion in Thy-Tau22 over time

To investigate the spatial distribution of phosphorylated Tau overtime, we performed immunostainings on brains of a separated cohort of Thy-Tau22, matching in age with mice tested in behavior and MRI (Fig. 9). Phosphorylated Tau at 3 months was observed mainly in the hippocampus, the amygdala and the septum (Fig. 9 A). From 7 months old, pathological Tau was detected in the frontal and somatosensory cortices, in addition with an increased

deposition of the phosphorylated protein in previously affected regions at 3 months (Fig. 9, B). In 12 months old Thy-Tau22 mice, accumulation of pathological Tau was found expanding in midbrain areas and most of cortical regions such as the motor and piriform cortices (Fig. 9, C).

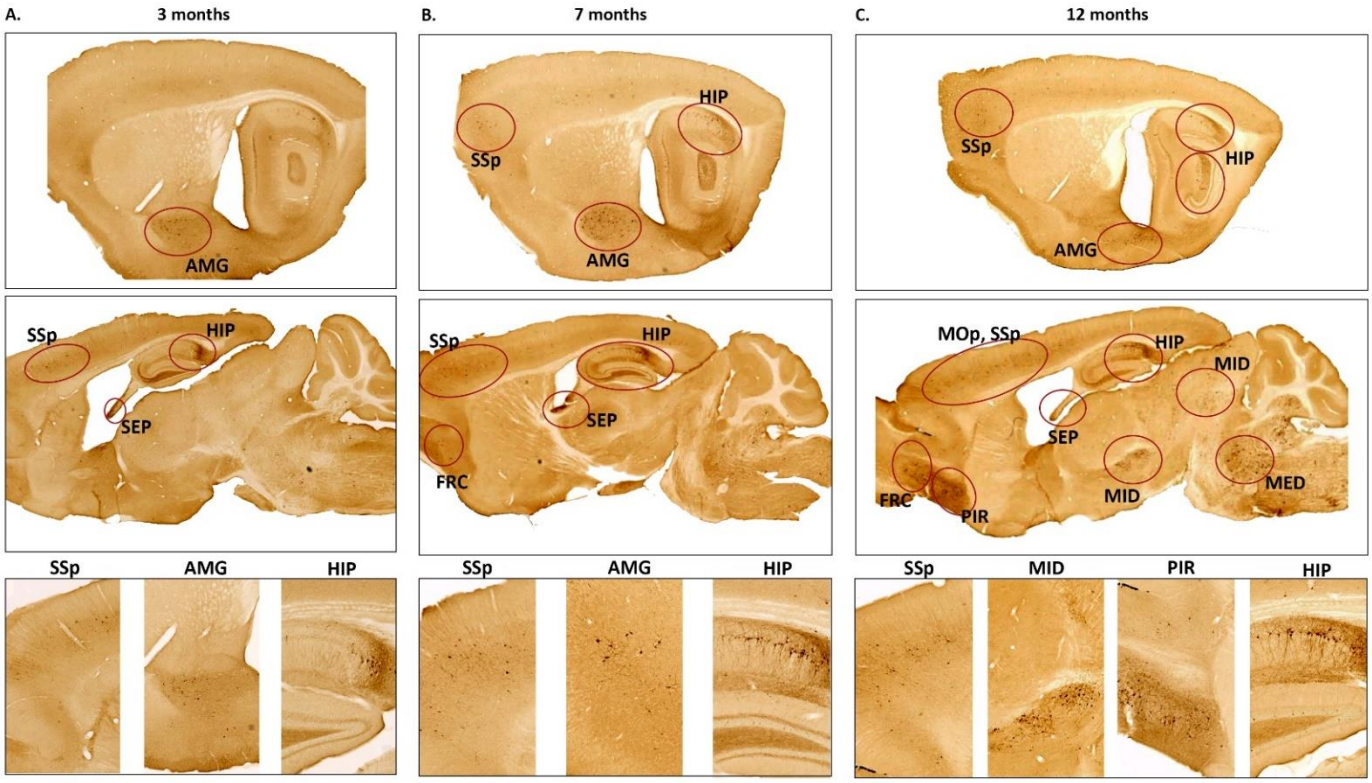

Figure 9: *Representative sagittal slices and corresponding magnified images of immunological staining at the pSer422 site of phosphorylation in the Tau protein, in Thy-Tau22 mice. Ellipses highlight the highest density deposition of phosphorylated Tau. (Amygdala: AMG; primary somatosensory cortex: SSp; hippocampus: HIP; septum: SEP; frontal cortex: FRC; primary motor cortex: MOp; piriform cortex: PIR; midbrain areas: MID; medulla: MED)*

4. Discussion

In this study we performed a longitudinal, non-invasive and in-vivo evaluation of the brain morphology and structural and functional brain networks organization, associated to behavioral and histological assessments in the Thy-Tau22 mouse model, relevant for tauopathy mechanisms of AD. This mechanism is so far largely unexplored at brain-wide circuitry level and only very few studies investigated by MRI the cerebral networks properties in rodent models of tauopathy [29,38]. We used a cohort of animals that underwent structural and functional MRI at early, intermediary and late stages in the development of the pathology, corresponding to 5, 9 and 13 months of age.

4.1. Microstructural substrate of cholinergic system alterations

At 5 months-old, Thy-Tau22 mice mirrored the prodromal clinical stages of the disease exhibiting neither memory impairment, nor morphological changes in the brain. Nevertheless, we demonstrated microstructural alterations at this age, combined with findings of pathological Tau deposition in corresponding brain areas.

Indeed, our major findings from DTI suggest compromised fiber integrity in the septum and the fornix. These early structural alterations could be associated in Thy-Tau22 with functional connectivity modifications, detected in septal nuclei and in the hippocampus networks. Hippocampal region is known to be the main projecting target from the septum through the fornix [39]. At the intermediate stage of the disease, Thy-Tau22 mice presented memory deficits in objects tests. This impaired phenotype could be related to a progression of microstructural alterations, as suggested by FA and fibers' density loss in the septum and the hippocampus, as well as the expansion of fornix' fibers affectations to the fimbria. This was accompanied by an increased Tau deposition in the hippocampus and the septum. Our imaging findings at early and intermediate stages of the disease are thus pointing towards early dysfunction of the septo-hippocampal circuitry. Using the same animal model Belarbi et al., [40] have shown at later stages of the pathology -13 months - synaptic dysfunctions of the septo-hippocampal pathway, associated with pathological Tau deposition in those same areas and in the fornix suggesting a disconnection between these two key brain regions. Other ex-vivo studies focused on the brain of a mouse model developing both hyperphosphorylated Tau and toxic amyloid peptides, and showed specific modifications in the fornix [41,42]. In addition, an ex vivo brain DTI study on Tg601 mice expressing tauopathy demonstrated age-related decrease in FA in the septo-hippocampal tract, in relation with a low glucose uptake in the septum and a high activity of acetylcholinesterase, showing a selective degeneration of this cholinergic pathway [43].

Structural connectivity analysis at 5, 9 and 13 months also showed affectation of the internal capsule and cerebral peduncle in transgenic mice at all ages, were cholinergic cells are projecting as well [44]. Connecting midbrain and cortical areas through the thalamus, where numerous motor and sensory fibers travel, the alterations of this pathway could underlie the early and longitudinal functional changes in cortical areas such as the motor cortex, the somatosensory cortex and the retrosplenial area [45,46]. Human studies also reported a decreased FA in the internal capsule of MCI subjects [47,48] and late AD patients [49–51].

Decrease of the FA in the internal capsule has also been associated with dysfunction in decision making, inhibition behavior, and psychomotor impairment [52,53] – the latter behavioral feature described in young Thy-Tau22 mice [54]. Sending axonal projections toward cortical areas, the caudate-putamen nucleus is an important relay particularly connecting frontal regions involved in cognitive and emotional functions in Human [55]. Lower than control FA values were found within this region starting from 5 months in transgenic mice, suggesting microstructural changes. Therefore, alterations of both the internal capsule-cerebral peduncle connectivity and caudate-putamen, may be associated with emotional and altered motivation, as described in Human in AD [56].

4.2. Functional connectivity signatures of the pathology in Thy-Tau22 Mice

We further explored the resting state functional network of Thy-Tau22 and WT animals with graph analysis approaches, and unraveled the septal area as one of the most altered node of the transgenic brain FC matrix at all stages of the disease, in agreement with structural MRI findings. Distinct patterns of changes were identified both from Thy-Tau22 vs. WT connectivity matrices comparison but also from seed-based analysis: septal areas consistently altered its FC with the somatosensory cortex and limbic areas such as the hippocampus and the amygdala. Likewise, the analysis of the Thy-Tau22 connectional evolution overtime (Thy-Tau22 from early to intermediate and late stages) showed persistent and progressive alterations of the septal connectivity towards three main brain complexes: (i) the hippocampus and peri-hippocampal memory areas; (ii) the aversive limbic nuclei of the amygdala - the integrative center for emotions, emotional behavior and motivation - and (iii) the retrosplenial cortex the core area of the rodent DMN [57,58].

1.2.1 Septo-hippocampal networks perturbations

Involved in memory circuit, the septum has been long associated to a modulatory role of the hippocampus [59,60], acting like a pacemaker for hippocampal rhythm oscillations [61] modulated by several neurotransmitter including cholinergic neurons [62]. In AD patients, the cholinergic system has been reported to be affected, especially in the basal ganglia -including the septal nucleus and the caudate putamen- and the basal nucleus of Meynert -projecting essentially to hippocampus and amygdala [63]. An autopsy study investigating the hyperphosphorylated Tau deposition, correlated a strong deposition of the pathological protein in the basal nucleus of Meynert, and tauopathy in the fornix, suggesting an important contribution of the fornix in spreading the neuropathology trough the septo-temporal axis of the brain [64]. In addition, a DTI study on AD patients correlated neurofibrillary tangles deposition with a low score in memory tests and a decreased FA in several white matter tracts including the fornix [9]. Using electrophysiological experiments to explore the functional connectivity between the hippocampus and the lateral septum, an in-vitro study of J20 mice expressing amyloïdopathy detected an early disruption in the communication of those two regions [65]. Our study revealed an affectation of the septo-hippocampal connectivity, in both functional and structural, connectivity occurring even before memory impairment. While several studies revealed functional connectivity alterations of the hippocampus in early AD patients [66,67], rsfMRI studies on Mild Cognitive Impairment (MCI) [68] or subjective memory complainers [69] also associated basal forebrain functional communication

dysfunction to impaired performance in memory tests. Using morphological measurements in MRI on a large cohort of age-matched older adults ranging from cognitively normal to AD, a study showed that basal forebrain degeneration precedes memory impairment [70]. In line with these observations we report in mice fibers density alterations along fornix and stria terminalis, connecting most forebrain limbic regions, such as the amygdala and the septum [71], which could represent a substrate for early functional modifications of the connectivity.

Fine grained mapping of the lateral septum functional network in Thy-Tau22 and WT mice with seed-based approaches, further provided voxel-wise information about the extent and the progression of alterations overtime. The whole septal functional system was affected in transgenic mice: the infralimbic, which mainly projects to the lateral septum [72], the medial septum, the diagonal band nucleus and the bed nuclei of the stria terminalis [73], relying on cholinergic neurotransmission [14,74]. The inter-group (Thy-Tau22 vs. WT) comparison of the evolution of the septal connectivity across lifespan highlighted as well strong alteration with the hippocampal and peri-hippocampal areas (including entorhinal and perirhinal areas).

1.2.2. Hippocampal network patterns

DTI structural measurements as well graph functional connectivity analysis in transgenic Thy-Tau22 mice consistently indicated dorsal and ventral hippocampal connectivity affectations over time. In mice, dorsal hippocampus is largely involved in cognitive processing and spatial memory while ventral regions of the hippocampus are important in emotional and affective processing [75]. Various approaches have revealed the differential molecular and structural characteristics, and functional roles of the two hippocampal regions. We therefore assumed that dorsal and ventral areas would be differentially modified along with tau pathology, and separately looked into their connections.

Dorsal hippocampus connectivity: From 5 to 9 months, the dorsal hippocampus showed alterations of its intrinsic connectivity and towards the subcortical limbic caudate putamen and accumbens nucleus, while most extensive modifications occurred towards somatosensory and other sensory and somatomotor cortical areas in transgenic mice. These patterns of modifications were strongly progressive from 9 to 13 month as well, and extending towards ventral hippocampus, insular cortex and thalamic nuclei.

FC modifications of somatomotor cortex were also seen in graph analysis and attest for an early and sustained involvement of this brain region in the disease progression. In rodents, in addition with the olfactory cortex, they are major systems for exploration. Tactile information from whiskers and paws stimulations are processed by hippocampus creating a representation of sensitive information [76]. Exploring anesthetized rat, a previous study highlighted - via electrophysiological recordings - the pathway of communication between the hippocampus and the somatosensory cortex following a mechanical stimulation of the forepaw or the whiskers [77]. The neuronal signal from the somatosensory cortex, reaching the hippocampus via the perforant path and the entorhinal cortex, was recorded. A differential and independent response coming from the dentate gyrus and CA1 was detected, reflecting a complex functional communication's organization between the somatosensory cortex and the hippocampus. In AD, this communication has already been shown disrupted in a mouse model of amyloïdopathy [78]. Using electrophysiology on brain tissue slices from 5XFAD rodent

model of amyloid, long-term potentiation (LTP) deficiency in the somatosensory cortex and reduced LTP in the hippocampus were detected and associated with a decrease of the hippocampal basal transmission and with amyloïd plaques deposition [78]. In Human, dysfunction of sensory modalities such as olfaction, auditory, visual or somatosensory, have been described in both aging and AD, and associated with pathological proteins disturbances in, *inter alia*, the hippocampus [79]. However, most studies only reported early affectations of visual [12], auditory [80] and olfactory [79,81] systems. In rodents, the somatosensory cortex is a highly organized area, especially when coming to the complex whisker-related integration. Indeed, mice are using whiskers as sensitive detectors for acquiring tactile information, in order to build spatial representation of their environment, locate objects, and perform fin-grain texture discrimination [82]. Comparatively, other sensory systems are way less developed in mice. For example, while many species present a highly functionally segregated visual cortex, mice do not present a structured functional map of this area [83]. These major differences are largely associated with the poor implication of this system in the daily life of rodent, which led to an evolutionary compensation illustrated by a complexification of the sensitive integration in rodent. Therefore, to assess sensory affectation in rodent models of neurodegenerative disease, the somatosensory cortex may present as a better candidate.

The functional connectivity of the dorsal hippocampus in Thy-Tau22 was also found changed with the insula from 9 to 13 months old in Thy-Tau22. Graph analysis also pointed the changed FC of insular cortex already at 5 months. At 13 months insula - ventral hippocampus was found as the most changed connection. Insular cortical structure is known to play a major role in emotional behavior and sensory-motor integration [84]. Studies have related insular dysfunction with AD in both MCI and late stages [85]. One group showed that functional alterations of the insular network would depend on the subregion affected in this cortical region [86]. In related neurodegeneratives diseases such as the Dementia with Lewy Body (DLB), the insula, more specifically the anterior part, has been shown early affected [87,88] and proposed as a potential biomarker in the differential diagnosis between AD and DLB at early onset.

Ventral hippocampus connectivity: We further described both dorsal and ventral hippocampus changed connectivity towards striatal limbic areas. Particularly, cholinergic connections between the hippocampus and the striatum are thought to sustain cooperate activity of limbic system regions through the consolidation of motor sequence especially during sleep [89,90]. Moreover, nucleus accumbens, hippocampus and septum nuclei [91,92] are all core areas of the reward circuit. This system has been largely exposed as vulnerable in neurodegenerative diseases, including AD [93].

In Tau-Thy22 mice ventral hippocampus showed alterations of its connectional pathways with caudate putamen nuclei from 5 to 9 months, sustained by a decreased FC towards this region and the accumbens nucleus when compared to WTs at 9 months. Interestingly, during this time interval, the ventral hippocampus displayed weaker than control changes towards amygdala, possibly accounting for less plasticity of the hippocampus-amygdala pathway in Thy-Tau22 mice. Our previous analysis at 5 months of age indicated already disrupted functional cross-talk between the two regions, known to modulate memory

consolidation in the context of fear and anxiety behavior. Indeed, ventral hippocampal and anterior cingulate cortex inputs to the basolateral amygdala selectively control generalized fear and contextual anxiety [94]. Optogenetic activation of ventral hippocampal inputs to the amygdala leads to an increase in anxiety behavior, whereas the inhibition of the same inputs results in a decrease in anxiety [95]. From 9 to 13 months, ventral hippocampus additionally altered its functional connectivity with the anterior cingulate cortex as well as with septal area in transgenic mice. Thus, our finding of dysfunctional signaling between ventral hippocampus and amygdala in Thy-Tau22 mice could underly the reduced anxiety and disinhibition behavior that was previously described in Thy-Tau22 mice [54]. In another model expressing both amyloidopathy and tauopathy, increased glucocorticoïde receptors in both hippocampus and amygdala at early stages, have been associated with a mild disinhibition behavior [96]. In AD patient alterations of ventral hippocampus, amygdala and frontal cortex were linked to emotional responses, impulsive behavior and disinhibition [75,97–99].

1.2.3. Amygdala circuitry alterations

In line with the previously discussed alterations of ventral hippocampus-amygdala pathway, graph analysis pointed to highly perturbed connectivity patterns of multiple amygdalar nuclei, evolving from 5 to 9 months and further increasing from 9 to 13 months in Thy-Tau22 mice. Further, multiple seed analysis evaluations indicate strong interactions of amygdala with septum and hippocampus, but also DMN centers. Indeed, among other connections, afferences to the septal nuclei arrive mainly from the amygdala, which receives reciprocal connections from the septum [100]. Amygdala and septum are both at the core of the limbic system and involved in regulating motivated behaviors and controlling emotions [97]. In association with the hippocampus this circuitry loop controls memory consolidation [101]. The substrate for this sustained dysfunction of amygdalar circuitry might reside in the specific accumulation of Tau pathologic proteins in this area, early in the disease, further leading to neuronal loss and specific atrophy as we report in Thy-Tau22 mice. A recent lifespan study in MRI from Coupé et al., 2019 [102] highlighted in AD patients early and longitudinal morphological alterations of the hippocampus and the amygdala along the disease progression, in coherence with our findings. Moreover, age-related affectations of the amygdala functional connectivity from MCI to AD patient was detected in an fMRI study [103], and morphological changes of the limbic system networks were associated with impaired emotional memory in AD [56].

1.2.4. DMN patterns and interactions with septal nuclei

Several rodent's studies showed cholinergic innervation of the retrosplenial cortex and the hippocampus through septal nuclei, and basal ganglia areas projections [104,105]. Indeed, cholinergic cells in the rat forebrain are organized into 4 subdivisions displaying different innervation patterns, with one originating from the medial septal area and the diagonal band of Broca, innervating the hippocampus and surrounding cortical areas such as the retrosplenial cortex [106,107]. We showed using graph theory that the most changed edge from 5 to 9 months and from 9 to 13 months was between the septum and retrosplenial cortex, sustaining a specific affectation of the DMN towards septal nuclei. Using the retrosplenial cortex as a seed to highlight DMN connectivity changes over time, we similarly revealed a changed

functional connectivity of the retrosplenial cortex with basal forebrain structures -including the septum and the caudate putamen- but also with the hippocampus.

The DMN, showing a synchronized functional activity at rest, has been highlighted as majorly affected in AD, and proposed as a biomarker to distinguish AD patient from healthy subject using rsfMRI [6]. This network is thought to be involved in multiple functional subsystems, communicating through "hubs", such as the posterior cingulate cortex (PCC), ventral prefrontal and inferior parietal cortices in human [108]. In prodromal Thy-Tau22, we detected increased DMN functional communication, particularly towards the amygdala and cortical areas.

Using MRI, a study in young carrier of APOE-4 risk allele of AD highlighted an increased functional connectivity of the DMN, particularly with medial temporal areas -including the hippocampus and the amygdala-, the retrosplenial and prefrontal cortices [109]. Increases in DMN connectivity have also been reported in amnestic MCI compared to healthy aged controls using regional homogeneity approach in rsfMRI. Particularly, this increase would be located within the PCC, frontal, lateral parietal, and middle temporal cortices in MCI [110]. At later stages of AD, the DMN activity within the PCC, frontal, occipital, parietal cortices was also found to be increased [108]. In mice, a rsfMRI study of model of amyloidosis showed a global functional hypersynchrony at pre-plaques stages, including within DMN areas [19]. This hypersynchony of DMN related areas have largely been interpreted as compensatory processes (Mevel et al., 2011). Moreover, an age-dependent evolution of the DMN's affectation in AD patient have been suggested to reflect interactions between B-amyoïd deposition and BOLD signal along time [111–113]. Using two-photon imaging on three mice model of amyloïdopathy, a study also showed an overlap distribution of amyloïd deposition with regions related to the DMN, in all three models [114]. Therefore, our findings could reflect a specific impact of the tauopathy deposition over time, leading to a steady pathological increase of the DMN functional connectivity. This hypothesis is sustained by our histological results, showing accumulations of pathological Tau deposition in the hippocampus, amygdala and somatosensory cortex over time.

To conclude, septal circuitry alterations - from early to late stages - were found as the main hallmark of the progression of the pathology. Septal hippocampal cholinergic pathway emerged as a crucial circuitry taking part in the brain network maladaptations prompted by Tau pathology and bringing out behavioral signatures of AD pathology. Moreover, septal connectivity with hippocampus, amygdala and DMN place this area at the intersection between limbic and default mode networks possibly modulating their interactions along the instalement of the pathology.

Septal area is known for its main implication in reward and reinforcement processes, working side by side with striatal areas -such as the accumbens nucleus-, and the hippocampus. The hippocampus is one of the main connections of the septum, reciprocally projecting to each other through the fornix that we found affected early in the line of the pathologic events. From these connections, the septum plays the role of relay center for connections of the hippocampus to the ventral tegmental area, associating reward signals with their context and thus, their memorization. The septal nucleus also plays a crucial role in emotional behavior sustained by,

among other, it’s mutual connection to the amygdala. The septal circuity is part of the cholinergic system and therefore, specific septal affectations most likely represent the neural substrate for the disruption of the cholinergic pathways known to be damaged in AD and triggering impairments of the limbic and memory systems.

Functional and structural modifications of these networks may induce neuronal loss in the amygdala and the hippocampus, both core nodes of those systems, finally leading to memory impairment. Our findings in mice are strongly coherent with recent human findings [102]. We also showed longitudinal functional and structural modification of the stria terminalis and related areas pathway that may strongly contribute to morphological alterations of the limbic system.

Therefore, the disfunctions highlighted in this study represent a strong lead toward the discovery of a potential biomarker of the disease or as a target for future treatment’s investigations that could be further explored in Human.

References

[1] Mohandas E, Rajmohan V, Raghunath B. Neurobiology of Alzheimer's disease. Indian Journal of Psychiatry 2009;51:55. doi:10.4103/0019-5545.44908.

[2] Fornito A, Zalesky A, Breakspear M. The connectomics of brain disorders. Nature Reviews Neuroscience 2015;16:159–72. doi:10.1038/nrn3901.

[3] Park H-J, Friston K. Structural and Functional Brain Networks: From Connections to Cognition. Science 2013;342:1238411–1238411. doi:10.1126/science.1238411.

[4] Sporns O. Graph theory methods: applications in brain networks. Dialogues Clin Neurosci 2018;20:111–21.

[5] Yan T, Wang W, Yang L, Chen K, Chen R, Han Y. Rich club disturbances of the human connectome from subjective cognitive decline to Alzheimer's disease. Theranostics 2018;8:3237–55. doi:10.7150/thno.23772.

[6] Greicius MD, Srivastava G, Reiss AL, Menon V. Default-mode network activity distinguishes Alzheimer's disease from healthy aging: evidence from functional MRI. Proceedings of the National Academy of Sciences of the United States of America 2004;101:4637–4642.

[7] Burggren A, Brown J. Imaging markers of structural and functional brain changes that precede cognitive symptoms in risk for Alzheimer's disease. Brain Imaging Behav 2014;8:251–61. doi:10.1007/s11682-013-9278-4.

[8] Yao H, Liu Y, Zhou B, Zhang Z, An N, Wang P, et al. Decreased functional connectivity of the amygdala in Alzheimer's disease revealed by resting-state fMRI. Eur J Radiol 2013;82:1531–8. doi:10.1016/j.ejrad.2013.03.019.

[9] Kantarci K, Murray ME, Schwarz CG, Reid R, Przybelski SA, Lesnick T, et al. White Matter Integrity on DTI and the Pathologic Staging of Alzheimer's Disease. Neurobiol Aging 2017;56:172–9. doi:10.1016/j.neurobiolaging.2017.04.024.

[10] Planche V, Coupé P, Helmer C, Le Goff M, Amieva H, Tison F, et al. Evolution of brain atrophy subtypes during aging predicts long-term cognitive decline and future Alzheimer's clinical syndrome. Neurobiology of Aging 2019;79:22–9. doi:10.1016/j.neurobiolaging.2019.03.006.

[11] Sivera R, Delingette H, Lorenzi M, Pennec X, Ayache N. A model of brain morphological changes related to aging and Alzheimer's disease from cross-sectional assessments. NeuroImage 2019;198:255–70. doi:10.1016/j.neuroimage.2019.05.040.

[12] Mitolo M, Stanzani-Maserati M, Capellari S, Testa C, Rucci P, Poda R, et al. Predicting conversion from mild cognitive impairment to Alzheimer's disease using brain 1H-MRS and volumetric changes: A two- year retrospective follow-up study. Neuroimage Clin 2019;23. doi:10.1016/j.nicl.2019.101843.

[13] Su L, Blamire AM, Watson R, He J, O'Brien BA and JT. Cortical and Subcortical Changes in Alzheimer's Disease: A Longitudinal and Quantitative MRI Study. Current Alzheimer Research 2016. http://www.eurekaselect.com/136989/article (accessed June 4, 2019).

[14] Schliebs R, Arendt T. The cholinergic system in aging and neuronal degeneration. Behavioural Brain Research 2011;221:555–63. doi:10.1016/j.bbr.2010.11.058.

[15] Serrano-Pozo A, Frosch MP, Masliah E, Hyman BT. Neuropathological alterations in Alzheimer disease. Cold Spring Harb Perspect Med 2011;1:a006189. doi:10.1101/cshperspect.a006189.

[16] Dong J, Revilla-Sanchez R, Moss S, Haydon PG. Multiphoton in vivo imaging of amyloid in animal models of Alzheimer's disease. Neuropharmacology 2010;59:268–75. doi:10.1016/j.neuropharm.2010.04.007.

[17] Sun S-W, Liang H-F, Trinkaus K, Cross AH, Armstrong RC, Song S-K. Noninvasive detection of cuprizone induced axonal damage and demyelination in the mouse corpus callosum. Magn Reson Med 2006;55:302–8. doi:10.1002/mrm.20774.

[18] Grandjean J, Schroeter A, He P, Tanadini M, Keist R, Krstic D, et al. Early Alterations in Functional Connectivity and White Matter Structure in a Transgenic Mouse Model of Cerebral Amyloidosis. J Neurosci 2014;34:13780–9. doi:10.1523/JNEUROSCI.4762-13.2014.

[19] Shah D, Praet J, Latif Hernandez A, Höfling C, Anckaerts C, Bard F, et al. Early pathologic amyloid induces hypersynchrony of BOLD resting-state networks in transgenic mice and provides an early therapeutic window before amyloid plaque deposition. Alzheimer's & Dementia 2016;12:964–76. doi:10.1016/j.jalz.2016.03.010.

[20] Nelson PT, Alafuzoff I, Bigio EH, Bouras C, Braak H, Cairns NJ, et al. Correlation of Alzheimer Disease Neuropathologic Changes With Cognitive Status: A Review of the Literature. Journal of Neuropathology & Experimental Neurology 2012;71:362–81. doi:10.1097/NEN.0b013e31825018f7.

[21] Braak H, Alafuzoff I, Arzberger T, Kretzschmar H, Del Tredici K. Staging of Alzheimer disease-associated neurofibrillary pathology using paraffin sections and immunocytochemistry. Acta Neuropathol 2006;112:389–404. doi:10.1007/s00401-006-0127-z.

[22] Arendt T, Holzer M, Brückner MK, Janke C, Gärtner U. The use of okadaic acid in vivo and the induction of molecular changes typical for Alzheimer's disease. Neuroscience 1998;85:1337–40. doi:10.1016/S0306-4522(97)00697-0.

[23] Gong CX, Singh TJ, Grundke-Iqbal I, Iqbal K. Phosphoprotein phosphatase activities in Alzheimer disease brain. J Neurochem 1993;61:921–7.

[24] Guo T, Noble W, Hanger DP. Roles of tau protein in health and disease. Acta Neuropathol 2017;133:665–704. doi:10.1007/s00401-017-1707-9.

[25] Buée L, Bussière T, Buée-Scherrer V, Delacourte A, Hof PR. Tau protein isoforms, phosphorylation and role in neurodegenerative disorders. Brain Res Brain Res Rev 2000;33:95–130.

[26] Snow WM, Dale R, O'Brien-Moran Z, Buist R, Peirson D, Martin M, et al. In Vivo Detection of Gray Matter Neuropathology in the 3xTg Mouse Model of Alzheimer's Disease with Diffusion Tensor Imaging. Journal of Alzheimer's Disease 2017;58:841–53. doi:10.3233/JAD-170136.

[27] Nie X, Falangola MF, Ward R, McKinnon ET, Helpern JA, Nietert PJ, et al. Diffusion MRI detects longitudinal white matter changes in the 3xTg-AD mouse model of Alzheimer's disease. Magnetic Resonance Imaging 2019;57:235–42. doi:10.1016/j.mri.2018.12.003.

[28] Liu D, Lu H, Stein E, Zhou Z, Yang Y, Mattson MP. Brain regional synchronous activity predicts tauopathy in 3×TgAD mice. Neurobiology of Aging 2018;70:160–9. doi:10.1016/j.neurobiolaging.2018.06.016.

[29] Sahara N, Perez PD, Lin W-L, Dickson DW, Ren Y, Zeng H, et al. Age-related decline in white matter integrity in a mouse model of tauopathy: an in vivo diffusion tensor magnetic resonance imaging study. Neurobiology of Aging 2014;35:1364–74. doi:10.1016/j.neurobiolaging.2013.12.009.

[30] Hamm V, Héraud C, Bott J-B, Herbeaux K, Strittmatter C, Mathis C, et al. Differential contribution of APP metabolites to early cognitive deficits in a TgCRND8 mouse model of Alzheimer's disease. Sci Adv 2017;3. doi:10.1126/sciadv.1601068.

[31] Chatterjee S, Cassel R, Schneider-Anthony A, Merienne K, Cosquer B, Tzeplaeff L, et al. Reinstating plasticity and memory in a tauopathy mouse model with an acetyltransferase activator. EMBO Molecular Medicine 2018:e8587. doi:10.15252/emmm.201708587.

[32] Veraart J, Novikov DS, Christiaens D, Ades-aron B, Sijbers J, Fieremans E. Denoising of diffusion MRI using random matrix theory. NeuroImage 2016;142:394–406. doi:10.1016/j.neuroimage.2016.08.016.

[33] Avants BB, Tustison NJ, Song G, Cook PA, Klein A, Gee JC. A reproducible evaluation of ANTs similarity metric performance in brain image registration. Neuroimage 2011;54:2033–44. doi:10.1016/j.neuroimage.2010.09.025.

[34] Reisert M, Mader I, Anastasopoulos C, Weigel M, Schnell S, Kiselev V. Global fiber reconstruction becomes practical. Neuroimage 2011;54:955–62. doi:10.1016/j.neuroimage.2010.09.016.

[35] Hübner NS, Mechling AE, Lee H-L, Reisert M, Bienert T, Hennig J, et al. The connectomics of brain demyelination: Functional and structural patterns in the cuprizone mouse model. NeuroImage 2017;146:1–18. doi:10.1016/j.neuroimage.2016.11.008.

[36] Smith SM, Miller KL, Salimi-Khorshidi G, Webster M, Beckmann CF, Nichols TE, et al. Network modelling methods for FMRI. Neuroimage 2011;54:875–91. doi:10.1016/j.neuroimage.2010.08.063.

[37] STOUFFER, SAMUEL A., EDWARD A. SUCHMAN, LELAND C. DEVINNEY, SHIRLEY A. STAR, and ROBIN M. WILLIAMS, JR. The American Soldier: Adjustment During Army Life. Vol. I. Pp. xii, 599. STOUFFER, SAMUEL A., ARTHUR A. LUMSDAINE, MARION HARPER LUMSDAINE, ROBIN M. WILLIAMS, JR., M. BREWSTER SMITH, IRVING L. JANIS, SHIRLEY A. STAR, and LEONARD S. COTTRELL, JR. The American Soldier: Combat and Its Aftermath. Vol. II. Pp. 675. Princeton: Princeton University Press, Studies in Social Psychology in World War II, 1949. Vols. I and II together, $13.50; separately, $7.50 per vol - Alfred McClung Lee, 1949 n.d. https://journals.sagepub.com/doi/abs/10.1177/000271624926500124 (accessed July 24, 2019).

[38] Green C, Sydow A, Vogel S, Anglada-Huguet M, Wiedermann D, Mandelkow E, et al. Functional networks are impaired by elevated tau-protein but reversible in a regulatable Alzheimer's disease mouse model. Mol Neurodegener 2019;14. doi:10.1186/s13024-019-0316-6.

[39] Dutar P, Bassant MH, Senut MC, Lamour Y. The septohippocampal pathway: structure and function of a central cholinergic system. Physiological Reviews 1995;75:393–427. doi:10.1152/physrev.1995.75.2.393.

[40] Belarbi K, Schindowski K, Burnouf S, Caillierez R, Grosjean M-E, Demeyer D, et al. Early Tau pathology involving the septo-hippocampal pathway in a Tau transgenic model: relevance to Alzheimer's disease. Curr Alzheimer Res 2009;6:152–7.

[41] Badea A, Kane L, Anderson RJ, Qi Y, Foster M, Cofer GP, et al. The fornix provides multiple biomarkers to characterize circuit disruption in a mouse model of Alzheimer's disease. NeuroImage 2016;142:498–511. doi:10.1016/j.neuroimage.2016.08.014.

[42] Badea A, Delpratt NA, Anderson RJ, Dibb R, Qi Y, Wei H, et al. Multivariate MR biomarkers better predict cognitive dysfunction in mouse models of Alzheimer's disease. Magn Reson Imaging 2019;60:52–67. doi:10.1016/j.mri.2019.03.022.

[43] Hara Y, Motoi Y, Hikishima K, Mizuma H, Onoe H, Matsumoto S-E, et al. Involvement of the Septo-Hippocampal Cholinergic Pathway in Association with Septal Acetylcholinesterase Upregulation in a Mouse Model of Tauopathy. Curr Alzheimer Res 2017;14:94–103.

[44] Watson C, Paxinos G, Puelles L. The Mouse Nervous System. Academic Press; 2012.

[45] Schmahmann JD, Rosene DL, Pandya DN. Motor projections to the basis pontis in rhesus monkey. J Comp Neurol 2004;478:248–68. doi:10.1002/cne.20286.

[46] Sullivan EV, Zahr NM, Rohlfing T, Pfefferbaum A. Fiber tracking functionally distinct components of the internal capsule. Neuropsychologia 2010;48:4155–63. doi:10.1016/j.neuropsychologia.2010.10.023.

[47] Thillainadesan S, Wen W, Zhuang L, Crawford J, Kochan N, Reppermund S, et al. Changes in mild cognitive impairment and its subtypes as seen on diffusion tensor imaging. Int Psychogeriatr 2012;24:1483–93. doi:10.1017/S1041610212000270.

[48] Cho H, Yang DW, Shon YM, Kim BS, Kim YI, Choi YB, et al. Abnormal Integrity of Corticocortical Tracts in Mild Cognitive Impairment: A Diffusion Tensor Imaging Study. J Korean Med Sci 2008;23:477–83. doi:10.3346/jkms.2008.23.3.477.

[49] Canu E, McLaren DG, Fitzgerald ME, Bendlin BB, Zoccatelli G, Alessandrini F, et al. Mapping the structural brain changes in Alzheimer's disease: The independent contribution of two imaging modalities. J Alzheimers Dis 2011;26:263–74. doi:10.3233/JAD-2011-0040.

[50] Rose SE, Janke AL, Chalk JB. Gray and white matter changes in Alzheimer's disease: a diffusion tensor imaging study. J Magn Reson Imaging 2008;27:20–6. doi:10.1002/jmri.21231.

[51] Xie R, Fang M, Zhou L, Fan S, Liu J, Quan H, et al. Diffusion tensor imaging detects Wallerian degeneration of the corticospinal tract early after cerebral infarction. Neural Regen Res 2012;7:900–5. doi:10.3969/j.issn.1673-5374.2012.12.004.

[52] Safadi Z, Grisot G, Jbabdi S, Behrens TE, Heilbronner SR, McLaughlin NCR, et al. Functional Segmentation of the Anterior Limb of the Internal Capsule: Linking White Matter Abnormalities to Specific Connections. J Neurosci 2018;38:2106–17. doi:10.1523/JNEUROSCI.2335-17.2017.

[53] Hyett MP, Perry A, Breakspear M, Wen W, Parker GB. White matter alterations in the internal capsule and psychomotor impairment in melancholic depression. PLOS ONE 2018;13:e0195672. doi:10.1371/journal.pone.0195672.

[54] Schindowski K, Bretteville A, Leroy K, Bégard S, Brion J-P, Hamdane M, et al. Alzheimer's Disease-Like Tau Neuropathology Leads to Memory Deficits and Loss of Functional Synapses in a Novel Mutated Tau Transgenic Mouse without Any Motor Deficits. The American Journal of Pathology 2006;169:599–616. doi:10.2353/ajpath.2006.060002.

[55] Graff-Radford J, Williams L, Jones DT, Benarroch EE. Caudate nucleus as a component of networks controlling behavior. Neurology 2017;89:2192–7. doi:10.1212/WNL.0000000000004680.

[56] Li X, Wang H, Tian Y, Zhou S, Li X, Wang K, et al. Impaired White Matter Connections of the Limbic System Networks Associated with Impaired Emotional Memory in Alzheimer's Disease. Front Aging Neurosci 2016;8:250. doi:10.3389/fnagi.2016.00250.

[57] Sforazzini F, Schwarz AJ, Galbusera A, Bifone A, Gozzi A. Distributed BOLD and CBV-weighted resting-state networks in the mouse brain. NeuroImage 2014;87:403–15. doi:10.1016/j.neuroimage.2013.09.050.

[58] Zerbi V, Grandjean J, Rudin M, Wenderoth N. Mapping the mouse brain with rs-fMRI: An optimized pipeline for functional network identification. NeuroImage 2015;123:11–21. doi:10.1016/j.neuroimage.2015.07.090.

[59] Winson J. Loss of hippocampal theta rhythm results in spatial memory deficit in the rat. Science 1978;201:160–3. doi:10.1126/science.663646.

[60] Oddie SD, Stefanek W, Kirk IJ, Bland BH. Intraseptal procaine abolishes hypothalamic stimulation-induced wheel-running and hippocampal theta field activity in rats. J Neurosci 1996;16:1948–56.

[61] Mamad O, McNamara HM, Reilly RB, Tsanov M. Medial septum regulates the hippocampal spatial representation. Front Behav Neurosci 2015;9. doi:10.3389/fnbeh.2015.00166.

[62] Khakpai F, Nasehi M, Haeri-Rohani A, Eidi A, Zarrindast MR. Septo-Hippocampo-Septal Loop and Memory Formation. Basic Clin Neurosci 2013;4:5–23.

[63] Ferreira-Vieira TH, Guimaraes IM, Silva FR, Ribeiro FM. Alzheimer's Disease: Targeting the Cholinergic System. Curr Neuropharmacol 2016;14:101–15. doi:10.2174/1570159X13666150716165726.

[64] Plowey ED, Ziskin JL. Hippocampal phospho-tau/MAPT neuropathology in the fornix in Alzheimer disease: an immunohistochemical autopsy study. Acta Neuropathol Commun 2016;4:114. doi:10.1186/s40478-016-0388-2.

[65] Mondragón-Rodríguez S, Gu N, Fasano C, Peña-Ortega F, Williams S. Functional Connectivity between Hippocampus and Lateral Septum is Affected in Very Young Alzheimer's Transgenic Mouse Model. Neuroscience 2019;401:96–105. doi:10.1016/j.neuroscience.2018.12.042.

[66] Quiroz YT, Budson AE, Celone K, Ruiz A, Newmark R, Castrillón G, et al. Hippocampal Hyperactivation in Presymptomatic Familial Alzheimer's Disease. Ann Neurol 2010;68:865–75. doi:10.1002/ana.22105.

[67] Dickerson BC, Salat DH, Greve DN, Chua EF, Rand-Giovannetti E, Rentz DM, et al. Increased hippocampal activation in mild cognitive impairment compared to normal aging and AD. Neurology 2005;65:404–11. doi:10.1212/01.wnl.0000171450.97464.49.

[68] Li H, Jia X, Qi Z, Fan X, Ma T, Ni H, et al. Altered Functional Connectivity of the Basal Nucleus of Meynert in Mild Cognitive Impairment: A Resting-State fMRI Study. Front Aging Neurosci 2017;9. doi:10.3389/fnagi.2017.00127.

[69] Chiesa PA, Cavedo E, Teipel SJ, Grothe MJ, Habert M-O, Lista S, et al. A FUNCTIONAL RESTING STATE STUDY OF BASAL FOREBRAIN FUNCTIONAL CONNECTIVITY IN ASYMPTOMATIC AT-RISK INDIVIDUALS FOR AD: THE INSIGHT-PREAD STUDY. Alzheimer's & Dementia: The Journal of the Alzheimer's Association 2017;13:P790. doi:10.1016/j.jalz.2017.06.1068.

[70] Schmitz TW, Nathan Spreng R, The Alzheimer's Disease Neuroimaging Initiative, Weiner MW, Aisen P, Petersen R, et al. Basal forebrain degeneration precedes and predicts the cortical spread of Alzheimer's pathology. Nature Communications 2016;7:13249. doi:10.1038/ncomms13249.

[71] Kamali A, Yousem DM, Lin DD, Sair HI, Jasti SP, Keser Z, et al. Mapping the trajectory of the stria terminalis of the human limbic system using high spatial resolution diffusion tensor tractography. Neuroscience Letters 2015;608:45–50. doi:10.1016/j.neulet.2015.09.035.

[72] Vertes RP. Differential projections of the infralimbic and prelimbic cortex in the rat. Synapse 2004;51:32–58. doi:10.1002/syn.10279.

[73] Swanson LW, Cowan WM. The connections of the septal region in the rat. J Comp Neurol 1979;186:621–55. doi:10.1002/cne.901860408.

[74] Masters CL, Bateman R, Blennow K, Rowe CC, Sperling RA, Cummings JL. Alzheimer's disease. Nature Reviews Disease Primers 2015;1. doi:10.1038/nrdp.2015.56.

[75] Fanselow MS, Dong H-W. Are the Dorsal and Ventral Hippocampus Functionally Distinct Structures? Neuron 2010;65:7–19. doi:10.1016/j.neuron.2009.11.031.

[76] Pereira A, Ribeiro S, Wiest M, Moore LC, Pantoja J, Lin S-C, et al. Processing of tactile information by the hippocampus. Proc Natl Acad Sci USA 2007;104:18286–91. doi:10.1073/pnas.0708611104.

[77] Bellistri E, Aguilar J, Brotons-Mas JR, Foffani G, de la Prida LM. Basic properties of somatosensory-evoked responses in the dorsal hippocampus of the rat. J Physiol 2013;591:2667–86. doi:10.1113/jphysiol.2013.251892.

[78] Crouzin N, Baranger K, Cavalier M, Marchalant Y, Cohen-Solal C, Roman FS, et al. Area-specific alterations of synaptic plasticity in the 5XFAD mouse model of Alzheimer's disease: dissociation between somatosensory cortex and hippocampus. PLoS ONE 2013;8:e74667. doi:10.1371/journal.pone.0074667.

[79] Daulatzai MA. Dysfunctional Sensory Modalities, Locus Coeruleus, and Basal Forebrain: Early Determinants that Promote Neuropathogenesis of Cognitive and Memory Decline and Alzheimer's Disease. Neurotoxicity Research 2016;30:295–337. doi:10.1007/s12640-016-9643-3.

[80] Gates GA, Anderson ML, Feeney MP, McCurry SM, Larson EB. Central Auditory Dysfunction in Older People with Memory Impairment or Alzheimer's Dementia. Arch Otolaryngol Head Neck Surg 2008;134:771–7. doi:10.1001/archotol.134.7.771.

[81] Wang Y, Risacher SL, West JD, McDonald BC, MaGee TR, Farlow MR, et al. Altered Default Mode Network Connectivity in Older Adults with Cognitive Complaints and Amnestic Mild Cognitive Impairment. J Alzheimers Dis 2013;35:751–60. doi:10.3233/JAD-130080.

[82] Petersen CCH. The Functional Organization of the Barrel Cortex. Neuron 2007;56:339–55. doi:10.1016/j.neuron.2007.09.017.

[83] Laramée M-E, Boire D. Visual cortical areas of the mouse: comparison of parcellation and network structure with primates. Front Neural Circuits 2015;8. doi:10.3389/fncir.2014.00149.

[84] Cauda F, D'Agata F, Sacco K, Duca S, Geminiani G, Vercelli A. Functional connectivity of the insula in the resting brain. Neuroimage 2011;55:8–23. doi:10.1016/j.neuroimage.2010.11.049.

[85] Bonthius DJ, Solodkin A, Van Hoesen GW. Pathology of the insular cortex in Alzheimer disease depends on cortical architecture. J Neuropathol Exp Neurol 2005;64:910–22. doi:10.1097/01.jnen.0000182983.87106.d1.

[86] Liu X, Chen X, Zheng W, Xia M, Han Y, Song H, et al. Altered Functional Connectivity of Insular Subregions in Alzheimer's Disease. Front Aging Neurosci 2018;10. doi:10.3389/fnagi.2018.00107.

[87] Roquet D, Noblet V, Anthony P, Philippi N, Demuynck C, Cretin B, et al. Insular atrophy at the prodromal stage of dementia with Lewy bodies: a VBM DARTEL study. Sci Rep 2017;7:9437. doi:10.1038/s41598-017-08667-7.

[88] Botzung A, Philippi N, Constans-Erbs M, Kemp J, Hamdaoui M, Ehrhard E, et al. INSULAR COGNITIVE IMPAIRMENT IN EARLY DEMENTIA WITH LEWY BODIES. Alzheimer's & Dementia: The Journal of the Alzheimer's Association 2017;13:P1462. doi:10.1016/j.jalz.2017.07.529.

[89] Albouy G, King BR, Maquet P, Doyon J. Hippocampus and striatum: dynamics and interaction during acquisition and sleep-related motor sequence memory consolidation. Hippocampus 2013;23:985–1004. doi:10.1002/hipo.22183.

[90] Pych JC, Chang Q, Colon-Rivera C, Haag R, Gold PE. Acetylcholine release in the hippocampus and striatum during place and response training. Learn Mem 2005;12:564–72. doi:10.1101/lm.33105.

[91] Salgado S, Kaplitt MG. The Nucleus Accumbens: A Comprehensive Review. SFN 2015;93:75–93. doi:10.1159/000368279.

[92] Mark GP, Rada P, Pothos E, Hoebel BG. Effects of feeding and drinking on acetylcholine release in the nucleus accumbens, striatum, and hippocampus of freely behaving rats. J Neurochem 1992;58:2269–74. doi:10.1111/j.1471-4159.1992.tb10973.x.

[93] Perry DC, Kramer JH. Reward processing in neurodegenerative disease. Neurocase 2015;21:120–33. doi:10.1080/13554794.2013.873063.

[94] Ortiz S, Latsko MS, Fouty JL, Dutta S, Adkins JM, Jasnow AM. Anterior cingulate cortex and ventral hippocampal inputs to the basolateral amygdala selectively control generalized fear. J Neurosci 2019:0810–9. doi:10.1523/JNEUROSCI.0810-19.2019.

[95] Allsop SA, Vander Weele CM, Wichmann R, Tye KM. Optogenetic insights on the relationship between anxiety-related behaviors and social deficits. Front Behav Neurosci 2014;8. doi:10.3389/fnbeh.2014.00241.

[96] Hebda-Bauer EK, Simmons TA, Sugg A, Ural E, Stewart JA, Beals JL, et al. 3xTg-AD Mice Exhibit an Activated Central Stress Axis during Early-Stage Pathology. J Alzheimers Dis 2013;33:407–22. doi:10.3233/JAD-2012-121438.

[97] Rajmohan V, Mohandas E. The limbic system. Indian J Psychiatry 2007;49:132–9. doi:10.4103/0019-5545.33264.

[98] Kirkby LA, Luongo FJ, Lee MB, Nahum M, Van Vleet TM, Rao VR, et al. An Amygdala-Hippocampus Subnetwork that Encodes Variation in Human Mood. Cell 2018;175:1688-1700.e14. doi:10.1016/j.cell.2018.10.005.

[99] Britt JP, Benaliouad F, McDevitt RA, Stuber GD, Wise RA, Bonci A. Synaptic and behavioral profile of multiple glutamatergic inputs to the nucleus accumbens. Neuron 2012;76:790–803. doi:10.1016/j.neuron.2012.09.040.

[100] Felten DL, O'Banion MK, Maida MS. 16 - Autonomic-Hypothalamic-Limbic Systems. In: Felten DL, O'Banion MK, Maida MS, editors. Netter's Atlas of Neuroscience (Third Edition), Philadelphia: Elsevier; 2016, p. 421–61. doi:10.1016/B978-0-323-26511-9.00016-3.

[101] Izquierdo I, da Cunha C, Rosat R, Jerusalinsky D, Ferreira MB, Medina JH. Neurotransmitter receptors involved in post-training memory processing by the amygdala, medial septum, and hippocampus of the rat. Behav Neural Biol 1992;58:16–26.

[102] Coupé P, Manjón JV, Lanuza E, Catheline G. Lifespan Changes of the Human Brain In Alzheimer's Disease. Sci Rep 2019;9. doi:10.1038/s41598-019-39809-8.

[103] Ortner M, Pasquini L, Barat M, Alexopoulos P, Grimmer T, Förster S, et al. Progressively Disrupted Intrinsic Functional Connectivity of Basolateral Amygdala in Very Early Alzheimer's Disease. Front Neurol 2016;7:132. doi:10.3389/fneur.2016.00132.

[104] Unal G, Joshi A, Viney TJ, Kis V, Somogyi P. Synaptic Targets of Medial Septal Projections in the Hippocampus and Extrahippocampal Cortices of the Mouse. J Neurosci 2015;35:15812–26. doi:10.1523/JNEUROSCI.2639-15.2015.

[105] Gonzalo-Ruiz A, Morte L. Localization of amino acids, neuropeptides and cholinergic markers in neurons of the septum-diagonal band complex projecting to the retrosplenial granular cortex of the rat. Brain Research Bulletin 2000;52:499–510. doi:10.1016/S0361-9230(00)00287-2.

[106] Dougherty KD, Turchin PI, Walsh TJ. Septocingulate and septohippocampal cholinergic pathways: involvement in working/episodic memory. Brain Res 1998;810:59–71. doi:10.1016/s0006-8993(98)00870-1.

[107] Senut MC, Menetrey D, Lamour Y. Cholinergic and peptidergic projections from the medial septum and the nucleus of the diagonal band of Broca to dorsal hippocampus, cingulate cortex and olfactory bulb: a combined wheatgerm agglutinin-apohorseradish peroxidase-gold immunohistochemical study. Neuroscience 1989;30:385–403. doi:10.1016/0306-4522(89)90260-1.

[108] Mevel K, Chételat G, Eustache F, Desgranges B. The Default Mode Network in Healthy Aging and Alzheimer's Disease. International Journal of Alzheimer's Disease 2011. doi:10.4061/2011/535816.

[109] Fleisher AS, Sherzai A, Taylor C, Langbaum JBS, Chen K, Buxton RB. Resting-state BOLD networks versus task-associated functional MRI for distinguishing Alzheimer's disease risk groups. Neuroimage 2009;47:1678–90. doi:10.1016/j.neuroimage.2009.06.021.

[110] Bai F, Zhang Z, Yu H, Shi Y, Yuan Y, Zhu W, et al. Default-mode network activity distinguishes amnestic type mild cognitive impairment from healthy aging: a combined structural and resting-state functional MRI study. Neurosci Lett 2008;438:111–5. doi:10.1016/j.neulet.2008.04.021.

[111] Buckner RL, Andrews-Hanna JR, Schacter DL. *The Brain's Default Network*: *Anatomy, Function, and Relevance to Disease*. Annals of the New York Academy of Sciences 2008;1124:1–38. doi:10.1196/annals.1440.011.

[112] Hafkemeijer A, van der Grond J, Rombouts SARB. Imaging the default mode network in aging and dementia. Biochimica et Biophysica Acta (BBA) - Molecular Basis of Disease 2012;1822:431–41. doi:10.1016/j.bbadis.2011.07.008.

[113] Filippini N, Ebmeier KP, MacIntosh BJ, Trachtenberg AJ, Frisoni GB, Wilcock GK, et al. Differential effects of the APOE genotype on brain function across the lifespan. Neuroimage 2011;54:602–10. doi:10.1016/j.neuroimage.2010.08.009.

[114] Whitesell JD, Buckley AR, Knox JE, Kuan L, Graddis N, Pelos A, et al. Whole brain imaging reveals distinct spatial patterns of amyloid beta deposition in three mouse models of Alzheimer's disease. BioRxiv 2018:395236. doi:10.1101/395236.

Supplementary material

4. Behavior tests

1.1. Objects tasks

We used a square Plexiglas open-field (52cmx52cm) for the object tests and spatial cues were disposed in the test room. Each task was divided in 2 phases: a habituation phase, and a retention phase. In the first phase of habituation, the mouse was allowed to explore the objects in the open-field for 10 minutes in the object recognition (OR) test, and for 15 minutes in the object in-place (OIP) test. The mouse was then put back in its cage and after 3h in the case of OR task, and 5min for the OIP task, one object was either changed or replaced for the retention phase. We then measured the time spent by the mouse exploring each object, and, based on the spontaneous behavior of rodents to preferentially explore novelty, we expected the mouse to spend significantly more time exploring the either changed, moved or replaced object (one-sample t-test comparing with the level of chance, $p<0.05$). Therefore, if the mouse doesn't detect the novelty, it is considered that it doesn't correctly remember the previous configuration of objects, and thus has memory impairments in this task.

1.2. The Morris Water Maze

In this test, mice had to learn the position of a platform hidden beneath opaque water in a circular pool, to get back in their cage. After 2 days of habituation, mice were trained for 5 days, 4 trials a day, to learn to locate the hidden platform using spatial cues in the room. The time spent and the path length before reaching the platform were measured using a video tracking system (Anymaze). 10 days after the learning phase, a probe test was performed for which the platform was removed. In this phase mice had 60s in the pool during which we evaluated the time spent in the target quadrant, corresponding to the quadrant where the platform was previously located. We used a one-way ANOVA with repeated measures and corrected for multiple comparisons by a Tukey test, to analyze and compare learning abilities of mice. For the probe test, the time spent in the target quadrant was compared with the chance level (15s for a test duration of 60s in four quadrants) using a one-sample t-test.

5. MRI experiments

2.1. Animal preparation

For rsfMRI acquisition, moderate MD sedation was initially induced by a subcutaneous (*sc*) bolus injection (0.6 mg MD per kg body weight in 100 µl 0.9% NaCl-solution). 15 min later, the animals received a continuous *sc* infusion of MD through an MRI compatible catheter (0.3 mg per kg body weight in 200 µl per hour) inserted at the mouse shoulder level. During the whole acquisition a 2 mm thick agar gel (2% in NaCl) was applied on the mouse head to

reduce any susceptibility artifacts arising at the coil/tissue interface. MD infusion was stopped and replaced by anesthesia through isoflurane (~1.5 % of volume) for further morphological and diffusion-based imaging protocol.

2.2. Preprocessing

The SPM function of co-registration was used to realign each functional scan to its corresponding T2-weighted image. A step of realignment of the 500 volumes to the first scan was applied as a motion correction (using a least square approach and a 6-parameters rigid body transformation in space). Normalization of the data was done on a template extracted from the Allen Brain Atlas (http://mouse.brain-map.org/static/atlas) involving a linear registration – 12-parameters affine transformation – accounting for major differences in head shape and position in between subjects as well as nonlinear registration – warping – accounting for smaller-scale anatomical differences. We performed a Gaussian smoothing with a kernel of 2 voxels FWHM to all fMRI image volumes and a zero-phase band-pass filter was applied to extract frequencies between 0.01-0.1 Hz, representatives of the Blood Oxygen Level Dependent (BOLD) signal. The signal from ventricles was regressed out using a least square approach in order to reduce non-neural detection from the cerebro-spinal fluid.

Supplementary table and figures

Supplementary table 1: *MRI acquisition parameters for the three used sequences.*

	T2-RARE	GE-EPI	DTI-EPI
Acquisition time	9min47sec	16min40sec	1h1min3sec
Field of view	2,1 x 2 cm^2	2.1 x 2 cm^2	2.1 x 2 cm^2
Resolution	0.08 x 0.07 mm^2	0.14 × 0.22 mm^2	0.1 x 0.1 mm^2
Slice thickness	0.4 mm	0.4 mm	0.5 mm
Echo time/repetition time	40/4500 ms	15ms/2000 ms	28/3000 ms
Number of volumes	/	500 volumes	/
B-values	/	/	500, 1000, 1500, 1750, 2000 s/mm^2
Diffusion parameters	/	/	Diffusion gradient duration (δ): 5 ms Time between the two diffusion gradients (Δ) = 10.64 ms

Supplementary table 2: *Abbreviations of regions of interests used in the partial correlation analysis*

Both_AAA_CEA	Bilateral Anterior and central amygdala
Both_LA_BLA_BMA	Bilateral Lateral, basolateral and basomedial amygdala
Both_MEA	Bilateral Medial amygdala
Both_ACA	Bilateral Anterior cingulate cortex
Both_RSP	Bilateral Retrosplenial cortex
Both_dhc	Bilateral Dorsal Hippocampus
Both_vhc	Bilateral Ventral Hippocampus

Both_ENT	Bilateral Entorhinal cortex
Both_SUB	Bilateral Subiculum
Both_PERI	Bilateral Perirhinal cortex
Both_ACB	Bilateral Nucleus accumbens
Both_LSX	Bilateral Lateral septum
Both_MSC	Bilateral Medial septum
Both_TRS	Bilateral Triangular nucleus of the septum
Left_SS	Left Primary somatosensory
Right_SS	Right Primary somatosensory
Both_MOp	Bilateral Primary motor cortex
Both_MOs	Bilateral Secondary motor cortex

Supplementary table 3: *Most changed edges (p<0.05, uncorr.) between Thy-Tau22 and WT at 5, 9 and 13 months from graph theory analysis (A, B, C) and from 5 to 9 months (D) and 9 to 13 months (E) in Thy-Tau22*

A. 5 months	B. 9 months	C. 13 months
Both_MSC <-> Both_RSP	Both_MSC <-> Both_LSX	Both_vhc <-> Both_AI
Both_TRS <-> Both_MSc	Both_RSP <-> Both_ACA	Both_MSC <-> Both_MOp
Left_SS <-> Both_dhc	Both_PERI <-> Both_ACB	Both_MOs <-> Both_MEA
Both_MSC <-> Both_LSX	Both_PERI <-> Both_dhc	Both_RSP <-> Both_ACA_CEA
Right_SS <-> Both_MOp	Both_MSC <-> Both_dhc	Both_TRS <-> Both_MOp
Right_SS <-> Both_MOs	Both_TRS <-> Both_MSC	Both_MSC <-> Both_LA_BLA_BMA
Both_PERI <-> Both_CP	Both_AI <-> Both_ACA_CEA	Left_SS <-> Both_MSC
Both_LA_BLA_BMA <-> Both_AI	Both_MOp <-> Both_MEA	Both_TRS <-> Both_AI
Both_LSX <-> Both_ENT	Both_SUB <-> Both_MOp	-
Both_TRS <-> Both_ACB	Both_MSC <-> Both_ACA_CEA	-
Both_AI <-> Both_ACB	Both_ACA <-> Both_ACA_CEA	-
Both_TRS <-> Both_ENT	Both_SUB <-> Both_MOs	-
Both_LA_BLA_BMA <-> Both_vhc	-	-

D. From 5 to 9 months	E. From 9 to 13 months
Both_RSP <-> Both_LSX	Both_RSP <-> Both_LSX
Both_LA_BLA_BMA <-> Both_ACA	Both_MOs <-> Both_MOp
Both_LA_BLA_BMA <-> Both_vhc	Both_dhc <-> Both_ACA_CEA
Right_SS <-> Both_MSC	Both_LA_BLA_BMA <-> Both_vhc
Both_RSP <-> Both_MOs	Both_TRS <-> Both_vhc
Both_MOp <-> Both_CP	Both_TRS <-> Both_RSP
Both_MOs <-> Both_CP	Both_MSC <-> Both_LA_BLA_BMA
Both_dhc <-> Both_ACB	Both_vhc <-> Both_ENT
Both_RSP <-> Both_CP	Both_SUB <-> Both_dhc
Both_LSX <-> Both_dhc	Both_vhc <-> Both_ACB
Both_RSP <-> Both_MOp	Both_vhc <-> Both_dhc
Both_dhc <-> Both_ACA_CEA	Both_MSC <-> Both_CP
Right_SS <-> Both_ACA_CEA	Both_MSC <-> Both_LSX
Both_RSP <-> Both_AI	Both_SUB <-> Both_ENT
-	Both_MOs <-> Both_ACA
-	Both_MSC <-> Both_vhc
-	Both_ENT <-> Both_CP
-	Both_LA_BLA_BMA <-> Both_ACA_CEA
-	Both_SUB <-> Both_CP
-	Both_LSX <-> Both_CP
-	Both_LSX <-> Both_ACA_CEA
-	Both_SUB <-> Both_ACB
-	Both_PERI <-> Both_LA_BLA_BMA
-	Both_LA_BLA_BMA <-> Both_ACB

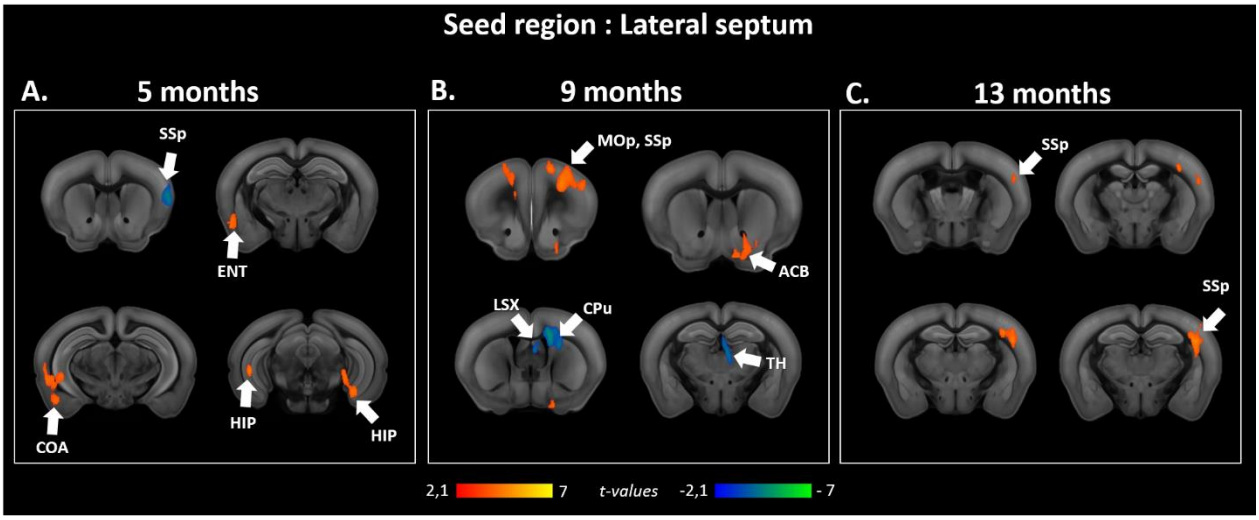

Supplementary figure 1: *Seed-based analysis of the lateral septum at 5, 9 and 13 months. Statistical comparison of the lateral septum functional connectivity between Thy-Tau22 and WT mice at (A) 5 months-old; (B) 9 months-old; and (C) 13 months-old (two sample t-test, p<0.05, FDR cluster corrected). Contrasts:* ***Thy-Tau22*** *< WT (blue scale);* ***Thy-Tau22*** *> WT (red scale).*

Group comparison between Thy-Tau22 and WT mice at 5 months-old (suppl. Fig.1, A) illustrated a significant increase of the septal (LSX) functional connectivity (FC) toward memory-related areas – the entorhinal cortex (ENT) and the hippocampus (HIP) -, and the

amygdala (COA) in Thy-Tau22 mice. A decreased FC was found between the lateral septum and the somatosensory cortex at this age in transgenic mice. At intermediate stage (suppl. Fig.1, B), the LSX showed a significantly higher FC with cortical areas -the somatosensory cortex (SSp), and the primary motor cortex (MOp)- and the accumbens nucleus (ACB) in transgenic mice; whereas a reduced FC was highlighted towards the striatal regions (LSX, and caudate putamen (CPu) in addition to the thalamus. 13 months-old Thy-Tau22 mice exclusively increased septal FC with the somatosensory cortex (suppl. Fig.1, C).

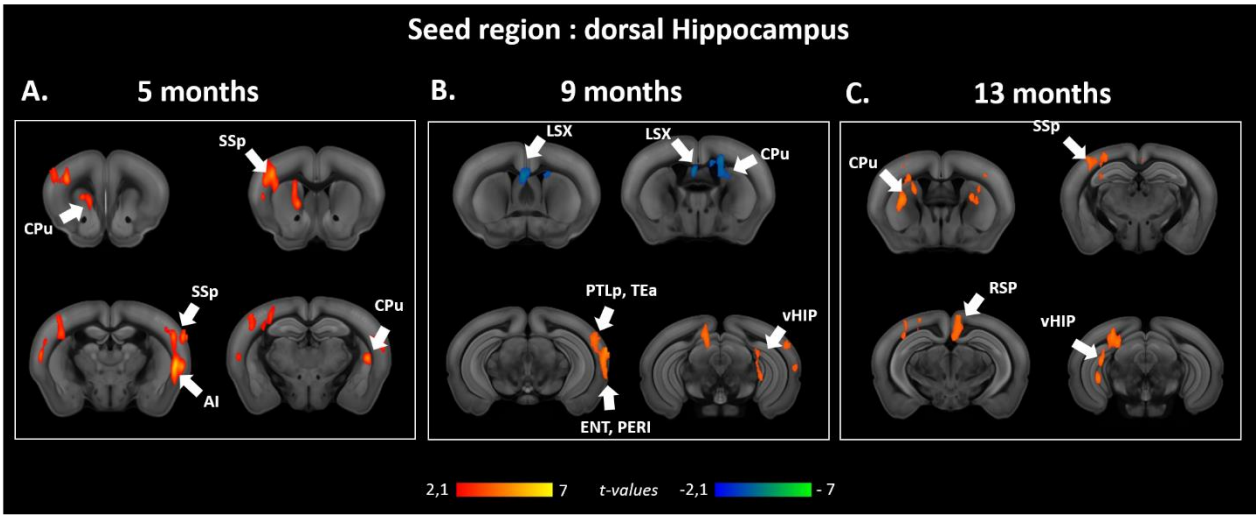

Supplementary figure 2: *Seed-based analysis of the dorsal hippocampus at 5, 9 and 13 months. Statistical comparison of the dorsal hippocampus functional connectivity between Thy-Tau22 and WT mice at (A) 5 months-old; (B) 9 months-old; and (C) 13 months-old (two sample t-test, p<0.05, FDR cluster corrected). Contrasts:* ***Thy-Tau22*** *< WT (blue scale);* ***Thy-Tau22*** *> WT (red scale). At 5 months-old, an increase of the FC of the dorsal hippocampus was found in Thy-Tau22 vs WT mice (suppl. Fig.2, A), exhibiting a hyperconnectivity towards: the somatosensory cortex (SSp), the insula (AI) and the caudate putamen (CPu). Significant differences were detected at 9 months between groups (suppl. Fig.2, B), highlighting an elevated functional communication in Thy-Tau22 mice with cortical associative areas (posterior parietal (PTLp) and temporal associative (TEa)), and memory related structures such as the entorhinal cortex (ENT), the perithinal cortex (PERI), and the ventral hippocampus (vHIP). Significant reduced FC of the dorsal hippocampus in transgenic mice was found, especially with the lateral septum (LSX) and the caudate putamen (CPu), at the intermediate stage of the disease. Significant increased FC was exclusively found in Thy-Tau22 at later stage of the disease (suppl. Fig.2, C): alteration of the dorsal hippocampus-retrosplenial (RSP) FC was found, in addition with an increased FC towards the SSp. Disrupted communication between the dorsal hippocampus and the ventral hippocampus (vHIP) was also illustrated, presenting a hypersynchronous FC, similarly as with the CPu.*

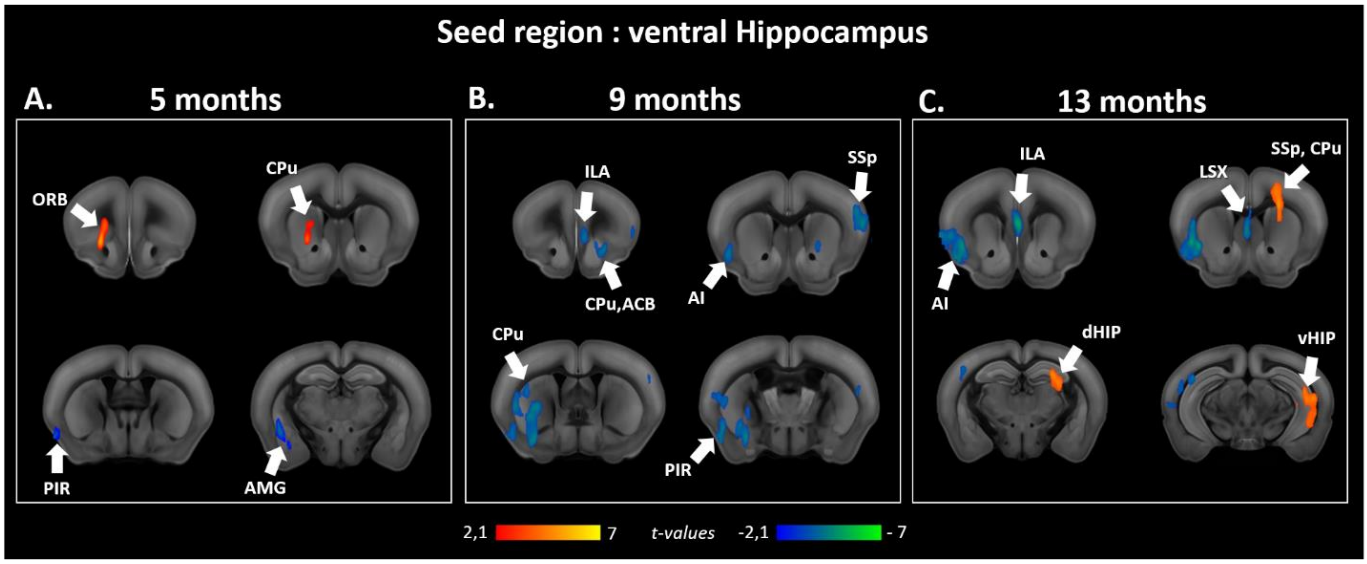

Supplementary figure 3: *Seed-based analysis of the ventral hippocampus at 5, 9 and 13 months. Statistical comparison of the dorsal hippocampus functional connectivity between Thy-Tau22 and WT mice at (A) 5 months-old; (B) 9 months-old; and (C) 13 months-old (two sample t-test, p<0.05, FDR cluster corrected). Contrasts:* ***Thy-Tau22*** *< WT (blue scale);* ***Thy-Tau22*** *> WT (red scale). Comparing groups at prodromal stage of the disease (suppl. Fig.3, A), we found a significant decrease of the functional relations between the ventral hippocampus and the amygdala (AMG). A remodeled FC was highlighted in the ventral hippocampus towards the olfactory system, showing a decreased communication with the piriform cortex (PIR), and an increase FC with the orbitofrontal cortex (ORB) and caudate putamen nucleus (CPu). At intermediate stage of the pathology, significant group differences were found, showing a decreased FC of the ventral hippocampus in Thy-Tau22 mice (suppl. Fig.3, B). Areas involved in the limbic system such as the infralimbic areas (ILA), the CPu and the accumbens nucleus (ACB) were presenting an altered FC with the ventral hippocampus at the same age. In addition, the communication of the ventral hippocampus was found disrupted towards several cortical areas including the somatosensory cortex, the agranular insula (AI), and the piriform cortex (PIR). Thy-Tau vs WT mice comparison at late stage, showed a hypersynchrony of the ventral hippocampus, in addition with the CPu and the somatosensory cortex (SSp) in Thy-Tau22 mice (suppl. Fig.3, C). Similarly to 9 months-old findings, limbic system related regions including the ILA, and the lateral septum (LSX) showed disrupted FC with the ventral hippocampus, as well as the AI.*

Additional results to the study 2:

Longitudinal microstructural alterations in Thy-Tau22 at 5, 9 and 13 months-old.

In order to better understand the specific microstructural substrate of DTI changes in Thy-Tau22 mice, we generated parametric maps of DTI derived indexes, exploring radial diffusivity (RD) and axial diffusivity (ADif) [222,250] changes between groups. These two measures may indirectly inform about specific myelin and axonal damage respectively [173]. We didn't find any group differences in 5 months-old mice. However, we further detected significant changes in RD starting at 9 months of age, and ADif from 13 months.

Investigating RD changes between groups, we found a significant RD increase in Thy-Tau22 mice compared to WT mice as of 9 months in several structures (annex figure 3): the amygdala, the hippocampus and the somatosensory cortex. In addition, cortical areas such as the visual and temporal associative areas exhibited an increased radial diffusivity, as well as the thalamus. White matter fiber bundles like the external capsule and the dorsal hippocampal commissure also showed a higher radial diffusivity in Thy-Tau2 mice than in WT mice. At 13 months, the same areas were affected showing an increased radial diffusivity in transgenic mice. In addition, the stria terminalis, the fimbria and the internal capsule pathways present a higher radial diffusivity, illustrating an increased affectation of the white matter in Thy-Tau22 mice at this age.

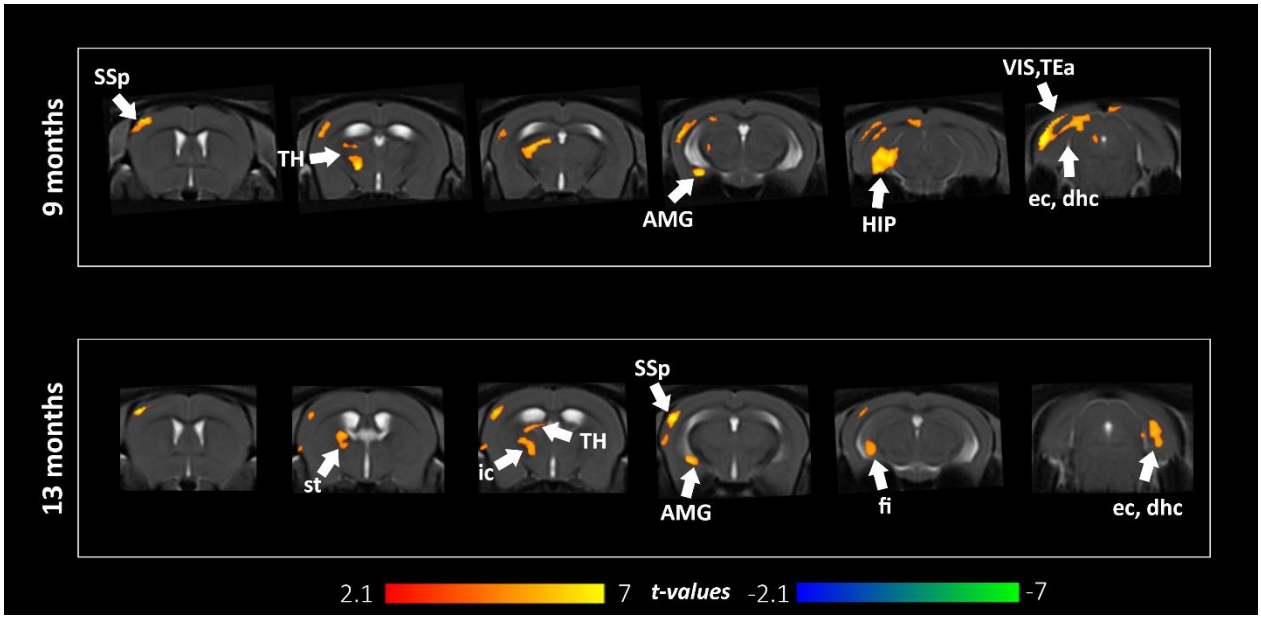

Annex figure 1: *Radial diffusivity increases over time in Thy-Tau22 mice. Coronal slices of the voxel-based quantification (VBQ) analysis of radial diffusivity (RD) showing statistical group comparison maps. An increased RD in Thy-Tau22 compared to WT mice is illustrated with positive values (red), and a decrease in negative values (blue). No statistical differences were found between groups at 5 months-old. The upper row show differences between groups at 9 months-old, and the lower row at 13 months-old. Only statistically significant differences calculated using a two-sample t-test, $p<0.05$, FDR cluster-corrected, are shown.*

We found a significant decreased RD (annex Fig.2) in Thy-Tau22 mice in several white matter tract such as the corpus callosum, the stria terminalis, the internal capsule, the fornix and the medial lemniscus. The peri-acqueducal grey areas and the thalamus, both grey matter areas, also exhibited a decreased ADif in 13 months-old transgenic mice.

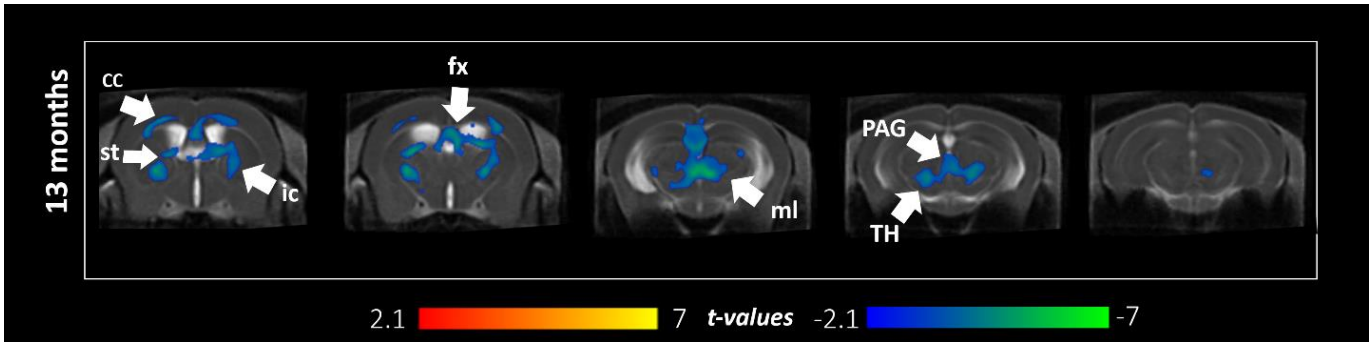

Annex figure 2: *Axial diffusivity modifications in Thy-Tau22 mice. Coronal slices of the voxel-based quantification (VBQ) analysis of axial diffusivity (ADif) showing statistical group comparison maps, a decrease in negative values (blue). No statistical differences were found between groups at 5 and 9 months-old. Only statistically significant differences calculated using a two-sample t-test, $p<0.05$, FDR cluster-corrected, are shown.*

Pilot translational study: Perspectives

To explore the translational potential of our preclinical results we conducted a very preliminary investigation, exploring changes in the hippocampal functional connectivity in Human AD patients in association with our findings of prodromal functional connectivity changes in the hippocampus in Thy-Tau22 mice.

A small cohort of 32 early AD patients displaying a score superior to 24 to the Mini Mental State Exam was compared to 19 healthy age-matching subjects in functional connectivity analysis of the left and right anterior and posterior hippocampal networks. A score inferior to 24 at MMS test denotes cognitive alterations and beginning of dementia.

Imaging was performed using a Siemens Verio 3T scanner equipped with a 32-channel head coil (Siemens, Erlangen, Germany). A resting-state BOLD-dependent sequence was used to acquire whole-brain T2*-weighted (gradient echo) echo planar images. The parameters were: repetition time = 3 s; echo time = 21 ms; field of view = 152 × 256 × 112 mm; 4-mm isotropic voxels.

Functional images were preprocessed with the following steps: low-pass filtering at 0.112 Hz to select the BOLD signal spontaneous resting-state fluctuations; slice-timing correction; rigid body registration and B0 field inhomogeneity correction; coregistration to the T1-weighted anatomical image; spatial normalization to Montreal Neurological Institute space using the DARTEL approach in SPM, with an 8-mm FWHM Gaussian kernel. We ensured that there were no between-group differences in the total amount of head motion (corresponding to the maximum absolute frame-wise displacement across scans), using ANOVA ($F(2, 156)=0.34$, $p=0.71$). Finally, a denoising step using the CompCor method [251] including cerebrospinal fluid, white matter and motion parameters was conducted to remove residual unwanted motion and physiological and artefactual effects from the BOLD signal, prior to connectivity analyses. (Methodology from Chabran E, Noblet V, Loureiro de Sousa P, Demuynck C, Philippi N, Mutter, Anthony P, Martin-Hunyadi C, Cretin B, Blanc F: Changes in gray matter volume and functional connectivity in dementia with Lewy bodies compared to Alzheimer's disease and normal aging: implications for fluctuations. Submitted to Alzheimer's Research and Therapy).

A seed-based analysis was then carried-out, using sphere ROIs of the left and right, anterior and posterior hippocampus, based on Damoiseaux et al., 2016 [252] coordinates. This segregation was chosen from literature, showing an antero-posterior functional axis of the hippocampus corresponding to the ventro-dorsal functional segregation in mice [253]. Statistical comparisons were performed using a two-sample t-test to compare AD patients and healthy subjects, and a significant cluster threshold ($p<0.05$, uncorr.) was further applied on the data.

The analysis of Thy-Tau22 mice functional connectivity of the dorsal and ventral hippocampus was performed as described in the first study at a prodromal stage of the disease (section *"2. Material and Methods"*, subsection "*2.3 MRI experiments: images acquisition and processing"*. See also annex 1, "*Processing pipeline of MRI images"* for further detailed processing steps). Results of the seed-based analysis of the dorso-ventral segregation of the

hippocampus functional communication comparison between Thy-Tau22 and WT mice, are developed in the section "*3. Results"*; subsection "*3.2 rsfMRI modifications in Thy-Tau22 before memory deficits"*, and illustrated in annex figure 4. B and D.

Evaluating the functional network modifications of the posterior left and right hippocampus (annex fig.4 A) in early AD patients *vs* healthy subjects, we revealed a hyperconnectivity of the intrinsic functional communication of the hippocampus (right). An increased functional connectivity of the posterior hippocampus with the amygdala, the putamen nucleus and the anterior insula was highlighted in early AD patients (right), but also a decreased functional relation with the superior temporal brain region and the posterior insula (right) in early AD compared to healthy patients. A higher functional connectivity of the left posterior hippocampus was detected with several cortical regions, such as the frontal cortex and the gyrus precentral sustaining motor integration.

Similarly, investigating the anterior left and right hippocampus (annex fig.4 C) we found an increased connectivity mainly with visual-related clusters such as the middle and inferior temporal gyrus, or the lateral occipital (right). A higher functional communication of the right anterior hippocampus was showed towards frontal areas and the anterior postcentral gyrus. In addition, we found a lower functional connectivity associated with angular gyrus and the postcentral posterior gyrus, both somatosensory areas (left and right respectively). We also described a decreased functional connectivity in early AD patient *vs* healthy control of the anterior hippocampus with the limbic system, including the amygdala, hippocampal-related areas, the pallidum, the accumbens nucleus, the putamen and the insula (right). The left anterior hippocampus exhibited a decreased connectivity with several cortical clusters including motor, and somatosensory areas.

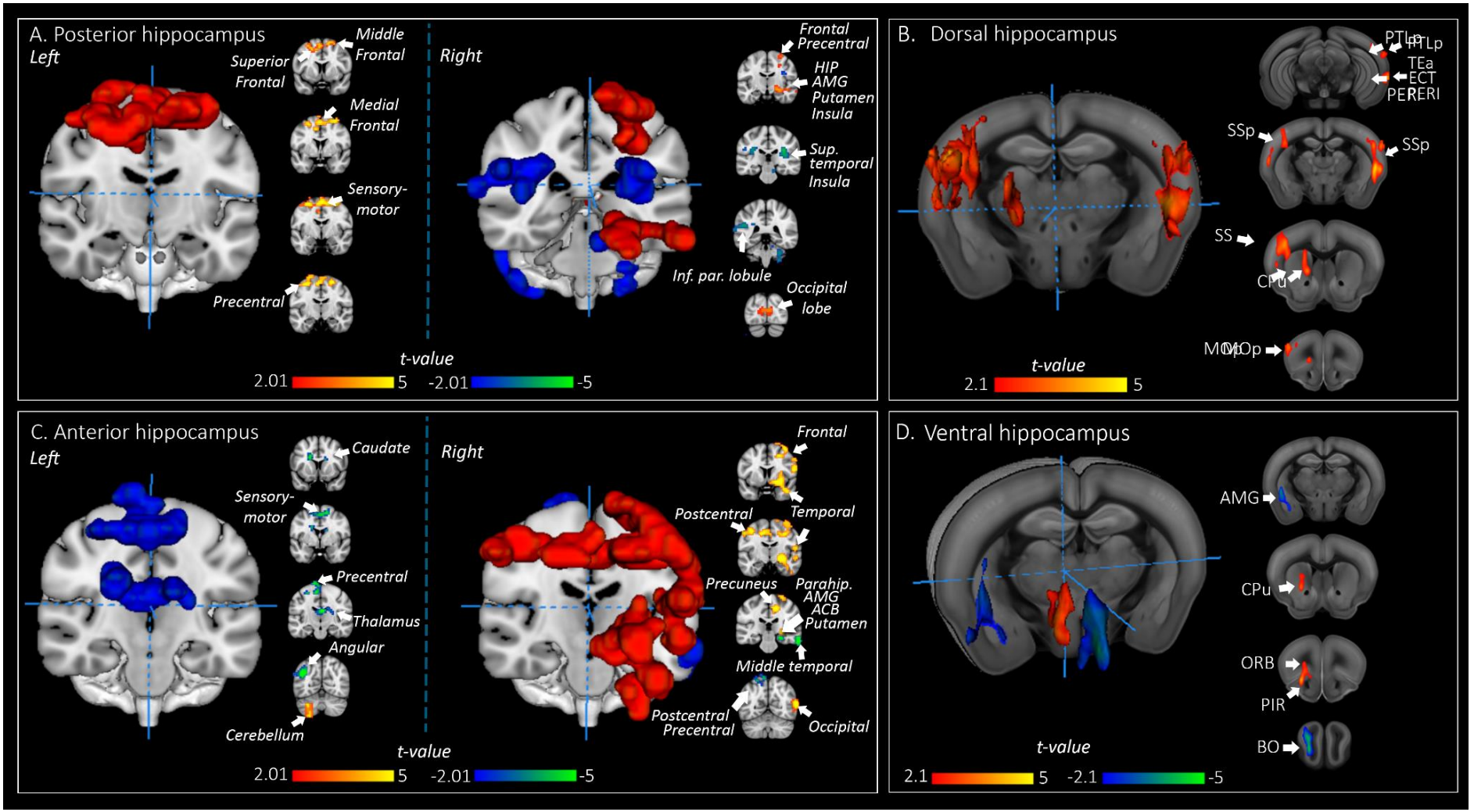
A. Posterior hippocampus
Left
Superior Frontal
Middle Frontal
Medial Frontal
Sensory-motor
Precentral
Right
Frontal Precentral
HIP
AMG
Putamen
Insula
Sup. temporal Insula
Inf. par. lobule
Occipital lobe
t-value
2.01
5
-2.01
-5
B. Dorsal hippocampus
PTLp
TEa
ECT
PERI
SSp
SS
CPu
MOp
t-value
2.1
5
C. Anterior hippocampus
Left
Caudate
Sensory-motor
Precentral
Thalamus
Angular
Cerebellum
Right
Frontal
Temporal
Postcentral
Precuneus
Parahip.
AMG
ACB
Putamen
Middle temporal
Postcentral
Precentral
Occipital
t-value
2.01
5
-2.01
-5
D. Ventral hippocampus
AMG
CPu
ORB
PIR
BO
t-value
2.1
5
-2.1
-5

Annex figure 3: *A preliminary evaluation of early hippocampal functional connectivity changes in early AD patients and prodromal Thy-Tau22 mice. Coronal slices of seed-based correlation analysis of the segregated hippocampus functional communication showing significant ($p<0.05$, uncorr.) differences between early AD patients and healthy controls in A) left and right posterior hippocampus and C) left and right anterior hippocampus. Corresponding seed-based comparison were performed comparing B) dorsal and D) ventral hippocampal functional connectivity between Thy-Tau22 and WT mice ($p<0.05$, cluster FDR corrected). Positive t-values showing a significant increase in AD patients/Thy-Tau22, and negative t-values a significant decrease in those same groups.*

D) Discussion

In this chapter, we'll discuss the results provided from the two previously presented studies, that is early and longitudinal investigations of the brain architecture in a mouse model of AD. Discussion about additional results of each study will also be included in the global interpretation of this work.

In this thesis, we aimed to uncover the evolution of the brain connectome with MRI, exploring functional connectivity modifications, structural network architecture changes, and morphological variations in a mouse model of tauopathy, from very early to late stage of the disease. For this purpose, we used resting state fMRI, diffusion MRI and brain morphometry measures in a longitudinal design. In parallel, we examined the overtime progression of the memory and learning phenotype of this model, to associate brain's circuitry alterations with behavioral output. Histological staining of pathologic proteins was additionally performed to identify the spatial distribution of phosphorylated Tau at all examined time-points.

This PhD study is thus providing a systematic characterization of the Thy-Tau22 model of tauopathy, revealing brain network signatures and structural modifications that might be used as potential biomarkers for both early diagnostic and characterizing the evolution of the disease, or as a target for future treatments.

1. Memory and learning behavioral profiles

To detect the emergence of memory deficits and to characterize its decline overtime, we submitted Thy-Tau22 mice to several tests involving specific cerebral regions of the temporal lobe areas such as the hippocampus, the entorhinal cortex and the perirhinal cortex. In AD patients, the hippocampus is one of the first and main affected brain region, after the entorhinal cortex [33]. From there, Tau lesions are spreading to other temporal regions, and to frontal association areas trough hippocampal projections in the prefrontal cortex, involved in memory consolidation [254]. At later stages of AD, pathological Tau finally reaches the occipital lobe, secondary, and primary brain areas. Using the MWM test, assessing spatial learning and memory abilities of mice, we investigated the hippocampus and the medial entorhinal cortex function in Thy-tau22 mice, both known to be strongly involved in spatial memory [255–258]. Indeed, grid cells in medial entorhinal cortex massively projecting to place cells in CA1 –a subfield of the hippocampus- through the perforant path [259], allows the hippocampus to mediate spatial cognitive processes such as learning, memory, navigation and exploration. We further refined the analysis applying the object localization tests that involve the same brain areas [260] but detecting more subtle possible alterations in spatial memory. To next assess the reliability of other memory-related regions, Thy-Tau22 mice underwent two supplementary object tests. In the object recognition test, the hippocampus would recruit the perirhinal cortex afferences to encode information about objects [261,262]. This region, which receive information about visual, olfactory and somatosensory stimulations, has been shown to be crucial for both object familiarity discrimination and object identification [263,264]. In addition, to evaluate multiple structure communication, we used the object-in-place test in which the hippocampus, perirhinal and prefrontal cortices are playing indispensable roles

[265–267] determining the reliability of interactions between the hippocampus and cortical regions in memory performance.

Our results illustrate the abilities of transgenic mice to learn and memorize environmental information's, creating a cognitive map in order to navigate and detect changes in their spatial context at 5 months. Thy-Tau22 mice also presented a reliable recognition memory at this age, contributing to combined perception and memory processes, by helping the identification of objects through the association of the different sensory features of an object [263]. Good performance in object in-place test as observed in 5 months-old Thy-Tau22 mice, have been associated with the ability to memorize features of a prior conformation -or occurrence- within an environment, making an association between an object and place in which it was previously encountered [266]. However, they exhibited memory impairment in both recognition test and object in-place test starting from 9 months, suggestive of initial manifestations of disrupted communication of the hippocampal-cortical circuits, sustaining associative memory processes, that have already been shown disrupted in AD [268,269]. At 13 months, Thy-Tau22 mice couldn't remember the location of the platform 10 days after a learning phase in the MWM test, showing spatial memory dysfunction, and therefore pointing to hippocampal affectations in mice at this age. Exploring the evolution of the phenotype in Thy-Tau22 mice, Van der Jeugd et al., in 2013b [79] highlighted comparable results, showing non-spatial memory impairment starting 6 months, and spatial memory impairment at 9 months. Among early affectations, Thy-Tau22 mice exhibited a reduced anxiety-like behavior, associated with disinhibition at 6 months-old [78]. In addition, this model has been found to present depression-like and aggressive behavior from 12 months of age, as well as "sundowning" -reflecting abnormal behavior during evening hours including activity or agitation- illustrated by an increased nocturnal activity in those mice [270]. The same group also emphasized that these mice do not present any motor impairment [78], reflecting a restricted deposition of pathological Tau in the brain, sparing the spinal cord unlike many other mice models of tauopathy [271–274] and thus displaying a closer phenotype to AD.

2. Patterns of functional and structural connectivity in Thy-Tau22 mouse model

a. Network signatures of early stage of the pathology:

a.1. Hippocampal connectivity

We showed specific functional and structural modifications of the hippocampus connectivity starting with 5 months in transgenic mice, before the occurrence of memory impairments that we detected only from 9 months on.

First, we discovered a global functional hyperconnectivity of hippocampal network, similarly to Human findings [198,217]. MRI studies in mice using either amyloid models, or mice expressing combined amyloid and tau mutations, also showed functional hippocampus hyperconnectivity at early stages of the pathology [224,231,232,275], but this was suggested to reflect the early accumulation of soluble Aβ, the overexpression of human APP, and/or the accumulation of different APP fragments, all three occurring before amyloid plaques' formation [224]. In our model, the hypersynchrony of the BOLD signal of the hippocampus and its connections could possibly reveal a compensatory mechanism ensuring the maintenance of the behavioral output following structural damage in the septo-hippocampal pathway and

the beginning of accumulation of pathological Tau and astrocytes in the same areas. The substrate of such mechanisms is worth further investigations and might stem from neuronal activity but also from transient astroglial and microglial responses, that can impact the resting state signal, via the neurovascular coupling. Despite the fact that we did not investigate the astrogliosis at 9 and 13 months, a previous study of the Thy-Tau model [78] indicates an age-dependent accumulation of astrocytes at from 3 to 6 and 12 months old, compared to WT mice.Particularly, recent studies point to astrocytes as additional cellular sources for the BOLD signal, as optogenetic astrocyte activation evokes BOLD fMRI response without neuronal activity modulation [276]. Furthermore, one has to take in account possible early inflammatory response to the tauopathy [277], impacting the BOLD rsfMRI.

We further refined our analysis by separately investigating dorsal and ventral hippocampal functional connectivity. Indeed, extensive literature is indicating a dorso-ventral functional and structural gradient in the hippocampus of mice [264,278]. In Human, this axis corresponds to an antero-posterior segregation of the hippocampus [279]. Exploring the hippocampus following such a separation has already been suggested as relevant for AD diagnosis, especially in volumetric analysis [280]. Compared to controls group, the anterior hippocampus would present a greater atrophy in AD patients than the posterior subregions [59]. In addition, functional differences have also been reported following the antero-posterior axis of the hippocampus [253]. Recently, a dynamic functional connectivity study in Human segregated the left and right hippocampus into six and five functional subregions respectively, reporting a dynamic state-dependent parcellation of the hippocampus [281], possibly with relevance for AD. In rodents, a study on a genetic mouse model of neurodegeneration also suggested that dorsal and ventral hippocampal areas present a differential susceptibility to neurodegenerative processes [282].

Dorsal hippocampus in mice receives its major input from the entorhinal lateral cortex, and projects to prefrontal areas such as the anterior cingulate cortex and retrosplenial cortex, both involved in cognitive, visuospatial information, and memory processing. Projections from the dorsal hippocampus to mamillar corpses and thalamus throughout the fornix, containing navigation related neurons, are also described. This area is therefore largely involved in spatial memory process [264]. Connections between the hippocampus and the somatosensory cortex have been showed highly segregated, has shown in the dorsal hippocampus [283]. Such communication is involved in episodic memory function, relying on the ability to integrate several features of sensory stimuli with their spatio-temporal context [284,285]. Moreover, a novel somatosensory navigational system has been recently described, sustaining by the findings of combined spatially-related cells such as place cells and head-direction cells in the somatosensory cortex, [286] and suggesting a strong involvement of this area in spatial memory process as well. Among main hippocampal connections, the septo-hippocampal communication has been largely described in literature [287] involving cholinergic reciprocal connections through the fornix. More precisely, a recent study highlighted specific connections from the dorsal hippocampus to the lateral septum that would be related to context-reinforcement in addiction behavior [288].

We demonstrated large patterns of increased dorsal hippocampal functional connectivity in Thy-Tau22 mice compared to WT mice, especially with the somatosensory cortex. This feature was also observed in amyloid mice [231] using rsfMRI and also using in vivo voltage sensitive dye imaging [289]. Maatuf et al., 2016 [290], showed with this latter technique that the whisker-evoked responses in the somatosensory cortex of amyloidopathy transgenic mice were much higher in amplitude and larger in spatial extent than in WTs at early stage of the disease. Similarly, a study combining three in vivo imaging methods detected an augmented and prolonged hemodynamic response to a sensory stimulation in a mouse model of amyloidopathy, when amyloid plaques were already developed [291]. In Human, a study used magneto-encephalography measurements after stimulation of the somatosensory cortex, and showed a larger amplitude of response in this area in MCI patients than AD or normal elderly, suggesting an early affectation of this region in AD [126], and sustaining our findings.

Ventral Hippocampus – Amygdala connectivity: One major finding of our study is the identification of hippocampus – amygdala connectivity as an early target of the Tau pathology. Indeed, while functional connection between the hippocampus and the amygdala are centralized to the ventral part of the hippocampus [292,293], we highlighted a functional hyperconnectivity of the dorsal hippocampus towards the amygdala. Acquisition of freezing responses in mice associated to contextual stimuli, strongly involving memory of sensory features, would rely on connections between the dorsal part of the hippocampus and the amygdala, whereas cued conditioned stimulus would rather be processed by the ventral hippocampus-amygdala connectivity [294]. In addition, to a functional hypersynchrony between the dorsal hippocampus and the amygdala, we depicted functional alterations of the ventral hippocampus - amygdala pathway in 5 months transgenic mice, associated with a high density of pathological tau depositions in both areas. Moreover, we highlighted dynamic functional connectivity (DFC) modifications of these specific two regions in Thy-Tau22 mice. We showed using DFC analysis that prodromal Thy-Tau22 mice spent more time in highly correlated states of the amygdala and the ventral hippocampus, than in sparse configurations, oppositely to Schumacher et al., 2018 [295] in late AD patient. Therefore, this dynamic functional pattern of connectivity might illustrate a crucial difference in dynamic communication of brain areas from early stages of the pathology to late onset.

The hippocampus and the amygdala are both key regions of the limbic system [249,296], exhibiting synchronous rhythmic oscillations [297]. Basolateral amygdala is especially involved in modulating the consolidation of emotional memories through projections to the hippocampus and the caudate-putamen nucleus [298]. Connections between hippocampus and amygdala are also crucial for fear conditioning and extinction behavior [299,300]. In AD, functional alterations of the amygdala and the hippocampus have already been reported in correlation with memory impairments at early stages of the disease [205]. Moreover, a group showed intrinsic functional connectivity alteration in early AD particularly with medial temporal lobe regions such as the hippocampus, independent of the atrophy of this same region [301]. Morphological assessment of the amygdala and hippocampus integrity have also been explored and correlated with memory functions alterations in early AD [302] and eldery with subtle cognitive decline [303]. Supporting those findings, a group recently showed that the morphological evolution during lifespan of both amygdala and hippocampus could

predict AD development in Human [212]. Interestingly, studies in both Human [304] and mice model of AD [305] highlighted the education or exercise as factors of influence to the size of amygdala and hippocampus, preventing risks of cognitive decline and neurodegenerative disease.

Therefore, the early differential modifications of the functional connectivity between dorsal and ventral hippocampus, and the amygdala, all regions also known to be strongly affected in AD at later stages and whose alterations mediate cognitive impairment, could serve as a lead toward the discovery of a non-invasive and early biomarker of AD.

In mice a huge bidirectional communication of the ventral hippocampus is shared with all amygdala nuclei, but they are also bidirectionnaly connected to prefrontal and agranular insular cortices. Those connections also mediate projections into septal nuclei, bed nucleus of stria terminalis and the hypothalamus [306–309]. Thus, the ventral hippocampus is mainly involved in emotional behavior, but also related to the integration of olfactory information by projecting to olfactory bulb and piriform cortex, before projecting to the orbitofrontal cortex [264].

At prodromal stages of the disease, functional connections of Thy-Tau22 mice exhibited also remodeled communication of the olfactory system, largely supported by human findings of early olfactory deficits in AD [310–314]. These functional alterations are however preceding olfactory dysfunctions starting at 12 months old in Thy-Tau22 mice, as shown by Martel et al in 2015 [315], despite an early detection of hyperphosphorylated tau in olfactory structures as described in this same study and sustaining by our histological findings. Therefore, this early functional alteration of the olfactory network could mediate later olfactory dysfunction in this model.

a.2 Early prefrontal cortex connectivity impairments in Thy-Tau22 mice

In AD, the prefrontal cortex of patients presents a strong deposition of toxic Aβ [316]. Recently, an atypical form of AD has been incorporated into the clinical diagnosis and research criterion of AD, called the frontal variant of AD [317]. This variant of the disease is presenting a specific affectation of the frontal lobe exhibiting a specific increase of NFT in frontal areas [318], but a similar deposition of toxic amyloid as in classical AD [319]. Clinically, patients presenting this AD variant are exhibiting similar memory symptoms as in classical AD. Based on literature and our results showing early deposition of pathological Tau in the prefrontal cortex, as well as an affected functional connectivity of the ventral hippocampus-orbitofrontal connectivity at prodromal stages, we further investigated the functional connectivity of the frontal pole in Thy-Tau22 compared to WT mice.

We detected a global increased functional communication of the frontal pole network in transgenic mice with several brain areas, including memory regions such as the entorhinal cortex, the hippocampus, and the subiculum. Using electrophysiology recording of hippocampal and prefrontal neurons of rat in a spatial memory test, a study detected a coordinated firing rhythm of both regions [320], underlying functional interactions of these two structures [321]. As suggested previously, this hyperconnectivity could reflect a

compensatory mechanism, especially in regions with a high deposition of pathological Tau. Indeed, several MRI and PET studies revealed an increased activity of prefrontal regions in AD patients, associated to a strong recruitment of neural resources during memory tasks [199,322,323]. In addition, we detected modifications of the frontal connectivity with primary and associative cortical brain areas. Indeed, the primary somatosensory, the temporal associative and the posterior parietal associative cortices also showed an increase functional connectivity with the frontal pole. These results are in line with our previous findings of a cortical hyperconnectivity at early stages in Thy-Tau22, and Human findings [198,199,217,218]. An increased functional communication was also found between the frontal area and the piriform cortex, sustaining the hypothesis of early affectations of the olfactory system in AD [313].

After presenting the extensive functional remodeling at early stage of AD, for fluency, we will continue by exposing the longitudinal functional network signatures. Their microstructural substrate is discussed afterwards (unlike in the discussion of the study 2).

b. Longitudinal profile of functional and structural brain networks alterations in Thy-Tau22 tauopathy model:

b.1 Functional network signatures

To identify functional changes over time, a longitudinal functional evaluation was performed, and revealed specific affectations of the septal communications with the hippocampus and the amygdala, and functional changes in the default-mode network were also observed.

Functional alterations through the septo-hippocampal pathway

Investigating the resting state functional network of Thy-Tau22 mice, we illustrated a specific functional affectation of the septal area toward the hippocampus, showing consistent alterations over time. This particular cholinergic circuit has been associated with working and episodic memory processes [324]. Indeed, one of the main functions of the septo-hippocampal pathway is to regulate the hippocampal theta activity [287]. In AD, affectations of this communication through the fornix/fimbria pathway would mediate the spreading of the neuropathology, and therefore enhanced the memory impairment in this disease.

Limbic system functional changes over time in Thy-Tau22

A growing affectation over time of the functional connections between the septum and the amygdala, receiving mutual innervation, was found in Thy-Tau22 mice. The communication between those two areas has been described to support memory formation, involved in consolidation of memories especially [325]. Both core nodes of the limbic system, the septum and the amygdala are also driving motivated behaviors and emotional responses [249]. Therefore, affectations of this functional circuitry have been associated in AD with impaired emotional memory, and in mice model of the pathology with disinhibitory behavior [209,326,327]. In Thy-Tau22, this same phenotype was found, starting at early stage of the disease [78], which may be linked to functional disruption of the septo-amygdala communication detected in this large-scale functional investigation.

The default-mode network: patterns of functional disruption in Thy-Tau22 mice

Strongly associated with AD, the default-mode network (DMN) have been mostly related to decrease functional communication at late stages of the disease [115], that would be mediated by amyloid deposition along time [111]. However, we described a continuous hyperactivity of this network in Thy-Tau22 mice. While some studies detected increases in the DMN connectivity in AD, most were associated with MCI or prodromal AD stages [328,329]. Here, we therefore suggest a specific interaction between pathological Tau and DMN's dysfunctions in AD, sustained by the detection of an overlapping spatial distribution of phosphorylated Tau with DMN nodes in Thy-Tau22 over time. In addition, we showed an altered function connectivity between the septum and the retrosplenial cortex, a core node of the DMN, sustaining a specific affectation of this network towards septal nuclei. Together, our findings on the functional remodeling in Thy-Tau22 mice position the septal area at the intersection of two important systems: the limbic and the default mode network, possibly regulating their interactions in AD.

Towards Dynamic functional connectivity investigations

Dynamic functional changes have already been shown in AD patients [330] but the interpretations of these findings can be very complex [101]. Fu et al in 2019 [331] associated dynamic features changes in AD with cognitive performances, highlighting the relevance of the exploration of dynamic networks to track cognitive impairment. Investigating the evolution of dynamic functional connectivity in AD, two other studies showed consistent results of decreased whole brain global dynamic functional interaction in patients at dementia stages [332,333]. Dynamic functional communication was also used to classify early and late AD [334], or MCI and controls patients [335], illustrating a change in dynamics from healthy controls, to early and late AD. Another group compared the dynamic functional connectivity between seven main networks of the brain in AD and Lewis Body dementia patients. They showed that both groups spent more time than controls in sparse connectivity configurations, and presented a reduced capacity to switch out from low inter-network connectivity [295]. Dynamic functional connectivity analysis has already been applied in mice as well, on social stress model or anesthetized mice [104]. Using a related measurement to dynamic called Quasi-Periodic Patterns (QPP), a group investigated functional networks in a mouse model of amyloidopathy [236]. They showed that transgenic mice presented an opposite dynamic DMN pattern to control mice, and a decrease of interaction between the DMN and task-positive network.

Therefore, to further explore the functional changes between areas showing specific affectation in static functional analysis, the use of dynamic functional connectivity investigation could provide a complementary insight of longitudinal functional alterations in the Thy-Tau22 mouse model.

b.2. Progressive microstructural alterations along major cholinergic pathways

Functional connectivity modifications described in Thy-Tau22 mice strongly correlate with FA and fiber density results, indicative of major microstructural damages of three main

cholinergic fiber tracts [246,268] starting at 5 months and increasing over time: (i) the septo-hippocampal pathway, (ii) the stria terminalis -a major efferent pathway of the amygdala projecting to the septum, the bed nucleus of stria terminalis (BST) the hypothalamus and the thalamus [308]-, and (iii) the cortico-thalamo-pontine tract combining the internal capsule pathway and descending fibers to the cerebral peduncle. This last tract is sending information from primary and supplementary motor areas, frontopontine, and thalamus to brain stem and cerebellar regions, and from thalamus to prefrontal cortex [336,337].

Associated brain areas to these white matter pathways were also presenting structural affectations, including septum, the caudate-putamen, the hippocampus, and the thalamus from 5 months, and the BST starting at 9 months.

In AD patients the cholinergic system that is particularly involved in memory processes [287], have been described to be damaged [338]. Indeed, the three pathway described earlier have been associated with AD dysfunction in Human, particularly at early stages of the disease [220,339–342] and in rodent studies [176,209,239,244,343]. More specifically, the septo-hippocampal pathway has been shown as mainly affected in an ex-vivo study of 13 months Thy-Tau22 mice [80,344] and in other mouse models of AD [345,346]. This cholinergic pathway is originating in the medial septal area, containing neurons projecting to the hippocampal formation through the fornix, strongly affected in AD [347], and the fimbria. Another route also innervates the amygdala to end mainly in the subiculum [287]. Related to FA and FD alterations of the septo-hippocampal pathway detected at prodromal stages and over time, we observed radial and axial diffusivity changes in Thy-Tau22 starting 9 months in this same tract. Indeed, FA and FD measurement are not specifically linked to myelin of axon's damage. Therefore, we refined our structural modifications assessment over time by carrying-out an analysis of radial and axial diffusivity, presented in the additional results to the second study. An increased radial diffusivity in the hippocampus and connecting fibers such as the dorsal hippocampal commissure was found, in addition to an increase of axial diffusivity in the hippocampus and the subiculum. While an increase of radial diffusivity has been strongly associated with myelin damaged in fibers [173,250], a higher axial diffusivity has already been found in AD and other neurodegenerative diseases such as Huntington's disease [178]. Studies have linked this unexpected increase of axial diffusivity to a potential increase of extracellular water content secondary to atrophy of the white matter, increasing the extra-axonal space, reducing the axonal caliber and therefore leading to higher water diffusion coefficients parallel to axons [177,178]. Similarly, we detected at 9 months an increased axial diffusivity in the amygdala, associated to an increased radial diffusivity in Thy-Tau22 mice. These results showed a potential axonal and myelin damages of the septo-hippocampal pathway and connected regions, that might contribute to functional modifications in those same brain areas. A similar affectation of the white matter has been observed in cortical areas of 9 months Thy-Tau22, which could be the result of a toxic functional hypersynchrony of this region at early and intermediary stages of the disease [215].

In 13 months old Thy-Tau22 mice, we found an important decrease of the axial diffusivity in the fornix, the stria terminalis, the internal capsule and the thalamus, suggesting axonal damage in these brain structures, in adequation with a decrease FA and FD. Moreover,

an increased radial diffusivity at the same age, in those same areas and related brain structures such as the fimbria, the dorsal hippocampal commissure and the amygdala, highlighted affectations of both axon and myelin in these pathways, that might reflect a Wallerian degeneration [173,250]. A decreased axial diffusivity was found in the corpus callosum in 13 months old Thy-Tau22 compared to WT mice. Similar findings were reported in AD patients in DTI studies as well, however at earlier stages, suggesting involvement of the tauopathy in degradation of this fiber bundle [339]. A DTI longitudinal study on a mouse model of tauopathy also detected alterations of the corpus callosum at later stages of the disease [244], sustaining this hypothesis.

Moreover, the atrophy of the hippocampus and the amygdala, which was detected in our study at the same time as the appearance of memory impairment in mice, is in agreement with measures in Human that point to the importance of the morphological features of two areas in the prediction of AD [212]. We showed that alterations of functional connectivity patterns of these two regions are preceding morphological changes. Thus, both prodromal and progressive longitudinal affectations of the septo-hippocampal pathway involving functional and microstructural communication can be seen as a potential signature of AD, and a target for treatment development.

Therefore, these microstructural findings could underlie the functional alterations that we characterize overtime in Thy-Tau22 mice. Indeed, structurally connected regions of the three cholinergic described pathways also presented functional connectivity modifications over time. As exposed in Fornito and Bullmore 2015 [185], changes in the functional connectome of the brain are mostly supported by structural architecture alterations. However, when looking at the extent of functional modifications that we identified in Thy-Tau22 mice, one has to take in account that functional networks shows flexibility and exceeds the confines of anatomically defined networks, as synchronous activity between two regions might exist due to polysynaptic connections or driven by a third region [93].

“From mice to men”:

To explore the translational potential of our preclinical results, we conducted a very preliminary study observing changes in the hippocampal functional connectivity of a small cohort of 32 early AD patient -displaying a high score at memory tests (Mini Mental State Exam score superior to 24)-, in relation with our result in Thy-Tau22 mice at prodromal stages. Based on literature, we segregated the Human hippocampus into the antero-posterior axis, corresponding to the ventro-dorsal functional gradient in mice [253]. In patients, the anterior hippocampus exhibited an increased connectivity with mainly visual-related clusters, and a higher functional connectivity with somatosensory areas. These results could be associated to the increased functional connectivity of the ventral hippocampus with olfactory related regions in Thy-Tau22 mice, corresponding to the one of the major exploration systems in mice [348,349], as the visual system in Human. We additionally found a decreased functional connectivity of the anterior hippocampus in early AD patients with the limbic system, a similar result as what we showed in Thy-Tau22 mice. In early AD patients, several cortical clusters exhibited a decreased connectivity with the anterior hippocampus, a functional connectivity change that we didn’t find in Thy-Tau22 mice.

Similarly investigating the functional network modifications of the posterior hippocampus in early AD patients, we revealed a hyperconnectivity of this region within the hippocampus, the amygdala and the putamen nucleus, reflecting very close results to our findings of functional connectivity of dorsal hippocampus in Thy-Tau22 mice. The increased connectivity in early AD patients of the posterior hippocampus with the amygdala, sustains our hypothesis of a compensatory mechanisms involved between those regions at this stage of the disease. Moreover, we found an increased connectivity with frontal regions, in coherence with the connectivity changes observed in the frontal functional network of Thy-Tau22 mice at 5 months old. However, several brain regions in humans and mice presented divergent patterns of connectivity early pathology phases.

In this preliminary study, we only included a very small cohort of patients, which leads to a high variability between subjects, and the use of a low threshold to detect significant modifications in group comparison. Therefore, differences in the findings of functional connectivity changes in AD patients and transgenic mice could be attributed to both, the preliminary state of this investigation including only a few patients, and the genotype of Thy-tau22 mice based on Tau mutations inducing only a tauopathy without mediating an amyloid pathology. However, we highlighted several similarities between our observations in Thy-Tau22 mice at prodromal stages and early AD patients, which underpin the translational potential of our findings to Human.

3. CONCLUSION and OUTLOOK

a. Major findings of the study

Early functional network signatures of Tau pathology in the Thy-Tau22 mouse model of Alzheimer's disease:

At prodromal stage of the disease, before the beginning of memory impairments, we detected functional communication disruption in Thy-Tau22 mice, involving areas of the brain strongly associated with AD.

1) First, we described a hypersynchronous signal between the dorsal hippocampus and isocortical areas, including the somatosensory cortex. Such mechanism could be related to the preserve episodic memory in Thy-Tau22, relying on the ability to integrate several features of sensory stimuli with their spatio-temporal context.
2) Second, we highlighted a remodeled hippocampus-amygdala functional communication, revealing a potential compensatory process driven by a hyperconnectivity between the dorsal hippocampus and the amygdala. This mechanism would sustain the maintainance of the integrity of dorsal memory processes at this age such as spatial navigation, and counterbalanced the decreased functional connectivity of the ventral hippocampus towards the amygdala. Dynamic functional interactions of both amygdala and ventral part of the hippocampus, are strongly supporting those findings.
3) Third, we showed a global increased functional communication of the frontal pole network, especially towards memory-related areas. As suggested previously, this

hyperconnectivity could reflect a compensatory mechanism to prevent cognitive impairment at this stage of the pathology, particularly frontal symptoms.

All those hypersynchronous mechanisms were found to highly overlap with the spatial distribution of the pathological Tau deposition, majorly found in the hippocampus, the amygdala and the somatosensory cortex at this age in Thy-Tau22 mice. Although we cannot demonstrate in our study, we could conjecture that the onset of this toxic pathological mechanisms, could drive a compensatory functional response in affected areas, and thus prevent memory impairment in those mice at early stage of the disease. This increased signaling could also capture early responses from other cellular sources such as the astrocytes impacting the BOLD rsfMRI signal. Whichever the source of these changes, these specific functional signatures at prodromal stage of the pathology constitute great clues to the encounter of potential early biomarkers of AD, a key item that remains to be overcome in this field of research.

Longitudinal profile of cerebral networks alterations inThy-Tau22 mice

Functional changes: We showed brain-wide functional connectivity alterations, highlighting the septum as a central node of the functional disruption over time.

Indeed, major functional circuits involving the septum were found continuously affected from early to late stage of the tauopathy: (i) the septo-hippocampal pathway and (ii) the interaction between the septal area and amygdala, both sustaining memory processes and emotional behavior alterations respectively, and largely described in AD. (iii) Moreover, we highlight DMN modifications and a specific affected functional communication between the DMN and the septum, communication through cholinergic projections from the septal nuclei towards the retrosplenial cortex. This last finding is reinforcing the crucial role of the septum communication in the functional longitudinal remodeling of networks in Thy-Tau22 mice.

Structural changes: We then described affectations of three cholinergic white matter pathways, a system highly affected in AD. The fornix/fimbria, majorly involved in the communication between the hippocampus and the septum, and associated with episodic memory processes, was found increasingly altered over time. Disruption of the stria terminalis, a fiber tract connecting the amygdala to the septum and involved in anxiety behavior, have been detected from early to late stage of the pathology. Finally, axonal damage of the internal capsule and descending fibers of the cerebral peduncle was found, carrying information between cortical areas, basal ganglia and midbrain nucleus, and may be associated with altered psychomotor, emotional and motivation behavior. From those findings, we thus highlighted microstructural affectations, correlated to main core symptoms of AD such as memory impairment, emotional affectations, sundowning, and disinhibition behavior.

Morphological atrophy of the hippocampus and the amygdala were detected from intermediate stage of the pathology. At the same time-point, Thy-Tau22 began to underperform in memory tests, suggesting a combined implication of the increasing microstructural affectations specifically connecting those areas -fornix/fimbria and stria terminalis- and atrophy of those brain regions in the development of memory impairments at this age.

b. Perspectives

In the present work, we described specific patterns of brain connectivity architecture remodeling, related to Alzheimer's disease. Exploring early and longitudinal evolution of the pathology enabled us to explore time-dependent evolution of the diseased brain functional and structural organization. Detailed work into the highlighted areas using further dynamic functional connectivity investigation over time, might provide insight into the pathological changes of brain interactions between affected brain regions along Alzheimer's disease, including both functional and structural dynamics evaluation. Moreover, comparative MRI studies to preclinical models of similar neurodegenerative diseases such as Lewy Body Dementia, would offer a lead towards potential biomarkers of differential diagnosis, a major black point in the early identification of neurodegenerative diseases. Moreover, brain MRI in this model might be used to investigate networks therapy responses to new pharmaceutical agents, that have already been shown to reinstating plasticity and memory in this same model.

References

[1] Stelzmann RA, Schnitzlein HN, Murtagh FR. An english translation of alzheimer's 1907 paper, "über eine eigenartige erkankung der hirnrinde." Clin Anat 1995;8:429–31. doi:10.1002/ca.980080612.

[2] Lambert J-C, Ibrahim-Verbaas CA, Harold D, Naj AC, Sims R, Bellenguez C, et al. Meta-analysis of 74,046 individuals identifies 11 new susceptibility loci for Alzheimer's disease. Nat Genet 2013;45:1452–8. doi:10.1038/ng.2802.

[3] Jansen IE, Savage JE, Watanabe K, Bryois J, Williams DM, Steinberg S, et al. Genome-wide meta-analysis identifies new loci and functional pathways influencing Alzheimer's disease risk. Nat Genet 2019;51:404–13. doi:10.1038/s41588-018-0311-9.

[4] World Alzheimer Report 2015, The Global Impact of Dementia: An analysis of prevalence, incidence, cost and trends n.d.:87.

[5] Galea LAM, Frick KM, Hampson E, Sohrabji F, Choleris E. Why estrogens matter for behavior and brain health. Neurosci Biobehav Rev 2017;76:363–79. doi:10.1016/j.neubiorev.2016.03.024.

[6] Snyder HM, Asthana S, Bain L, Brinton R, Craft S, Dubal DB, et al. Sex biology contributions to vulnerability to Alzheimer's disease: A think tank convened by the Women's Alzheimer's Research Initiative. Alzheimers Dement J Alzheimers Assoc 2016;12:1186–96. doi:10.1016/j.jalz.2016.08.004.

[7] Andrew MK, Tierney MC. The puzzle of sex, gender and Alzheimer's disease: Why are women more often affected than men? Womens Health 2018;14:1745506518817995. doi:10.1177/1745506518817995.

[8] Alzheimer (maladie d'). Inserm - Sci Pour Santé n.d. https://www.inserm.fr/information-en-sante/dossiers-information/alzheimer-maladie (accessed May 6, 2019).

[9] Wolters FJ, Ikram MA. Epidemiology of Dementia: The Burden on Society, the Challenges for Research. In: Perneczky R, editor. Biomark. Alzheimer's Dis. Drug Dev., vol. 1750, New York, NY: Springer New York; 2018, p. 3–14. doi:10.1007/978-1-4939-7704-8_1.

[10] La maladie d'Alzheimer en chiffres. Fr Alzheimer n.d. https://www.francealzheimer.org/maladie-dalzheimer-vos-questions-nos-reponses/maladie-dalzheimer-chiffres/ (accessed May 6, 2019).

[11] Tanzi RE, Bertram L. Twenty Years of the Alzheimer's Disease Amyloid Hypothesis: A Genetic Perspective. Cell 2005;120:545–55. doi:10.1016/j.cell.2005.02.008.

[12] Querfurth HW, LaFerla FM. Alzheimer's Disease. N Engl J Med 2010;362:329–44. doi:10.1056/NEJMra0909142.

[13] Kayed R, Head E, Thompson JL, McIntire TM, Milton SC, Cotman CW, et al. Common Structure of Soluble Amyloid Oligomers Implies Common Mechanism of Pathogenesis. Science 2003;300:486–9. doi:10.1126/science.1079469.

[14] Walsh DM, Selkoe DJ. Aβ Oligomers – a decade of discovery. J Neurochem 2007;101:1172–84. doi:10.1111/j.1471-4159.2006.04426.x.

[15] Lue L-F, Kuo Y-M, Roher AE, Brachova L, Shen Y, Sue L, et al. Soluble Amyloid β Peptide Concentration as a Predictor of Synaptic Change in Alzheimer's Disease. Am J Pathol 1999;155:853–62.

[16] Mena MA, Rodríguez-Navarro JA, García de Yébenes J. The multiple mechanisms of amyloid deposition. Prion 2009;3:5–11.

[17] Thinakaran G, Koo EH. Amyloid Precursor Protein Trafficking, Processing, and Function. J Biol Chem 2008;283:29615–9. doi:10.1074/jbc.R800019200.

[18] Tam JH, Seah C, Pasternak SH. The Amyloid Precursor Protein is rapidly transported from the Golgi apparatus to the lysosome and where it is processed into beta-amyloid. Mol Brain 2014;7:54. doi:10.1186/s13041-014-0054-1.

[19] Yu WH, Kumar A, Peterhoff C, Shapiro Kulnane L, Uchiyama Y, Lamb BT, et al. Autophagic vacuoles are enriched in amyloid precursor protein-secretase activities: implications for β-amyloid peptide over-production and localization in Alzheimer's disease. Int J Biochem Cell Biol 2004;36:2531–40. doi:10.1016/j.biocel.2004.05.010.

[20] Yu WH, Cuervo AM, Kumar A, Peterhoff CM, Schmidt SD, Lee J-H, et al. Macroautophagy—a novel β-amyloid peptide-generating pathway activated in Alzheimer's disease. J Cell Biol 2005;171:87–98. doi:10.1083/jcb.200505082.

[21] Selkoe DJ. Alzheimer's Disease Is a Synaptic Failure. Science 2002;298:789–91. doi:10.1126/science.1074069.

[22] Du H, Guo L, Yan S, Sosunov AA, McKhann GM, Yan SS. Early deficits in synaptic mitochondria in an Alzheimer's disease mouse model. Proc Natl Acad Sci 2010;107:18670–5. doi:10.1073/pnas.1006586107.

[23] Krafft GA, Klein WL. ADDLs and the signaling web that leads to Alzheimer's disease. Neuropharmacology 2010;59:230–42. doi:10.1016/j.neuropharm.2010.07.012.

[24] Braak H, Alafuzoff I, Arzberger T, Kretzschmar H, Del Tredici K. Staging of Alzheimer disease-associated neurofibrillary pathology using paraffin sections and immunocytochemistry. Acta Neuropathol (Berl) 2006;112:389–404. doi:10.1007/s00401-006-0127-z.

[25] Arendt T, Holzer M, Brückner MK, Janke C, Gärtner U. The use of okadaic acid in vivo and the induction of molecular changes typical for Alzheimer's disease. Neuroscience 1998;85:1337–40. doi:10.1016/S0306-4522(97)00697-0.

[26] Gong CX, Singh TJ, Grundke-Iqbal I, Iqbal K. Phosphoprotein phosphatase activities in Alzheimer disease brain. J Neurochem 1993;61:921–7.

[27] Guo T, Noble W, Hanger DP. Roles of tau protein in health and disease. Acta Neuropathol (Berl) 2017;133:665–704. doi:10.1007/s00401-017-1707-9.

[28] Weingarten MD, Lockwood AH, Hwo SY, Kirschner MW. A protein factor essential for microtubule assembly. Proc Natl Acad Sci 1975;72:1858–62. doi:10.1073/pnas.72.5.1858.

[29] Patterson KR, Remmers C, Fu Y, Brooker S, Kanaan NM, Vana L, et al. Characterization of prefibrillar Tau oligomers in vitro and in Alzheimer disease. J Biol Chem 2011;286:23063–76. doi:10.1074/jbc.M111.237974.

[30] Brion JP, Passareiro H, Nunez J, Flament Durand J. Mise en évidence immunologique de la protéine tau au niveau des lésions de dégénérescence neurofibrillaire de la maladie d'Alzheimer. Arch Biol (Liege) 1985;95:229–35.

[31] Buée L, Bussière T, Buée-Scherrer V, Delacourte A, Hof PR. Tau protein isoforms, phosphorylation and role in neurodegenerative disorders. Brain Res Brain Res Rev 2000;33:95–130.

[32] Mandelkow E, von Bergen M, Biernat J, Mandelkow E-M. Structural principles of tau and the paired helical filaments of Alzheimer's disease. Brain Pathol Zurich Switz 2007;17:83–90. doi:10.1111/j.1750-3639.2007.00053.x.

[33] Braak H, Braak E. Frequency of Stages of Alzheimer-Related Lesions in Different Age Categories n.d.:7.

[34] Masters CL, Bateman R, Blennow K, Rowe CC, Sperling RA, Cummings JL. Alzheimer's disease. Nat Rev Dis Primer 2015;1. doi:10.1038/nrdp.2015.56.

[35] Hardy JA, Higgins GA. Alzheimer's disease: the amyloid cascade hypothesis. Science 1992;256:184–5. doi:10.1126/science.1566067.

[36] Bilousova T, Miller CA, Poon WW, Vinters HV, Corrada M, Kawas C, et al. Synaptic Amyloid-β Oligomers Precede p-Tau and Differentiate High Pathology Control Cases. Am J Pathol 2016;186:185–98. doi:10.1016/j.ajpath.2015.09.018.

[37] Duyckaerts C, Braak H, Brion J-P, Buée L, Del Tredici K, Goedert M, et al. PART is part of Alzheimer disease. Acta Neuropathol (Berl) 2015;129:749–56. doi:10.1007/s00401-015-1390-7.

[38] Karran E, Mercken M, De Strooper B. The amyloid cascade hypothesis for Alzheimer's disease: an appraisal for the development of therapeutics. Nat Rev Drug Discov 2011;10:698–712. doi:10.1038/nrd3505.

[39] Korczyn AD. The amyloid cascade hypothesis. Alzheimers Dement J Alzheimers Assoc 2008;4:176–8. doi:10.1016/j.jalz.2007.11.008.

[40] Lee H, Casadesus G, Zhu X, Joseph JA, Perry G, Smith MA. Perspectives on the amyloid-beta cascade hypothesis. J Alzheimers Dis JAD 2004;6:137–45.

[41] Pimplikar SW. Reassessing the amyloid cascade hypothesis of Alzheimer's disease. Int J Biochem Cell Biol 2009;41:1261–8. doi:10.1016/j.biocel.2008.12.015.

[42] Nelson PT, Alafuzoff I, Bigio EH, Bouras C, Braak H, Cairns NJ, et al. Correlation of Alzheimer Disease Neuropathologic Changes With Cognitive Status: A Review of the Literature. J Neuropathol Exp Neurol 2012;71:362–81. doi:10.1097/NEN.0b013e31825018f7.

[43] Galvan V, Gorostiza OF, Banwait S, Ataie M, Logvinova AV, Sitaraman S, et al. Reversal of Alzheimer's-like pathology and behavior in human APP transgenic mice by mutation of Asp664. Proc Natl Acad Sci U S A 2006;103:7130–5. doi:10.1073/pnas.0509695103.

[44] Mohandas E, Rajmohan V, Raghunath B. Neurobiology of Alzheimer's disease. Indian J Psychiatry 2009;51:55. doi:10.4103/0019-5545.44908.

[45] Heneka MT, Carson MJ, El Khoury J, Landreth GE, Brosseron F, Feinstein DL, et al. Neuroinflammation in Alzheimer's Disease. Lancet Neurol 2015;14:388–405. doi:10.1016/S1474-4422(15)70016-5.

[46] Kinney JW, Bemiller SM, Murtishaw AS, Leisgang AM, Salazar AM, Lamb BT. Inflammation as a central mechanism in Alzheimer's disease. Alzheimers Dement Transl Res Clin Interv 2018;4:575–90. doi:10.1016/j.trci.2018.06.014.

[47] Carmona S, Zahs K, Wu E, Dakin K, Bras J, Guerreiro R. The role of TREM2 in Alzheimer's disease and other neurodegenerative disorders. Lancet Neurol 2018;17:721–30. doi:10.1016/S1474-4422(18)30232-1.

[48] Chun H, Lee CJ. Reactive astrocytes in Alzheimer's disease: A double-edged sword. Neurosci Res 2018;126:44–52. doi:10.1016/j.neures.2017.11.012.

[49] N.d. https://www.bioscience.org/2013/v5e/af/605/fulltext.htm (accessed May 6, 2019).

[50] Association AP. DSM-5 - Manuel diagnostique et statistique des troubles mentaux. Elsevier Masson; 2015.

[51] Serrano-Pozo A, Frosch MP, Masliah E, Hyman BT. Neuropathological alterations in Alzheimer disease. Cold Spring Harb Perspect Med 2011;1:a006189. doi:10.1101/cshperspect.a006189.

[52] Conway MA. Episodic memories. Neuropsychologia 2009;47:2305–13. doi:10.1016/j.neuropsychologia.2009.02.003.

[53] Nicholas M, Connor LT, Obler LK, Albert ML. 12 - Aging, Language, and Language Disorders. In: Taylor Sarno M, editor. Acquir. Aphasia Third Ed., San Diego: Academic Press; 1998, p. 413–49. doi:10.1016/B978-012619322-0/50015-4.

[54] Matthews BR. Memory Dysfunction. Contin Lifelong Learn Neurol 2015;21:613–26. doi:10.1212/01.CON.0000466656.59413.29.

[55] Bature F, Guinn B-A, Pang D, Pappas Y. Signs and symptoms preceding the diagnosis of Alzheimer's disease: a systematic scoping review of literature from 1937 to 2016. BMJ Open 2017;7:e015746. doi:10.1136/bmjopen-2016-015746.

[56] Attems J, Jellinger KA. The overlap between vascular disease and Alzheimer's disease - lessons from pathology. BMC Med 2014;12. doi:10.1186/s12916-014-0206-2.

[57] Park J. Mortality from Alzheimer's disease in Canada: A multiple-cause-of-death analysis, 2004 to 201. Health Rep 2015;27:7.

[58] Tschampa HJ, Kallenberg K, Urbach H, Meissner B, Nicolay C, Kretzschmar HA, et al. MRI in the diagnosis of sporadic Creutzfeldt–Jakob disease: a study on inter-observer agreement. Brain 2005;128:2026–33. doi:10.1093/brain/awh575.

[59] Raji CA, Lopez OL, Kuller LH, Carmichael OT, Becker JT. Age, Alzheimer disease, and brain structure. Neurology 2009;73:1899–905. doi:10.1212/WNL.0b013e3181c3f293.

[60] Niemantsverdriet E, Valckx S, Bjerke M, Engelborghs S. Alzheimer's disease CSF biomarkers: clinical indications and rational use. Acta Neurol Belg 2017;117:591–602. doi:10.1007/s13760-017-0816-5.

[61] Jack CR, Knopman DS, Jagust WJ, Petersen RC, Weiner MW, Aisen PS, et al. Tracking pathophysiological processes in Alzheimer's disease: an updated hypothetical model of dynamic biomarkers. Lancet Neurol 2013;12:207–16. doi:10.1016/S1474-4422(12)70291-0.

[62] Burns A, Iliffe S. Alzheimer's disease. BMJ 2009;338:b158–b158. doi:10.1136/bmj.b158.

[63] Korolev IO. Alzheimer's Disease: A Clinical and Basic Science Review 2014;04:10.

[64] Counts SE, Lahiri DK. Overview of Immunotherapy in Alzheimer's Disease (AD) and Mechanisms of IVIG Neuroprotection in Preclinical Models of AD. Curr Alzheimer Res 2014;11:623–5.

[65] LaFerla FM, Green KN. Animal Models of Alzheimer Disease. Cold Spring Harb Perspect Med 2012;2. doi:10.1101/cshperspect.a006320.

[66] Sasaguri H, Nilsson P, Hashimoto S, Nagata K, Saito T, De Strooper B, et al. APP mouse models for Alzheimer's disease preclinical studies. EMBO J 2017;36:2473–87. doi:10.15252/embj.201797397.

[67] Oddo S, Caccamo A, Shepherd JD, Murphy MP, Golde TE, Kayed R, et al. Triple-transgenic model of Alzheimer's disease with plaques and tangles: intracellular Abeta and synaptic dysfunction. Neuron 2003;39:409–21.

[68] Drummond E, Wisniewski T. Alzheimer's Disease: Experimental Models and Reality. Acta Neuropathol (Berl) 2017;133:155–75. doi:10.1007/s00401-016-1662-x.

[69] Lossos A, Reches A, Gal A, Newman JP, Soffer D, Gomori JM, et al. Frontotemporal dementia and parkinsonism with the P301S tau gene mutation in a Jewish family. J Neurol 2003;250:733–40. doi:10.1007/s00415-003-1074-4.

[70] Ghetti B, Oblak AL, Boeve BF, Johnson KA, Dickerson BC, Goedert M. Invited review: Frontotemporal dementia caused by *microtubule-associated protein tau* gene (*MAPT*) mutations: a chameleon for neuropathology and neuroimaging: *MAPT* mutations and FTD. Neuropathol Appl Neurobiol 2015;41:24–46. doi:10.1111/nan.12213.

[71] Borrego-Écija S, Morgado J, Palencia-Madrid L, Grau-Rivera O, Reñé R, Hernández I, et al. Frontotemporal Dementia Caused by the P301L Mutation in the MAPT Gene: Clinicopathological Features of 13 Cases from the Same Geographical Origin in Barcelona, Spain. Dement Geriatr Cogn Disord 2017;44:213–21. doi:10.1159/000480077.

[72] Ameen-Ali KE, Wharton SB, Simpson JE, Heath PR, Sharp P, Berwick J. Review: Neuropathology and behavioural features of transgenic murine models of Alzheimer's disease. Neuropathol Appl Neurobiol 2017;43:553–70. doi:10.1111/nan.12440.

[73] Götz J, Tolnay M, Barmettler R, Chen F, Probst A, Nitsch RM. Oligodendroglial tau filament formation in transgenic mice expressing G272V tau. Eur J Neurosci 2001;13:2131–40.

[74] Tanemura K, Murayama M, Akagi T, Hashikawa T, Tominaga T, Ichikawa M, et al. Neurodegeneration with tau accumulation in a transgenic mouse expressing V337M human tau. J Neurosci Off J Soc Neurosci 2002;22:133–41.

[75] Tatebayashi Y, Miyasaka T, Chui D-H, Akagi T, Mishima K, Iwasaki K, et al. Tau filament formation and associative memory deficit in aged mice expressing mutant (R406W) human tau. Proc Natl Acad Sci U S A 2002;99:13896–901. doi:10.1073/pnas.202205599.

[76] Jankowsky JL, Zheng H. Practical considerations for choosing a mouse model of Alzheimer's disease. Mol Neurodegener 2017;12:89. doi:10.1186/s13024-017-0231-7.

[77] Andorfer C, Kress Y, Espinoza M, de Silva R, Tucker KL, Barde Y-A, et al. Hyperphosphorylation and aggregation of tau in mice expressing normal human tau isoforms. J Neurochem 2003;86:582–90. doi:10.1046/j.1471-4159.2003.01879.x.

[78] Schindowski K, Bretteville A, Leroy K, Bégard S, Brion J-P, Hamdane M, et al. Alzheimer's Disease-Like Tau Neuropathology Leads to Memory Deficits and Loss of Functional Synapses in a Novel Mutated Tau Transgenic Mouse without Any Motor Deficits. Am J Pathol 2006;169:599–616. doi:10.2353/ajpath.2006.060002.

[79] Van der Jeugd A, Vermaercke B, Derisbourg M, Lo AC, Hamdane M, Blum D, et al. Progressive age-related cognitive decline in tau mice. J Alzheimers JAD 2013;37:777–788.

[80] Belarbi K, Schindowski K, Burnouf S, Caillierez R, Grosjean M-E, Demeyer D, et al. Early Tau pathology involving the septo-hippocampal pathway in a Tau transgenic model: relevance to Alzheimer's disease. Curr Alzheimer Res 2009;6:152–7.

[81] Pauling L, Coryell CD. The Magnetic Properties and Structure of Hemoglobin, Oxyhemoglobin and Carbonmonoxyhemoglobin. Proc Natl Acad Sci U S A 1936;22:210–6.

[82] Shetty PK, Galeffi F, Turner DA. Cellular Links between Neuronal Activity and Energy Homeostasis. Front Pharmacol 2012;3. doi:10.3389/fphar.2012.00043.

[83] Cinciute S. Translating the hemodynamic response: why focused interdisciplinary integration should matter for the future of functional neuroimaging. PeerJ 2019;7:e6621. doi:10.7717/peerj.6621.

[84] Ratering D, Baltes C, Nordmeyer-Massner J, Marek D, Rudin M. Performance of a 200-MHz cryogenic RF probe designed for MRI and MRS of the murine brain. Magn Reson Med 2008;59:1440–7. doi:10.1002/mrm.21629.

[85] Bernstein MA, Huston J, Ward HA. Imaging artifacts at 3.0T. J Magn Reson Imaging 2006;24:735–46. doi:10.1002/jmri.20698.

[86] Jonckers E, Shah D, Hamaide J, Verhoye M, Van der Linden A. The power of using functional fMRI on small rodents to study brain pharmacology and disease. Front Pharmacol 2015;6. doi:10.3389/fphar.2015.00231.

[87] Jonckers E, Delgado y Palacios R, Shah D, Guglielmetti C, Verhoye M, Van der Linden A. Different anesthesia regimes modulate the functional connectivity outcome in mice: Anesthesia and Functional Connectivity Outcome in Mice. Magn Reson Med 2014;72:1103–12. doi:10.1002/mrm.24990.

[88] Grandjean J, Schroeter A, Batata I, Rudin M. Optimization of anesthesia protocol for resting-state fMRI in mice based on differential effects of anesthetics on functional connectivity patterns. NeuroImage 2014;102:838–47. doi:10.1016/j.neuroimage.2014.08.043.

[89] King JA, Garelick TS, Brevard ME, Chen W, Messenger TL, Duong TQ, et al. Procedure for minimizing stress for fMRI studies in conscious rats. J Neurosci Methods 2005;148:154–60. doi:10.1016/j.jneumeth.2005.04.011.

[90] Madularu D, Mathieu AP, Kumaragamage C, Reynolds LM, Near J, Flores C, et al. A non-invasive restraining system for awake mouse imaging. J Neurosci Methods 2017;287:53–7. doi:10.1016/j.jneumeth.2017.06.008.

[91] Biswal B, Yetkin FZ, Haughton VM, Hyde JS. Functional connectivity in the motor cortex of resting human brain using echo-planar MRI. Magn Reson Med 1995;34:537–41.

[92] Raichle ME, MacLeod AM, Snyder AZ, Powers WJ, Gusnard DA, Shulman GL. A default mode of brain function. Proc Natl Acad Sci U S A 2001;98:676–82. doi:10.1073/pnas.98.2.676.

[93] Park H-J, Friston K. Structural and Functional Brain Networks: From Connections to Cognition. Science 2013;342:1238411–1238411. doi:10.1126/science.1238411.

[94] Smith SM, Miller KL, Salimi-Khorshidi G, Webster M, Beckmann CF, Nichols TE, et al. Network modelling methods for FMRI. NeuroImage 2011;54:875–91. doi:10.1016/j.neuroimage.2010.08.063.

[95] van den Heuvel MP, Hulshoff Pol HE. Exploring the brain network: A review on resting-state fMRI functional connectivity. Eur Neuropsychopharmacol 2010;20:519–34. doi:10.1016/j.euroneuro.2010.03.008.

[96] McKeown MJ, Makeig S, Brown GG, Jung TP, Kindermann SS, Bell AJ, et al. Analysis of fMRI data by blind separation into independent spatial components. Hum Brain Mapp 1998;6:160–88.

[97] Calhoun VD, Adali T, Pearlson GD, Pekar JJ. A method for making group inferences from functional MRI data using independent component analysis. Hum Brain Mapp 2001;14:140–51.

[98] Margulies DS, Böttger J, Long X, Lv Y, Kelly C, Schäfer A, et al. Resting developments: a review of fMRI post-processing methodologies for spontaneous brain activity. Magma N Y N 2010;23:289–307. doi:10.1007/s10334-010-0228-5.

[99] Varoquaux G, Gramfort A, Pedregosa F, Michel V, Thirion B. Multi-subject dictionary learning to segment an atlas of brain spontaneous activity. Inf Process Med Imaging Proc Conf 2011;22:562–73.

[100] Eavani H, Filipovych R, Davatzikos C, Satterthwaite TD, Gur RE, Gur RC. Sparse dictionary learning of resting state fMRI networks. Proc. - 2012 2nd Int. Workshop Pattern Recognit. NeuroImaging PRNI 2012, 2012, p. 73–6. doi:10.1109/PRNI.2012.25.

[101] Preti MG, Bolton TA, Van De Ville D. The dynamic functional connectome: State-of-the-art and perspectives. NeuroImage 2017;160:41–54. doi:10.1016/j.neuroimage.2016.12.061.

[102] Du Y, Pearlson GD, Yu Q, He H, Lin D, Sui J, et al. Interaction among subsystems within default mode network diminished in schizophrenia patients: A dynamic connectivity approach. Schizophr Res 2016;170:55–65. doi:10.1016/j.schres.2015.11.021.

[103] Damaraju E, Allen EA, Belger A, Ford JM, McEwen S, Mathalon DH, et al. Dynamic functional connectivity analysis reveals transient states of dysconnectivity in schizophrenia. NeuroImage Clin 2014;5:298–308. doi:10.1016/j.nicl.2014.07.003.

[104] Grandjean J, Preti MG, Bolton TAW, Buerge M, Seifritz E, Pryce CR, et al. Dynamic reorganization of intrinsic functional networks in the mouse brain. NeuroImage 2017;152:497–508. doi:10.1016/j.neuroimage.2017.03.026.

[105] Biswal BB. Resting state fMRI: A personal history. NeuroImage 2012;62:938–44. doi:10.1016/j.neuroimage.2012.01.090.

[106] Beckmann CF, DeLuca M, Devlin JT, Smith SM. Investigations into resting-state connectivity using independent component analysis. Philos Trans R Soc Lond B Biol Sci 2005;360:1001–13. doi:10.1098/rstb.2005.1634.

[107] Fox MD, Snyder AZ, Vincent JL, Corbetta M, Essen DCV, Raichle ME. The human brain is intrinsically organized into dynamic, anticorrelated functional networks. Proc Natl Acad Sci 2005;102:9673–8. doi:10.1073/pnas.0504136102.

[108] Damoiseaux JS, Rombouts SARB, Barkhof F, Scheltens P, Stam CJ, Smith SM, et al. Consistent resting-state networks across healthy subjects. Proc Natl Acad Sci U S A 2006;103:13848–53. doi:10.1073/pnas.0601417103.

[109] Heuvel M van den, Mandl R, Pol HH. Normalized Cut Group Clustering of Resting-State fMRI Data. PLOS ONE 2008;3:e2001. doi:10.1371/journal.pone.0002001.

[110] Raichle ME. The Restless Brain. Brain Connect 2011;1:3–12. doi:10.1089/brain.2011.0019.

[111] Buckner RL, Andrews-Hanna JR, Schacter DL. *The Brain's Default Network*: *Anatomy, Function, and Relevance to Disease*. Ann N Y Acad Sci 2008;1124:1–38. doi:10.1196/annals.1440.011.

[112] Poerio GL, Sormaz M, Wang H-T, Margulies D, Jefferies E, Smallwood J. The role of the default mode network in component processes underlying the wandering mind. Soc Cogn Affect Neurosci 2017;12:1047–62. doi:10.1093/scan/nsx041.

[113] Guo W, Liu F, Zhang J, Zhang Z, Yu L, Liu J, et al. Abnormal Default-Mode Network Homogeneity in First-Episode, Drug-Naive Major Depressive Disorder. PLOS ONE 2014;9:e91102. doi:10.1371/journal.pone.0091102.

[114] Mingoia G, Wagner G, Langbein K, Maitra R, Smesny S, Dietzek M, et al. Default mode network activity in schizophrenia studied at resting state using probabilistic ICA. Schizophr Res 2012;138:143–9. doi:10.1016/j.schres.2012.01.036.

[115] Greicius MD, Srivastava G, Reiss AL, Menon V. Default-mode network activity distinguishes Alzheimer's disease from healthy aging: evidence from functional MRI. Proc Natl Acad Sci U S A 2004;101:4637–4642.

[116] Menon V, Uddin LQ. Saliency, switching, attention and control: a network model of insula function. Brain Struct Funct 2010;214:655–67. doi:10.1007/s00429-010-0262-0.

[117] Andreano JM, Touroutoglou A, Dickerson BC, Barrett LF. Resting connectivity between salience nodes predicts recognition memory. Soc Cogn Affect Neurosci 2017;12:948–55. doi:10.1093/scan/nsx026.

[118] Balthazar MLF, Pereira FRS, Lopes TM, da Silva EL, Coan AC, Campos BM, et al. Neuropsychiatric symptoms in Alzheimer's disease are related to functional connectivity alterations in the salience network. Hum Brain Mapp 2014;35:1237–46. doi:10.1002/hbm.22248.

[119] Chand GB, Wu J, Hajjar I, Qiu D. Interactions of the Salience Network and Its Subsystems with the Default-Mode and the Central-Executive Networks in Normal Aging and Mild Cognitive Impairment. Brain Connect 2017;7:401–12. doi:10.1089/brain.2017.0509.

[120] Koechlin E, Summerfield C. An information theoretical approach to prefrontal executive function. Trends Cogn Sci 2007;11:229–35. doi:10.1016/j.tics.2007.04.005.

[121] Menon V. Large-Scale Brain Networks in Cognition: Emerging Principles 2010:11.

[122] Miller EK, Cohen JD. An integrative theory of prefrontal cortex function. Annu Rev Neurosci 2001;24:167–202. doi:10.1146/annurev.neuro.24.1.167.

[123] Wu L, Soder RB, Schoemaker D, Carbonnell F, Sziklas V, Rowley J, et al. Resting State Executive Control Network Adaptations in Amnestic Mild Cognitive Impairment. J Alzheimers Dis 2014;40:993–1004. doi:10.3233/JAD-131574.

[124] Hobkirk AL, Bell RP, Utevsky AV, Huettel S, Meade CS. Reward and executive control network resting-state functional connectivity is associated with impulsivity during reward-based decision making for cocaine users. Drug Alcohol Depend 2019;194:32–9. doi:10.1016/j.drugalcdep.2018.09.013.

[125] Chenji S, Jha S, Lee D, Brown M, Seres P, Mah D, et al. Investigating Default Mode and Sensorimotor Network Connectivity in Amyotrophic Lateral Sclerosis. PLoS ONE 2016;11. doi:10.1371/journal.pone.0157443.

[126] Stephen JM, Montaño R, Donahue CH, Adair JC, Knoefel J, Qualls C, et al. Somatosensory responses in normal aging, mild cognitive impairment, and Alzheimer's disease. J Neural Transm Vienna Austria 1996 2010;117:217–25. doi:10.1007/s00702-009-0343-5.

[127] Maatuf Y, Stern EA, Slovin H. Abnormal Population Responses in the Somatosensory Cortex of Alzheimer's Disease Model Mice. Sci Rep 2016;6. doi:10.1038/srep24560.

[128] Albin RL, Young AB, Penney JB. The functional anatomy of basal ganglia disorders. Trends Neurosci 1989;12:366–75.

[129] Cacciola A, Calamuneri A, Milardi D, Mormina E, Chillemi G, Marino S, et al. A Connectomic Analysis of the Human Basal Ganglia Network. Front Neuroanat 2017;11. doi:10.3389/fnana.2017.00085.

[130] Robinson S, Basso G, Soldati N, Sailer U, Jovicich J, Bruzzone L, et al. A resting state network in the motor control circuit of the basal ganglia. BMC Neurosci 2009;10:137. doi:10.1186/1471-2202-10-137.

[131] Szewczyk-Krolikowski K, Menke RAL, Rolinski M, Duff E, Salimi-Khorshidi G, Filippini N, et al. Functional connectivity in the basal ganglia network differentiates PD patients from controls. Neurology 2014;83:208–14. doi:10.1212/WNL.0000000000000592.

[132] Rodriguez-Sabate C, Morales I, Lorenzo JN, Rodriguez M. The organization of the basal ganglia functional connectivity network is non-linear in Parkinson's disease. NeuroImage Clin 2019;22:101708. doi:10.1016/j.nicl.2019.101708.

[133] Palesi F, Castellazzi G, Casiraghi L, Sinforiani E, Vitali P, Gandini Wheeler-Kingshott CAM, et al. Exploring Patterns of Alteration in Alzheimer's Disease Brain Networks: A Combined Structural and Functional Connectomics Analysis. Front Neurosci 2016;10. doi:10.3389/fnins.2016.00380.

[134] Fornito A, Zalesky A, Breakspear M. The connectomics of brain disorders. Nat Rev Neurosci 2015;16:159–72. doi:10.1038/nrn3901.

[135] Zerbi V, Grandjean J, Rudin M, Wenderoth N. Mapping the mouse brain with rs-fMRI: An optimized pipeline for functional network identification. NeuroImage 2015;123:11–21. doi:10.1016/j.neuroimage.2015.07.090.

[136] Jonckers E, Van Audekerke J, De Visscher G, Van der Linden A, Verhoye M. Functional Connectivity fMRI of the Rodent Brain: Comparison of Functional Connectivity Networks in Rat and Mouse. PLoS ONE 2011;6:e18876. doi:10.1371/journal.pone.0018876.

[137] Sforazzini F, Schwarz AJ, Galbusera A, Bifone A, Gozzi A. Distributed BOLD and CBV-weighted resting-state networks in the mouse brain. NeuroImage 2014;87:403–15. doi:10.1016/j.neuroimage.2013.09.050.

[138] Stafford JM, Jarrett BR, Miranda-Dominguez O, Mills BD, Cain N, Mihalas S, et al. Large-scale topology and the default mode network in the mouse connectome. Proc Natl Acad Sci 2014;111:18745–50. doi:10.1073/pnas.1404346111.

[139] Nasrallah FA, Tay H-C, Chuang K-H. Detection of functional connectivity in the resting mouse brain. NeuroImage 2014;86:417–24. doi:10.1016/j.neuroimage.2013.10.025.

[140] Gozzi A, Schwarz AJ. Large-scale functional connectivity networks in the rodent brain. NeuroImage 2016;127:496–509. doi:10.1016/j.neuroimage.2015.12.017.

[141] Wright IC, Rabe-Hesketh S, Woodruff PW, David AS, Murray RM, Bullmore ET. Meta-analysis of regional brain volumes in schizophrenia. Am J Psychiatry 2000;157:16–25. doi:10.1176/ajp.157.1.16.

[142] Ashburner J, Friston KJ. Voxel-based morphometry--the methods. NeuroImage 2000;11:805–21. doi:10.1006/nimg.2000.0582.

[143] Chételat G, Landeau B, Eustache F, Mézenge F, Viader F, de la Sayette V, et al. Using voxel-based morphometry to map the structural changes associated with rapid conversion in MCI: a longitudinal MRI study. NeuroImage 2005;27:934–46. doi:10.1016/j.neuroimage.2005.05.015.

[144] Kurth F, Gaser C, Luders E. A 12-step user guide for analyzing voxel-wise gray matter asymmetries in statistical parametric mapping (SPM). Nat Protoc 2015;10:293–304. doi:10.1038/nprot.2015.014.

[145] Bansal R, Gerber AJ, Peterson BS. Brain Morphometry Using Anatomical Magnetic Resonance Imaging. J Am Acad Child Adolesc Psychiatry 2008;47:619–21. doi:10.1097/CHI.0b013e31816c54ed.

[146] Badea A, Johnson GA, Jankowsky JL. Remote sites of structural atrophy predict later amyloid formation in a mouse model of Alzheimer's disease. NeuroImage 2010;50:416–27. doi:10.1016/j.neuroimage.2009.12.070.

[147] Redwine JM, Kosofsky B, Jacobs RE, Games D, Reilly JF, Morrison JH, et al. Dentate gyrus volume is reduced before onset of plaque formation in PDAPP mice: a magnetic resonance microscopy and stereologic analysis. Proc Natl Acad Sci U S A 2003;100:1381–6. doi:10.1073/pnas.242746599.

[148] Maheswaran S, Barjat H, Bate ST, Aljabar P, Hill DLG, Tilling L, et al. Analysis of serial magnetic resonance images of mouse brains using image registration. NeuroImage 2009;44:692–700. doi:10.1016/j.neuroimage.2008.10.016.

[149] Lau JC, Lerch JP, Sled JG, Henkelman RM, Evans AC, Bedell BJ. Longitudinal neuroanatomical changes determined by deformation-based morphometry in a mouse model of Alzheimer's disease. NeuroImage 2008;42:19–27. doi:10.1016/j.neuroimage.2008.04.252.

[150] Badea A, Delpratt NA, Anderson RJ, Dibb R, Qi Y, Wei H, et al. Multivariate MR biomarkers better predict cognitive dysfunction in mouse models of Alzheimer's disease. Magn Reson Imaging 2019;60:52–67. doi:10.1016/j.mri.2019.03.022.

[151] Le Bihan D. Looking into the functional architecture of the brain with diffusion MRI. Nat Rev Neurosci 2003;4:469–80. doi:10.1038/nrn1119.

[152] Le Bihan D, Johansen-Berg H. Diffusion MRI at 25: exploring brain tissue structure and function. NeuroImage 2012;61:324–41. doi:10.1016/j.neuroimage.2011.11.006.

[153] Bihan DL, Mangin J-F, Poupon C, Clark CA, Pappata S, Molko N, et al. Diffusion tensor imaging: Concepts and applications. J Magn Reson Imaging 2001;13:534–46. doi:10.1002/jmri.1076.

[154] Le Bihan D. Molecular diffusion, tissue microdynamics and microstructure. NMR Biomed 1995;8:375–86.

[155] Mori S, Zhang J. Principles of diffusion tensor imaging and its applications to basic neuroscience research. Neuron 2006;51:527–39. doi:10.1016/j.neuron.2006.08.012.

[156] Basser PJ, Mattiello J, LeBihan D. MR diffusion tensor spectroscopy and imaging. Biophys J 1994;66:259–67. doi:10.1016/S0006-3495(94)80775-1.

[157] Basser PJ, Mattiello J, LeBihan D. Estimation of the effective self-diffusion tensor from the NMR spin echo. J Magn Reson B 1994;103:247–54.

[158] Basser PJ, Mattiello J, LeBihan D. MR diffusion tensor spectroscopy and imaging. Biophys J 1994;66:259–67. doi:10.1016/S0006-3495(94)80775-1.

[159] Basser PJ, Pierpaoli C. Microstructural and physiological features of tissues elucidated by quantitative-diffusion-tensor MRI. J Magn Reson B 1996;111:209–19.

[160] Mukherjee P, Berman JI, Chung SW, Hess CP, Henry RG. Diffusion tensor MR imaging and fiber tractography: theoretic underpinnings. AJNR Am J Neuroradiol 2008;29:632–41. doi:10.3174/ajnr.A1051.

[161] Basser PJ, Jones DK. Diffusion-tensor MRI: theory, experimental design and data analysis - a technical review. NMR Biomed 2002;15:456–67. doi:10.1002/nbm.783.

[162] Jones DK. Challenges and limitations of quantifying brain connectivity *in vivo* with diffusion MRI. Imaging Med 2010;2:341–55. doi:10.2217/iim.10.21.

[163] Jones DK, Knösche TR, Turner R. White matter integrity, fiber count, and other fallacies: The do's and don'ts of diffusion MRI. NeuroImage 2013;73:239–54. doi:10.1016/j.neuroimage.2012.06.081.

[164] Jones DK. Tractography gone wild: probabilistic fibre tracking using the wild bootstrap with diffusion tensor MRI. IEEE Trans Med Imaging 2008;27:1268–74. doi:10.1109/TMI.2008.922191.

[165] Tuch DS, Reese TG, Wiegell MR, Makris N, Belliveau JW, Wedeen VJ. High angular resolution diffusion imaging reveals intravoxel white matter fiber heterogeneity. Magn Reson Med 2002;48:577–82. doi:10.1002/mrm.10268.

[166] Reisert M, Mader I, Anastasopoulos C, Weigel M, Schnell S, Kiselev V. Global fiber reconstruction becomes practical. NeuroImage 2011;54:955–62. doi:10.1016/j.neuroimage.2010.09.016.

[167] Daducci A, Dal Palú A, Descoteaux M, Thiran J-P. Microstructure Informed Tractography: Pitfalls and Open Challenges. Front Neurosci 2016;10:247. doi:10.3389/fnins.2016.00247.

[168] Stämpfli P, Sommer S, Manoliu A, Burrer A, Schmidt A, Herdener M, et al. Subtle white matter alterations in schizophrenia identified with a new measure of fiber density. Sci Rep 2019;9:4636. doi:10.1038/s41598-019-40070-2.

[169] Stadlbauer A, Ganslandt O, Salomonowitz E, Buchfelder M, Hammen T, Bachmair J, et al. Magnetic resonance fiber density mapping of age-related white matter changes. Eur J Radiol 2012;81:4005–12. doi:10.1016/j.ejrad.2012.05.029.

[170] Roberts TPL, Liu F, Kassner A, Mori S, Guha A. Fiber Density Index Correlates with Reduced Fractional Anisotropy in White Matter of Patients with Glioblastoma 2005:4.

[171] Prasad G, Nir TM, Toga AW, Thompson PM. TRACTOGRAPHY DENSITY AND NETWORK MEASURES IN ALZHEIMER'S DISEASE. Proc IEEE Int Symp Biomed Imaging 2013;2013:692–5. doi:10.1109/ISBI.2013.6556569.

[172] Alexander AL, Lee JE, Lazar M, Field AS. Diffusion Tensor Imaging of the Brain. Neurother J Am Soc Exp Neurother 2007;4:316–29. doi:10.1016/j.nurt.2007.05.011.

[173] Winklewski PJ, Sabisz A, Naumczyk P, Jodzio K, Szurowska E, Szarmach A. Understanding the Physiopathology Behind Axial and Radial Diffusivity Changes—What Do We Know? Front Neurol 2018;9. doi:10.3389/fneur.2018.00092.

[174] Sun S-W, Liang H-F, Trinkaus K, Cross AH, Armstrong RC, Song S-K. Noninvasive detection of cuprizone induced axonal damage and demyelination in the mouse corpus callosum. Magn Reson Med 2006;55:302–8. doi:10.1002/mrm.20774.

[175] Song S-K, Sun S-W, Ju W-K, Lin S-J, Cross AH, Neufeld AH. Diffusion tensor imaging detects and differentiates axon and myelin degeneration in mouse optic nerve after retinal ischemia. NeuroImage 2003;20:1714–22.

[176] Lancaster MA, Seidenberg M, Smith JC, Nielson KA, Woodard JL, Durgerian S, et al. Diffusion Tensor Imaging Predictors of Episodic Memory Decline in Healthy Elders at Genetic Risk for Alzheimer's Disease. J Int Neuropsychol Soc JINS 2016;22:1005–15. doi:10.1017/S1355617716000904.

[177] Della Nave R, Ginestroni A, Diciotti S, Salvatore E, Soricelli A, Mascalchi M. Axial diffusivity is increased in the degenerating superior cerebellar peduncles of Friedreich's ataxia. Neuroradiology 2011;53:367–72. doi:10.1007/s00234-010-0807-1.

[178] Diana Rosas H, Lee SY, Bender A, Zaleta AK, Vange M, Yu P, et al. Altered White Matter Microstructure in the Corpus Callosum in Huntington's Disease: implications for cortical "disconnection." NeuroImage 2010;49:2995–3004. doi:10.1016/j.neuroimage.2009.10.015.

[179] Kamagata K, Motoi Y, Abe O, Shimoji K, Hori M, Nakanishi A, et al. White Matter Alteration of the Cingulum in Parkinson Disease with and without Dementia: Evaluation by Diffusion Tensor Tract–Specific Analysis. Am J Neuroradiol 2012;33:890–5. doi:10.3174/ajnr.A2860.

[180] Kochunov P, Thompson PM, Lancaster JL, Bartzokis G, Smith S, Coyle T, et al. Relationship between white matter fractional anisotropy and other indices of cerebral health in normal aging: Tract-based spatial statistics study of aging. NeuroImage 2007;35:478–87. doi:10.1016/j.neuroimage.2006.12.021.

[181] Wakamoto H, Eluvathingal TJ, Makki M, Juhász C, Chugani HT. Diffusion tensor imaging of the corticospinal tract following cerebral hemispherectomy. J Child Neurol 2006;21:566–71. doi:10.1177/08830738060210071401.

[182] Xie R, Fang M, Zhou L, Fan S, Liu J, Quan H, et al. Diffusion tensor imaging detects Wallerian degeneration of the corticospinal tract early after cerebral infarction. Neural Regen Res 2012;7:900–5. doi:10.3969/j.issn.1673-5374.2012.12.004.

[183] Thomalla G, Glauche V, Koch MA, Beaulieu C, Weiller C, Röther J. Diffusion tensor imaging detects early Wallerian degeneration of the pyramidal tract after ischemic stroke. NeuroImage 2004;22:1767–74. doi:10.1016/j.neuroimage.2004.03.041.

[184] Zhan J, Lin T-H, Libbey JE, Sun P, Ye Z, Song C, et al. Diffusion Basis Spectrum and Diffusion Tensor Imaging Detect Hippocampal Inflammation and Dendritic Injury in a Virus-Induced Mouse Model of Epilepsy. Front Neurosci 2018;12. doi:10.3389/fnins.2018.00077.

[185] Fornito A, Bullmore ET. Connectomics: a new paradigm for understanding brain disease. Eur Neuropsychopharmacol J Eur Coll Neuropsychopharmacol 2015;25:733–48. doi:10.1016/j.euroneuro.2014.02.011.

[186] Sporns O. Structure and function of complex brain networks. Dialogues Clin Neurosci 2013;15:247–62.

[187] Aertsen AM, Gerstein GL, Habib MK, Palm G. Dynamics of neuronal firing correlation: modulation of "effective connectivity." J Neurophysiol 1989;61:900–17. doi:10.1152/jn.1989.61.5.900.

[188] Friston KJ. Functional and Effective Connectivity: A Review. Brain Connect 2011;1:13–36. doi:10.1089/brain.2011.0008.

[189] Sporns O. THE HUMAN CONNECTOME: A COMPLEX NETWORK. Schizophr Res 2012;136:S28. doi:10.1016/S0920-9964(12)70100-7.

[190] Sporns O. Graph theory methods: applications in brain networks. Dialogues Clin Neurosci 2018;20:111–21.

[191] van den Heuvel MP, Sporns O. Rich-Club Organization of the Human Connectome. J Neurosci 2011;31:15775–86. doi:10.1523/JNEUROSCI.3539-11.2011.

[192] Finger S, Koehler PJ, Jagella C. The Monakow concept of diaschisis: origins and perspectives. Arch Neurol 2004;61:283–8. doi:10.1001/archneur.61.2.283.

[193] Feeney DM, Baron JC. Diaschisis. Stroke 1986;17:817–30.

[194] Cowan WM. Anterograde and Retrograde Transneuronal Degeneration in the Central and Peripheral Nervous System. In: Nauta WJH, Ebbesson SOE, editors. Contemp. Res. Methods

Neuroanat., Berlin, Heidelberg: Springer Berlin Heidelberg; 1970, p. 217–51. doi:10.1007/978-3-642-85986-1_11.

[195] Klupp E, Förster S, Grimmer T, Tahmasian M, Yakushev I, Sorg C, et al. In Alzheimer's Disease, Hypometabolism in Low-Amyloid Brain Regions May Be a Functional Consequence of Pathologies in Connected Brain Regions. Brain Connect 2014;4:371–83. doi:10.1089/brain.2013.0212.

[196] Koen JD, Rugg MD. Neural Dedifferentiation in the Aging Brain. Trends Cogn Sci 2019. doi:10.1016/j.tics.2019.04.012.

[197] Li S-C, Lindenberger U, Sikström S. Aging cognition: from neuromodulation to representation. Trends Cogn Sci 2001;5:479–86. doi:10.1016/S1364-6613(00)01769-1.

[198] Quiroz YT, Budson AE, Celone K, Ruiz A, Newmark R, Castrillón G, et al. Hippocampal Hyperactivation in Presymptomatic Familial Alzheimer's Disease. Ann Neurol 2010;68:865–75. doi:10.1002/ana.22105.

[199] Grady CL, McIntosh AR, Beig S, Keightley ML, Burian H, Black SE. Evidence from functional neuroimaging of a compensatory prefrontal network in Alzheimer's disease. J Neurosci Off J Soc Neurosci 2003;23:986–93.

[200] Jack CR, Knopman DS, Jagust WJ, Petersen RC, Weiner MW, Aisen PS, et al. Update on hypothetical model of Alzheimer's disease biomarkers. Lancet Neurol 2013;12:207–16. doi:10.1016/S1474-4422(12)70291-0.

[201] Noppeney U, Friston KJ, Price CJ. Degenerate neuronal systems sustaining cognitive functions. J Anat 2004;205:433–42. doi:10.1111/j.0021-8782.2004.00343.x.

[202] Mevel K, Chételat G, Eustache F, Desgranges B. The Default Mode Network in Healthy Aging and Alzheimer's Disease. Int J Alzheimer's Dis 2011. doi:10.4061/2011/535816.

[203] Burggren A, Brown J. Imaging markers of structural and functional brain changes that precede cognitive symptoms in risk for Alzheimer's disease. Brain Imaging Behav 2014;8:251–61. doi:10.1007/s11682-013-9278-4.

[204] Wang Y, Risacher SL, West JD, McDonald BC, MaGee TR, Farlow MR, et al. Altered Default Mode Network Connectivity in Older Adults with Cognitive Complaints and Amnestic Mild Cognitive Impairment. J Alzheimers Dis JAD 2013;35:751–60. doi:10.3233/JAD-130080.

[205] Yao H, Liu Y, Zhou B, Zhang Z, An N, Wang P, et al. Decreased functional connectivity of the amygdala in Alzheimer's disease revealed by resting-state fMRI. Eur J Radiol 2013;82:1531–8. doi:10.1016/j.ejrad.2013.03.019.

[206] Zhang B, Hua R, Qing Z, Ni L, Zhang X, Zhao H, et al. Abnormal brain functional connectivity coupled with hypoperfusion measured by Resting-State fMRI: An additional contributing factor for cognitive impairment in patients with Alzheimer's disease. Psychiatry Res Neuroimaging 2019;289:18–25. doi:10.1016/j.pscychresns.2019.04.007.

[207] Kaneta T, Katsuse O, Hirano T, Ogawa M, Shihikura-Hino A, Yoshida K, et al. Voxel-wise correlations between cognition and cerebral blood flow using arterial spin-labeled perfusion MRI in patients with Alzheimer's disease: a cross-sectional study. BMC Neurol 2017;17:91. doi:10.1186/s12883-017-0870-x.

[208] Kantarci K, Murray ME, Schwarz CG, Reid R, Przybelski SA, Lesnick T, et al. White Matter Integrity on DTI and the Pathologic Staging of Alzheimer's Disease. Neurobiol Aging 2017;56:172–9. doi:10.1016/j.neurobiolaging.2017.04.024.

[209] Li X, Wang H, Tian Y, Zhou S, Li X, Wang K, et al. Impaired White Matter Connections of the Limbic System Networks Associated with Impaired Emotional Memory in Alzheimer's Disease. Front Aging Neurosci 2016;8:250. doi:10.3389/fnagi.2016.00250.

[210] Matsuda H. MRI morphometry in Alzheimer's disease. Ageing Res Rev 2016;30:17–24. doi:10.1016/j.arr.2016.01.003.

[211] Nho K, Risacher SL, Crane PK, DeCarli C, Glymour MM, Habeck C, et al. Voxel and Surface-Based Topography of Memory and Executive Deficits in Mild Cognitive Impairment and Alzheimer's Disease. Brain Imaging Behav 2012;6:551–67. doi:10.1007/s11682-012-9203-2.

[212] Coupé P, Manjón JV, Lanuza E, Catheline G. Lifespan Changes of the Human Brain In Alzheimer's Disease. Sci Rep 2019;9. doi:10.1038/s41598-019-39809-8.

[213] Bernard C, Helmer C, Dilharreguy B, Amieva H, Auriacombe S, Dartigues J-F, et al. Time course of brain volume changes in the preclinical phase of Alzheimer's disease. Alzheimers Dement 2014;10:143-151.e1. doi:10.1016/j.jalz.2013.08.279.

[214] Sivera R, Delingette H, Lorenzi M, Pennec X, Ayache N. A model of brain morphological changes related to aging and Alzheimer's disease from cross-sectional assessments. NeuroImage 2019;198:255–70. doi:10.1016/j.neuroimage.2019.05.040.

[215] Bakker A, Krauss GL, Albert MS, Speck CL, Jones LR, Stark CE, et al. Reduction of Hippocampal Hyperactivity Improves Cognition in Amnestic Mild Cognitive Impairment. Neuron 2012;74:467–74. doi:10.1016/j.neuron.2012.03.023.

[216] Celone KA, Calhoun VD, Dickerson BC, Atri A, Chua EF, Miller SL, et al. Alterations in Memory Networks in Mild Cognitive Impairment and Alzheimer's Disease: An Independent Component Analysis. J Neurosci 2006;26:10222–31. doi:10.1523/JNEUROSCI.2250-06.2006.

[217] Dickerson BC, Salat DH, Greve DN, Chua EF, Rand-Giovannetti E, Rentz DM, et al. Increased hippocampal activation in mild cognitive impairment compared to normal aging and AD. Neurology 2005;65:404–11. doi:10.1212/01.wnl.0000171450.97464.49.

[218] Hämäläinen A, Pihlajamäki M, Tanila H, Hänninen T, Niskanen E, Tervo S, et al. Increased fMRI responses during encoding in mild cognitive impairment. Neurobiol Aging 2007;28:1889–903. doi:10.1016/j.neurobiolaging.2006.08.008.

[219] Stephen JM, Montaño R, Donahue CH, Adair JC, Knoefel J, Qualls C, et al. Somatosensory responses in normal aging, mild cognitive impairment, and Alzheimer's disease. J Neural Transm Vienna Austria 1996 2010;117:217–25. doi:10.1007/s00702-009-0343-5.

[220] Ringman JM, O'Neill J, Geschwind D, Medina L, Apostolova LG, Rodriguez Y, et al. Diffusion tensor imaging in preclinical and presymptomatic carriers of familial Alzheimer's disease mutations. Brain J Neurol 2007;130:1767–76. doi:10.1093/brain/awm102.

[221] Tijms BM, Wink AM, de Haan W, van der Flier WM, Stam CJ, Scheltens P, et al. Alzheimer's disease: connecting findings from graph theoretical studies of brain networks. Neurobiol Aging 2013;34:2023–36. doi:10.1016/j.neurobiolaging.2013.02.020.

[222] Harsan L-A, Paul D, Schnell S, Kreher BW, Hennig J, Staiger JF, et al. In vivo diffusion tensor magnetic resonance imaging and fiber tracking of the mouse brain. NMR Biomed 2010;23:884–96. doi:10.1002/nbm.1496.

[223] Liska A, Galbusera A, Schwarz AJ, Gozzi A. Functional connectivity hubs of the mouse brain. NeuroImage 2015;115:281–91. doi:10.1016/j.neuroimage.2015.04.033.

[224] Shah D, Praet J, Latif Hernandez A, Höfling C, Anckaerts C, Bard F, et al. Early pathologic amyloid induces hypersynchrony of BOLD resting-state networks in transgenic mice and provides an early therapeutic window before amyloid plaque deposition. Alzheimers Dement 2016;12:964–76. doi:10.1016/j.jalz.2016.03.010.

[225] Dodart JC, Mathis C, Saura J, Bales KR, Paul SM, Ungerer A. Neuroanatomical abnormalities in behaviorally characterized APP(V717F) transgenic mice. Neurobiol Dis 2000;7:71–85. doi:10.1006/nbdi.1999.0278.

[226] Gonzalez-Lima F, Berndt JD, Valla JE, Games D, Reiman EM. Reduced corpus callosum, fornix and hippocampus in PDAPP transgenic mouse model of Alzheimer's disease. Neuroreport 2001;12:2375–9. doi:10.1097/00001756-200108080-00018.

[227] Weiss C, Venkatasubramanian PN, Aguado AS, Power JM, Tom BC, Li L, et al. Impaired Eyeblink Conditioning and Decreased Hippocampal Volume in PDAPP V717F Mice. Neurobiol Dis 2002;11:425–33. doi:10.1006/nbdi.2002.0555.

[228] Redwine JM, Kosofsky B, Jacobs RE, Games D, Reilly JF, Morrison JH, et al. Dentate gyrus volume is reduced before onset of plaque formation in PDAPP mice: a magnetic resonance microscopy and stereologic analysis. Proc Natl Acad Sci U S A 2003;100:1381–6. doi:10.1073/pnas.242746599.

[229] Dhenain M. Preclinical MRI and NMR Biomarkers of Alzheimer's Disease: Concepts and Applications. Magn Reson Insights 2008;2:MRI.S971. doi:10.4137/MRI.S971.

[230] Latif-Hernandez A, Shah D, Craessaerts K, Saido T, Saito T, De Strooper B, et al. Subtle behavioral changes and increased prefrontal-hippocampal network synchronicity in APPNL−G−F mice before prominent plaque deposition. Behav Brain Res 2019;364:431–41. doi:10.1016/j.bbr.2017.11.017.

[231] Grandjean J, Schroeter A, He P, Tanadini M, Keist R, Krstic D, et al. Early Alterations in Functional Connectivity and White Matter Structure in a Transgenic Mouse Model of Cerebral Amyloidosis. J Neurosci 2014;34:13780–9. doi:10.1523/JNEUROSCI.4762-13.2014.

[232] Liu D, Lu H, Stein E, Zhou Z, Yang Y, Mattson MP. Brain regional synchronous activity predicts tauopathy in 3×TgAD mice. Neurobiol Aging 2018;70:160–9. doi:10.1016/j.neurobiolaging.2018.06.016.

[233] Govaerts K, Lechat B, Struys T, Kremer A, Borghgraef P, Van Leuven F, et al. Longitudinal assessment of cerebral perfusion and vascular response to hypoventilation in a bigenic mouse model of Alzheimer's disease with amyloid and tau pathology. NMR Biomed 2019;32:e4037. doi:10.1002/nbm.4037.

[234] El Tannir El Tayara N, Delatour B, Le Cudennec C, Guégan M, Volk A, Dhenain M. Age-related evolution of amyloid burden, iron load, and MR relaxation times in a transgenic mouse model of Alzheimer's disease. Neurobiol Dis 2006;22:199–208. doi:10.1016/j.nbd.2005.10.013.

[235] Shah D, Jonckers E, Praet J, Vanhoutte G, Palacios RD y, Bigot C, et al. Resting State fMRI Reveals Diminished Functional Connectivity in a Mouse Model of Amyloidosis. PLOS ONE 2013;8:e84241. doi:10.1371/journal.pone.0084241.

[236] Belloy ME, Shah D, Abbas A, Kashyap A, Roßner S, Van der Linden A, et al. Quasi-Periodic Patterns of Neural Activity improve Classification of Alzheimer's Disease in Mice. Sci Rep 2018;8. doi:10.1038/s41598-018-28237-9.

[237] Zerbi V, Wiesmann M, Emmerzaal TL, Jansen D, Van Beek M, Mutsaers MPC, et al. Resting-State Functional Connectivity Changes in Aging apoE4 and apoE-KO Mice. J Neurosci 2014;34:13963–75. doi:10.1523/JNEUROSCI.0684-14.2014.

[238] Praet J, Manyakov NV, Muchene L, Mai Z, Terzopoulos V, de Backer S, et al. Diffusion kurtosis imaging allows the early detection and longitudinal follow-up of amyloid-β-induced pathology. Alzheimers Res Ther 2018;10. doi:10.1186/s13195-017-0329-8.

[239] Nie X, Falangola MF, Ward R, McKinnon ET, Helpern JA, Nietert PJ, et al. Diffusion MRI detects longitudinal white matter changes in the 3xTg-AD mouse model of Alzheimer's disease. Magn Reson Imaging 2019;57:235–42. doi:10.1016/j.mri.2018.12.003.

[240] Snow WM, Dale R, O'Brien-Moran Z, Buist R, Peirson D, Martin M, et al. In Vivo Detection of Gray Matter Neuropathology in the 3xTg Mouse Model of Alzheimer's Disease with Diffusion Tensor Imaging. J Alzheimers Dis 2017;58:841–53. doi:10.3233/JAD-170136.

[241] Kesler SR, Acton P, Rao V, Ray WJ. Functional and structural connectome properties in the 5XFAD transgenic mouse model of Alzheimer's disease. Netw Neurosci 2018;2:241–58. doi:10.1162/netn_a_00048.

[242] Poisnel G, Hérard A-S, El Tannir El Tayara N, Bourrin E, Volk A, Kober F, et al. Increased regional cerebral glucose uptake in an APP/PS1 model of Alzheimer's disease. Neurobiol Aging 2012;33:1995–2005. doi:10.1016/j.neurobiolaging.2011.09.026.

[243] Micotti E, Paladini A, Balducci C, Tolomeo D, Frasca A, Marizzoni M, et al. Striatum and entorhinal cortex atrophy in AD mouse models: MRI comprehensive analysis. Neurobiol Aging 2015;36:776–88. doi:10.1016/j.neurobiolaging.2014.10.027.

[244] Sahara N, Perez PD, Lin W-L, Dickson DW, Ren Y, Zeng H, et al. Age-related decline in white matter integrity in a mouse model of tauopathy: an in vivo diffusion tensor magnetic resonance imaging study. Neurobiol Aging 2014;35:1364–74. doi:10.1016/j.neurobiolaging.2013.12.009.

[245] Green C, Sydow A, Vogel S, Anglada-Huguet M, Wiedermann D, Mandelkow E, et al. Functional networks are impaired by elevated tau-protein but reversible in a regulatable Alzheimer's disease mouse model. Mol Neurodegener 2019;14. doi:10.1186/s13024-019-0316-6.

[246] Lyketsos CG, Carrillo MC, Ryan JM, Khachaturian AS, Trzepacz P, Amatniek J, et al. Neuropsychiatric symptoms in Alzheimer's disease. Alzheimers Dement J Alzheimers Assoc 2011;7:532–9. doi:10.1016/j.jalz.2011.05.2410.

[247] Victoroff J, Lin FV, Coburn KL, Shillcutt SD, Voon V, Ducharme S. Noncognitive Behavioral Changes Associated With Alzheimer's Disease: Implications of Neuroimaging Findings. J Neuropsychiatry Clin Neurosci 2018;30:14–21. doi:10.1176/appi.neuropsych.16080155.

[248] Gariano RF, Groves PM. Burst firing induced in midbrain dopamine neurons by stimulation of the medial prefrontal and anterior cingulate cortices. Brain Res 1988;462:194–8. doi:10.1016/0006-8993(88)90606-3.

[249] Rajmohan V, Mohandas E. The limbic system. Indian J Psychiatry 2007;49:132–9. doi:10.4103/0019-5545.33264.

[250] Song S-K, Sun S-W, Ju W-K, Lin S-J, Cross AH, Neufeld AH. Diffusion tensor imaging detects and differentiates axon and myelin degeneration in mouse optic nerve after retinal ischemia. NeuroImage 2003;20:1714–22.

[251] A component based noise correction method (CompCor) for BOLD and perfusion based fMRI. - PubMed - NCBI n.d. https://www.ncbi.nlm.nih.gov/pubmed/17560126 (accessed July 29, 2019).

[252] Damoiseaux JS, Viviano RP, Yuan P, Raz N. Differential effect of age on posterior and anterior hippocampal functional connectivity. NeuroImage 2016;133:468–76. doi:10.1016/j.neuroimage.2016.03.047.

[253] Zarei M, Beckmann CF, Binnewijzend MAA, Schoonheim MM, Oghabian MA, Sanz-Arigita EJ, et al. Functional segmentation of the hippocampus in the healthy human brain and in Alzheimer's disease. NeuroImage 2013;66:28–35. doi:10.1016/j.neuroimage.2012.10.071.

[254] Preston AR, Eichenbaum H. Interplay of hippocampus and prefrontal cortex in memory. Curr Biol CB 2013;23:R764–73. doi:10.1016/j.cub.2013.05.041.

[255] D'Hooge R, De Deyn PP. Applications of the Morris water maze in the study of learning and memory. Brain Res Rev 2001;36:60–90. doi:10.1016/S0165-0173(01)00067-4.

[256] Bird CM, Burgess N. The Hippocampus Supports Recognition Memory for Familiar Words but Not Unfamiliar Faces. Curr Biol 2008;18:1932–6. doi:10.1016/j.cub.2008.10.046.

[257] Van Cauter T, Camon J, Alvernhe A, Elduayen C, Sargolini F, Save E. Distinct Roles of Medial and Lateral Entorhinal Cortex in Spatial Cognition. Cereb Cortex 2013;23:451–9. doi:10.1093/cercor/bhs033.

[258] Sasaki T, Leutgeb S, Leutgeb JK. Spatial and memory circuits in the medial entorhinal cortex. Curr Opin Neurobiol 2015;32:16–23. doi:10.1016/j.conb.2014.10.008.

[259] Moser EI, Kropff E, Moser M-B. Place Cells, Grid Cells, and the Brain's Spatial Representation System. Annu Rev Neurosci 2008;31:69–89. doi:10.1146/annurev.neuro.31.061307.090723.

[260] Assini FL, Duzzioni M, Takahashi RN. Object location memory in mice: Pharmacological validation and further evidence of hippocampal CA1 participation. Behav Brain Res 2009;204:206–11. doi:10.1016/j.bbr.2009.06.005.

[261] Clarke JR, Cammarota M, Gruart A, Izquierdo I, Delgado-García JM. Plastic modifications induced by object recognition memory processing. Proc Natl Acad Sci U S A 2010;107:2652–7. doi:10.1073/pnas.0915059107.

[262] Dere E, Huston JP, De Souza Silva MA. The pharmacology, neuroanatomy and neurogenetics of one-trial object recognition in rodents. Neurosci Biobehav Rev 2007;31:673–704. doi:10.1016/j.neubiorev.2007.01.005.

[263] Murray EA, Richmond BJ. Role of perirhinal cortex in object perception, memory, and associations. Curr Opin Neurobiol 2001;11:188–93. doi:10.1016/S0959-4388(00)00195-1.

[264] Fanselow MS, Dong H-W. Are the Dorsal and Ventral Hippocampus Functionally Distinct Structures? Neuron 2010;65:7–19. doi:10.1016/j.neuron.2009.11.031.

[265] Lee I, Solivan F. The roles of the medial prefrontal cortex and hippocampus in a spatial paired-association task. Learn Mem 2008;15:357–67. doi:10.1101/lm.902708.

[266] Barker GRI, Warburton EC. Object-in-Place Associative Recognition Memory Depends on Glutamate Receptor Neurotransmission Within Two Defined Hippocampal-Cortical Circuits: A Critical Role for AMPA and NMDA Receptors in the Hippocampus, Perirhinal, and Prefrontal Cortices. Cereb Cortex N Y NY 2015;25:472–81. doi:10.1093/cercor/bht245.

[267] Jo YS, Lee I. Perirhinal cortex is necessary for acquiring, but not for retrieving object-place paired association. Learn Mem Cold Spring Harb N 2010;17:97–103. doi:10.1101/lm.1620410.

[268] Fowler KS, Saling MM, Conway EL, Semple JM, Louis WJ. Paired associate performance in the early detection of DAT. J Int Neuropsychol Soc JINS 2002;8:58–71.

[269] Hart SA, Smith CM, Swash M. Recognition memory in Alzheimer's disease. Neurobiol Aging 1985;6:287–92.

[270] Van der Jeugd A, Blum D, Raison S, Eddarkaoui S, Buée L, D'Hooge R. Observations in THY-Tau22 mice that resemble behavioral and psychological signs and symptoms of dementia. Behav Brain Res 2013;242:34–9. doi:10.1016/j.bbr.2012.12.008.

[271] Lewis J, McGowan E, Rockwood J, Melrose H, Nacharaju P, Van Slegtenhorst M, et al. Neurofibrillary tangles, amyotrophy and progressive motor disturbance in mice expressing mutant (P301L) tau protein. Nat Genet 2000;25:402–5. doi:10.1038/78078.

[272] Allen B, Ingram E, Takao M, Smith MJ, Jakes R, Virdee K, et al. Abundant tau filaments and nonapoptotic neurodegeneration in transgenic mice expressing human P301S tau protein. J Neurosci Off J Soc Neurosci 2002;22:9340–51.

[273] Ikeda M, Shoji M, Kawarai T, Kawarabayashi T, Matsubara E, Murakami T, et al. Accumulation of filamentous tau in the cerebral cortex of human tau R406W transgenic mice. Am J Pathol 2005;166:521–31. doi:10.1016/S0002-9440(10)62274-2.

[274] Terwel D, Lasrado R, Snauwaert J, Vandeweert E, Van Haesendonck C, Borghgraef P, et al. Changed conformation of mutant Tau-P301L underlies the moribund tauopathy, absent in progressive, nonlethal axonopathy of Tau-4R/2N transgenic mice. J Biol Chem 2005;280:3963–73. doi:10.1074/jbc.M409876200.

[275] Busche MA, Chen X, Henning HA, Reichwald J, Staufenbiel M, Sakmann B, et al. Critical role of soluble amyloid- for early hippocampal hyperactivity in a mouse model of Alzheimer's disease. Proc Natl Acad Sci 2012;109:8740–5. doi:10.1073/pnas.1206171109.

[276] Takata N, Sugiura Y, Yoshida K, Koizumi M, Hiroshi N, Honda K, et al. Optogenetic astrocyte activation evokes BOLD fMRI response with oxygen consumption without neuronal activity modulation. Glia 2018;66:2013–23. doi:10.1002/glia.23454.

[277] Kuchibhotla KV, Lattarulo CR, Hyman BT, Bacskai BJ. Synchronous Hyperactivity and Intercellular Calcium Waves in Astrocytes in Alzheimer Mice. Science 2009;323:1211–5. doi:10.1126/science.1169096.

[278] Moser MB, Moser EI. Functional differentiation in the hippocampus. Hippocampus 1998;8:608–19. doi:10.1002/(SICI)1098-1063(1998)8:6<608::AID-HIPO3>3.0.CO;2-7.

[279] Tanti A, Belzung C. Neurogenesis along the septo-temporal axis of the hippocampus: are depression and the action of antidepressants region-specific? Neuroscience 2013;252:234–52. doi:10.1016/j.neuroscience.2013.08.017.

[280] Maruszak A, Thuret S. Why looking at the whole hippocampus is not enough—a critical role for anteroposterior axis, subfield and activation analyses to enhance predictive value of hippocampal changes for Alzheimer's disease diagnosis. Front Cell Neurosci 2014;8. doi:10.3389/fncel.2014.00095.

[281] Zhong Q, Xu H, Qin J, Zeng L-L, Hu D, Shen H. Functional parcellation of the hippocampus from resting-state dynamic functional connectivity. Brain Res 2019;1715:165–75. doi:10.1016/j.brainres.2019.03.023.

[282] Fuster-Matanzo A, Llorens-Martín M, Barreda EG de, Ávila J, Hernández F. Different Susceptibility to Neurodegeneration of Dorsal and Ventral Hippocampal Dentate Gyrus: A Study with Transgenic Mice Overexpressing GSK3β. PLOS ONE 2011;6:e27262. doi:10.1371/journal.pone.0027262.

[283] Bellistri E, Aguilar J, Brotons-Mas JR, Foffani G, de la Prida LM. Basic properties of somatosensory-evoked responses in the dorsal hippocampus of the rat. J Physiol 2013;591:2667–86. doi:10.1113/jphysiol.2013.251892.

[284] The Hippocampus as a Cognitive Map n.d. https://repository.arizona.edu/handle/10150/620894 (accessed July 29, 2019).

[285] Eacott MJ, Norman G. Integrated memory for object, place, and context in rats: a possible model of episodic-like memory? J Neurosci Off J Soc Neurosci 2004;24:1948–53. doi:10.1523/JNEUROSCI.2975-03.2004.

[286] Long X, Zhang S-J. A novel somatosensory spatial navigation system outside the hippocampal formation. BioRxiv 2018:473090. doi:10.1101/473090.

[287] Dutar P, Bassant MH, Senut MC, Lamour Y. The septohippocampal pathway: structure and function of a central cholinergic system. Physiol Rev 1995;75:393–427. doi:10.1152/physrev.1995.75.2.393.

[288] McGlinchey EM, Aston-Jones G. Dorsal Hippocampus Drives Context-Induced Cocaine Seeking via Inputs to Lateral Septum. Neuropsychopharmacology 2018;43:987–1000. doi:10.1038/npp.2017.144.

[289] Grinvald A, Hildesheim R. VSDI: a new era in functional imaging of cortical dynamics. Nat Rev Neurosci 2004;5:874–85. doi:10.1038/nrn1536.

[290] Maatuf Y, Stern EA, Slovin H. Abnormal Population Responses in the Somatosensory Cortex of Alzheimer's Disease Model Mice. Sci Rep 2016;6. doi:10.1038/srep24560.

[291] Kim J, Jeong Y. Augmentation of sensory-evoked hemodynamic response in an early Alzheimer's disease mouse model. J Alzheimers Dis JAD 2013;37:857–68. doi:10.3233/JAD-121900.

[292] Pitkänen A, Pikkarainen M, Nurminen N, Ylinen A. Reciprocal Connections between the Amygdala and the Hippocampal Formation, Perirhinal Cortex, and Postrhinal Cortex in Rat: A Review. Ann N Y Acad Sci 2000;911:369–91. doi:10.1111/j.1749-6632.2000.tb06738.x.

[293] Ritov G, Ardi Z, Richter-Levin G. Differential activation of amygdala, dorsal and ventral hippocampus following an exposure to a reminder of underwater trauma. Front Behav Neurosci 2014;8. doi:10.3389/fnbeh.2014.00018.

[294] Phillips RG, LeDoux JE. Differential Contribution of Amygdala and Hippocampus to Cued and Contextual Fear Conditioning n.d.:12.

[295] Schumacher J, Peraza LR, Firbank M, Thomas AJ, Kaiser M, Gallagher P, et al. Dynamic functional connectivity changes in dementia with Lewy bodies and Alzheimer's disease. NeuroImage Clin 2019;22:101812. doi:10.1016/j.nicl.2019.101812.

[296] McDonald AJ, Mott DD. Functional Neuroanatomy of Amygdalohippocampal Interconnections and Their Role in Learning and Memory. J Neurosci Res 2017;95:797–820. doi:10.1002/jnr.23709.

[297] Paré D, Collins DR, Pelletier JG. Amygdala oscillations and the consolidation of emotional memories. Trends Cogn Sci 2002;6:306–14.

[298] Packard MG, Cahill L, McGaugh JL. Amygdala modulation of hippocampal-dependent and caudate nucleus-dependent memory processes. Proc Natl Acad Sci U S A 1994;91:8477–81. doi:10.1073/pnas.91.18.8477.

[299] Hobin JA, Ji J, Maren S. Ventral hippocampal muscimol disrupts context-specific fear memory retrieval after extinction in rats. Hippocampus 2006;16:174–82. doi:10.1002/hipo.20144.

[300] Orsini CA, Kim JH, Knapska E, Maren S. Hippocampal and prefrontal projections to the basal amygdala mediate contextual regulation of fear after extinction. J Neurosci Off J Soc Neurosci 2011;31:17269–77. doi:10.1523/JNEUROSCI.4095-11.2011.

[301] Ortner M, Pasquini L, Barat M, Alexopoulos P, Grimmer T, Förster S, et al. Progressively Disrupted Intrinsic Functional Connectivity of Basolateral Amygdala in Very Early Alzheimer's Disease. Front Neurol 2016;7. doi:10.3389/fneur.2016.00132.

[302] Laakso MP, Soininen H, Partanen K, Helkala E-L, Hartikainen P, Vainio P, et al. Volumes of hippocampus, amygdala and frontal lobes in the MRI-based diagnosis of early Alzheimer's disease: Correlation with memory functions. J Neural Transm - Park Dis Dement Sect 1995;9:73–86. doi:10.1007/BF02252964.

[303] Zanchi D, Giannakopoulos P, Borgwardt S, Rodriguez C, Haller S. Hippocampal and Amygdala Gray Matter Loss in Elderly Controls with Subtle Cognitive Decline. Front Aging Neurosci 2017;9. doi:10.3389/fnagi.2017.00050.

[304] Tang X, Varma VR, Miller MI, Carlson MC. Education is associated with sub-regions of the hippocampus and the amygdala vulnerable to neuropathologies of Alzheimer's disease. Brain Struct Funct 2017;222:1469–79. doi:10.1007/s00429-016-1287-9.

[305] Lin T-W, Shih Y-H, Chen S-J, Lien C-H, Chang C-Y, Huang T-Y, et al. Running exercise delays neurodegeneration in amygdala and hippocampus of Alzheimer's disease (APP/PS1) transgenic mice. Neurobiol Learn Mem 2015;118:189–97. doi:10.1016/j.nlm.2014.12.005.

[306] Swanson LW, Cowan WM. The connections of the septal region in the rat. J Comp Neurol 1979;186:621–55. doi:10.1002/cne.901860408.

[307] Chiba T. Collateral projection from the amygdalo--hippocampal transition area and CA1 to the hypothalamus and medial prefrontal cortex in the rat. Neurosci Res 2000;38:373–83.

[308] Dong HW, Petrovich GD, Swanson LW. Topography of projections from amygdala to bed nuclei of the stria terminalis. Brain Res Brain Res Rev 2001;38:192–246.

[309] Petrovich GD, Canteras NS, Swanson LW. Combinatorial amygdalar inputs to hippocampal domains and hypothalamic behavior systems. Brain Res Rev 2001;38:247–89. doi:10.1016/S0165-0173(01)00080-7.

[310] Kovács T. Mechanisms of olfactory dysfunction in aging and neurodegenerative disorders. Ageing Res Rev 2004;3:215–32. doi:10.1016/j.arr.2003.10.003.

[311] Djordjevic J, Jones-Gotman M, De Sousa K, Chertkow H. Olfaction in patients with mild cognitive impairment and Alzheimer's disease. Neurobiol Aging 2008;29:693–706. doi:10.1016/j.neurobiolaging.2006.11.014.

[312] Olofsson JK, Rönnlund M, Nordin S, Nyberg L, Nilsson L-G, Larsson M. Odor Identification Deficit as a Predictor of Five-Year Global Cognitive Change: Interactive Effects with Age and ApoE-ε4. Behav Genet 2009;39:496–503. doi:10.1007/s10519-009-9289-5.

[313] Wilson RS, Arnold SE, Schneider JA, Boyle PA, Buchman AS, Bennett DA. Olfactory Impairment in Presymptomatic Alzheimer's Disease. Ann N Y Acad Sci 2009;1170:730–5. doi:10.1111/j.1749-6632.2009.04013.x.

[314] Devanand DP, Tabert MH, Cuasay K, Manly J, Schupf N, Brickman AM, et al. Olfactory identification deficits and MCI in a multi-ethnic elderly community sample. Neurobiol Aging 2010;31:1593–600. doi:10.1016/j.neurobiolaging.2008.09.008.

[315] Martel G, Simon A, Nocera S, Kalainathan S, Pidoux L, Blum D, et al. Aging, but not tau pathology, impacts olfactory performances and somatostatin systems in THY-Tau22 mice. Neurobiol Aging 2015;36:1013–28. doi:10.1016/j.neurobiolaging.2014.10.033.

[316] La Joie R, Perrotin A, Barré L, Hommet C, Mézenge F, Ibazizene M, et al. Region-specific hierarchy between atrophy, hypometabolism, and β-amyloid (Aβ) load in Alzheimer's disease dementia. J Neurosci Off J Soc Neurosci 2012;32:16265–73. doi:10.1523/JNEUROSCI.2170-12.2012.

[317] Duclos H, Sayette V de L, Eustache F, Desgranges B, Laisney M. La variante frontale de la maladie d'Alzheimer Frontal variant of Alzheimer's disease n.d.:18.

[318] Kawakatsu S, Kobayashi R, Hayashi H. Typical and atypical appearance of early-onset Alzheimer's disease: A clinical, neuroimaging and neuropathological study. Neuropathology 2017;37:150–73. doi:10.1111/neup.12364.

[319] Johnson JK, Head E, Kim R, Starr A, Cotman CW. Clinical and pathological evidence for a frontal variant of Alzheimer disease. Arch Neurol 1999;56:1233–9.

[320] Jones MW, Wilson MA. Theta Rhythms Coordinate Hippocampal–Prefrontal Interactions in a Spatial Memory Task. PLoS Biol 2005;3. doi:10.1371/journal.pbio.0030402.

[321] Singer W. Neuronal synchrony: a versatile code for the definition of relations? Neuron 1999;24:49–65, 111–25.

[322] Becker JT, Mintun MA, Aleva K, Wiseman MB, Nichols T, DeKosky ST. Compensatory reallocation of brain resources supporting verbal episodic memory in Alzheimer's disease. Neurology 1996;46:692–700. doi:10.1212/WNL.46.3.692.

[323] Woodard JL, Grafton ST, Votaw JR, Green RC, Dobraski ME, Hoffman JM. Compensatory recruitment of neural resources during overt rehearsal of word lists in Alzheimer's disease. Neuropsychology 1998;12:491–504.

[324] Dougherty KD, Turchin PI, Walsh TJ. Septocingulate and septohippocampal cholinergic pathways: involvement in working/episodic memory. Brain Res 1998;810:59–71. doi:10.1016/s0006-8993(98)00870-1.

[325] Izquierdo I, da Cunha C, Rosat R, Jerusalinsky D, Ferreira MB, Medina JH. Neurotransmitter receptors involved in post-training memory processing by the amygdala, medial septum, and hippocampus of the rat. Behav Neural Biol 1992;58:16–26.

[326] Ortner M, Pasquini L, Barat M, Alexopoulos P, Grimmer T, Förster S, et al. Progressively Disrupted Intrinsic Functional Connectivity of Basolateral Amygdala in Very Early Alzheimer's Disease. Front Neurol 2016;7. doi:10.3389/fneur.2016.00132.

[327] Hebda-Bauer EK, Simmons TA, Sugg A, Ural E, Stewart JA, Beals JL, et al. 3xTg-AD Mice Exhibit an Activated Central Stress Axis during Early-Stage Pathology. J Alzheimers Dis JAD 2013;33:407–22. doi:10.3233/JAD-2012-121438.

[328] Fleisher AS, Sherzai A, Taylor C, Langbaum JBS, Chen K, Buxton RB. Resting-state BOLD networks versus task-associated functional MRI for distinguishing Alzheimer's disease risk groups. NeuroImage 2009;47:1678–90. doi:10.1016/j.neuroimage.2009.06.021.

[329] Bai F, Zhang Z, Yu H, Shi Y, Yuan Y, Zhu W, et al. Default-mode network activity distinguishes amnestic type mild cognitive impairment from healthy aging: a combined structural and resting-state functional MRI study. Neurosci Lett 2008;438:111–5. doi:10.1016/j.neulet.2008.04.021.

[330] Filippi M, Spinelli EG, Cividini C, Agosta F. Resting State Dynamic Functional Connectivity in Neurodegenerative Conditions: A Review of Magnetic Resonance Imaging Findings. Front Neurosci 2019;13. doi:10.3389/fnins.2019.00657.

[331] Fu Z, Caprihan A, Chen J, Du Y, Adair JC, Sui J, et al. Altered static and dynamic functional network connectivity in Alzheimer's disease and subcortical ischemic vascular disease: shared and specific brain connectivity abnormalities. Hum Brain Mapp 2019;40:3203–21. doi:10.1002/hbm.24591.

[332] Demirtaş M, Tornador C, Falcón C, López-Solà M, Hernández-Ribas R, Pujol J, et al. Dynamic functional connectivity reveals altered variability in functional connectivity among patients with major depressive disorder. Hum Brain Mapp 2016;37:2918–30. doi:10.1002/hbm.23215.

[333] Córdova-Palomera A, Kaufmann T, Persson K, Alnæs D, Doan NT, Moberget T, et al. Disrupted global metastability and static and dynamic brain connectivity across individuals in the Alzheimer's disease continuum. Sci Rep 2017;7. doi:10.1038/srep40268.

[334] Jie B, Wee C-Y, Shen D, Zhang D. Hyper-connectivity of functional networks for brain disease diagnosis. Med Image Anal 2016;32:84–100. doi:10.1016/j.media.2016.03.003.

[335] Wee C-Y, Yap P-T, Zhang D, Denny K, Browndyke JN, Potter GG, et al. Identification of MCI individuals using structural and functional connectivity networks. NeuroImage 2012;59:2045–56. doi:10.1016/j.neuroimage.2011.10.015.

[336] Sullivan EV, Zahr NM, Rohlfing T, Pfefferbaum A. Fiber tracking functionally distinct components of the internal capsule. Neuropsychologia 2010;48:4155–63. doi:10.1016/j.neuropsychologia.2010.10.023.

[337] Schmahmann JD, Rosene DL, Pandya DN. Motor projections to the basis pontis in rhesus monkey. J Comp Neurol 2004;478:248–68. doi:10.1002/cne.20286.

[338] Ferreira-Vieira TH, Guimaraes IM, Silva FR, Ribeiro FM. Alzheimer's Disease: Targeting the Cholinergic System. Curr Neuropharmacol 2016;14:101–15. doi:10.2174/1570159X13666150716165726.

[339] Cho H, Yang DW, Shon YM, Kim BS, Kim YI, Choi YB, et al. Abnormal Integrity of Corticocortical Tracts in Mild Cognitive Impairment: A Diffusion Tensor Imaging Study. J Korean Med Sci 2008;23:477–83. doi:10.3346/jkms.2008.23.3.477.

[340] Thillainadesan S, Wen W, Zhuang L, Crawford J, Kochan N, Reppermund S, et al. Changes in mild cognitive impairment and its subtypes as seen on diffusion tensor imaging. Int Psychogeriatr 2012;24:1483–93. doi:10.1017/S1041610212000270.

[341] Copenhaver BR, Rabin LA, Saykin AJ, Roth RM, Wishart HA, Flashman LA, et al. The fornix and mammillary bodies in older adults with Alzheimer's disease, mild cognitive impairment, and cognitive complaints: A volumetric MRI study. Psychiatry Res Neuroimaging 2006;147:93–103. doi:10.1016/j.pscychresns.2006.01.015.

[342] Rose SE, Janke AL, Chalk JB. Gray and white matter changes in Alzheimer's disease: a diffusion tensor imaging study. J Magn Reson Imaging JMRI 2008;27:20–6. doi:10.1002/jmri.21231.

[343] Shim G, Choi K-Y, Kim D, Suh S-I, Lee S, Jeong H-G, et al. Predicting neurocognitive function with hippocampal volumes and DTI metrics in patients with Alzheimer's dementia and mild cognitive impairment. Brain Behav 2017;7:e00766. doi:10.1002/brb3.766.

[344] Belarbi K, Burnouf S, Fernandez-Gomez F-J, Desmercières J, Troquier L, Brouillette J, et al. Loss of medial septum cholinergic neurons in THY-Tau22 mouse model: what links with tau pathology? Curr Alzheimer Res 2011;8:633–638.

[345] Hara Y, Motoi Y, Hikishima K, Mizuma H, Onoe H, Matsumoto S-E, et al. Involvement of the Septo-Hippocampal Cholinergic Pathway in Association with Septal Acetylcholinesterase Upregulation in a Mouse Model of Tauopathy. Curr Alzheimer Res 2017;14:94–103.

[346] Mondragón-Rodríguez S, Gu N, Fasano C, Peña-Ortega F, Williams S. Functional Connectivity between Hippocampus and Lateral Septum is Affected in Very Young Alzheimer's Transgenic Mouse Model. Neuroscience 2019;401:96–105. doi:10.1016/j.neuroscience.2018.12.042.

[347] Thomas AG, Koumellis P, Dineen RA. The Fornix in Health and Disease: An Imaging Review. RadioGraphics 2011;31:1107–21. doi:10.1148/rg.314105729.

[348] Pereira A, Ribeiro S, Wiest M, Moore LC, Pantoja J, Lin S-C, et al. Processing of tactile information by the hippocampus. Proc Natl Acad Sci U S A 2007;104:18286–91. doi:10.1073/pnas.0708611104.

[349] Itskov PM, Vinnik E, Diamond ME. Hippocampal representation of touch-guided behavior in rats: persistent and independent traces of stimulus and reward location. PloS One 2011;6:e16462. doi:10.1371/journal.pone.0016462.

ANNEXE 1: Processing pipeline of MRI images

1. Preprocessing of resting-state fMRI images

In order to explore the functional connectivity in mice, resting-state fMRI images were processed over several steps. The preprocessing of acquired resting-state fMRI volumes was performed on a tool implemented on MATLAB (The MathWorks, Natick, Massachusetts) in association with the fMRI tool of Statistical Parametric Mapping (SPM8, http://www.fil.ion.ucl.ac.uk/spm/), and its SPMmouse toolbox (http://www.spmmouse.org). We followed the steps illustrated in the figure 1, and applied them for each mouse:

1. The SPM function of **co-registration** was first used to align the first fMRI scan to its corresponding T2-weighted contrast-based image.

2. Variation of the signal intensity was corrected using the ANTS tool (Avants et al. 2011) on morphological T2-weighted images, which were then **normalized** to a template extracted from the Allen Mouse Brain Atlas (AMBA, Lein et al., 2007, http://mouse.brain-map.org/static/atlas). Information on standard locations of grey matter, white matter and cerebro-spinal fluid were provided from AMBA tissue probability maps. T2-weighted images were **segmented** and aligned to the atlas template using linear registration (12-parameter affine transformation, accounting for major differences in head shape and position between subjects), and non-linear registration (warping, accounting for small-scale anatomical differences)

3. A step of **realignment** of the 500 volumes to the first scan was applied as a motion correction (using a least square approach and a 6-parameters rigid body transformation in space), in addition to a bias intensity correction on each volume of each mouse.

4. The individual 4th degree B-Spline deformation (warping) information gained from the **normalization** and **segmentation** of the T2-weighted image was further applied to the rsfMRI contrast data to bring them into the high-resolution template space (0.15x0.15x0.15 mm^3).

5. A **spatial smoothing** of normalized resting-state fMRI data was performed with a Gaussian kernel of full width at half maximum (FWHM) of two voxels

6. Thanks to the normalization of the resting-state fMRI images to the AMBA, time-courses of the Blood Oxygen Level Dependent (BOLD) signal were precisely extracted from ROIs defined by this atlas.

7. Time-courses of each mouse for each chosen ROI were then detrended. We performed a Gaussian smoothing with a kernel of 2 voxels FWHM to all fMRI image volumes and a zero-phase band-pass filter was applied to extract frequencies between 0.01-0.1 Hz, representatives of the BOLD signal. The signal from ventricles was regressed out using a least square approach in order to reduce non-neural detection from the cerebro-spinal fluid.

From these processed images, we further performed static functional connectivity investigations - including correlations analysis, and graph theory measurements- and dynamic functional connectivity analysis.

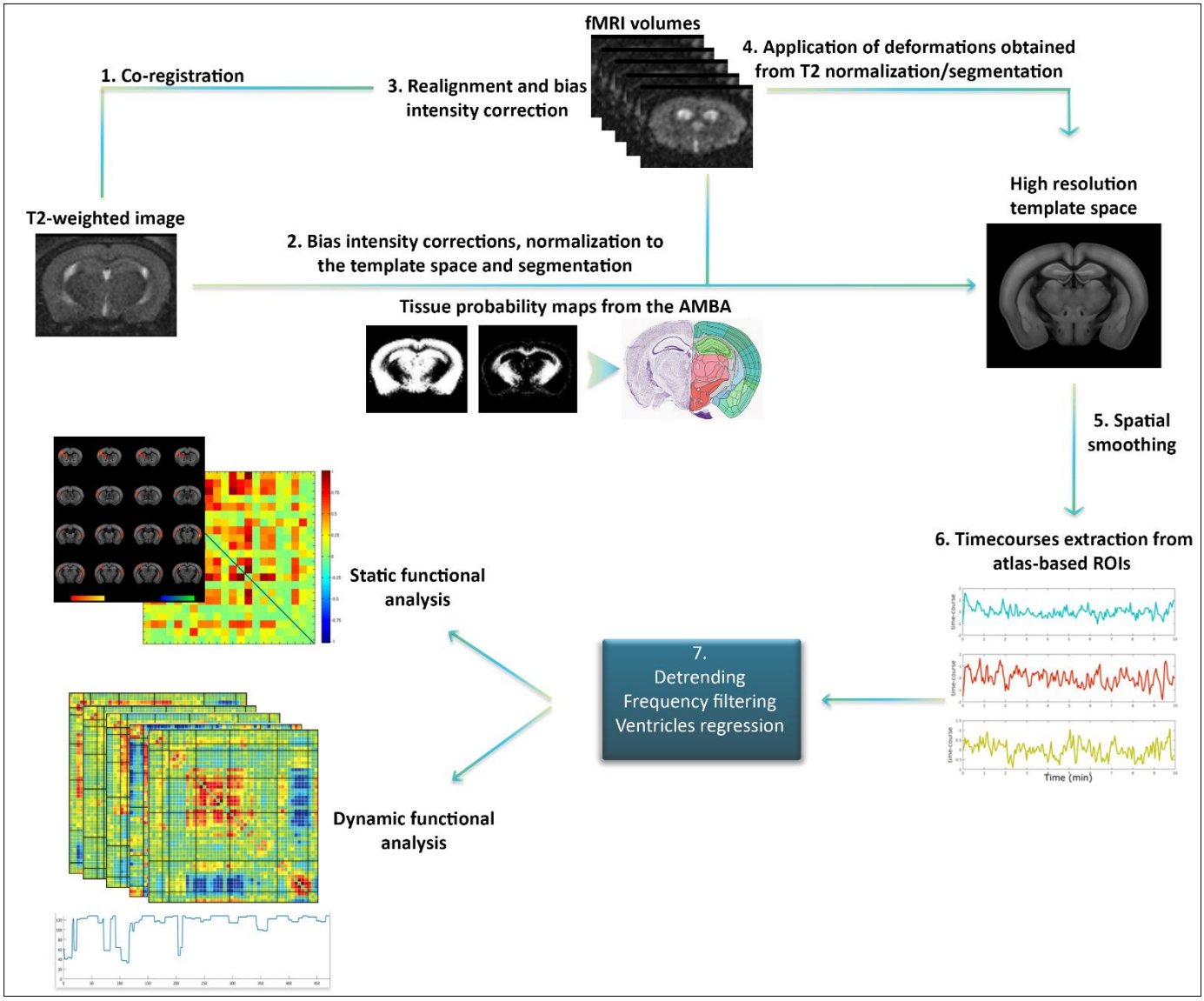

Figure 1: *Pre-processing pipeline of resting-state fMRI data*

2. Preprocessing of DTI images

HARDI images were acquired for all animals and fiber tracking was performed via global fiber tracking algorithm developed by Reisert et al., 2011; optimized and validated for in-vivo mouse brain tractography (Harsan et al., 201 3). To analyze diffusion-weighted images, we first went through several processing steps as illustrated in the figure 2, and followingexplained:

1. B-vector and b-values – representing respectively the collected gradient directions (30) and the amount of diffusion weighted used for each volume- were extracted from HARDI data and denoised using the MRtrix software (Veraart et al., 2016), to obtaine denoised diffusion weighted images.

2. Tensor-derived maps were calculated from denoised diffusion weighted images: the Axial Diffusivity (λ_1, Adif) maps were obtained from the measurement of longitudinal diffusivity in voxels, the Radial Diffusivity ((λ_{2+} λ_3)/2, RD) maps were extracted from measures of

diffusivity on the perpendicular axis of the tensor, and Fractional Anisotropy (FA) maps were computed by a normalization of diffusion measures from all three axis of the tensor.

2'. From denoised HARDI data, we applied global tractography for each individual mouse brain included in the studies to reconstruct fibers (Mechling et al., 2016), and extracted fiber density maps (FD).

3. From each parametric map (ADif, RD, FA, FD), an average template was created using the ANTS multivariate template construction function (Avants et al. 2011), and individuals' images were co-registered to the corresponding template, allowing rigid and non-rigid deformations.

4. A spatial gaussian smoothing of 0.5mm FWHM was applied to all images, to further performed voxel-based quantification analysis on deformations maps.

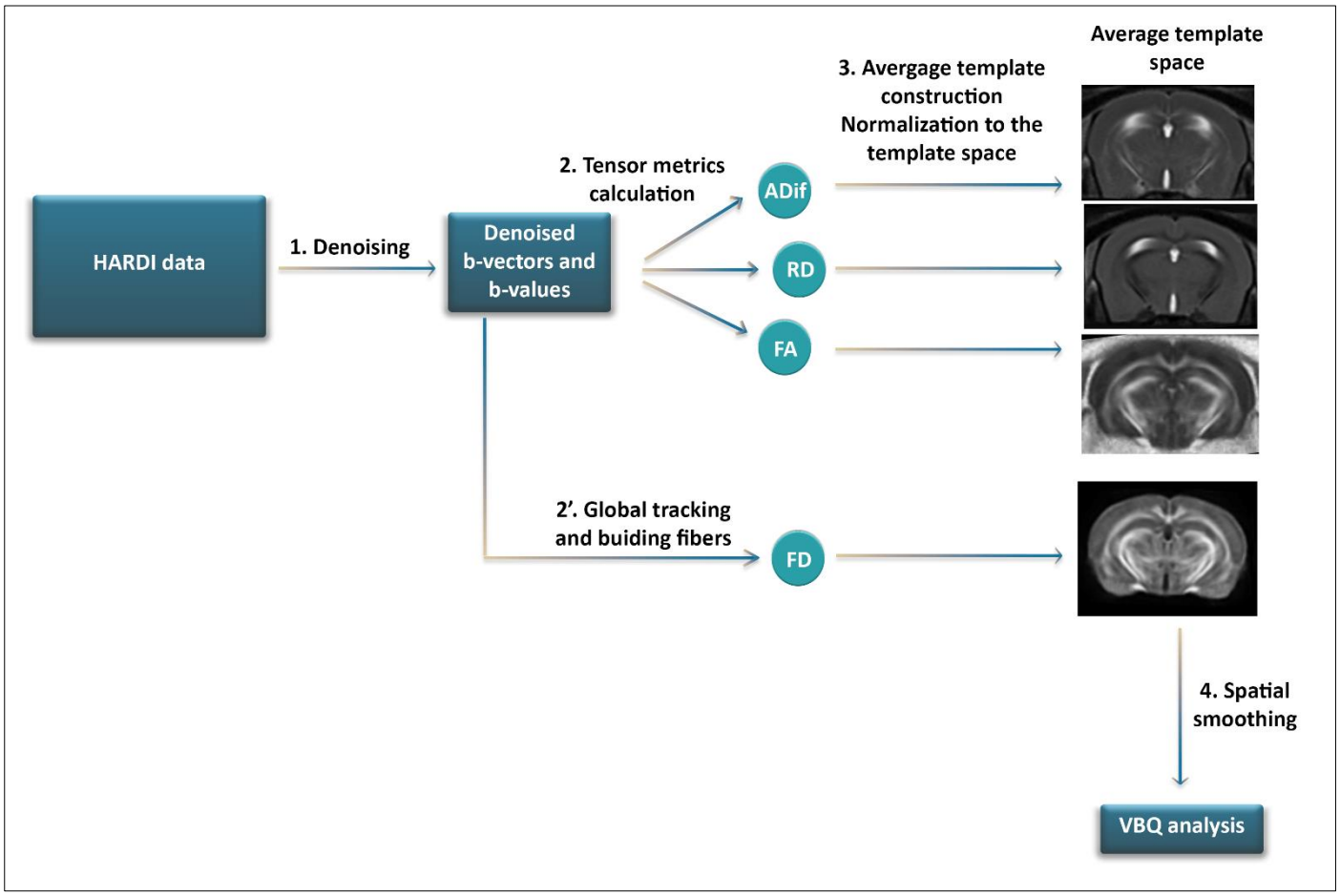

Figure 2: Pre-processing pipeline of HARDI data

ANNEXE 2 : Résumé de la thèse en français

Introduction

Notre cerveau est un réseau, une association très efficace de régions structurellement et fonctionnellement interconnectées, partageant continuellement des informations entre elles. L'étude du cerveau comme un tel système d'intégration permet d'apporter des indications uniques sur la communication neuronale à grande échelle. Elle permet de fournir une plate-forme pour étudier et tenter de comprendre comment les connectivités structurelle et fonctionnelle sont affectées par les changements du métabolisme cérébral ou du comportement, et plus particulièrement, comment cette organisation peut être modifiée ou réorganisée dans des pathologies neurodégénératives telle que la maladie d'Alzheimer (MA)

En 1907, Aloïs Alzheimer -un médecin allemand psychiatre, neurologue et neuropathologiste - décrivit pour la première fois les symptômes de la pathologie qui portera plus tard son nom. Sa patiente, Auguste Deter, était âgée de 51 ans quand Aloïs Alzheimer détecta chez elle des perturbations importantes de la mémoire. A son décès, le médecin réalisa une autopsie cérébrale lui permettant de mettre en évidence les deux principales lésions de la pathologie : les plaques amyloïdes et les dégénérescences neurofibrillaires (DNF). Depuis ces découvertes, de nombreuses connaissances sur la maladie d'Alzheimer (MA) ont été rassemblées, comme la détection d'altérations génétiques impliquées dans la pathologie, de facteurs de risques génétiques comme l'allèle E4 du gène de l'apolipoprotéine ou un variant du gène TREM2 impliqué dans la neuroinflammation, ainsi que les principaux composants des plaques amyloïdes et DNF. Malgré ces avancées, la MA est à l'heure actuelle la pathologie la plus fréquente chez les personnes âgées, en concernant 900 000 personnes en France, et 35 millions autour du globe. Ainsi, dans le but d'améliorer le diagnostic de cette pathologie et de développer des traitements efficaces, une meilleure compréhension des altérations biologiques sous-jacentes des symptômes cognitifs chez les patients est aujourd'hui cruciale.

On admet qu'il existe dans la MA deux mécanismes principaux : l'amyloïdopathie et la tauopathie. L'hypothèse de la « cascade amyloïde » selon laquelle la neurotoxicité amyloïde serait à l'origine du développement de toutes les autres altérations biologiques dans la MA, est à l'heure actuelle la plus acceptée et explorée par la communauté scientifique. La tauopathie est, quant à elle, considérée comme le second mécanisme le plus important dans la MA, et est responsable du développement des déficits cognitifs dans la pathologie, dont la progression est décrite par les stades de Braak. Dans la MA, la modification de conformation de la protéine Tau entraine son dysfonctionnement, menant à une désintégration axonale puis à une mort neuronale. Bien qu'étant des lésions caractéristiques de la MA, des plaques amyloïdes et DNF sont aussi retrouvées chez des personnes âgées saines, ou dans d'autres pathologies, induisant des difficultés de diagnostic importantes.

En raison de son caractère non-invasif, l'Imagerie par Résonance Magnétique (IRM) est un des outils les plus utilisé pour diagnostiquer la MA, permettant le suivi au cours du temps des altérations chez les patients. Cette technique est à l'heure actuelle employée pour mettre en évidence les modifications morphologiques cérébrales des patients, souvent présentes à des stades déjà tardifs de la maladie. Cependant, grâce à l'étude de la connectivité cérébrale, des

études en IRM chez l'Homme ont su révéler le potentiel de cet outil dans la mise en évidence d'un biomarqueur diagnostic plus précoce, montrant des altérations des connectivités fonctionnelle et structurelle du cerveau dans la MA. En effet, des études IRM ont pu identifier des modifications de configuration de réseaux cérébraux en corrélation avec la symptomatologie de patients atteints de la MA. Sonder les réseaux et le métabolisme du cerveau chez la souris, le modèle le plus largement utilisé dans les neurosciences expérimentales représente ainsi une étape cruciale pour cette recherche translationnelle, comblant le fossé entre les investigations précliniques et cliniques. En effet, cette recherche de nouveaux biomarqueurs précis, robustes et non-invasifs, à la fois pour le diagnostic et la caractérisation de l'évolution de la maladie, constitue une phase essentielle pour permettre le développement de traitements, sous-tendues notamment par des études pré-cliniques des modèles animaux de la MA. Afin de mettre en évidence des patterns spécifiques de la pathologie, l'IRM constitue un outil unique permettant l'analyse longitudinale, non invasive et *in vivo* de la connectivité cérébrale.

C'est pourquoi, l'objectif de ce projet de thèse est de caractériser l'évolution au cours du temps de l'architecture des réseaux cérébraux d'un modèle murin de la maladie d'Alzheimer, en combinant des informations sur l'organisation cérébrale à la fois structurelle et fonctionnelle -ou connectome- obtenues en utilisant des techniques d'IRM de pointes nous permettant d'ouvrir une fenêtre non-invasive sur le cerveau et de reconstruire l'architecture globale des voies fonctionnelles de communication ainsi que leur substrat microstructural. De manière originale, le projet a porté sur une souris modèle de tauopathie, faisant l'objet de beaucoup moins d'études que l'amyloïdopathie, particulièrement en IRM. Une cartographie du connectome du modèle transgénique Thy-Tau22, exprimant la tauopathie, et un suivi de la dynamique de ces réseaux au cours du temps en parallèle avec l'évolution de la pathologie a été réalisé, en association avec une investigation comportementale et histologique des atteintes, afin de mettre en évidence de potentiels biomarqueurs de la pathologie ainsi que de potentielles cibles pour le développement de stratégies thérapeutiques.

Approches méthodologiques

Chez les souris Thy-Tau22 les premières dégénérescences neurofibrillaires, caractéristiques d'une perturbation de la fonction de la protéine Tau, apparaissent dans l'hippocampe à l'âge de 4 mois d'après la littérature. Parallèlement, une étude a montré que les premiers signes d'un déclin cognitif se manifestent, eux, à l'âge de 8 mois. Se basant sur ce décours temporel, deux groupes de souris saines (n = 13, C57Bl6/J) et Thy-Tau22 (n = 16) ont été suivis de manière longitudinale par IRM et analyse comportementale, aux âges de 5, 9 et 13 mois reflétant respectivement les stades prodromal, précoce et tardif de la pathologie. En parallèle, des marquages histologiques de la Tau pathologique ont été effectués afin de caractériser la localisation des dépôts de la protéine au cours du temps, en association avec l'évolution comportemental et du connectome.

L'unique technique, chez l'Homme et l'animal, permettant d'étudier le connectome cérébrale de manière longitudinale, non invasive et in vivo, est l'IRM. Celle-ci permet par exemple d'obtenir des informations sur la connectivité fonctionnelle via l'imagerie

fonctionnelle de repos (IRMfr), et structurelle grâce à l'imagerie du tenseur de diffusion (DTI). Pour étudier le connectome des souris Thy-Tau22, des acquisitions en imagerie anatomique, en IRMfr et en DTI ont été réalisées au sein de la plateforme « IRIS » de Strasbourg, à l'aide d'une antenne d'émission 86 mm et une antenne de réception à température ambiante adaptée à la tête des souris. Ces trois approches méthodologiques permettent d'étudier les potentielles modifications morphologiques cérébrales, de connectivité fonctionnelle, et de connectivité structurelle du cerveau, dans le but de révéler l'organisation complexe du connectome cérébral dans ce modèle.

Pour ce projet, une première partie d'optimisation de l'anesthésie des animaux au cours de l'examen d'IRMfr a été réalisée. En effet, d'après des études comparant l'effet de différents anesthésiques en IRMfr, le Domitor (médétomidine) est actuellement un des sédatifs les plus adapté pour observer la connectivité fonctionnelle cérébrale au repos chez la souris. Ces études ont montré que d'autres anesthésiques comme l'isoflurane, classiquement utilisé en IRM du petit animal, perturbait le système hémodynamique cérébral sur lequel se base le signal observé en IRMfr. Ainsi en fonction de la littérature, pour les examens d'IRMfr, les souris sont mises sous infusion sous-cutanée de Domitor, parfois précédée d'un bolus lui aussi injecté en sous-cutanée. Il n'existe à l'heure actuelle pas de dose standard pour une infusion sous-cutanée de Domitor chez la souris. Nous avons donc testé des doses le plus souvent utilisées dans la littérature allant de 0 à 0.6 mg/kg dans 100µl de NaCl 0.9% pour le bolus, et 0.3 à 0.6 mg/kg dilué dans 200µl/h de NaCl 0.9% pour l'infusion. Le but de cette procédure est de réduire la dose de Domitor au maximum afin de s'assurer un état de repos tel qu'il est défini par électroencéphalographie (EEG). Après cette optimisation, des doses de 0.3 mg/kg pour 100µl de NaCl 0.9% pour le bolus et de 0.6 mg/kg dans 200µl/h de NaCl 0.9% pour l'infusion ont été choisi.

Imagerie anatomique

Dans un premier temps, des analyses morphométriques basées-voxel (VBM) ont été effectuées pour détecter les éventuelles variations anatomiques du cerveau entre les groupes, et au cours du temps au sein du même groupe expérimental. Ces changements anatomiques peuvent être associés à une mort neuronale importante dans des régions cérébrales spécifiques, induisant une atrophie de ces mêmes aires. Au contraire, une hypertrophie du cerveau peut aussi être observée, associée au recrutement massif de cellules neuroinflammatoires induit par la pathologie Tau.

Imagerie fonctionnelle

Afin de mettre en évidence les relations de connectivités fonctionnelles entre différentes régions cérébrales, une analyse des fluctuations d'un signal hémodynamique appelé signal BOLD (Blood-Oxygen-Level Dependant), a été réalisée chez les souris à l'état de repos par IRMfr. Cette méthode se base sur la détection des fluctuations spontanées de basses fréquences (inférieures à 0,1Hz) du signal BOLD, et il est aujourd'hui admis que la synchronisation de ces fluctuations entre des régions cérébrales distinctes reflète une connexion fonctionnelle entre elles. L'évaluation des corrélations entre le décours temporel de ce signal dans différentes régions d'intérêts, et le reste du cerveau a donc été effectuée. Ce type d'analyse permet de révéler les réseaux fonctionnels de ces régions. Ainsi, une forte corrélation entre deux décours

temporels est considérée comme une connexion fonctionnelle entre deux régions. Deux approches ont été utilisées pour ces analyses : statique et dynamique :

1) On parle de connectivité fonctionnelle *statique* lorsque l'on s'intéresse uniquement aux relations spatiales entre les décours temporels du signal BOLD d'une région d'intérêt avec le reste du cerveau, créant une carte de connectivité fonctionnelle de cette région. Pour cette étude, deux principales méthodes d'analyse statique ont été employées. Dans un premier temps, des analyses par régions d'intérêt (ROI) ont été effectuées. L'utilisation de cette technique permet d'évaluer la connectivité fonctionnelle d'une ROI spécifique, en calculant la corrélation entre le décours temporel moyen du signal BOLD de cette région, avec tout les autres décours des voxels du cerveau. Ainsi, on obtient une carte de la connectivité fonctionnelle de cette région cible pour un individu.

Une seconde approche, basée sur la théorie des graphs pouvant être appliquée à la fois aux connectivités fonctionnelle et structurelle, a été utilisée pour caractériser l'organisation fonctionnelle hiérarchique entre plusieurs régions cérébrales, appelées des *nœuds*. Cette méthode permet de mettre en évidence différentes caractéristiques spécifiques du modèle mathématiques de la théorie des graphs : on appelle *edge*, un lien entre deux régions cérébrales, qu'il soit fonctionnel ou structurel. Le nombre de liens d'une région est regroupé sous la nomination de *degré*, définissant l'influence d'une aire du cerveau sur les autres régions. Au niveau cérébrale, les réseaux sont organisés sous forme de *module*, correspondant à une communication neuronale intrinsèque de régions fortement liées fonctionnellement et structurellement. Permettant l'interaction entre ces différents modules, certains nœuds sont définis comme *hubs* et possède une influence particulièrement importante sur l'organisation et la communication cérébrale. L'analyse de la connectivité fonctionnelle suivant la théorie des graphs dans le cadre de l'étude de maladie neurodégénérative permet donc d'évaluer les modifications hiérarchiques entre les différentes régions cérébrales d'intérêts et de détecter les altérations liées au différents paramètres du modèles tel que le *degré*.

2) En ajoutant une composante temporelle à notre analyse, on peut révéler la dynamique de la connectivité fonctionnelle. En effet, bien qu'intégrant l'ensemble des interactions simultanément, l'analyse statique est toujours réalisée sur toute la durée du signal BOLD enregistrées au cours de l'acquisition. Les variations temporelles des interactions et corrélations entre différentes régions cérébrales ne sont donc pas perçues. Si cette hypothèse a été faite pour faciliter la mise en œuvre des techniques de mesure de la connectivité fonctionnelle, les nouvelles approches tendent depuis quelques années à caractériser la dynamique de la connectivité fonctionnelle. Plusieurs méthodes ont été développées afin d'analyser les fluctuations de cette connectivité fonctionnelle. Des variations de communication entre deux régions cérébrales sont observées en mesurant leur connectivité fonctionnelle sur différentes fenêtres temporelles, de durée inférieure à la durée globale de l'acquisition. En effet, au cours d'une session d'IRMfr, la connectivité fonctionnelle entre deux régions cérébrales peut varier, présentant des changement dans leur état de connectivité pouvant être corrélé ou décorrélé. Ces états décrivent les variations d'associations ou de dissociation de ces régions à un réseau de régions d'intérêt défini. Grâce à l'utilisation d'un algorithme de fenêtre glissante, la détection des variations d'états de connectivités entre

plusieurs régions d'intérêts, tout au long d'une session d'acquisition IRM, a pu être réalisée dans cette étude, et associée aux analyses statique de la connectivité fonctionnelle.

Pour analyser les images acquises en IRMfr, un protocole de traitement a été développé, suivant les étapes classique du traitement d'images médicales :

1. Les images ont dans un premier temps été prétraitées par un réalignement des données fonctionnelles afin de corriger les éventuels artefacts de mouvements, associé à une correction du biais d'intensité du signal (ANTS tool, Avants et al. 2011) ; suivi d'un recalage sur une image anatomique ainsi qu'une normalisation sur un atlas du cerveau de la souris, l'Allen Mouse Brain Atlas (AMBA, Lein et al., 2007, http://mouse.brain-map.org/static/atlas). Des déformations rigides puis non-rigides ont été appliquées sur les images, impliquant des transformation affines suivant 12 paramètres et une déformation non affine B-Spline de degré 4, permettant de placer les images dans le même espace fonctionnelle à haute résolution spatiale ($0.15x0.15x0.15mm^3$) que l'AMBA.

2. Une segmentation des images fonctionnelles suivant une ségrégation issues de l'AMBA basée sur des cartes de probabilités de la matière grise, la matière blanche et le liquide céphalo-rachidien, a ensuite été réalisée. Cette dernière étape permettra par la suite de cibler de manière très précise les régions d'intérêts de notre étude.

3. Pour finir les images ont été lissées spatialement suivant un filtre gaussien, à une échelle de deux voxels.

4. Dans un second temps, les images fonctionnelles prétraitées ont été post-traitées par une filtration des basses fréquences afin de ne sélectionner que les fréquences BOLD spontanées (0.01Hz-0.1Hz), associées à l'état de repos. Une éventuelle tendance du signal a été normalisée par un étape dites de « *detrending* », et le signal provenant des ventricules a été régressé selon la méthode des moindres carrées afin de ne s'intéresser qu'aux signaux issues des matières grises et blanches.

Imagerie structurelle

L'imagerie DTI illustre, elle, la diffusion des molécules d'eau le long des fibres axonales de la matière blanche ; fibres pouvant ensuite être cartographiées grâce à l'utilisation d'algorithmes de suivi des fibres et permettre ainsi d'étudier la connectivité structurelle dans la cerveau. Cette méthode se base sur la détection par IRM des mouvements de diffusion des molécules d'eau au sein des différents tissus biologiques, ces mouvements pouvant être de type isotrope ou anisotrope. Au niveau cérébral, un mouvement de l'eau de type isotrope sera associé indirectement à la détection de matière grise (neurones, cellules gliales) ou de liquide céphalo-rachidien. En revanche, un mouvement de diffusion anisotrope sera associé au déplacement des molécules d'eau au sein des fibres nerveuses. L'analyse grâce à l'utilisation d'un modèle mathématique de tenseur permet de quantifier le degré d'anisotropie de la diffusion de l'eau au sein du cerveau ainsi que son orientation préférentielle, mettant donc en évidence l'organisation des fibres nerveuses, et leurs caractéristiques microstructurelles.

Les images obtenues par imagerie du tenseur de diffusion ont été utilisées pour effectuer une cartographie à haute résolution des fibres nerveuses, et extraire des cartes statistiques de diffusion. Pour cette analyses, les données utilisées ont été prétraitées de la même manière suivante :

1. Les images de diffusion ont dans un premier temps été débruitées grâce à l'utilisation d'un algorithme de débruitage développé par MRtrix (Veraart et al., 2016).

2. Les cartes paramétriques issues du tenseur ont été extraites en utilisant un fonction de Mrtrix (Veraart et al., 2016), reflétant les différentes directions de diffusion. Ces cartes permettent d'observer la diffusion radiale (RD) dans le cerveau, obtenue par la mesure de diffusion perpendiculaire à l'axe principale du tenseur, la diffusion axiale (ADif) des molécules d'eau dans le cerveau des souris correspondant à la diffusion le long de l'axe principale du tenseur, et enfin la fraction d'anisotropie (FA) reflétant une mesure normalisée combinant le degrés d'anisotropie de la diffusion de l'eau dans les 3 axes du tenseur.

3. En parallèle, un algorithme complexe a été utilisé afin de réaliser une tractographie globale des fibres nerveuses sur les cartes debruitées issues de l'imagerie DTI, et d'en évaluer la densité (FD) dans chacun des groupes.

4. Toutes les cartes générées (RD, ADif, FA et FD) ont ensuite été utilisées pour créer une image de référence, ou « *template* », moyenne pour chacun des paramètres extraits, et ont été normalisées sur ce-dernier à l'aide de déformations linéaire et non linéaires.

5. Un filtre spatial Gaussien de 0.5mm a été appliqué a toutes les images, afin d'effectuer par la suite des analyse de quantification basées-voxel.

Evaluation comportementales et histologiques

En parallèle des résultats obtenus en imagerie, des études comportementales et histologiques ont été effectuées. La MA étant une pathologie induisant, entre autres, des perturbations mnésiques, l'étude comportementale a donc été faite à l'aide de tests évaluant la mémoire. Une étude longitudinale de la pathologie a été réalisée sur les mêmes groupes de souris analysés en IRM, et aux mêmes stades critiques. Les capacités mnésiques des souris ont été testé via des tests classiques évaluant la mémoire chez la souris tel que la piscine de Morris, et la reconnaissance d'objets.

Trois types de tests dits « tests objets » ont tout d'abord été réalisés. Ces tests se basent sur le comportement spontané des souris consistant à explorer préférentiellement la nouveauté dans leur environnement. Ainsi, les souris sont dans un premier temps placées dans un champ ouvert en présence d'objets qu'elles passeront 10 minutes à explorer. Puis, dans une seconde phase et après avoir été remise dans leur cages pendant 15 minutes ou 1h en fonction du test effectué, l'un des objets est soit déplacé, remplacé ou changé. On considère alors que si la souris passe plus de temps à explorer cet objet modifié, elle aura bien détecté le changement dans son environnement, sous-entendant qu'elle a mémorisé la conformation initiale des objets lors de la première phase. Ces trois tests permettent de mettre en évidence de manière

spécifique d'éventuelles atteintes du cortex entorhinal, du cortex périrhinal ou de l'hippocampe, 3 régions très impliquées dans le traitement de la mémoire, et atteintes dans la maladie d'Alzheimer chez l'Homme.

Le test de la piscine de Morris, classiquement utilisé pour évaluer la mémoire spatiale chez la souris, a ensuite été effectué. Ce test est un labyrinthe aquatique réalisé dans une piscine circulaire rempli avec d'eau à 22°C. La piscine, placée dans une pièce comportant des indices spatiaux, contient une plateforme circulaire "échappatoire" au centre d'un des quadrants de ces quadrant appelé quadrant-cible. Ainsi dans ce test, les souris doivent apprendre à localiser la plateforme immergée afin de pouvoir retourner dans leur cage et sortir de ce milieu aversif. La première phase du test consiste à apprendre aux souris la localisation de la plateforme et se déroule sur 5 jours consécutifs à raison de 4 essais par jours. Comme indicateur d'un apprentissage, le temps mis par l'animal pour atteindre la plate-forme au cours des essais et des jours est mesuré. Une seconde phase du test consiste ensuite à évaluer les capacités de rétention des souris. Pour cela, 10 jours après l'apprentissage, les animaux sont à nouveaux mis dans la piscine où cette fois la plateforme a été retirée et le temps passé dans le quadrant cible est mesuré sur 60 secondes. Ainsi, un animal qui se souvient de l'emplacement de la plate-forme passera plus de temps que le hasard dans le quadrant cible.

En plus des tests comportementaux de mémoire, des marquages immunologiques de la protéine Tau hyperphosphorylée ont été effectués sur des cerveaux de souris du même âge que les groupes étudiés en IRM et en comportement, afin d'associer l'accumulation des dépôts de Tau pathologiques (AT8 et pSer422) avec des perturbations du connectome et des affectations cognitives. Au stade prodromal, un marquage des cellules astrocytaires impliquées dans la réaction inflammatoire a aussi été réalisé (GFAP).

Résultats et discussion

Dans un premier temps, plusieurs tests comportementaux ont été effectués sur les souris âgées de 5 mois. D'après les résultats, les souris Thy-Tau22 ne présentent pas de déficits mnésiques à cet âge, confirmant le stade prodromal de la maladie. Ces mêmes souris ont ensuite été examinées *in vivo* par IRM cérébrale. L'analyse morphométrique a révélé qu'à 5 mois, les souris Thy-Tau22 ne présentent pas de modifications morphologiques par rapport aux souris saines. Malgré l'absence de troubles mnésiques et de mort neuronale chez les souris transgéniques à ce stade de la pathologie, des modifications de la connectivité fonctionnelle cérébrale à la fois statique et dynamique ont pu être mises en évidence. En effet, l'analyse de la connectivité fonctionnelle cérébrale statique du modèle a révélé une hyperconnectivité de certaines régions spécifiques comme l'hippocampe -région clé impliquée dans les processus de mémoire-, et l'amygdale -impliquée dans le système de traitements des émotions, le système limbique. Appuyant ces résultats, des modifications significatives de la dynamique de connectivité fonctionnelle de ces mêmes régions ont été détectées. Parallèlement, la connectivité d'autres régions cérébrales comme le cortex entorhinal et le cortex périrhinal, des régions pourtant connues pour être impliquées dans la maladie, ne présente pas de modifications par rapport aux souris saines. Ainsi les altérations de communications fonctionnelles de régions spécifiques à un stade où aucun déficit mnésique, ni atrophie

cérébrale n'est observé chez les souris Thy-Tau22, semblent mettre en évidence un potentiel marqueur d'imagerie pour les stades précoce de la pathologie.

Suite aux analyses en imagerie fonctionnelle, des images obtenues par la technique de DTI ont été utilisées afin d'effectuer une cartographie à haute résolution des fibres nerveuses, et extraire les cartes paramétriques issues du tenseur de diffusion. Un algorithme complexe a été utilisé afin de réaliser une tractographie globale du cerveau, et d'en évaluer la densité de fibres (FD) dans chacun des groupes. Les cartes paramétriques extraites ont permis de calculer la fraction d'anisotropie (FA), la diffusion radiale (RD), et la diffusion axiale (AD) des molécules d'eau dans le cerveau des souris. L'analyse de ces résultats a montré une atteinte de la FA et de la FD au niveau de la fimbria et du fornix dès l'âge de 5 mois, indiquant de possibles modifications microstructurelles au long de ces voies cholinergiques reliant essentiellement l'hippocampe et le septum. L'hyperconnectivité fonctionnelle du réseau hippocampique au même âge pourrait donc être interprétée comme un mécanisme compensatoire à ce stade précoce de la maladie. Les résultats combinés des analyses de la connectivité fonctionnelle et structurelle à 5 mois semblent donc montrer une atteinte précoce de la voie septo-hippocampique, connue pour être affectée dans la MA chez l'Homme également. De plus, chez les souris Thy-Tau22, des modifications de la connectivité fonctionnelle de l'hippocampe sont détectables avant l'émergence de troubles de mémoire ou d'apprentissage.

Cependant l'étude du connectome en IRM ne permettant pas de mettre en évidence de manière direct le substrat biologique impliqué dans les modifications observées, des analyses immunohistologiques ont été conduites sur le cerveau de souris du même âge. Différents marquages ont été réalisés afin de confirmer ou non les hypothèses possibles. En effet l'hyperconnectivité de réseaux spécifiques chez les souris Thy-Tau22 à 5 mois pourrait être le résultat d'une activation des cellules gliales – incluant les astrocytes-, une réaction inflammatoire qui dans un premier temps pourrait induire un effet de compensation, ou encore refléter la progression de la pathologie Tau dans des régions spécifiques. C'est pourquoi, un marquage des cellules astrocytaires impliquées dans la réaction inflammatoire a été réalisé (GFAP), ainsi qu'un marquage de la protéine tau pathologique (AT8). D'après les résultats, on remarque une cohérence entre la localisation des deux marqueurs biologiques et l'hyperconnectivité du réseau hippocampique chez les souris Thy-Tau22 à 5 mois. Ces résultats suggèrent donc que l'augmentation de la connectivité fonctionnelle de ce réseau serait liée à une densité importante de tau pathologique dans les régions qui le constituent, additionnée à un important recrutement de cellules astrogliales. Cette accumulation de Tau pathologique pourrait en même temps entrainer des perturbations des voies de connectivité de l'hippocampe, amplifiant la réponse fonctionnelle anormale de cette région.

Le but de l'étude étant de faire une analyse longitudinale, non invasive et in vivo des souris modèles de la MA, les souris scannées à 5 mois ont donc été soumises aux mêmes tests comportementaux et analyses d'IRM à un stade intermédiaire (9 mois) et avancé (13 mois) de la maladie. Parallèlement, une autre cohorte de souris a été utilisée pour effectuer des analyses histologiques aux mêmes âges.

Les résultats comportementaux à 9 et 13 mois ont montré des perturbations mnésiques débutant à 9 mois chez les souris Thy-Tau22, présentant des performances significativement

plus faibles que les souris saines dans tous les tests effectués. Associée à ces altérations, une atrophie spécifique de l'hippocampe et de l'amygdale a été détectée dès l'âge de 9 mois, et renforcée à 13 mois. Une analyse longitudinale a aussi permis de révéler un impact de la connectivité fonctionnelle affectant particulièrement le septum et sa connectivité avec l'hippocampe, l'amygdale et le cortex retrosplénial -un nœud central du réseau par défaut- au cours du temps chez les souris Thy-Tau22. Parallèlement, les analyses des données structurelles à 9 et 13 mois ont pu mettre en évidence une augmentation des perturbations microstructurelles, particulièrement des voies cholinergiques septo-hippocampique, septo-amygdalienne et cortico-subcortical qui pourraient être associées à la diminution de connectivité fonctionnelle de l'hippocampe, et aux altérations fonctionnelles septales. L'analyse histologique a confirmé la densité importante de protéine Tau pathologique dans les régions affectées à la fois au niveau morphologique, structurel et fonctionnel.

L'émergence des perturbations de la mémoire de ces souris à 9 mois pourrait donc être liée à une perte de mécanismes compensatoires fonctionnels du réseau hippocampique associée à une atrophie cérébrale de cette même région, ainsi qu'à l'amplification des altérations des fibres nerveuses et régions cérébrales associées -septum, hippocampe, amygdale, et nœuds réseau par défaut. Les perturbations microstructurelles de la voie cholinergique septo-hippocampique pourraient être responsables du début d'atrophie cérébrale observée dans l'hippocampe, sous-tendues par la présence de Tau pathologique ainsi que d'une inflammation chronique dans ces mêmes régions.

Ainsi, grâce à l'analyse longitudinale, non invasive et *in vivo* du connectome chez un modèle souris de la MA, cette étude a permis de mettre en évidence des patterns de connectivité spécifiques de la pathologie pouvant servir de potentiel biomarqueur de la maladie. Par ailleurs, la détection d'altérations de connectivité (à la fois fonctionnelle et structurelle) à des stades très précoces de la pathologie, avant l'apparition d'atrophie cérébrale et de symptômes mnésiques, pourrait correspondre aux prémices de la maladie, lorsque celle-ci est encore indétectable chez l'Homme. Afin d'aller plus loin dans cette analyse, il serait donc intéressant de réaliser une étude translationnelle permettant une comparaison directe entre des résultats précliniques et cliniques via une analyse du connectome cérébral chez des patients atteints de la MA, particulièrement à des stades précoces. Les voies de connectivité mises en évidence ainsi que la signature fonctionnelle détectée à un stade prodromal chez les souris modèles, pourraient ainsi servir de points de départ pour une exploration similaire chez l'Homme, et permettre de progresser dans la révélation d'un biomarqueur précoce de diagnostic et de l'évolution de la pathologie.

ANNEXE 3: Other study: Karatas, Degiorgis et., al; in preparation

Time-dependent alterations in structural and functional brain networks in rodent neuropathic pain-induced depression

1. Introduction

Neuropathic pain is a neurological syndrome that associates both sensory nociceptive and aversive emotional components. It can also lead to anxio-depressive consequences, which increases the pain burden. The existence of neuropathic pain-induced affective disorders is further supported by preclinical studies showing that neuropathic pain models can induce anxiety- and/or depression-like behaviors in a time dependent manner (Yalcin et al., 2011, 2014a).

Previous imaging studies frequently focused on the transition from an acute to chronic pain state and demonstrated that the nucleus accumbens (ACB), hippocampus (HIP), prefrontal cortex (PFC)(M. N. Baliki et al., 2014; Bilbao et al., 2018; Chang et al., 2014), somatosensory and insular cortices (Baliki et al., 2012; Hubbard et al., 2015) are involved in the pain chronicity. However, we still do not know how the brain reorganizes functional connectivity when chronic pain comorbid with anxiety and depressive-like behaviors, which may stem from the fact that experiments in humans are generally cross-sectional in nature. Longitudinal experimental designs are thus the unique tool to study how changes occur overtime.

Longitudinal neuroimaging studies in rodent neuropathic pain models (M. N. Baliki et al., 2014; Bilbao et al., 2018; Hubbard et al., 2015; Seminowicz et al., 2009) demonstrated time-dependent changes in brain morphology, metabolism and functional connectivity. For instance, volume abnormalities in medial PFC and limbic brain regions (Bilbao et al., 2018; Seminowicz et al., 2009), altered glutamatergic transmission in the anterior cingulate area (ACA) and HIP (Bilbao et al., 2018; Hubbard et al., 2015) and an overall reorganization of corticolimbic system functional connectivity highlighting ACB, PFC and hippocampus connectivity changes (M. N. Baliki et al., 2014; Bilbao et al., 2018; Chang et al., 2014) were reported at different time points. However, the main focus of these aforementioned studies once again was nociception-related behaviors and pain chronicity.

Affective consequences of pain can be attributed to plasticity changes caused by chronic pain conditions in brain regions processing both pain and emotional/motivational information (Shelton et al., 2012; Yalcin et al., 2014a). In this framework, mesocortico-limbic circuits, encompassing reward/aversion areas such as ACB and ventral tegmental area (VTA) (Borsook et al., 2016; Mitsi and Zachariou, 2016), mPFC, ACA (Barthas et al., 2015; Wang et al., 2015; Zhang et al., 2015; Zhuo, 2013) and limbic regions (e.g. amygdala, HIP) (Gonçalves et al., 2008; Mutso et al.,

2013) have been shown to play important roles in negative moods associated with pain conditions. Rodent brain imaging studies using stress-based animal models of depression also highlighted the role of mesocortico-limbic areas (Anacker et al., 2016; Clemm von Hohenberg et al., 2018; Gass et al., 2014) in particular, the major role of reward/aversion system comprising ACB, VTA, and lateral habenula (LHb). Moreover, hyperactivity of default mode network (DMN)- a large scale network of interacting brain regions that are activated during rest and deactivated during task performance- and its increased connectivity with subgenual cingulate characterizes major depressive disorder (MDD) in clinics. This hyper-connectivity is often interpreted as rumination, where depressed subjects persevere on negative, self-referential thoughts (Berman et al., 2011; Greicius et al., 2007). Similarly, these DMN alterations were also reported in rodent with stress-induced depression models (Grandjean et al., 2016; Henckens et al., 2015). Whether the brain network alterations in stress-induced and pain-induced depression overlap or diverge is an important research question that needs to be answered for a better understanding of pain-depression comorbidity.

In this study, we combined neuroimaging methods with behavioral measurements for a global characterization of structural and functional brain changes in the neuropathic pain and depression comorbidity. For this purpose, we used the cuff model of neuropathic pain in mice (Benbouzid et al., 2008; Yalcin et al., 2014b), inducing mechanical allodynia and anxio-depressive phenotype in a time-dependent manner. We evaluated mechanical allodynia weekly and tested depressive-like behaviors at 8 weeks after cuff surgery, timepoint that animals develop the phenotype (Sellmeijer et al., 2018; Yalcin et al., 2011). We longitudinally followed brain functional and structural connectivity changes along with morphology at different time points by using resting-state fMRI (rs-fMRI), high angular resolution diffusion MRI (HARDI) and fiber tractography and anatomical imaging. Our objective was to identify brain structural and functional network signatures of pain-induced depression and to define specific imaging-related biomarkers for this condition.

Our main results showed that the cingulate area displays significant structural alterations over time with diffusion MRI. Furthermore, resting-state fMRI revealed the reorganization of the functional connectivity of brain structures involved in reward, DMN and salience pathways in a time-dependent manner.

2. Material and Methods

Animals

14 adult male C57BL/6J mice (Charles River Laboratories, L'Arbresle, France) were used for the MRI experiments. Mice were housed under standard animal facility conditions (4-5 per cage, temperature 21°C, humidity 55-60%, food and water were given ad libitum, 12h/12h light-dark cycle). All experiments were conducted in accordance with the European Directive 2010/63/EU on the protection of animals used for scientific purposes and approved by the local ethical committee of the University of Strasbourg (CREMEAS, No: 2016072818151694).

Neuropathic pain model and relevant behavioral tests

We used the cuff model to induce neuropathic pain in mice (Barthas et al., 2017). Cuff surgery was performed as described in the previous literature (Yalcin et al., 2014b). Briefly, mice were anesthetized with ketamine/xylazine (80/10 mg/kg) and then a polyethylene cuff was placed around right main branch of the sciatic nerve (cuff group, n=7). The nerve was simply exposed for the controls (sham surgery group, n=7).

Since mechanical allodynia is one of the main symptoms of neuropathic pain, we used von Frey filaments (Bioseb, Vitrolles, France) to evaluate the mechanical hypersensitivity weekly. For this, mice were placed in Plexiglas® boxes (7 cm x 9 cm x 7 cm) on an elevated mesh screen. After a 15-minute habituation, animals were tested by applying a series of ascending forces (0.6 to 8 grams) on the plantar surface of each hind paw. Each filament was tested 5 times per paw, applied until it just bent (Barthas et al., 2017; Yalcin et al., 2014b). The threshold was defined as 3 or more withdrawals observed out of the 5 trials. In order to characterize changes in mechanical thresholds during an extended period, we tested animals before and at given time points after sciatic nerve surgery.

Depressive-like phenotype was assessed eight weeks after the surgery using splash test. This test was used to measure grooming behavior indirectly (Barthas et al., 2017; Yalcin et al., 2011), as decreased grooming can be related to the loss of interest in performing self-relevant tasks. This behavior was measured for 5 minutes after spraying a 10% sucrose solution on the coat of the animals.

Experimental design

After baseline MRI acquisition, we separated animals into two groups (i.e. Control and Cuff) on the basis of baseline mechanical hypersensitivity. Second MRI acquisition was performed 2 weeks after the peripheral nerve injury (timepoint 1-TP1). The development of depressive-like phenotype was confirmed using the splash test 7 weeks after the neuropathic pain induction. The last MRI acquisition was

conducted at 8-9 weeks post-surgery (timepoint 2- TP2). Mechanical threshold was checked once a week throughout the whole procedure (*see* Figure 2-1).

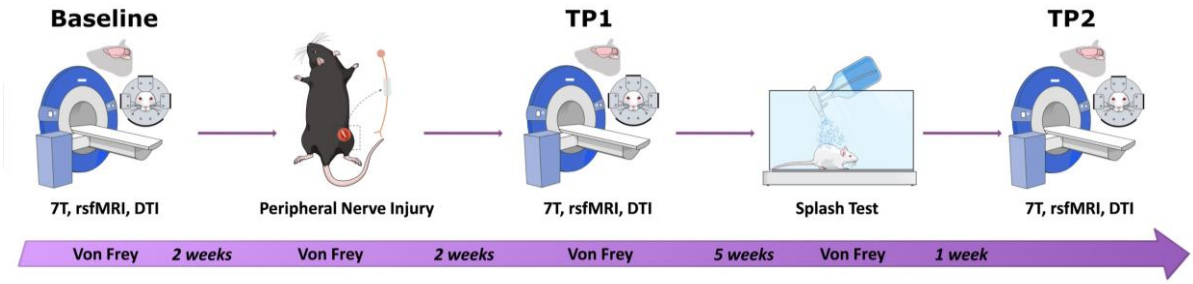

Figure 2-1 Experimental timeline.

After baseline resting state functional magnetic resonance imaging (rs-fMRI) and diffusion MRI acquisition, we separated animals into two groups, cuff and sham surgery groups (neuropathic pain and control mice, respectively) based on their mechanical hypersensitivity. Second MRI acquisition was performed 2 weeks after the peripheral nerve injury (TP1). The development of depressive-like phenotype was confirmed using the splash test 7 weeks after the neuropathic pain induction. Last MRI acquisition was conducted at 8-9 weeks post-surgery (TP2). Mechanical threshold was checked once a week throughout the entire procedure.

MRI data acquisition

All scans were performed with a 7T Bruker BioSpec 70/30 USR animal scanner, room temperature surface coil for the acquisition of the MRI signal and ParaVision software version 6.1 (Bruker, Ettlingen, Germany) at baseline and at 2 (TP1) and 8 weeks (TP2) after cuff surgery.

Animal preparation and placement were done under 2% isoflurane; a bolus of medetomidine (0.15 mg/kg body weight sc) was administered during preparation. 10 minutes after the bolus injection, isoflurane was discontinued, and animal bed was placed in the scanner. Medetomidine infusion was started (0.3 mg/kg bw /h sc) right before the rs-fMRI scans, within 35 minutes of bolus injection. Respiration and body temperature were monitored throughout the imaging session. Acquisition parameters for rs-fMRI were: single shot GE-EPI sequence, 31 axial slices of 0.5 mm thickness, FOV=2.12×1.8 cm, matrix=147× 59, TE/TR= 15 ms /2000 ms, 500 image volumes, 0.14× 0.23× 0.5 mm^3 resolution. Acquisition time was 16 minutes.

Morphological T2-weighted brain images (resolution of 0.08 × 0.08 × 0.4 mm^3) were acquired with a RARE sequence using the following parameters: TE/TR =40 ms/4591 ms; 48 slices, 0.4 mm slice thickness, interlaced sampling, RARE factor of 8, 4 averages; an acquisition matrix of 256 × 256 and FOV of 2.12×2 cm^2. For the diffusion MRI, medetomidine infusion was replaced with 1.5% isoflurane anesthesia. HARDI (High Angular Resolution Diffusion Imaging) acquisitions were carried out using a single shot DTI-EPI sequence, 27 axial slices, 0.1×0.1×0.5 mm^3 resolution, TE/TR= 28.9 ms/3000 ms, 4 averages, diffusion gradients applied along 30 non-collinear directions,

2 b-values (1000/2000 s/mm^2), gradient duration (δ)/separation(Δ)= 5 ms/10.6 ms for an acquisition time of 1 hour 13 minutes.

Statistical analysis of behavioral parameters

Data are presented as mean± SEM. For behavioral data, statistical analyses were performed with Statistica 7.1 software (StatSoft, Tulsa, OK) by using multifactor analysis of variance (ANOVA) with repeated measures and Duncan post hoc analyses for von Frey test and unpaired Student's t tests for splash test. Significance level was set to $p<0.05$.

MRI data processing

Resting-state fMRI data

Rs-fMRI images were spatially normalized into a template using Advanced Normalization Tools (ANTs) software (Avants et al., 2011) using SyN algorithm and smoothed (FWHM=0.28×0.46×1 mm^3) with SPM8.

Seed-based functional connectivity analysis was performed with a MATLAB tool developed in-house. Regions of interest (ROI) were extracted from Allen Mouse Brain Atlas (Lein et al., 2007) which were later normalized into the template space. Resting-state time series were de-trended, band-pass filtered (0.01-0.1 Hz) and regressed for cerebrospinal fluid signal from the ventricles. Principal component analysis (PCA) of the BOLD time courses across voxels within a given ROI was performed and first principal component accounting for the largest variability was selected as the representative time course for further analysis.

Partial correlation (PC) between the representative time courses of selected ROIs were computed to construct individual connectivity matrices for each mouse (76 pre-selected regions comprising limbic, cortical, reward, and nociceptive areas and covering the entire isocortex and major subcortical areas). Fisher's r-to-z transformation was applied to individual matrices and average PC matrices were computed by pooling the two groups at baseline, and for each group at TP1 and T2. Connections surviving $p<0.001$ (uncorrected) threshold for one sample t-test were selected for graph theoretical analysis using NetworkX software package for Python (https://networkx.github.io). A ranking of hub regions (nodes) are reported for each timepoint. For statistical comparison between the two groups, individual baseline matrices were subtracted from those belonging to TP1 and TP2, and two sample t-test was applied for subtraction matrices at each post-injury time point. Most changed connections (edges, expressed as degrees) and most changed nodes (expressed as Stouffer coefficients) were ranked among connections surviving $p<0.05$ (uncorrected) threshold. Briefly, Stouffer method uses a single p-value computed for each region based on the combination of the p-values derived from the statistical tests made on

the correlations with all other regions, highlighting the regions with major changes in the inter-group comparison (Stouffer et al., 1949).

Furthermore, Spearman correlations between the PCA time course of single ROIs and each voxel of the brain was computed at the group and individual levels and r values were converted to z using Fisher's r-to-z transformation. Individual connectivity maps for baseline rs-fMRI acquisitions were subtracted from TP1 and TP2 counterparts for each subject. Baseline subtracted TP1 and TP2 connectivity maps were subsequently used for two sample t-test with SPM8 to perform group comparison at two post-injury timepoints. Family-wise error rate (FWER) correction was applied at the cluster level ($p<0.05$) for each statistical image. Additionally, statistical analysis of baseline-subtracted connectivity maps was performed using SPM full factorial ANOVA of the two factors group and time point, associated with two levels respectively (Neuropathic and control for the group factor; TP1 and TP2 for the time point factor) to compare longitudinal evolution of functional modifications between groups. The group effect results on the evolution functional connectivity of several ROIs from TP1 to TP2 in mice were reported ($p<0.05$, FWER cluster corrected).

Diffusion MRI data

Post-processing of the diffusion data was performed using an in-house developed DTI and FiberTool software package (*see* www.uniklinik-freiburg.de/mr-en/research-groups/diffperf/fibertools.html) for SPM on MATLAB. Diffusion-based parameter maps were generated, including fractional anisotropy (FA), mean diffusivity (MD), radial (RD) and axial diffusivities (AD). Mouse brain diffusion tractograpy using a global fiber tracking algorithm (Harsan et al., 2013) was also performed and fiber density (FD) maps were generated (Reisert et al., 2011). Diffusion MRI parametric maps were also compared across groups using a voxel-based analysis. The FA and FD maps were jointly registered using the multimodal group-wise registration procedure implemented in the ANTs; the analysis was then conducted using the voxel-based quantification (VBQ) method (Draganski et al., 2011). This method implements a combined weighting/smoothing procedure, which avoids parameter value changes by Gaussian smoothing applied in standardized space. Furthermore, we conducted voxel-wise analysis on FD maps modulated by jacobian values in order to quantify the amount of fibers in the standardized space which accurately reflects that of the native space. A Gaussian kernel with a FWHM of 0.5 mm was applied here. Baseline VBQ images were subtracted from images for later time points. Intergroup comparisons were conducted at the voxel level using the general linear model in SPM8. Statistical maps were corrected with family-wise error rate (FWER) applied at the cluster level for $p<0.05$.

3. Results

Behavioral results

von Frey and splash tests were carried-out as shown in Figure 2-1 at timepoints selected in correlation with MRI experiments to assess mechanical allodynia and emergence of depressive phenotype, respectively. The mechanical allodynia was evaluated at baseline (before surgery) and overtime (after cuff or sham surgeries). Mice were then scanned at 2 weeks, the time point corresponding to animals displaying only mechanical hypersensitivity (TP1) (Figure 3-1-A, $F_{(6,72)}=6.26$ $p=0.000025$; post-hoc: Neuropathic vs. Control from 1 to 7 weeks, $p<0.00001$) but not depressive-like behaviors, and at 8 weeks, the time point corresponding to cuff animals displaying both mechanical hypersensitivity and depressive-like behaviors as demonstrated by decreased grooming behavior in the splash test (TP2) (Figure 3-1-B, $p<0.00001$).

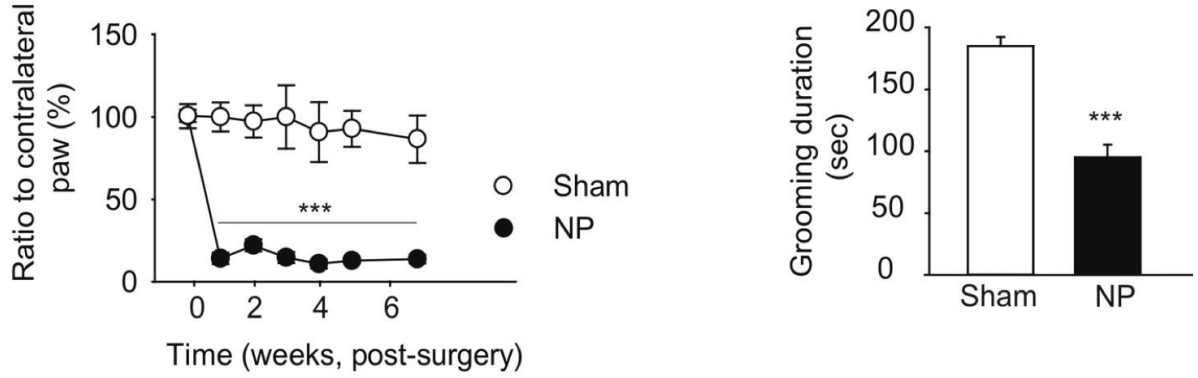

Figure 3-1 Nerve injury induces mechanical hypersensitivity and depressive-like behavior.

(A) *In C57BL/6J mice, unilateral sciatic nerve compression induces an ipsilateral long-lasting mechanical hypersensitivity. Results are presented as a ratio to contralateral paw (%).* ***(B)*** *Splash test at 7 weeks after the peripheral nerve injury illustrating decreased grooming behavior in neuropathic (NP) animals compared to sham-operated littermates. ***p<0.0001.*

HARDI measures of structural connectivity

Fractional anisotropy (FA) is a measure of water diffusion directedness within the tissue where values approach 0 for free unrestricted diffusion (i.e. isotropic) and 1 for oriented diffusion direction (i.e. anisotropy, such as seen in muscle and axonal fibers). FA could be an indicator of brain microstructural integrity, fiber organization and density, myelination, and axon diameters as well as other tissue characteristics unrelated to white matter (e.g. glial processes) (Scholz et al., 2009)We used voxel-based quantification (VBQ, *see* Material and Methods section) method for the inter-group analysis (TP1/TP2 neuropathic group vs. control group) of FA parametric

maps. VBQ comparisons were performed after the subtraction of the baseline VBQ images from TP1 and TP2 counterparts.

Our results showed lower FA values in the neuropathic group in several areas involved in pain processing, including ACA, thalamus (TH), hypothalamus (HY), HIP and retrosplenial area (RSP) at TP1 (Figure 3-2-A). However, at TP2 these differences persist only for ACA and RSP (Figure 3-2-B) - core areas of rodent default mode network (DMN).

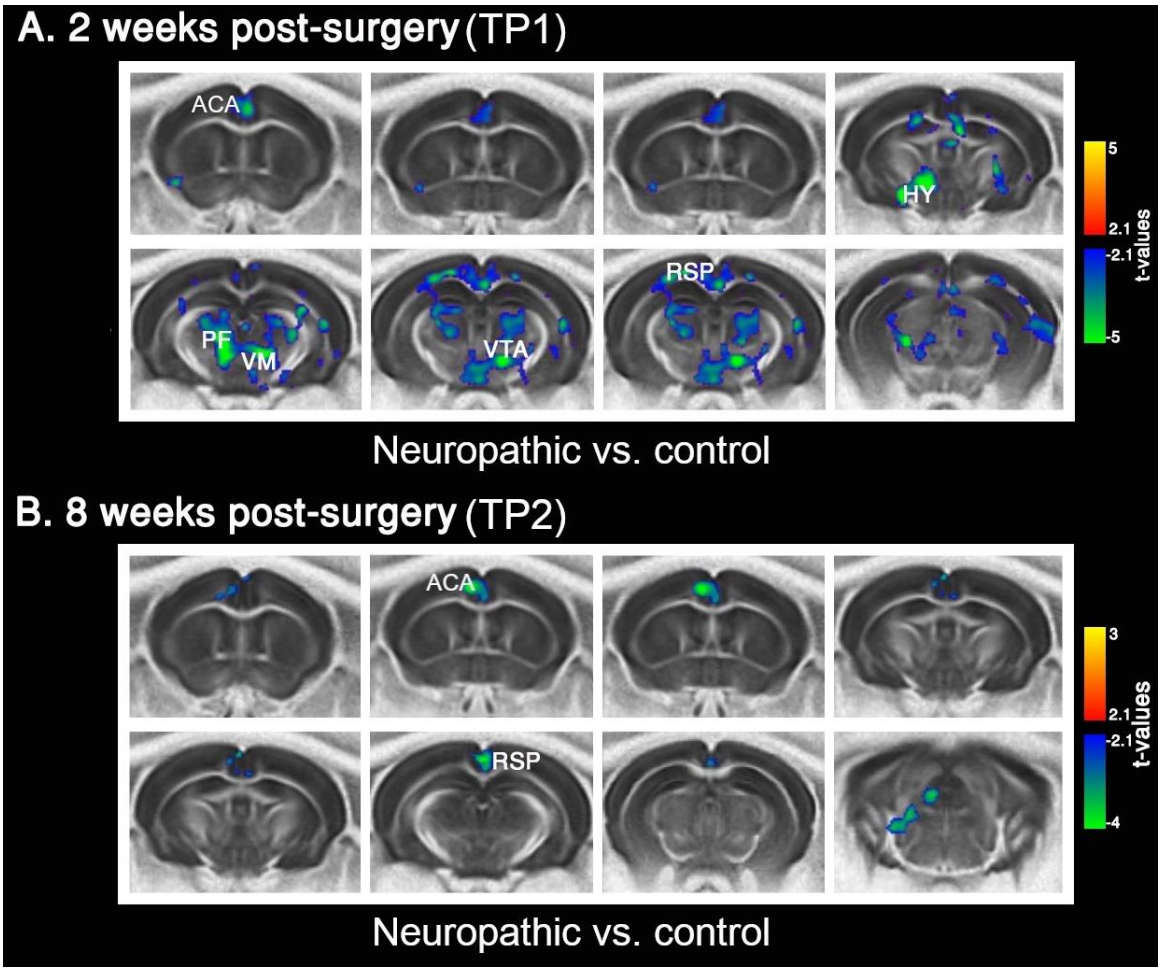

Figure 3-2 Fractional anisotropy (FA) differences between groups at 2 weeks (TP1) and 8 weeks (TP2) after peripheral nerve injury. ***(A)*** *At TP1, neuropathic group displayed lower FA values than controls in the anterior cingulate (ACA) and hypothalamus, ventral tegmental area (VTA), parafascicular (PF) and ventromedial (VM) nuclei of thalamus (TH), and retrosplenial area (RSP).* ***(B)*** *At TP2, neuropathic mice showed lower FA than controls only in ACA and RSP. FWER correction used at cluster level for $p<0.05$ for statistical images.*

Functional connectivity (FC) via resting-state fMRI

Next, we created functional connectivity matrices for each timepoint to obtain a global view of the potential functional changes associated with neuropathic pain and subsequent depressive behaviors. We selected 76 unilateral ROIs which cover the entire isocortex and major subcortical areas including limbic, cortical, reward, and nociceptive areas. Figure 3-3 demonstrates the significant connectivity changes between neuropathic and control group matrices (Figure 3-3-AA and D, $p<0.05$, uncorrected) overlaid on the mouse brain. We then calculated the connections (edges) and regions (nodes) showing most changes between the two groups at TP1 (Figure 3-3-A shows edge strength changes as correlation coefficients and node degree changes as Stouffer coefficients, node sizes correspond to ranking of most changed nodes; Figure 3-3-B, C list the most changed edges and nodes, respectively) and TP2 (3.3-D, E, F). At TP1, most changed nodes consisted of areas related to pain processing (e.g. TH and agranular insula-AI), and areas associated with aversion (e.g. amygdala, septum, ACB, hypothalamus, hippocampal formation and thalamus), highlighting pain-related functional alterations in the mouse brain (Figure 3-3-C). At TP2, however, the emergence of depressive phenotype coincided with functional changes mainly in reward/aversion areas (e.g. ACB, pallidum (PAL), ventral tegmental area (VTA), hippocampal formation, bed nucleus of stria terminalis (BST), and septum) and areas of rodent DMN (e.g. RSP, hippocampus, midbrain) which are known to be involved in major depression (Figure 3-3-F).

In light of the Stouffer analysis results determining the nodes with the most significant FC changes (Figure 3-3-C, F) and the structural connectivity results previously presented (Figure 3-2), we chose ACA, VTA, habenula (Hb), HIP, ACB, insula and periaqueductal gray (PAG) as regions of interest for inter-group analysis.

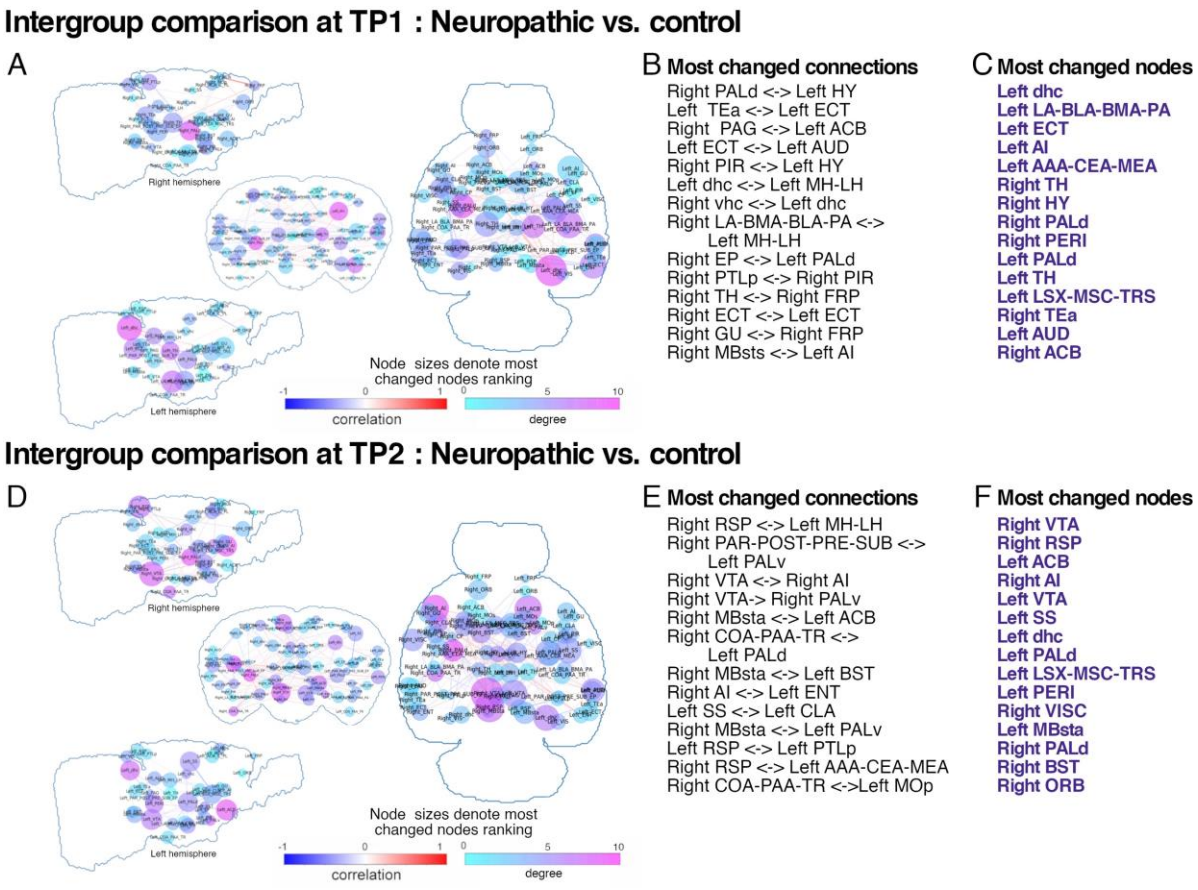

Figure 3-3 Graph theoretical analysis for functional connectivity matrices. (A and D) *Significant changes between neuropathic and control groups for connection (edge) strengths and nodes are shown as mouse brain overlays at TP1* ***(A)*** *and TP2* ***(D).*** *Edge strength changes are displayed on a scale of correlation coefficients. The relevance of FC chances for each node was assessed using two measures: the degree (color coded) denoting the number of significantly changed connections / node; and the Stouffer coefficient (node size) that is also introducing the weight of the changes for each connection. Stouffer coefficients and therefore the node sizes correspond to ranking of most changed nodes.* ***(B and E)*** *List of most changed edges (according to the p value) are ranked for TP1* ***(B)*** *and TP2* ***(E)****.* ***(C and F)*** *List of most changed nodes from Stouffer analysis are ranked for the two post-injury timepoints.* ***(C)*** *At TP1, most changed nodes are areas related to pain processing (e.g. thalamus [TH] and agranular insula [AI]) and aversion (e.g. amygdala, septum, nucleus accumbens [ACB], hypothalamus [HY], hippocampal formation and thalamus [TH]).* ***(F)*** *At TP2, mainly reward/aversion areas (e.g. ACB, pallidum (PAL), ventral tegmental area (VTA), hippocampal formation, bed nucleus of stria terminalis (BST), and septum) and areas of rodent default-mode network (DMN) (e.g. RSP, hippocampus, midbrain) are listed as the nodes with most changes. All results are p<0.05, uncorrected.*

(***Abbreviations:*** *AAA-CEA-MEA: Anterior-central-medial amygdala; ACB: Nucleus accumbens; AI: Agranular insula; AUD: Auditory areas; BST: Bed nucleus of stria terminalis; CLA: Claustrum; COA-PAA-TR: Cortical-piriform amygdalar areas, post-piriform transition area; dhc: Dorsal hippocampus; ECT: Ectorhinal area; ENT: Entorhinal area; EP: Endopiriform nucleus; FRP: Frontal pole; GU: Gustatory area; HY: Hypothalamus; LA-BMA-BLA-PA: Lateral-basomedial-basolateral-posterior amygdala; LSX-MSC-TRS: Lateral-medial septum, triangular nucleus; MBsta: Behavioral state-related midbrain; MH-LH: Medial-lateral habenula; MOp: Primary motor area; ORB: Orbital*

area; PAG: Periaqueductal gray; PALd: Dorsal pallidum; PALv: Ventral pallidum; PAR-POST-PRE-SUB: Para-/post-/pre-/subiculum; PERI: Perirhinal area; PIR: Piriform area; PTLp: Posterior parietal association area; RSP: Retrosplenial area; SS: Somatosensory area; TEa: Temporal association area ; TH: Thalamus; vhc: Ventral hippocampus; VISC: Visceral area; VTA: Ventral tegmental area.)

Functional connectivity of cingulate area, a region showing structural alterations in the neuropathic group, was assessed at both TP1 and TP2 Figure 3-4, FWER corrected at cluster level for $p<0.05$). At TP1, ACA connectivity towards AI, caudate-putamen (CP), dorsal hippocampus (dHIP), Hb, and PAG was decreased in the neuropathic mice; whereas a stronger ACA-hypothalamus connectivity was observed in this group compared with control (Figure 3-4-A). At TP2, when neuropathic mice display depressive-like behaviors, ACA was found more connected to RSP, amygdala (AMY), and temporal association areas (TeA) in neuropathic mice, while the ACA connectivity with CP, dHIP, Hb, and PAG was lower in neuropathic animals than controls at this time, similar to TP1 results in this seed (Figure 3-4-B).

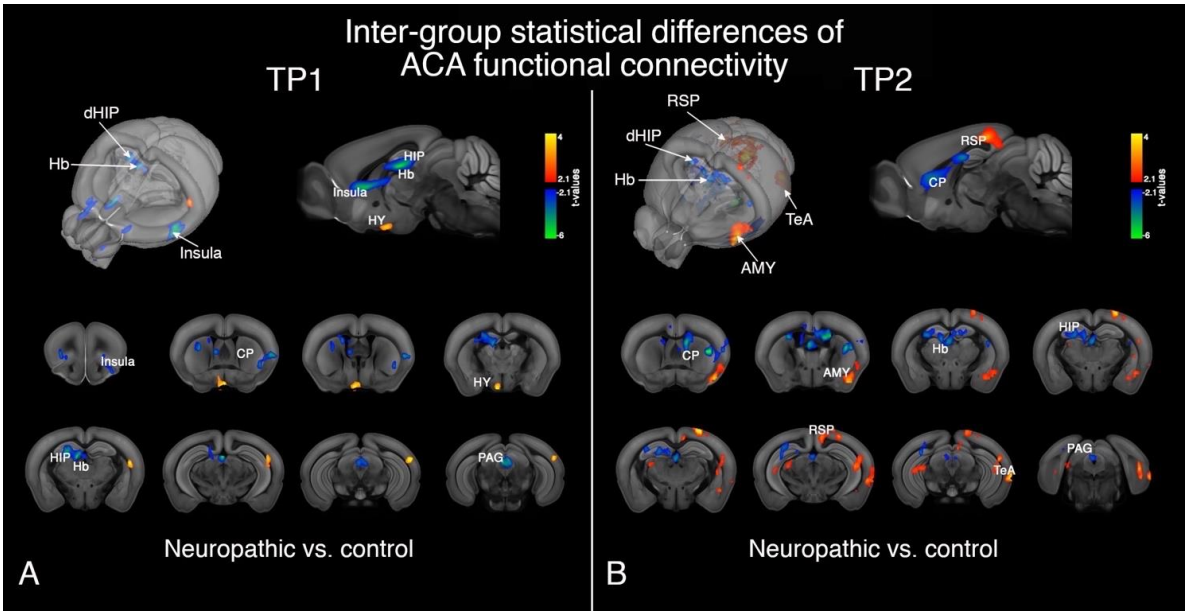

Figure 3-4 Inter-group differences in anterior cingulate area (ACA) functional connectivity at TP1 and TP2. ***(A)*** *At TP1, ACA connectivity towards agranular insula (AI), caudate-putamen (CP), dorsal hippocampus (dHIP), habenula (Hb), periaqueductal gray (PAG) was lower and ACA-hypothalamus connectivity was higher in the neuropathic group.* ***(B)*** *At TP2 weeks, ACA was more connected to retrosplenial area (RSP), amygdala (AMY), and temporal association areas (TeA) for neuropathic mice whereas ACA connectivity with CP, dHIP, Hb, and PAG was reduced. FWER corrected at cluster level for $p<0.05$.*

Inter-group statistical comparisons suggest strong remodeling of the VTA functional connectivity in the neuropathic animals. Indeed, at TP1, neuropathic animals showed higher synchrony of the BOLD rs-fMRI signal towards somatosensory cortex (SS), CP, and RSP areas (Figure 3-5,, FWER corrected at cluster level for $p<0.05$; Figure 3-5-A) while at TP2, the VTA FC changes detected towards ACA, ACB, CP, BST, Hb, PF and medial dorsal (MD) nuclei of thalamus, as well as higher intra-region connectivity within VTA (Figure 3-5-B). Many of these areas belong to the reward circuitry, a system concerned with incentive salience, motivated behaviors, and reward learning (Borsook et al., 2016; Hu, 2016; Russo and Nestler, 2013). Figure 3-6 shows 3D reconstruction of inter-group statistical differences in longitudinal evolution of VTA FC from T1 to T2 (Figure 3-6, FWER correction applied at cluster level for $p<0.05$).

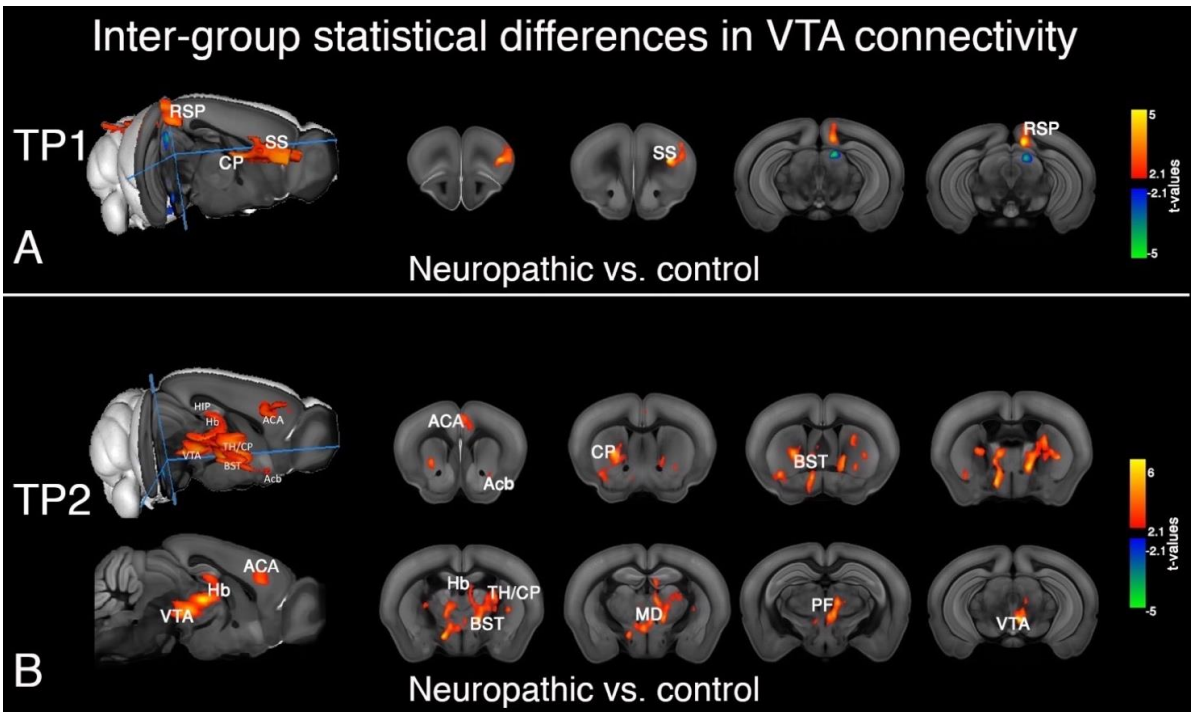

Figure 3-5 Inter-group differences in ventral tegmental area (VTA) functional connectivity at TP1 and TP2. (A) *At TP1, somatosensory (SS), caudate-putamen (CP) and retrosplenial area (RSP) connectivity towards VTA was higher in neuropathic mice than in controls.* ***(B)*** *At TP2, neuropathic group showed greater VTA synchrony towards anterior cingulate (ACA), nucleus accumbens (ACB), CP, bed nucleus of stria terminalis (BST), habenula (Hb), parafascicular (PF) and medial dorsal (MD) nuclei of thalamus and higher intra-region connectivity at VTA. FWER corrected at cluster level for $p<0.05$.*

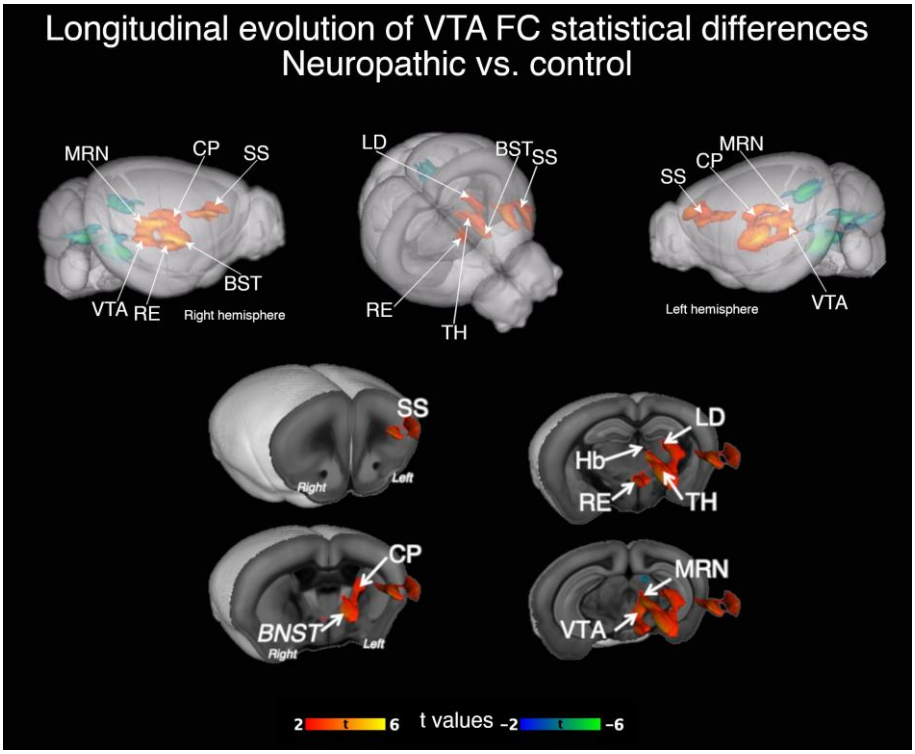

Figure 3-6 3D reconstruction of inter-group statistical differences in longitudinal evolution of VTA functional connectivity from T1 to T2. *Full factorial ANOVA results, FWER correction applied at cluster level for p<0.05.*

Lateral habenula (LHb) is an important brain region encoding negative value/ aversion and inhibition of reward signals via its extensive connections to limbic forebrain and aminergic brainstem centers. At TP1, LHb connectivity towards amygdala, TeA, midbrain reticular nucleus (MRN) and ventral hippocampus (vHIP) were increased in neuropathic animals compared to controls (Figure 3-7-A, FWER cluster correction at p<0.05). At TP2, higher connectivity of LHb with thalamus, HY, VTA, and MRN and lower connectivity with AI and secondary motor area (MOs) were observed for neuropathic group (Figure 3-7-B, FWER correction at cluster level at p<0.05).

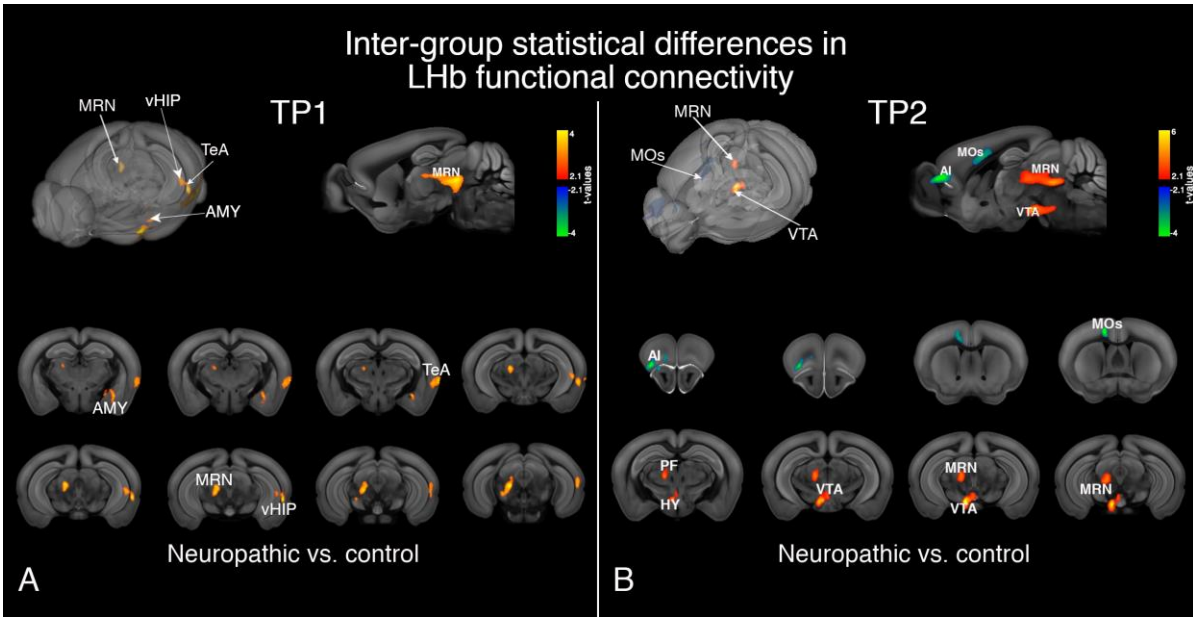

Figure 3-7 Inter-group differences in lateral habenula (LHb) functional connectivity at TP1 and TP2. (A) *At TP1, LHb connectivity towards amygdala (AMY), temporal association area (TeA), ventral hippocampus (vHIP) and midbrain reticular nucleus (MRN) were increased in neuropathic mice.* ***(B)*** *At TP2, neuropathic animals displayed higher connectivity of LHb with parafascicular (PF) nucleus of thalamus, hypothalamus (HY), ventral tegmental area (VTA), and MRN; lower connectivity with agranular insula (AI) and secondary motor area (MOs). FWER correction at cluster level was applied for p<0.05.*

Based on the graph analysis results that highlighted important inter-group differences of FC involving pain and reward/aversion areas, we further performed fine-grained mapping of FC using ACB, dorsal HIP (dHIP), insula (AI), and PAG as seeds. Figure 3-8 presents the functional connectivity alterations of these ROIs in the neuropathic pain group compared with controls at TP1 and TP2 (All statistical results are FWER corrected at cluster level for $p<0.05$). At TP1, ACB displays reduced connectivity towards CP, SS, lateral geniculate nucleus (LGN) of thalamus and vHIP in neuropathic mice (Figure 3-8-A). At TP2, reduced ACB connectivity to CP, SS, and primary MO (MOp) areas were accompanied with greater connectivity towards zona incerta (ZI), TeA, vHIP, and substantia nigra (SN) for neuropathic animals (Figure 3-8-B).

dHIP connectivity at TP1 was higher towards AMY, RSP, superior colliculus (SC), and LGN and lower towards CP in neuropathic pain group (Figure 3-8-C). dHIP demonstrated increased connectivity with AMY and posterior parietal association areas (PTLp) and decreased connectivity with ACA and septum in neuropathic animals with depressive phenotype at TP2 (Figure 3-8-D).

Insula and PAG, areas known to be involved in pain processing, also showed connectivity alterations in the neuropathic pain group. Insular connectivity towards

RSP and PAG was greater and its connectivity towards MOs, TH and vHIP was lower in neuropathic mice at TP1 (Figure 3-8-E). At TP2, neuropathic pain group presenting depressive behaviors showed insular connectivity patterns increased towards HY, LGN, and entorhinal areas (ENT) and decreased towards CP, PF nucleus, TeA, and MRN (Figure 3-8-F). PAG connectivity at TP1 (Figure 3-8-G) was higher towards ACB, CP and HY and lower towards Hb, PTLp and SS areas in neuropathic mice compared to controls. At TP2, connectivity of PAG with ACB, piriform area (PIR), olfactory tubercle (OT), and LGN was stronger and PAG-SS connections were weaker for neuropathic pain-induced depression group (Figure 3-8-H).

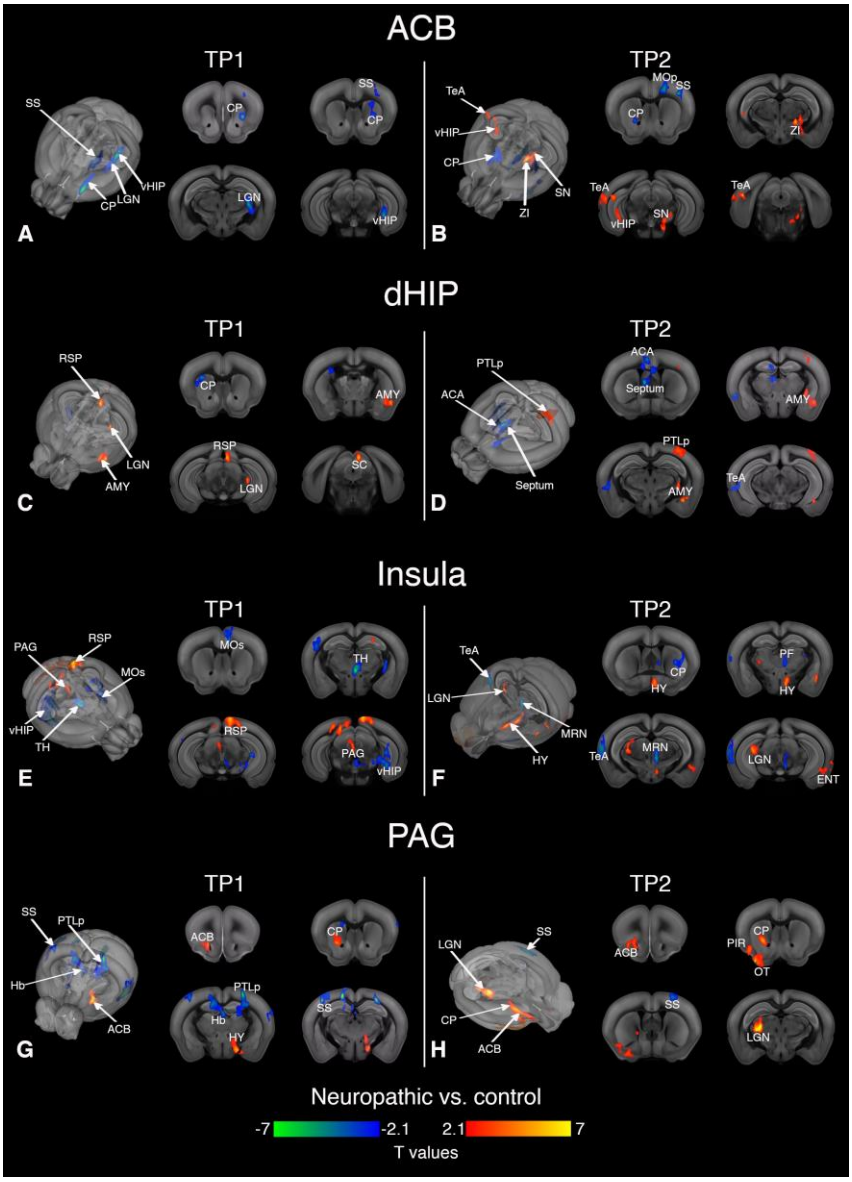

Figure 3-8 Inter-group differences in the nucleus accumbens (ACB), dorsal hippocampus (dHIP), agranular insula (AI), and periaqueductal gray (PAG) functional connectivity at TP1 and TP2. ***(A)*** *ACB displays reduced connectivity towards caudate-putamen (CP), somatosensory areas (SS), lateral geniculate nucleus (LGN) of the thalamus and ventral HIP (vHIP) in neuropathic mice at TP1.* ***(B)*** *At TP2, reduced ACB connectivity to CP, SS, and primary MO (MOp) areas and greater connectivity towards zona incerta (ZI), temporal association area (TeA), vHIP, and substantia nigra (SN) were shown for neuropathic animals.* ***(C)*** *dHIP connectivity at TP1 was higher towards amygdala (AMY), retrosplenial area (RSP), superior colliculus (SC), and LGN and lower towards CP in neuropathic pain group.* ***(D)*** *dHIP demonstrated increased connectivity with AMY and posterior parietal association areas (PTLp) and decreased connectivity with anterior cingulate (ACA) and septum in neuropathic animals with depressive phenotype at TP2.* ***(E)*** *Insular connectivity towards RSP and periaqueductal gray (PAG) was greater and its connectivity towards secondary motor (MOs), thalamus (TH) and ventral hippocampus (vHIP) was lower in neuropathic mice at TP1.* ***(F)*** *At TP2, neuropathic pain group showed increased insular connectivity patterns towards hypothalamus (HY), LGN, and entorhinal areas (ENT) and*

decreased towards CP, parafascicular (PF) nucleus, TeA, and MRN. ***(G)*** *PAG connectivity at TP1 was higher towards ACB, CP and HY and lower towards Hb, PTLp and SS areas in neuropathic mice compared to controls.* ***(H)*** *At TP2, connectivity of PAG with ACB, piriform area (PIR), olfactory tubercle (OT), and LGN was stronger and PAG-SS connections were weaker for neuropathic pain-induced depression group. All statistical results were FWER corrected at cluster level for p<0.05.*

Longitudinal evolution

Additionally, we performed full factorial ANOVA to highlight group-differences in the evolution of the FC patterns from TP1 to TP2 (Figure 3-9, FWER corrected at cluster level for $p<0.05$). Overall, neuropathic mice showed stronger connectivity modifications of the ACA FC with basolateral amygdala (BLA), RSP, and VTA and reduced variations towards claustrum (CLA), insula, Hb, and dHIP when compared to the control animals (Figure 3-9-A). Overtime, RSP functional connectivity was reduced towards thalamus and dHIP in neuropathic group in comparison to controls (Figure 3-9-B). In neuropathic mice, insular cortex displayed greater FC modifications towards RSP and PAG areas and lower variations towards SS and thalamus compared to controls overtime (Figure 3-9-C). These time-dependent changes were also observed for PAG which exhibited stronger FC modifications towards ACB, CP, thalamus and dHIP in the neuropathic group while modifications towards SS were reduced compared to controls (Figure 3-9-D).

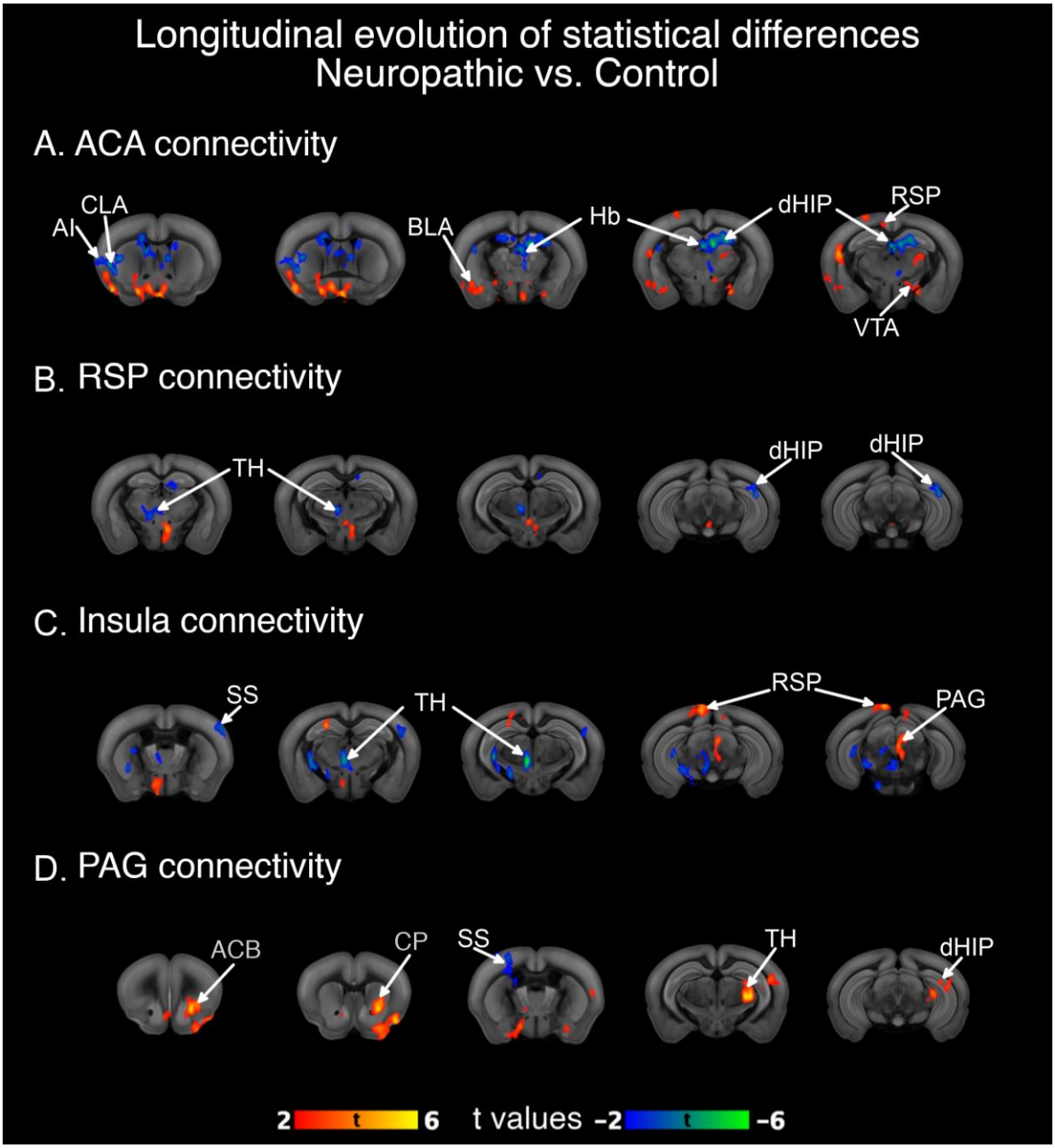

Figure 3-9 Group-differences in the evolution of the FC patterns from TP1 to TP2 for anterior cingulate (ACA), retrosplenial area (RSP), agranular insula (AI) and periaqueductal gray (PAG). ***(A)*** *Stronger modifications of the ACA connectivity towards basolateral amygdala (BLA), RSP, and ventral tegmental area (VTA) were found neuropathic animals (red). ACA had reduced connectivity modifications towards claustrum (CLA), insula, habenula (Hb), and dorsal hippocampus (dHIP) in neuropathic mice as compared to control group (blue).* ***(B)*** *RSP connectivity showed stronger modifications towards thalamus and dHIP in neuropathic group than in controls.* ***(C)*** *Neuropathic mice showed greater insula-RSP and insula-PAG connectivity alterations ovetime when compared to the sham group, while insula-SS and insula - thalamus connectivity showed lower variations from TP1 to TP2****(D)*** *Connectivity modifications between PAG and ACB, CP, thalamus, and dHIP were higher in neuropathic mice as compared to*

sham; SS connectivity showed less changes to PAG in this group. FWER corrected at cluster level for $p<0.05$.

Aside from structures implicated in pain processing, structures involved in reward-aversion processes showed a distinct evolution profile of FC in neuropathic animals with depressive-like behaviors in comparison with controls. For instance, ACB connectivity changes became dominant towards vHIP and VTA in neuropathic animals (Figure 3-10-A). In regard to LHb, we observed stronger FC changes with amygdala, VTA, and midbrain reticular nuclei (MRN) and weaker FC alterations with dHIP (Figure 3-10-B). The main changes of the VTA FC were observed with SS, CP, BST, and thalamus in neuropathic animals (Figure 3-10-C).

Hippocampus, a structure implicated in both pain and depression also showed time-dependent changes in neuropathic animals compared to controls. The vHIP (Figure 3-10-D) displayed stronger FC alterations with infralimbic (IL), prelimbic (PL), SS, insula and dHIP in animals displaying depressive-like behaviors while dHIP (Figure 3-10-E) revealed stronger changes towards insula and amygdala and reduced connectivity alterations towards ACA, Hb and within dHIP in neuropathic mice with depressive phenotype compared to controls.

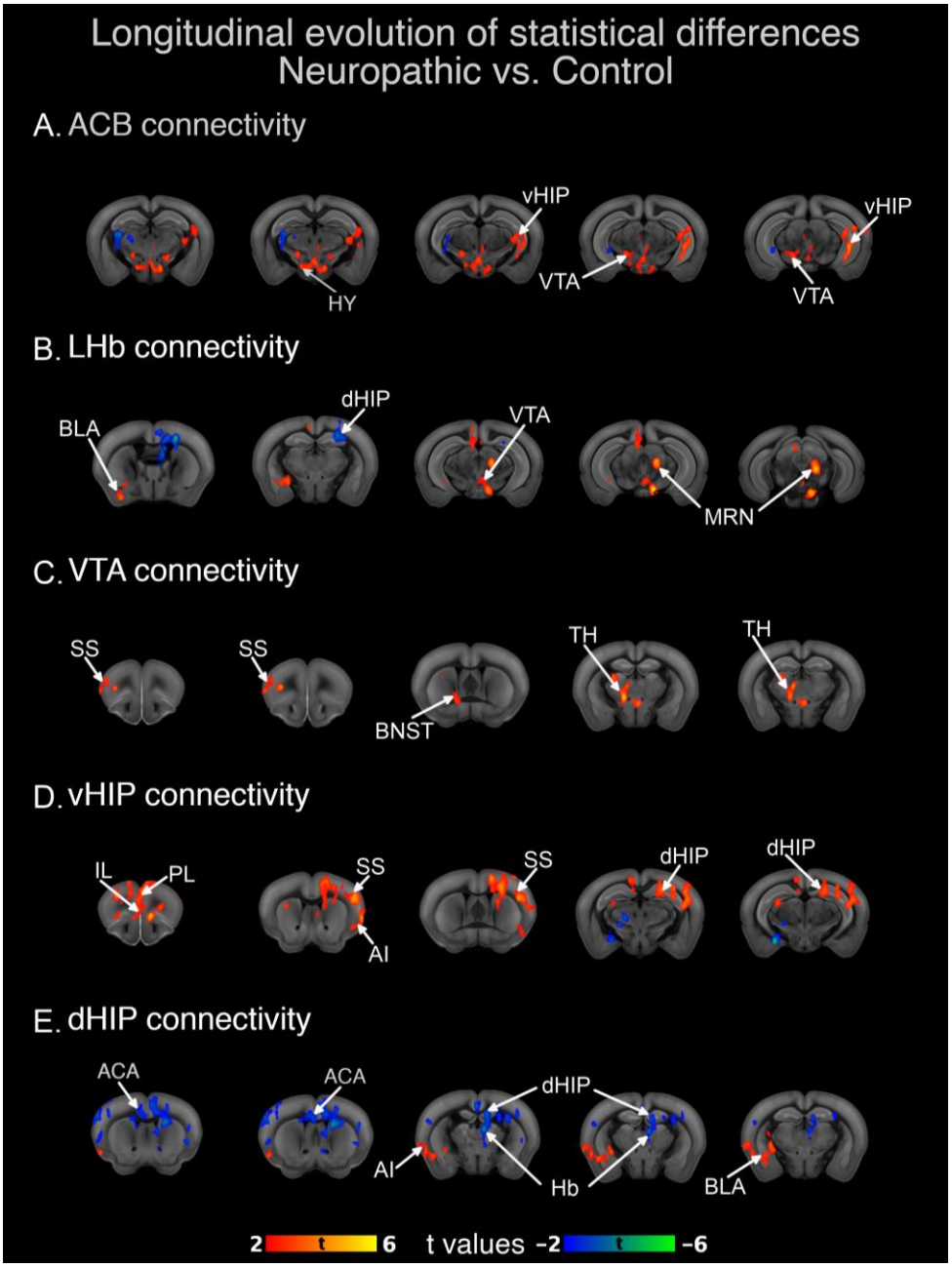

Figure 3-2 Group-differences in the evolution of the FC patterns for nucleus accumbens (ACB), ventral tegmental area (VTA), lateral habenula (LHb) and two main hippocampal divisions (dorsal and ventral hippocampus (dHIP and vHIP, respectively) from TP1 to TP2. ***(A)*** *ACB connectivity with vHIP and VTA showed stronger overtime modifications for neuropathic animals in comparison with controls.* ***(B)*** *LHb area displayed greater connectivity changes towards BLA, VTA, and midbrain reticular nuclei (MRN) in neuropathic pain group; they also had lower connectivity changes between LHb-dHIP.* ***(C)*** *VTA revealed stronger than control modifications in neuropathic mice towards somatosensory area (SS), bed nucleus of stria terminalis (BST), and thalamus.* ***(D)*** *Ventral part of the hippocampus (vHIP) displayed in neuropathic animals greater connectivity changes towards infralimbic (IL), prelimbic (PL), and SS areas, insula, dHIP than in controls.* ***(E)*** *Dorsal part of hippocampal area (dHIP) exhibited in neuropathic animals greater than control connectivity variations from TP1 to TP2*

towards insula and BLA and reduced connectivity changes with ACA, Hb, and within dHIP when compared to the sham group. FWER corrected at cluster level for p<0.05.

4. Discussion

In this study, we aimed to uncover the evolution of the brain structural and functional connectivity associated with the establishment of chronic pain and later, the emergence of depressive behaviors in a mouse model of neuropathic pain. For this purpose, we used diffusion MRI and resting state fMRI in parallel with behavioral measures in a longitudinal design. We were able to show structural differences at two post-injury timepoints for neuropathic mice. ACA and RSP displayed lower FA values at both 2 weeks and 8 weeks following cuff surgery while TH, HY, and hippocampus had reduced FA values only at 2 weeks post-surgery.

Brain functional connectivity networks had also undergone a substantial remodeling throughout the period of neuropathic pain. As expected, following cuff surgery, mice developed long lasting mechanical allodynia (Yalcin et al., 2011). Thus at 2 weeks, corresponding to the early stages of the neuropathy, we observed regions involved in pain processing and aversion taking predominant roles in neuropathic mouse brain networks determined from graph theoretical analysis. At 8 weeks when animals display not only mechanical allodynia but also depressive-like behavior, we demonstrated alterations in the reward circuitry and default mode network (DMN).

Further, we investigated functional connectivity profiles of brain areas showing structural changes or changes in graph measures between groups in more detail. Several regions exhibited connectivity changes for neuropathic pain group at 2-week (TP1) and 8-week (TP2) time points. Most notable results were obtained in ACA, VTA, and LHb nodes along with other reward areas and DMN components.

Neuropathic pain leads to brain structural modifications

Our results revealed that FA values are reduced at the early stages of neuropathy (2 weeks) in ACA and RSP, core regions of mouse DMN, along with TH, HY and hippocampus in neuropathic mice. Moreover, ACA and RSP changes persisted at TP2, where a depressive phenotype manifests in behavioral tests.

Preclinical and clinical studies focusing on pain research showed several structural alterations which support the results of our present study. Indeed, reduced volumes of prefrontal cortex (PFC) and RSP were reported in a rat spared nerve injury (SNI) model, coinciding with anxious behavior (Seminowicz et al., 2009). Prefrontal volume reduction was also described in the SNI model using mice (Bilbao et al., 2018). In addition, patients with neuropathic pain following spinal cord injury (Yoon et al., 2013) displayed gray matter decrease in subgenual ACC while decreased FA in thalamic areas was reported for patients with migraine (DaSilva et al., 2007),

fibromyalgia (Lutz et al., 2008) and temporomandibular disorder (Moayedi et al., 2012). In addition, gray matter atrophy in ventromedial prefrontal cortex (vmPFC) along with lower FA in cingulum and decreased vmPFC-basal ganglia connectivity were found in complex regional pain syndrome (CRPS) (Geha et al., 2008)

Furthermore, studies in major depressive disorder (MDD) showed reduced volume of anterior cingulate, related to both glial and neuronal losses (Drevets et al., 1997; Mayberg, 2009; Rajkowska, 2000; Russo and Nestler, 2013; Uranova et al., 2004). Structural changes found in the same brain region for chronic pain and MDD suggest a contribution of anterior cingulate in their comorbidity. Indeed, ACA is thought to play an important role in pain-induced depression. Previous research from our group showed that the hyperactivity of this region is associated with anxio-depressive consequences of the cuff model (Sellmeijer et al., 2018) and the optogenetic inhibition of this area abolishes aversion to pain without affecting mechanical hypersensitivity.

Longitudinal nature of our experimental design enabled us to assess time-dependent evolution of brain connectivity, which is difficult to capture with cross-sectional designs often used in clinical settings. We thus could detect the disappearance of FA alterations in TH, HY, and hippocampal areas at TP2, which points to an early but short-lasting reaction to cuff surgery. TH, HY, and hippocampus were identified as parts of aversion circuitry (Hayes and Northoff, 2011) and thalamus is well-known to be involved in pain processing (Garcia-Larrea and Peyron, 2013) thus, transient structural changes in these areas might correspond to initiation of chronic pain and related aversive behaviors. Concerning the long-lasting changes that we observed in ACA and RSP might be associated with steady neuroplastic changes resulting from activity-dependent or inflammatory and glial processes, leading to depressive behavior. In line with this, ACA shows long term potentiation (LTP) of glutamatergic synapses following nerve injury in mice (Xu et al., 2008). Astrocytic processes in ACA were also shown to be involved in the establishment of LTP and pain hypersensitivity (Ikeda et al., 2013) in an inflammatory injury model. Chemotherapy-induced neuropathic pain resulted in a significant increase in ACA astrocytes in rats (Mannelli et al., 2013) and Narita Minoru et al. (2006) reported role of the cortical δ-opioid receptor dysfunction in ACA astrogliosis, potentially leading to anxiety state. Putative role of glial processes in depression were also investigated. Postmortem brains of depressed patients showed increased microglial quinolinic acid, an NMDA agonist which is considered to modulate the link between immune and neurotransmitter staple changes, in subgenual ACC and mid-cingulate areas (Steiner et al., 2011). Impairment of gap junction-mediated communication between astrocytes and oligodendrocytes in ACA was discovered in postmortem brain tissues from depressed suicides (Tanti et al., 2019), emphasizing the importance of glia in normal brain function.

RSP is a principal area of rodent DMN (Stafford et al., 2014; Upadhyay et al., 2011) together with ACA. Default mode network (DMN) is a set of regions that show synchronous activity at rest and deactivate during task performance (Greicius et al., 2003; Raichle et al., 2001). DMN alterations are found across several neurologic and psychiatric disorders (Baliki et al., 2014; Berman et al., 2011; Broyd et al., 2009; Buckner et al., 2008). Deactivation of DMN was reduced while switching from rest to attentional task in patients suffering from chronic back pain (Baliki et al., 2008). In a diabetic neuropathy cohort, DMN connectivity was increased towards dorsal ACA and MO/SS cortices and decreased towards dlPFC, insula and TH (Cauda et al., 2010), whereas in fibromyalgia, DMN-insula connectivity and coherence within DMN were increased (Napadow et al., 2011). In three distinct pain conditions, mPFC connectivity with posterior part of DMN was found to be decreased and mPFC-insula FC was increased (Baliki et al., 2014). In short, while the DMN connectivity changes are not consistent across conditions, DMN dysfunction seems to be important maladaptation in chronic pain.

DMN modifications in major depression are also well-documented(Wang et al., 2012; Zhu et al., 2012). For instance, Greicius et al. (2007) has shown greater subgenual ACC connectivity towards DMN regions which is correlated with the length of current depressive episode in MDD. On the preclinical side, DMN connectivity was enhanced with chronic stress (Henckens et al., 2015) in a model of depression in mice (Grandjean et al., 2016) and in rats. In rats with genetic predisposition for major depression, enhancement of DMN connectivity (Gass et al., 2016) was observed while the optogenetic perturbation of LHb in this model resulted in diminished DMN connectivity and rescued the rats from depressive phenotype (Clemm von Hohenberg et al., 2018). Hence, RSP structural modifications might be giving rise to network-level functional connectivity reorganization, promoting aversive and anxio-depressive behaviors.

Functional connectivity remodeling in limbic circuitry

To obtain a global perspective on brain functional connectivity in neuropathic pain, we generated large connectivity matrices. We extracted ROIs from anatomical segmentation of Allen mouse brain atlas (Lein et al., 2007), covering isocortex and subcortical regions. The connectivity matrices were constructed with partial correlation, which computes correlation between any two nodes while excluding the influence of all others. Difference between neuropathic and control groups were analyzed for TP1 and TP2, graph theoretical parameters were assessed and most changed connections (edges) and regions (nodes) were ranked. In this manner, we were able to evaluate the longitudinal evolution of brain-wide FC.

At TP1, the point where mechanical hypersensitivity is established, the most prominent changes appeared in pain and aversion-related regions such as thalamus and insula (Iannetti and Mouraux, 2010) along with amygdala, hypothalamus, and parts of hippocampal formation. These areas were shown to be parts of aversion circuitry (Hayes and Northoff, 2011) in humans and in animals. Chronic pain is thought to reflect a shift from pain-related circuitry to meso-corticolimbic circuitry over time (Farmer et al., 2012), different pain conditions displaying divergent patterns of network reorganization. Transition from subacute to chronic back pain, as followed by rs-fMRI over time, could be predicted from initial cortico-striatal FC patterns (Baliki et al., 2012). Here, we observed limbic/reward areas and DMN components as most changed nodes at TP2 for neuropathic animals. These areas included VTA, ACB, pallidum, hippocampus, midbrain, septum, BST as well as SS, insula and RSP- implicating them in the development of anxiety and depression as a consequence of neuropathic pain.

On the basis of the nodes with most marked changes determined from graph theoretical approach and the areas showing structural alterations, we chose several ROIs to perform fine-grained seed analyses.

ACA functional connectivity presented major changes at both timepoints: At TP1, lower connectivity of ACA towards nociceptive areas (insula, PAG) might reflect the loss of descending pain modulation from this area, exacerbating pain. FC reductions towards CP, dHIP, and Hb also imply deficits in top-down control, allowing negative affect to prevail. At TP2, along with the changes observed at TP1, ACA displayed stronger connectivity towards RSP; thus, enhanced within-DMN connectivity patterns coinciding with depressive phenotype. ACA-AMY FC also showed enhancements, denoting an amplification of aversive inputs from amygdala into ACA or alterations of the negative loop between ACA and AMY. As mentioned earlier, ACA structural and functional connectivity changes are quite prevalent in depression and chronic pain conditions in their comorbidity. Combined with our observations, ACA emerges as a crucial node taking part in brain network reconstruction prompted by nerve injury and bringing out the behavioral signatures of depressive pathology.

VTA, a dopaminergic midbrain center encoding reward and coordinating meso-corticolimbic pathway, was one of the most changed areas at TP2 in the graph analysis. At this time point, VTA demonstrated stronger connectivity towards several other limbic areas, namely, ACA, ACB, CP, BST, Hb, PF and MD nuclei of thalamus in neuropathic mice with depressive phenotype. VTA connectivity increases both within reward circuitry and towards ACA, a DMN node which position VTA and ACA at the intersection of two important networks, possibly regulating their interactions. VTA takes part in both reward and aversion (Lammel et al., 2014), pain

processing (Ezzatpanah et al., 2016; Hipólito et al., 2015; Ko et al., 2018; Sotres-Bayón et al., 2001; Watanabe et al., 2018), stress- and pain-induced depressive behaviors (Fu et al., 2018; Isingrini et al., 2017; Ji et al., 2018). In rodent chronic pain models, VTA activity and reward behaviors are shown to be disrupted since rats with peripheral nerve injury had reduced dopaminergic signaling due to microglia-regulated activation of GABAergic VTA interneurons (Taylor et al., 2015) and increased GABAergic and decreased dopaminergic signaling was also reported for spinal cord injury in rats (Ko et al., 2018). In a spared nerve injury model, VTA activity and dopamine concentration in ACB were reduced (Ren et al., 2015). Both nerve injury and cancer pain models resulted in reduced neuronal excitability in VTA (Devonshire et al., 2017; Watanabe et al., 2018), while optogenetic stimulation of VTA dopaminergic neurons projecting to ACB alleviated allodynia (Watanabe et al., 2018). While preclinical studies such as chronic unpredictable mild stress (CUMS) model of depression reported lower VTA activity in VTA-mPFC pathway (Liu et al., 2018; Redlich et al., 2015) showed higher functional connectivity of ventral striatum (VS) and VTA in depressed patients. However, contradicting findings of increased VTA activity were reported in social defeat stress model (Berton et al., 2006; Walsh et al., 2014) and in chronic constriction injury (CCI) model (Liu et al., 2018). These contradictions might stem from VTA heterogeneity with respect to projections, activity patterns, and neurotransmitter types. Although we cannot determine activity levels in VTA with rs-fMRI, we might conjecture the increased connectivity towards reward/aversion areas as either compensatory mechanisms counteracting reward deficit or increased signaling for anti-reward, or a combination of both mechanisms.

LHb is another key reward/aversion structure which presents with connectivity alterations in neuropathic mice. LHb encodes aversion relevant to avoidance and escape behaviors and inhibits reward signals. At TP1, LHb connectivity towards AMY, TeA, vHIP and MRN were increased in neuropathic animals, which point to an augmented aversive signaling. The higher connectivity of LHb with PF nucleus of thalamus, HY, VTA, and MRN and lower connectivity with AI and MOs at TP2 can be interpreted as the enhancement of the inhibitory influence of LHb over reward areas. This effect can likely cause reward deficits associated with depressive phenotype. Longitudinal evolution of LHb FC in neuropathic animals identified stronger connections towards amygdala, VTA, and MRN and weaker connections to dHIP, indicating heightened LHb influence over reward areas promoting aversion and reward deficiency in a time dependent manner.

LHb is implicated in pain modulation (Shelton et al., 2012) via its connections to monoaminergic and opioidergic centers. Similar to our results, LHb connectivity towards PFC divisions and MO cortices were decreased in pediatric CRPS patients (Erpelding et al., 2013).

LHb is also involved in depressive pathologies (Proulx et al., 2014). For instance, increased blood flow to LHb (Gass et al., 2014) and LHb hyperactivity (Gass et al., 2016) was reported in rodent models of depression model while the lesion of the LHb diminish depressive behaviors. In addition, increased LHb burst activity drives depressive phenotype and rapid antidepressant ketamine acts to suppress this hyperactivity, reversing depressive behaviors and anhedonia (Yang et al., 2018) and inactivation of habenula with deep brain stimulation (DBS) in treatment resistant depression resulted in full remission in a patient (Sartorius et al., 2010). Even more relevant, some recent studies showed the involvement of the LHb in depression-pain comorbidity. Indeed, it has been shown that CUMS model in rats induces pain hypersensitivity and LHb hyperactivity, and its lesion relieves both the pain hypersensitivity and depressive phenotype (Li et al., 2016). Moreover, chronic constriction injury in rats also caused increased LHb activity and depressive behaviors which were eliminated by lesioning the LHb (Li et al., 2017). To conclude, increased LHb activity might be the common denominator in pain and depression comorbidity, regardless of initial pathology.

Moreover, functional connectivity of dorsal hippocampus (dHIP) showed higher connectivity towards RSP, SC, and LGN at TP1 which might be associated with amplified nociceptive inputs or compensation for lower dHIP activation in chronic pain. Indeed, impaired neurogenesis and synaptic plasticity were detected in hippocampus, which contribute to memory deficits commonly observed in chronic pain (Mutso et al., 2013). At TP2, dHIP connectivity towards ACA and septum was lower and its connectivity towards AMY and PTLp was greater in neuropathic mice. Reduced ACA-dHIP connectivity was also shown in a mouse model of metastatic bone cancer pain (Buehlmann et al., 2018). Decreased hippocampal connectivity towards mPFC was predictive of chronification of back pain in patients (Mutso et al., 2013) and may correlate with reduced reward learning signals in depressive disorder (Kumar et al., 2008). Overall, dHIP FC was higher with insula and amygdala, pain and aversion areas, and reduced towards ACA, Hb, and within itself in neuropathic pain-induced depression model.

On the other hand, ventral HIP showed stronger overall connectivity to mPFC, SS and insular area, and dHIP underlining their distinct functionalities. In fact, dorsal hippocampus engages in cognitive functions whereas vHIP is related to stress and emotional processing (Fanselow and Dong, 2010) and the two hippocampal divisions show differential gene expression patterns (Lee et al., 2017). Taken together, hippocampal FC patterns we observe might correspond to cognitive deficits and heightened emotional processing encountered in chronic pain (Simons et al., 2014) and depression.

While our study brought valuable information concerning the functional and structural reorganization of the brain in pain and depression comorbidity, it has some methodological limitations. Even though we started with the bigger animal cohort, due to a variation in the prevalence of relevant behavioral phenotype our sample size became smaller. Reproduction of our findings in a larger cohort would confirm their biological significance. Another caveat was the use of male subjects only. Recently, the stance on higher hormonal variability in female subjects was abandoned (Shansky, 2019) citing similar variability in males as well as the effects of male social hierarchy. There is a pronounced gender bias in basic research (Alderton, 2019) which might lead to false generalizations and public health problems. As depression prevalence is higher in women (Abate, 2013) and pain responses might differ between sexes (Fillingim et al., 2009), it is especially important to use female subjects in pain-induced depression results.

5. Conclusion

To recapitulate, we assessed the longitudinal evolution of the brain structural and functional connectivity coinciding with pain- and depression-related phenotypes. We observed time-dependent brain structural alterations and functional connectivity remodeling in several relevant brain areas for neuropathic mice in comparison to controls. Predominance of pain and aversion circuitries in the earlier post-injury time point accounted for the establishment of pain hypersensitivity. Development of depressive behaviors were accompanied by reorganization of reward system and DMN delineating causal relations between pain and depression. A prominent role of ACA, LHb, and VTA regions was discovered in pain-induced depression.

6. References

Abate, K.H., 2013. Gender Disparity in Prevalence of Depression Among Patient Population: A Systematic Review. Ethiop. J. Health Sci. 23, 283–288.

Alderton, G., 2019. Sex bias in research animals. Science 364, 846–848. https://doi.org/10.1126/science.364.6443.846-p

Anacker, C., Scholz, J., O'Donnell, K.J., Allemang-Grand, R., Diorio, J., Bagot, R.C., Nestler, E.J., Hen, R., Lerch, J.P., Meaney, M.J., 2016. Neuroanatomic Differences Associated With Stress Susceptibility and Resilience. Biol. Psychiatry, Mechanisms of Resilience to Stress Effects 79, 840–849. https://doi.org/10.1016/j.biopsych.2015.08.009

Avants, B.B., Tustison, N.J., Song, G., Cook, P.A., Klein, A., Gee, J.C., 2011. A reproducible evaluation of ANTs similarity metric performance in brain image registration. Neuroimage 54, 2033–2044. https://doi.org/10.1016/j.neuroimage.2010.09.025

Baliki, M. N., Chang, P.C., Baria, A.T., Centeno, M.V., Apkarian, A.V., 2014. Resting-sate functional reorganization of the rat limbic system following neuropathic injury. Sci. Rep. 4, 6186. https://doi.org/10.1038/srep06186

Baliki, M.N., Geha, P.Y., Jabakhanji, R., Harden, N., Schnitzer, T.J., Apkarian, A.V., 2008. A Preliminary fMRI Study of Analgesic Treatment in Chronic Back Pain and Knee Osteoarthritis. Mol. Pain 4, 1744-8069-4–47. https://doi.org/10.1186/1744-8069-4-47

Baliki, Marwan N., Mansour, A.R., Baria, A.T., Apkarian, A.V., 2014. Functional reorganization of the default mode network across chronic pain conditions. PloS One 9, e106133. https://doi.org/10.1371/journal.pone.0106133

Baliki, M.N., Petre, B., Torbey, S., Herrmann, K.M., Huang, L., Schnitzer, T.J., Fields, H.L., Apkarian, A.V., 2012. Corticostriatal functional connectivity predicts transition to chronic back pain. Nat. Neurosci. 15, 1117–1119. https://doi.org/10.1038/nn.3153

Barthas, F., Humo, M., Gilsbach, R., Waltisperger, E., Karatas, M., Leman, S., Hein, L., Belzung, C., Boutillier, A.-L., Barrot, M., Yalcin, I., 2017. Cingulate Overexpression of Mitogen-Activated Protein Kinase Phosphatase-1 as a Key Factor for Depression. Biol. Psychiatry 82, 370–379. https://doi.org/10.1016/j.biopsych.2017.01.019

Barthas, F., Sellmeijer, J., Hugel, S., Waltisperger, E., Barrot, M., Yalcin, I., 2015. The anterior cingulate cortex is a critical hub for pain-induced depression. Biol. Psychiatry 77, 236–245. https://doi.org/10.1016/j.biopsych.2014.08.004

Benbouzid, M., Pallage, V., Rajalu, M., Waltisperger, E., Doridot, S., Poisbeau, P., Freund-Mercier, M.J., Barrot, M., 2008. Sciatic nerve cuffing in mice: A model of sustained neuropathic pain. Eur. J. Pain 12, 591–599. https://doi.org/10.1016/j.ejpain.2007.10.002

Berman, M.G., Peltier, S., Nee, D.E., Kross, E., Deldin, P.J., Jonides, J., 2011. Depression, rumination and the default network. Soc. Cogn. Affect. Neurosci. 6, 548–555. https://doi.org/10.1093/scan/nsq080

Berton, O., McClung, C.A., DiLeone, R.J., Krishnan, V., Renthal, W., Russo, S.J., Graham, D., Tsankova, N.M., Bolanos, C.A., Rios, M., Monteggia, L.M., Self, D.W., Nestler, E.J., 2006. Essential Role of BDNF in the Mesolimbic Dopamine Pathway in Social Defeat Stress. Science 311, 864–868. https://doi.org/10.1126/science.1120972

Bilbao, A., Falfán-Melgoza, C., Leixner, S., Becker, R., Singaravelu, S.K., Sack, M., Sartorius, A., Spanagel, R., Weber-Fahr, W., 2018. Longitudinal Structural and Functional Brain Network Alterations in a Mouse Model of Neuropathic Pain. Neuroscience. https://doi.org/10.1016/j.neuroscience.2018.04.020

Borsook, D., Linnman, C., Faria, V., Strassman, A.M., Becerra, L., Elman, I., 2016. Reward deficiency and anti-reward in pain chronification. Neurosci. Biobehav. Rev. 68, 282–297. https://doi.org/10.1016/j.neubiorev.2016.05.033

Broyd, S.J., Demanuele, C., Debener, S., Helps, S.K., James, C.J., Sonuga-Bark, E.J.S., 2009. Default-mode brain dysfunction in mental disorders: A systematic review. Neurosci. Biobehav. Rev. 33, 279–296. https://doi.org/10.1016/j.neubiorev.2008.09.002

Buckner, R.L., Andrews-Hanna, J.R., Schacter, D.L., 2008. The Brain's Default Network: Anatomy, Function, and Relevance to Disease. Ann. N. Y. Acad. Sci. 1124, 1–38. https://doi.org/10.1196/annals.1440.011

Buehlmann, D., Grandjeanc, J., Xandryd, J., Rudin, M., 2018. Longitudinal resting-state fmri in a mouse model of metastatic bone cancer reveals distinct functional reorganizations along a developing chronic pain state. Pain Publish Ahead of Print. https://doi.org/10.1097/j.pain.0000000000001148

Cauda, F., D'Agata, F., Sacco, K., Duca, S., Cocito, D., Paolasso, I., Isoardo, G., Geminiani, G., 2010. Altered resting state attentional networks in diabetic neuropathic pain. J. Neurol. Neurosurg. Psychiatry 81, 806–811. https://doi.org/10.1136/jnnp.2009.188631

Chang, P.-C., Pollema-Mays, S.L., Centeno, M.V., Procissi, D., Contini, M., Baria, A.T., Martina, M., Apkarian, A.V., 2014. Role of nucleus accumbens in neuropathic pain: Linked multi-scale evidence in

the rat transitioning to neuropathic pain: Pain 155, 1128–1139. https://doi.org/10.1016/j.pain.2014.02.019

Clemm von Hohenberg, C., Weber-Fahr, W., Lebhardt, P., Ravi, N., Braun, U., Gass, N., Becker, R., Sack, M., Cosa Linan, A., Gerchen, M.F., Reinwald, J.R., Oettl, L.-L., Meyer-Lindenberg, A., Vollmayr, B., Kelsch, W., Sartorius, A., 2018. Lateral habenula perturbation reduces default-mode network connectivity in a rat model of depression. Transl. Psychiatry 8, 68. https://doi.org/10.1038/s41398-018-0121-y

DaSilva, A.F.M., Granziera, C., Tuch, D.S., Snyder, J., Vincent, M., Hadjikhani, N., 2007. Interictal alterations of the trigeminal somatosensory pathway and PAG in migraine. Neuroreport 18, 301–305. https://doi.org/10.1097/WNR.0b013e32801776bb

Devonshire, I.M., Burston, J.J., Xu, L., Lillywhite, A., Prior, M.J., Watson, D.J.G., Greenspon, C.M., Iwabuchi, S.J., Auer, D.P., Chapman, V., 2017. Manganese-enhanced magnetic resonance imaging depicts brain activity in models of acute and chronic pain: A new window to study experimental spontaneous pain? NeuroImage 157, 500–510. https://doi.org/10.1016/j.neuroimage.2017.06.034

Draganski, B., Ashburner, J., Hutton, C., Kherif, F., Frackowiak, R.S.J., Helms, G., Weiskopf, N., 2011. Regional specificity of MRI contrast parameter changes in normal ageing revealed by voxel-based quantification (VBQ). NeuroImage 55, 1423–1434. https://doi.org/10.1016/j.neuroimage.2011.01.052

Drevets, W.C., Price, J.L., Jr, J.R.S., Todd, R.D., Reich, T., Vannier, M., Raichle, M.E., 1997. Subgenual prefrontal cortex abnormalities in mood disorders. Nature 386, 824–827. https://doi.org/10.1038/386824a0

Erpelding, N., Sava, S., Simons, L.E., Lebel, A., Serrano, P., Becerra, L., Borsook, D., 2013. Habenula functional resting-state connectivity in pediatric CRPS. J. Neurophysiol. 111, 239–247. https://doi.org/10.1152/jn.00405.2013

Ezzatpanah, S., Babapour, V., Haghparast, A., 2016. Differential contribution of orexin receptors within the ventral tegmental area to modulation of persistent inflammatory pain. Eur. J. Pain 20, 1090–1101. https://doi.org/10.1002/ejp.833

Fanselow, M.S., Dong, H.-W., 2010. Are the Dorsal and Ventral Hippocampus Functionally Distinct Structures? Neuron 65, 7–19. https://doi.org/10.1016/j.neuron.2009.11.031

Farmer, M.A., Baliki, M.N., Apkarian, A.V., 2012. A dynamic network perspective of chronic pain. Neurosci. Lett. 520, 197–203. https://doi.org/10.1016/j.neulet.2012.05.001

Fillingim, R.B., King, C.D., Ribeiro-Dasilva, M.C., Rahim-Williams, B., Riley, J.L., 2009. Sex, Gender, and Pain: A Review of Recent Clinical and Experimental Findings. J. Pain Off. J. Am. Pain Soc. 10, 447–485. https://doi.org/10.1016/j.jpain.2008.12.001

Fu, B., Wen, S.-N., Wang, B., Wang, K., Zhang, J.-Y., Weng, X.-C., Liu, S.-J., 2018. Gabapentin regulates dopaminergic neuron firing and theta oscillation in the ventral tegmental area to reverse depression-like behavior in chronic neuropathic pain state [WWW Document]. J. Pain Res. https://doi.org/10.2147/JPR.S170167

Garcia-Larrea, L., Peyron, R., 2013. Pain matrices and neuropathic pain matrices: a review. Pain 154 Suppl 1, S29-43. https://doi.org/10.1016/j.pain.2013.09.001

Gass, N., Becker, R., Schwarz, A.J., Weber-Fahr, W., Clemm von Hohenberg, C., Vollmayr, B., Sartorius, A., 2016. Brain network reorganization differs in response to stress in rats genetically predisposed to depression and stress-resilient rats. Transl. Psychiatry 6, e970–e970. https://doi.org/10.1038/tp.2016.233

Gass, N., Cleppien, D., Zheng, L., Schwarz, A.J., Meyer-Lindenberg, A., Vollmayr, B., Weber-Fahr, W., Sartorius, A., 2014. Functionally altered neurocircuits in a rat model of treatment-resistant depression show prominent role of the habenula. Eur. Neuropsychopharmacol. 24, 381–390. https://doi.org/10.1016/j.euroneuro.2013.12.004

Geha, P.Y., Baliki, M.N., Harden, R.N., Bauer, W.R., Parrish, T.B., Apkarian, A.V., 2008. The Brain in Chronic CRPS Pain: Abnormal Gray-White Matter Interactions in Emotional and Autonomic Regions. Neuron 60, 570–581. https://doi.org/10.1016/j.neuron.2008.08.022

Gonçalves, L., Silva, R., Pinto-Ribeiro, F., Pêgo, J.M., Bessa, J.M., Pertovaara, A., Sousa, N., Almeida, A., 2008. Neuropathic pain is associated with depressive behaviour and induces neuroplasticity in the amygdala of the rat. Exp. Neurol. 213, 48–56. https://doi.org/10.1016/j.expneurol.2008.04.043

Grandjean, J., Azzinnari, D., Seuwen, A., Sigrist, H., Seifritz, E., Pryce, C.R., Rudin, M., 2016. Chronic psychosocial stress in mice leads to changes in brain functional connectivity and metabolite levels comparable to human depression. NeuroImage 142, 544–552. https://doi.org/10.1016/j.neuroimage.2016.08.013

Greicius, M.D., Flores, B.H., Menon, V., Glover, G.H., Solvason, H.B., Kenna, H., Reiss, A.L., Schatzberg, A.F., 2007. Resting-State Functional Connectivity in Major Depression: Abnormally Increased Contributions from Subgenual Cingulate Cortex and Thalamus. Biol. Psychiatry 62, 429–437. https://doi.org/10.1016/j.biopsych.2006.09.020

Greicius, M.D., Krasnow, B., Reiss, A.L., Menon, V., 2003. Functional connectivity in the resting brain: a network analysis of the default mode hypothesis. Proc. Natl. Acad. Sci. 100, 253–258.

Harsan, L.-A., Dávid, C., Reisert, M., Schnell, S., Hennig, J., von Elverfeldt, D., Staiger, J.F., 2013. Mapping remodeling of thalamocortical projections in the living reeler mouse brain by diffusion tractography. Proc. Natl. Acad. Sci. U. S. A. 110, E1797-1806. https://doi.org/10.1073/pnas.1218330110

Hayes, D.J., Northoff, G., 2011. Identifying a Network of Brain Regions Involved in Aversion-Related Processing: A Cross-Species Translational Investigation. Front. Integr. Neurosci. 5. https://doi.org/10.3389/fnint.2011.00049

Henckens, M.J.A.G., van der Marel, K., van der Toorn, A., Pillai, A.G., Fernández, G., Dijkhuizen, R.M., Joëls, M., 2015. Stress-induced alterations in large-scale functional networks of the rodent brain. NeuroImage 105, 312–322. https://doi.org/10.1016/j.neuroimage.2014.10.037

Hipólito, L., Wilson-Poe, A., Campos-Jurado, Y., Zhong, E., Gonzalez-Romero, J., Virag, L., Whittington, R., Comer, S.D., Carlton, S.M., Walker, B.M., Bruchas, M.R., Morón, J.A., 2015. Inflammatory Pain Promotes Increased Opioid Self-Administration: Role of Dysregulated Ventral Tegmental Area μ Opioid Receptors. J. Neurosci. 35, 12217–12231. https://doi.org/10.1523/JNEUROSCI.1053-15.2015

Hubbard, C.S., Khan, S.A., Xu, S., Cha, M., Masri, R., Seminowicz, D.A., 2015. Behavioral, metabolic and functional brain changes in a rat model of chronic neuropathic pain: A longitudinal MRI study. NeuroImage 107, 333–344. https://doi.org/10.1016/j.neuroimage.2014.12.024

Iannetti, G.D., Mouraux, A., 2010. From the neuromatrix to the pain matrix (and back). Exp. Brain Res. 205, 1–12. https://doi.org/10.1007/s00221-010-2340-1

Ikeda, H., Mochizuki, K., Murase, K., 2013. Astrocytes are involved in long-term facilitation of neuronal excitation in the anterior cingulate cortex of mice with inflammatory pain: Pain 154, 2836–2843. https://doi.org/10.1016/j.pain.2013.08.023

Isingrini, E., Perret, L., Rainer, Q., Amilhon, B., Guma, E., Tanti, A., Martin, G., Robinson, J., Moquin, L., Marti, F., 2017. 695. Resilience against Chronic Stress is Mediated by Noradrenergic Regulation of the Ventral Tegmental Area. Biol. Psychiatry 81, S282.

Ji, N.-N., Kang, J., Hua, R., Zhang, Y.-M., 2018. Involvement of dopamine system in the regulation of the brain corticotropin-releasing hormone in paraventricular nucleus in a rat model of chronic visceral pain. Neurol. Res. 0, 1–8. https://doi.org/10.1080/01616412.2018.1460702

Ko, M.Y., Jang, E.Y., Lee, J.Y., Kim, S.P., Whang, S.H., Lee, B.H., Kim, H.Y., Yang, C.H., Cho, H.J., Gwak, Y.S., 2018. The Role of Ventral Tegmental Area Gamma-Aminobutyric Acid in Chronic Neuropathic

Pain after Spinal Cord Injury in Rats. J. Neurotrauma 35, 1755–1764. https://doi.org/10.1089/neu.2017.5381

Kumar, P., Waiter, G., Ahearn, T., Milders, M., Reid, I., Steele, J.D., 2008. Abnormal temporal difference reward-learning signals in major depression. Brain 131, 2084–2093. https://doi.org/10.1093/brain/awn136

Lammel, S., Lim, B.K., Malenka, R.C., 2014. Reward and aversion in a heterogeneous midbrain dopamine system. Neuropharmacology 76, 351–359. https://doi.org/10.1016/j.neuropharm.2013.03.019

Lee, A.-R., Kim, J.-H., Cho, E., Kim, M., Park, M., 2017. Dorsal and Ventral Hippocampus Differentiate in Functional Pathways and Differentially Associate with Neurological Disease-Related Genes during Postnatal Development. Front. Mol. Neurosci. 10. https://doi.org/10.3389/fnmol.2017.00331

Lein, E.S., Hawrylycz, M.J., Ao, N., Ayres, M., Bensinger, A., Bernard, A., Boe, A.F., Boguski, M.S., Brockway, K.S., Byrnes, E.J., Chen, Lin, Chen, Li, Chen, T.-M., Chi Chin, M., Chong, J., Crook, B.E., Czaplinska, A., Dang, C.N., Datta, S., Dee, N.R., Desaki, A.L., Desta, T., Diep, E., Dolbeare, T.A., Donelan, M.J., Dong, H.-W., Dougherty, J.G., Duncan, B.J., Ebbert, A.J., Eichele, G., Estin, L.K., Faber, C., Facer, B.A., Fields, R., Fischer, S.R., Fliss, T.P., Frensley, C., Gates, S.N., Glattfelder, K.J., Halverson, K.R., Hart, M.R., Hohmann, J.G., Howell, M.P., Jeung, D.P., Johnson, R.A., Karr, P.T., Kawal, R., Kidney, J.M., Knapik, R.H., Kuan, C.L., Lake, J.H., Laramee, A.R., Larsen, K.D., Lau, C., Lemon, T.A., Liang, A.J., Liu, Y., Luong, L.T., Michaels, J., Morgan, J.J., Morgan, R.J., Mortrud, M.T., Mosqueda, N.F., Ng, L.L., Ng, R., Orta, G.J., Overly, C.C., Pak, T.H., Parry, S.E., Pathak, S.D., Pearson, O.C., Puchalski, R.B., Riley, Z.L., Rockett, H.R., Rowland, S.A., Royall, J.J., Ruiz, M.J., Sarno, N.R., Schaffnit, K., Shapovalova, N.V., Sivisay, T., Slaughterbeck, C.R., Smith, S.C., Smith, K.A., Smith, B.I., Sodt, A.J., Stewart, N.N., Stumpf, K.-R., Sunkin, S.M., Sutram, M., Tam, A., Teemer, C.D., Thaller, C., Thompson, C.L., Varnam, L.R., Visel, A., Whitlock, R.M., Wohnoutka, P.E., Wolkey, C.K., Wong, V.Y., Wood, M., Yaylaoglu, M.B., Young, R.C., Youngstrom, B.L., Feng Yuan, X., Zhang, B., Zwingman, T.A., Jones, A.R., 2007. Genome-wide atlas of gene expression in the adult mouse brain. Nature 445, 168–176. https://doi.org/10.1038/nature05453

Li, J., Li, Y., Zhang, B., Shen, X., Zhao, H., 2016. Why depression and pain often coexist and mutually reinforce: Role of the lateral habenula. Exp. Neurol. 284, 106–113. https://doi.org/10.1016/j.expneurol.2016.08.010

Li, Yanhui, Wang, Y., Xuan, C., Li, Yang, Piao, L., Li, J., Zhao, H., 2017. Role of the Lateral Habenula in Pain-Associated Depression. Front. Behav. Neurosci. 11. https://doi.org/10.3389/fnbeh.2017.00031

Liu, D., Tang, Q.-Q., Yin, C., Song, Yu, Liu, Y., Yang, J.-X., Liu, H., Zhang, Y.-M., Wu, S.-Y., Song, Ying, Juarez, B., Ding, H.-L., Han, M.-H., Zhang, H., Cao, J.-L., 2018. Brain-derived neurotrophic factor–mediated projection-specific regulation of depressive-like and nociceptive behaviors in the mesolimbic reward circuitry: PAIN 159, 175. https://doi.org/10.1097/j.pain.0000000000001083

Lutz, J., Jäger, L., Quervain, D. de, Krauseneck, T., Padberg, F., Wichnalek, M., Beyer, A., Stahl, R., Zirngibl, B., Morhard, D., Reiser, M., Schelling, G., 2008. White and gray matter abnormalities in the brain of patients with fibromyalgia: A diffusion-tensor and volumetric imaging study. Arthritis Rheum. 58, 3960–3969. https://doi.org/10.1002/art.24070

Mannelli, L.D.C., Pacini, A., Bonaccini, L., Zanardelli, M., Mello, T., Ghelardini, C., 2013. Morphologic Features and Glial Activation in Rat Oxaliplatin-Dependent Neuropathic Pain. J. Pain 14, 1585–1600. https://doi.org/10.1016/j.jpain.2013.08.002

Mayberg, H.S., 2009. Targeted electrode-based modulation of neural circuits for depression. J. Clin. Invest. 119, 717–725. https://doi.org/10.1172/JCI38454

Mitsi, V., Zachariou, V., 2016. Modulation of pain, nociception, and analgesia by the brain reward center. Neuroscience. https://doi.org/10.1016/j.neuroscience.2016.05.017

Moayedi, M., Weissman-Fogel, I., Salomons, T.V., Crawley, A.P., Goldberg, M.B., Freeman, B.V., Tenenbaum, H.C., Davis, K.D., 2012. White matter brain and trigeminal nerve abnormalities in temporomandibular disorder. Pain 153, 1467–1477. https://doi.org/10.1016/j.pain.2012.04.003

Mutso, A.A., Petre, B., Huang, L., Baliki, M.N., Torbey, S., Herrmann, K.M., Schnitzer, T.J., Apkarian, A.V., 2013. Reorganization of hippocampal functional connectivity with transition to chronic back pain. J. Neurophysiol. 111, 1065–1076. https://doi.org/10.1152/jn.00611.2013

Napadow, V., LaCount, L., Park, K., As-Sanie, S., Clauw, D.J., Harris, R.E., 2011. Intrinsic brain connectivity in fibromyalgia is associated with chronic pain intensity. Arthritis Rheum. 62, 2545–2555. https://doi.org/10.1002/art.27497

Narita Minoru, Kuzumaki Naoko, Narita Michiko, Kaneko Chihiro, Hareyama Nana, Miyatake Mayumi, Shindo Keiko, Miyoshi Kan, Nakajima Mayumi, Nagumo Yasuyuki, Sato Fumiaki, Wachi Hiroshi, Seyama Yoshiyuki, Suzuki Tsutomu, 2006. Chronic pain-induced emotional dysfunction is associated with astrogliosis due to cortical δ-opioid receptor dysfunction. J. Neurochem. 97, 1369–1378. https://doi.org/10.1111/j.1471-4159.2006.03824.x

Proulx, C.D., Hikosaka, O., Malinow, R., 2014. Reward processing by the lateral habenula in normal and depressive behaviors. Nat. Neurosci. 17, 1146–1152. https://doi.org/10.1038/nn.3779

Raichle, M.E., MacLeod, A.M., Snyder, A.Z., Powers, W.J., Gusnard, D.A., Shulman, G.L., 2001. A default mode of brain function. Proc. Natl. Acad. Sci. 98, 676–682.

Rajkowska, G., 2000. Postmortem studies in mood disorders indicate altered numbers of neurons and glial cells. Biol. Psychiatry 48, 766–777. https://doi.org/10.1016/S0006-3223(00)00950-1

Redlich, R., Dohm, K., Grotegerd, D., Opel, N., Zwitserlood, P., Heindel, W., Arolt, V., Kugel, H., Dannlowski, U., 2015. Reward Processing in Unipolar and Bipolar Depression: A Functional MRI Study. Neuropsychopharmacology 40, 2623–2631. https://doi.org/10.1038/npp.2015.110

Reisert, M., Mader, I., Anastasopoulos, C., Weigel, M., Schnell, S., Kiselev, V., 2011. Global fiber reconstruction becomes practical. NeuroImage 54, 955–962. https://doi.org/10.1016/j.neuroimage.2010.09.016

Ren, W., Centeno, M.V., Berger, S., Wu, Y., Na, X., Liu, X., Kondapalli, J., Apkarian, A.V., Martina, M., Surmeier, D.J., 2015. The indirect pathway of the nucleus accumbens shell amplifies neuropathic pain. Nat. Neurosci. 19, 220–222. https://doi.org/10.1038/nn.4199

Russo, S.J., Nestler, E.J., 2013. The brain reward circuitry in mood disorders. Nat. Rev. Neurosci. 14, 609–625. https://doi.org/10.1038/nrn3381

Sartorius, A., Kiening, K.L., Kirsch, P., Gall, C.C. von, Haberkorn, U., Unterberg, A.W., Henn, F.A., Meyer-Lindenberg, A., 2010. Remission of Major Depression Under Deep Brain Stimulation of the Lateral Habenula in a Therapy-Refractory Patient. Biol. Psychiatry 67, e9–e11. https://doi.org/10.1016/j.biopsych.2009.08.027

Scholz, J., Tomassini, V., Johansen-Berg, H., 2009. Chapter 11 - Individual Differences in White Matter Microstructure in the Healthy Brain, in: Johansen-Berg, H., Behrens, T.E.J. (Eds.), Diffusion MRI. Academic Press, San Diego, pp. 237–249. https://doi.org/10.1016/B978-0-12-374709-9.00011-0

Sellmeijer, J., Mathis, V., Hugel, S., Li, X.-H., Song, Q., Chen, Q.-Y., Barthas, F., Lutz, P.-E., Karatas, M., Luthi, A., Veinante, P., Aertsen, A., Barrot, M., Zhuo, M., Yalcin, I., 2018. Hyperactivity of Anterior Cingulate Cortex Areas 24a/24b Drives Chronic Pain-Induced Anxiodepressive-like Consequences. J. Neurosci. 38, 3102–3115. https://doi.org/10.1523/JNEUROSCI.3195-17.2018

Seminowicz, D.A., Laferriere, A.L., Millecamps, M., Yu, J.S.C., Coderre, T.J., Bushnell, M.C., 2009. MRI structural brain changes associated with sensory and emotional function in a rat model of long-term neuropathic pain. NeuroImage, Brain Body Medicine 47, 1007–1014. https://doi.org/10.1016/j.neuroimage.2009.05.068

Shansky, R.M., 2019. Are hormones a "female problem" for animal research? Science 364, 825–826. https://doi.org/10.1126/science.aaw7570

Shelton, L., Becerra, L., Borsook, D., 2012. Unmasking the mysteries of the habenula in pain and analgesia. Prog. Neurobiol. 96, 208–219. https://doi.org/10.1016/j.pneurobio.2012.01.004

Simons, L.E., Elman, I., Borsook, D., 2014. Psychological processing in chronic pain: a neural systems approach. Neurosci. Biobehav. Rev. 39, 61–78. https://doi.org/10.1016/j.neubiorev.2013.12.006

Sotres-Bayón, F., Torres-López, E., López-Ávila, A., del Ángel, R., Pellicer, F., 2001. Lesion and electrical stimulation of the ventral tegmental area modify persistent nociceptive behavior in the rat. Brain Res. 898, 342–349. https://doi.org/10.1016/S0006-8993(01)02213-2

Stafford, J.M., Jarrett, B.R., Miranda-Dominguez, O., Mills, B.D., Cain, N., Mihalas, S., Lahvis, G.P., Lattal, K.M., Mitchell, S.H., David, S.V., Fryer, J.D., Nigg, J.T., Fair, D.A., 2014. Large-scale topology and the default mode network in the mouse connectome. Proc. Natl. Acad. Sci. 111, 18745–18750. https://doi.org/10.1073/pnas.1404346111

Steiner, J., Walter, M., Gos, T., Guillemin, G.J., Bernstein, H.-G., Sarnyai, Z., Mawrin, C., Brisch, R., Bielau, H., zu Schwabedissen, L.M., Bogerts, B., Myint, A.-M., 2011. Severe depression is associated with increased microglial quinolinic acid in subregions of the anterior cingulate gyrus: Evidence for an immune-modulated glutamatergic neurotransmission? J. Neuroinflammation 8, 94. https://doi.org/10.1186/1742-2094-8-94

Stouffer, S.A., Suchman, E.A., DeVinney, L.C., Star, S.A., Williams, R.M.J., 1949. Adjustment During Army Life. Princet. NJ Princet. Univ. Press.

Tanti, A., Lutz, P.-E., Kim, J., O'Leary, L., Turecki, G., Mechawar, N., 2019. Evidence of decreased gap junction coupling between astrocytes and oligodendrocytes in the anterior cingulate cortex of depressed suicides. bioRxiv 578807. https://doi.org/10.1101/578807

Taylor, A.M.W., Castonguay, A., Taylor, A.J., Murphy, N.P., Ghogha, A., Cook, C., Xue, L., Olmstead, M.C., De Koninck, Y., Evans, C.J., Cahill, C.M., 2015. Microglia Disrupt Mesolimbic Reward Circuitry in Chronic Pain. J. Neurosci. 35, 8442–8450. https://doi.org/10.1523/JNEUROSCI.4036-14.2015

Upadhyay, J., Baker, S.J., Chandran, P., Miller, L., Lee, Y., Marek, G.J., Sakoglu, U., Chin, C.-L., Luo, F., Fox, G.B., Day, M., 2011. Default-mode-like network activation in awake rodents. PloS One 6, e27839. https://doi.org/10.1371/journal.pone.0027839

Uranova, N.A., Vostrikov, V.M., Orlovskaya, D.D., Rachmanova, V.I., 2004. Oligodendroglial density in the prefrontal cortex in schizophrenia and mood disorders: a study from the Stanley Neuropathology Consortium. Schizophr. Res. 67, 269–275. https://doi.org/10.1016/S0920-9964(03)00181-6

Walsh, J.J., Friedman, A.K., Sun, H., Heller, E.A., Ku, S.M., Juarez, B., Burnham, V.L., Mazei-Robison, M.S., Ferguson, D., Golden, S.A., Koo, J.W., Chaudhury, D., Christoffel, D.J., Pomeranz, L., Friedman, J.M., Russo, S.J., Nestler, E.J., Han, M.-H., 2014. Stress and CRF gate neural activation of BDNF in the mesolimbic reward pathway. Nat. Neurosci. 17, 27–29. https://doi.org/10.1038/nn.3591

Wang, G.-Q., Cen, C., Li, C., Cao, S., Wang, N., Zhou, Z., Liu, X.-M., Xu, Y., Tian, N.-X., Zhang, Y., Wang, J., Wang, L.-P., Wang, Y., 2015. Deactivation of excitatory neurons in the prelimbic cortex via Cdk5 promotes pain sensation and anxiety. Nat. Commun. 6, 7660. https://doi.org/10.1038/ncomms8660

Wang, L., Hermens, D.F., Hickie, I.B., Lagopoulos, J., 2012. A systematic review of resting-state functional-MRI studies in major depression. J. Affect. Disord. 142, 6–12. https://doi.org/10.1016/j.jad.2012.04.013

Watanabe, M., Narita, Michiko, Hamada, Y., Yamashita, A., Tamura, H., Ikegami, D., Kondo, T., Shinzato, T., Shimizu, T., Fukuchi, Y., Muto, A., Okano, H., Yamanaka, A., Tawfik, V.L., Kuzumaki, N., Navratilova, E., Porreca, F., Narita, Minoru, 2018. Activation of ventral tegmental area dopaminergic

neurons reverses pathological allodynia resulting from nerve injury or bone cancer. Mol. Pain 14, 1744806918756406. https://doi.org/10.1177/1744806918756406

Xu, H., Wu, L.-J., Wang, H., Zhang, X., Vadakkan, K.I., Kim, S.S., Steenland, H.W., Zhuo, M., 2008. Presynaptic and Postsynaptic Amplifications of Neuropathic Pain in the Anterior Cingulate Cortex. J. Neurosci. 28, 7445–7453. https://doi.org/10.1523/JNEUROSCI.1812-08.2008

Yalcin, I., Barthas, F., Barrot, M., 2014a. Emotional consequences of neuropathic pain: Insight from preclinical studies. Neurosci. Biobehav. Rev. 47, 154–164. https://doi.org/10.1016/j.neubiorev.2014.08.002

Yalcin, I., Bohren, Y., Waltisperger, E., Sage-Ciocca, D., Yin, J.C., Freund-Mercier, M.-J., Barrot, M., 2011. A time-dependent history of mood disorders in a murine model of neuropathic pain. Biol. Psychiatry 70, 946–953. https://doi.org/10.1016/j.biopsych.2011.07.017

Yalcin, I., Megat, S., Barthas, F., Waltisperger, E., Kremer, M., Salvat, E., Barrot, M., 2014b. The Sciatic Nerve Cuffing Model of Neuropathic Pain in Mice. J. Vis. Exp. https://doi.org/10.3791/51608

Yang, Y., Wang, H., Hu, J., Hu, H., 2018. Lateral habenula in the pathophysiology of depression. Curr. Opin. Neurobiol., Neurobiology of Disease 48, 90–96. https://doi.org/10.1016/j.conb.2017.10.024

Yoon, E.J., Kim, Y.K., Shin, H.I., Lee, Y., Kim, S.E., 2013. Cortical and white matter alterations in patients with neuropathic pain after spinal cord injury. Brain Res. 1540, 64–73. https://doi.org/10.1016/j.brainres.2013.10.007

Zhang, Z., Gadotti, V.M., Chen, L., Souza, I.A., Stemkowski, P.L., Zamponi, G.W., 2015. Role of Prelimbic GABAergic Circuits in Sensory and Emotional Aspects of Neuropathic Pain. Cell Rep. 12, 752–759. https://doi.org/10.1016/j.celrep.2015.07.001

Zhu, X., Wang, X., Xiao, J., Liao, J., Zhong, M., Wang, W., Yao, S., 2012. Evidence of a Dissociation Pattern in Resting-State Default Mode Network Connectivity in First-Episode, Treatment-Naive Major Depression Patients. Biol. Psychiatry 71, 611–617. https://doi.org/10.1016/j.biopsych.2011.10.035

Zhuo, M., 2013. Long-term potentiation in the anterior cingulate cortex and chronic pain. Philos. Trans. R. Soc. B Biol. Sci. 369, 20130146–20130146. https://doi.org/10.1098/rstb.2013.0146

Annexe 4: List of presentations

Congress presentations:

SFRMBM, Bordeaux 2017, Poster (Awarded):

- *Connectivité fonctionnelle au repos au stade prodromal de la maladie d'Alzheimer : étude d'un modèle murin de la tauopathie* ; **Auteurs** : Laetitia Degiorgis, Meltem Karatas, Marion Sourty, Chrystelle Po, Thomas Bienert, Hsu Lei Lee, Dominik von Elverfeldt, Anne-Laurence Boutillier, Chantal Mathis, David Blum, Jean-Paul Armspach, Frédéric Blanc and Laura Adela Harsan.

ISMRM, Honolulu 2017, E-poster:

- *Patterns of resting-state functional connectivity in the prodromal phase of Alzheimer's disease: Insights from a tauopathy mouse model (Thy-Tau22) ;* **Auteurs** : Laetitia Degiorgis, Meltem Karatas, Marion Sourty, Chrystelle Po, Thomas Bienert, Hsu Lei Lee, Dominik von Elverfeldt, Chantal Mathis, Anne-Laurence Boutiller, Frédéric Blanc, Jean-Paul Armspach and Laura Adela Harsan.

EMIM, Cologne 2017, Poster:

- *Remodeled functional connectivity in the early phase of Alzheimer's pathology in a tauopathy mouse model (Thy-Tau22) ;* ***Auteurs :*** Laetitia Degiorgis, Meltem Karatas, Marion Sourty, Chrystelle Po, Thomas Bienert, Hsu Lei Lee, Dominik von Elverfeldt, Anne-Laurence Boutillier, Chantal Mathis, David Blum, Jean-Paul Armspach, Frédéric Blanc and Laura Adela Harsan.

FMTS, Strasbourg 2018, Oral presentation:

- *Mapping functional connectivity alterations in a mouse model of Alzheimer's disease ;* **Auteurs** : Laetitia Degiorgis, Meltem Karatas, Marion Sourty, Thomas Bienert, Marco Reisert, Chantal Mathis, Anne-Laurence Boutiller, Frédéric Blanc, Jean-Paul Armspach and Laura Adela Harsan.

IRMGE, Strasbourg 2018, Oral presentation:

- *Analyse des réseaux cérébraux par IRM fonctionnelle et structurelle chez un modèle souris de la maladie d'Alzheimer ;* **Auteurs** *:* Laetitia Degiorgis, Meltem Karatas, Marion Sourty, Thomas Bienert, Marco Reisert, Chantal Mathis, Anne-Laurence Boutiller, Frédéric Blanc, Jean-Paul Armspach and Laura Adela Harsan.

ISMRM, Paris 2018, Oral presentation:

- *Longitudinal alterations of resting-state functional connectivity in Alzheimer's disease in a tauopathy mouse model* ; **Auteurs :** Laetitia Degiorgis, Meltem Karatas, Marion Sourty, Thomas Bienert, Marco Reisert, Chantal Mathis, Anne-Laurence Boutiller, Frédéric Blanc, Jean-Paul Armspach and Laura Adela Harsan.

AD/PD, Lisbonne 2019, Poster :

- *Longitudinal modifications of the connectome of a mouse model of Alzheimer's disease ;* Laetitia Degiorgis, Meltem Karatas, Marion Sourty, Thomas Bienert, Marco Reisert, Chantal Mathis, Anne-Laurence Boutiller, David Blum, Frédéric Blanc, Jean-Paul Armspach and Laura-Adela Harsan.

SFRMBM, Strasbourg 2019, Oral presentations

- *Modifications précoces de la dynamique de la connectivité fonctionnelle chez un modèle souris de la Maladie d'Alzheimer ;* **Authors** : Degiorgis Laetitia, Sourty Marion, Boutillier Anne-Laurence, Faivre Emilie, Blum David, Armspach Jean-Paul, Blanc Frédéric, Harsan Laura-Adela

- *Altérations longitudinales du connectome cérébral chez une souris modèle de la maladie d'Alzheimer ;* **Authors** : Degiorgis Laetitia, Karatas Meltem, Sourty Marion, Bienert Thomas, Reisert Marco, Mathis Chantal, Faivre Emilie, Blum David, Boutillier Anne-Laurence, Armspach Jean-Paul, Blanc Frédéric, Harsan Laura-Adela

Publications:

- Submitted in Alzheimer and Dementia:

  "Remodeling of cerebral networks architecture anticipate behavioral deficits in a tauopathy mouse model of Alzheimer's disease"; **Authors**: Laetitia Degiorgis, Meltem Karatas, Marion Sourty, Emilie Faivre Julien Lamy, Vincent Noblet, Thomas Bienert, Marco Reisert, Dominik Elverfeldt, Luc Buée, David Blum, Anne-Laurence Boutillier, Jean-Paul Armspach, Frédéric Blanc, Laura- Harsan

- Article in preparation:

  Longitudinal evaluation of the cerebral connectome in a tauopathy mouse model of Alzheimer's disease; **Authors**: Laetitia Degiorgis, Meltem Karatas, Marion Sourty, Emilie Faivre Julien Lamy, Vincent Noblet, Thomas Bienert, Marco Reisert, Dominik Elverfeldt, Luc Buée, David Blum, Anne-Laurence Boutillier, Jean-Paul Armspach, Frédéric Blanc, Laura- Harsan